INVESTIGATIONS INTO THE EFFECTS OF CHAIN-LENGTH-DEPENDENT TERMINATION AND PROPAGATION ON THE KINETICS OF RADICAL POLYMERISATION

▲

by

Gregory Brian Smith

First Submitted June 2007

Final Version January 2008

▼

A thesis submitted in partial fulfilment of the requirements for the Degree of

Doctor of Philosophy in Chemistry

The Difficult is that which can be done immediately; the Impossible that which takes a little longer. – George Santayana (1863–1952)

Nature laughs at the difficulties of integration. – Pierre-Simon Laplace (1749–1827)

Acknowledgements

Firstly, I gratefully acknowledge the contributions of my supervisor, Greg Russell. His temperate guidance through the thickets of research and his unwavering confidence in my abilities has been invaluable to the completion of my Ph.D. The support and patience of my parents, Jan and Alister, has likewise played a vital role. Thanks to Robert Maclagan, who first cultivated my interest in Chemistry.

I thank many office-mates over the years for companionship and scintillating conversations: Mark Rees, Chris Ferguson, Kim van Berkel, Jung Hye Choi, Uma Adash, Darby Brooke, Mary Gower, Briar Schwalger-Smith, Bryce Jackson and Omar El-Hadad.

The Chemistry Department at the University of Canterbury is acknowledged for a Teaching Assistantship and opportunities for personal growth and paid employment in undergraduate teaching laboratories.

Table of Contents

List of Figures

List of Tables

Abstract

Radical polymerisation (RP) has for many years been an industrially important process, and the kinetics of the process remains an active area of research. As polymerisation proceeds, converting monomer (small molecules) into polymer (long chain molecules), chemical species of a variety of chain lengths are produced. Recent work has pointed toward the fact that rate coefficients for polymerisation reactions (specifically, termination and propagation) are often dependent on the chain-length of the reacting species. The focus of this thesis is to study the effects of chain-length-dependent reactions on the kinetics of RP, by using computer-based modeling and comparing the results of such modeling with experimental data. This enables the understanding of otherwise inexplicable trends and the building of more mechanistically detailed and accurate models for RP kinetics.

In Chapter 2, a new model for termination is developed, connecting observations and analyses of termination kinetics at short chain lengths (particularly small molecule studies) with other observations and analyses at long chain lengths (conventional RP kinetics studies) in order to construct a model for termination that is shown to be capable of coherently describing termination kinetics at any chain length. In Chapter 3, this new model for termination is tested at short chain lengths on polymerisations with large quantities of added chain transfer agent. With the inclusion of chain-length-dependent propagation in the model, the model for termination is validated. Chapter 4 is aimed at extending an existing reduced-variable, compact, 'universal' description of steady-state RP kinetics by incorporating all known chain-length dependent reactivities. This both increases computational efficiency over other approaches and provides easily evaluated, approximate analytical expressions for RP kinetics. This foundational theory is applied in Chapter 5 to reach a deeper understanding of the behaviour of the model, and show how experimental data may readily be analysed to

extract information about chain-length-dependent termination kinetics. In Chapter 6, the effect of chain-length dependent reactivities on the important technique of single-pulse pulsed-laser polymerisation is investigated, and this technique is validated as the best experimental method for investigation of termination kinetics.

In general, a central result of this thesis is that chain-length-dependent reactivities, when acknowledged and properly incorporated into models, can explain many phenomena in RP kinetics which otherwise seem difficult to account for. No exceptions to this principle have been found.

List of Published Papers Associated with Thesis Work

Chapter 2: Smith, G. B.; Russell, G. T.; Heuts, J. P. A. *Macromol. Theory Simul.* **2003**, *12*, 299-314.

Chapter 3: Smith, G. B.; Russell, G. T.; Yin, M.; Heuts, J. P. A. *Eur. Polym. J.* **2005**, *41*, 225.

Smith, G. B.; Heuts, J. P. A.; Russell, G. T. *Macromol. Symp.* **2005**, *226*, 133-146.

Heuts, J. P. A.; Russell, G. T.; Smith, G. B.; van Herk, A. M. *Macromol. Symp.* **2007**, *248*, 12-22.

Chapter 5: Smith, G. B.; Russell, G. T. *Macromol. Symp.* **2007**, *248*, 1-11.

Chapter 6: Smith, G. B.; Russell, G. T. *Z. Phys. Chem.* **2005**, *219*, 295-323.

Chapter 7: Heuts, J. P. A.; Russell, G. T.; Smith, G. B. *Aust. J. Chem.* **2007**, *60*, 754-764.

Chapter 8: Tanaka, K.; Yamada, B.; Fellows, C. M.; Gilbert, R. G.; Davis, T. P.; Yee, L. H.; Smith, G. B.; Rees, M. T. L.; Russell, G. T. *J. Polym. Sci., Polym. Chem. Ed.* **2001**, *39*, 3902-3915.

1 Introduction

1.1 Preamble

Worldwide polymer production now comfortably exceeds 100 million tons per annum, approximately half of which is by radical polymerisation (RP). One would expect therefore that the kinetics of RP are intimately understood. While the basic mechanisms have been known since the 1930s, detailed knowledge, of the sort that would allow prediction of the characteristics of novel polymerisation reactions, remains elusive. One may speculate as to the reasons for this. One possibility is simply that detailed knowledge is not really required. Another is that polymer science is a field in which technological development has generally come first, leaving behind unanswered scientific questions to be addressed at a later date. A third explanation is that the traditional framework does a reasonable job. Each of these suggestions will now be discussed in more detail.

To what extent is detailed knowledge required? After all, the history of polymer science contains many examples (see below) of materials that were discovered by accident. While there is no denying this, it is equally true that serendipity can only take one so far, and further, that it is no basis for progress. Not only does detailed knowledge provide a more sound basis for progress, but it is essential both for optimisation and control of processes. This is perhaps the main reason that development of materials in the modern age can progress much faster than in earlier times. Control of processes involves variables such as the production rate and material properties. Sophisticated programs are used to control industrial reactors. This obviously requires some level of knowledge of polymer composition, structure, reactions and kinetics. Once control is achieved, optimisation of the process can be performed on the basis of economics, safety and convenience, and material properties. Economics may involve factors such as which of several chemically similar starting materials

is cheaper. Most obviously and most importantly it also involves the fact that time is money, so the more product one can make in a given time, the more money can be earned. When safety is an issue, for example when heat is evolved in polymerisation reactions, there is a trade-off between production rate and reactor temperature. Material properties such as transparency and tensile strength may be optimised. We have seen that while detailed knowledge is not absolutely required, it is a superior approach to blind trial and error.

In general with reference to the second point raised above, in materials science an empirical, trial-and-error approach to discovery of novel materials for applications yields good results. The role of accidental, fortuitous discovery ("serendipity") is often underestimated.[1] Some examples of serendipitous discoveries in the field of polymer science will now be considered.[1]

Probably the best known example of serendipity in polymer science is the first, that of vulcanization of natural rubber by Charles Goodyear.[1] Natural rubber was discovered in South America and introduced to Europe in the early 16th century. However, it was of limited use because its elastic properties are restricted to a narrow range of temperatures (at low temperature it is glassy, at high temperature it melts). In 1844 Charles Goodyear applied for a patent for the process of vulcanisation, which eventually revolutionised the rubber industry. What he had discovered purely by accident is that heating a mixture of natural rubber and sulphur led to a product with improved resistance to temperature changes. We now know that Goodyear's process linked the linear natural rubber molecules together, which formed a 3-dimensional network. It is noteworthy that this was done in ignorance of the structure of rubber and the mechanism of vulcanisation.

Even more relevant to RP was the discovery of polyethylene. The initial discovery was made in 1933 by workers at the Alkali Division of I.C.I. directed by Perrin and Swallow,[1] as part of

an investigation of the effect on various chemical reactions of very high pressures. Efforts to intentionally produce the polymer in 1935 succeeded due to a fortuitous accident: a leaky joint caused the introduction of the right amount of oxygen to catalyse the radical polymerisation. Control of the polymerisation process was achieved by a lengthy process of trial and error, since the mechanism was totally unknown: it was not even appreciated that radicals were involved! Even at this stage the success of the product was not assured as it was expensive to produce in large quantities. With the advent of World War II, polyethylene found immediate application as an insulator for cabling used in radar equipment. After the war, development focused on films and moulds, and the volume of production rapidly increased.

The story of the development of Teflon (polytetrafluoroethylene) closely resembles that of polyethylene. The discovery in 1938 by Roy Plunkett[1] occurred as part of research into non-toxic refrigerants. Gaseous tetrafluoroethylene was stored in a sealed tank, but when the valve was opened no gas emerged. Since the weight of the tank suggested that the gas could not have escaped, further investigation was undertaken by sawing open the tank. It was thereby discovered that the gas had polymerised, forming a waxy white powder. This was an accidental discovery because it was not appreciated that the chemical structure of the monomer ensured that it was susceptible to polymerisation. The product was highly inert: unaffected by acids, bases, heat or solvents, and also formed a low friction surface. The refrigerant research program eventually led to development of chlorofluorocarbons (CFCs) which were later implicated in damage to the ozone layer. However, the impact of Teflon has been far more positive. Like polyethylene, Teflon was initially used in war materials, this time in the atomic bomb program, compounded into gaskets and valves resistant to the corrosive gas uranium hexafluoride. After the war, development of non-stick cooking surfaces based on Teflon was rather slow due to expense and difficulties with bonding the

non-stick material to metal surfaces. However, it has also found use in medical applications, where its inert nature is again useful: it is not rejected by the human body, so it is often used to coat artificial valves and joints.

For the present thesis a highly pertinent example is that commercial production of polystyrene by RP began in the late 1920s, a full 8 years before it was realised that radicals were even involved in this process![2]

What do we learn from this? From the above historical considerations, we can conclude that discovery and development of polymers is certainly *possible* in the absence of detailed knowledge of structures and mechanisms, but it should not be forgotten that further advances may depend on the acquisition of such knowledge. Before addressing the third explanation above, that the traditional framework does a reasonable job, we must examine the traditional framework itself. This is done in the following two sections.

1.2 Radical Polymerisation Reactions

The fundamental processes in radical polymerisation are initiation (generation of the initial source of free radicals), propagation (stepwise growth of the polymer chain by addition of monomer molecules) and termination (removal of free radicals to form stable products).[3] These processes are fundamental in that they encapsulate the 'life cycle' of radicals, so that the processes must be present in some form in all radical polymerisations. However, whether they are intended to occur or not, additional reactions such as chain transfer (transfer of the active radical to a different molecular species) may also be important in some systems.[3] These reactions will now be discussed in turn in more detail.

Initiation

Generation of the initial source of free radicals may be achieved by a variety of means. Broadly speaking, these may be divided into continuous and pulsed initiation.[3] Continuous initiation is typically achieved by decomposition of a thermally labile compound, producing two radical fragments. In pulsed initiation, the stimulus for initiation is radiation, which can be readily modulated and even switched on and off, if for example a laser is used. The control over the experiment afforded by this can be a powerful investigative tool, as will be seen in later chapters of this thesis.

A commonly used thermal initiator is AIBN (azobisisobutyronitrile). Since the molecule is symmetrical (as are many thermal initiators) decomposition produces two identical radical fragments.

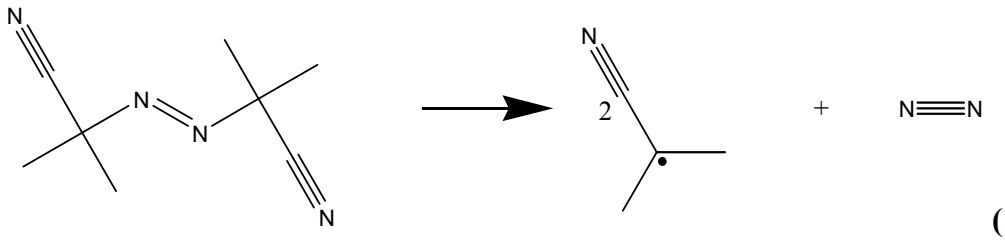

(1.1)

Since there are many possible fates for the radical fragments, initiation is considered incomplete until they add to monomer. The fraction of initiator-derived ('primary') radicals that add to monomer is termed the initiator efficiency (denoted *f*) and is dependent on (at least) temperature and degree of conversion of monomer into polymer.

A general scheme for continuous initiation is given by eqs. **(1.2)**, where I is the initiator, R_0 is the initiator fragment, M monomer, R_1 is a radical of chain length 1, k_d is the initiator decomposition rate coefficient and k_i is the rate coefficient for the first propagation step (see later). The total rate of initiation is given by $R_{init} = 2fk_d[I]$.

$$I \xrightarrow{k_d} 2R_0 \qquad \textbf{(1.2a)}$$

$$R_0 + M \xrightarrow{k_i} R_1 \qquad \textbf{(1.2b)}$$

In contrast to thermal initiators, many commonly used photoinitiators are nonsymmetric molecules. This can complicate the kinetics of initiation, particularly if the primary radicals have significantly different reactivities toward monomer. An example of such a nonideal photoinitiator is 2,2-dimethoxy-2-phenylacetophenone (DMPA).[4] Ideally, both free-radical species from photoinitiator decomposition will readily add to monomer. α-Methyl-4-(methylmercapto)-α-morpholinopropiophenone (MMMP) meets this requirement (eq. **(1.3)**). Also, MMMP is readily soluble in most common monomers.

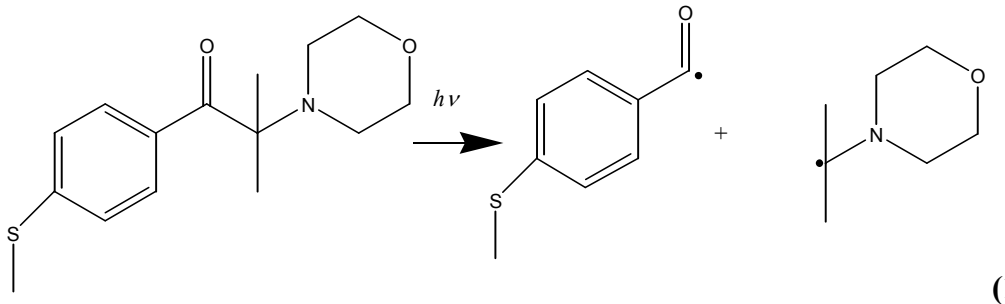

(1.3)

In general, the photoinitator-derived radicals will react with monomer as per eq. **(1.2b)**. Typically a photoinitiation event is characterised by the concentration of radicals of chain length 1 added by the laser pulse, and this quantity is denoted by ρ.

Propagation

A wide variety of monomers are used in RP to produce polymer with desirable properties. The structural feature common to all RP monomers is the carbon-carbon double bond. The propagation reaction involves a radical centre attacking the double bond, shifting the radical centre and adding the monomer molecule to the growing polymer molecule. The number of

monomer molecules incorporated is termed the chain length of the polymer molecule. This process is exemplified by the propagation of methyl methacrylate as depicted in eq. **(1.4)**.

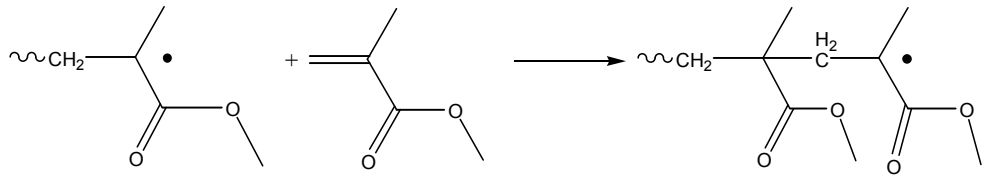

(1.4)

Although polymerisation of monomer molecules with higher degrees of substitution are known, most monomers are mono- or di-substituted olefins. One example of the former, polytetrafluoroethylene (Teflon), has been mentioned. Radical attack usually occurs at the unsubstituted end of the carbon-carbon double bond for both steric and electronic reasons.

$$R_i + M \xrightarrow{k_p^{\,i}} R_{i+1} \qquad \textbf{(1.5)}$$

The rate coefficient for propagation, k_p, depends on chain length for the first few propagation steps: k_p for radicals of chain length one may be about ten times higher than k_p for radicals of chain length 10, at which point the value converges to a 'long-chain' value. This will be discussed further in a later section of this chapter. A general scheme for propagation is therefore given by eq. **(1.5)**, where R_i is a radical of chain length i, and $k_p^{\,i}$ is their propagation rate coefficient.

Termination

Termination reactions involve loss of free radicals, forming 'dead' polymer chains. The two mechanisms operative in RP are distinguished by their products: in disproportionation (eq. **(1.6)**) hydrogen atom abstraction by one of the radicals leads to formation of two dead polymer chains, whereas in combination (eq. **(1.7)**) the two reacting radicals bond to form a single dead polymer chain.

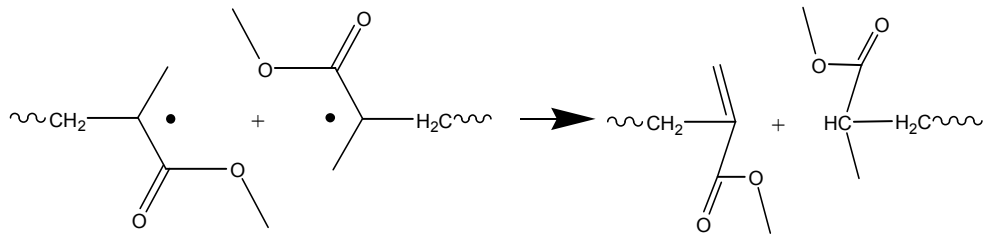

(1.6)

The products of the disproportionation reaction are chemically distinct. In particular, one of the dead polymer chains is unsaturated, which implies that it can undergo further propagation. When this occurs it is termed 'terminal double bond polymerisation'.

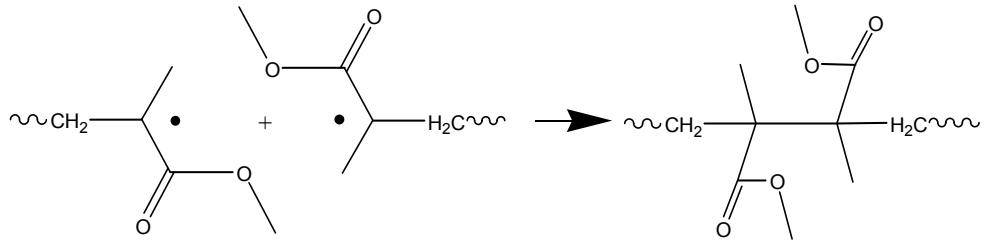

(1.7)

The fraction of termination events that occur by disproportionation is denoted by λ. This value is close to 1 for polymers with sterically hindered end-groups, such as poly(methyl methacrylate) (pMMA), and close to 0 for less sterically hindered polymers such as polystyrene. Rate constants for termination reactions are usually so high that it can be assumed that the reaction has near zero activation energy, and is thus diffusion controlled. Consequently, termination is chain-length dependent (and this has further consequences that will be examined in a later section). In general therefore, the termination reaction is described by eq. **(1.8)**, where $k_t^{i,j}$ is the rate coefficient for termination of radicals with chain lengths i and j, and D_i is 'dead' polymer of chain length i. The fraction of products due to disproportionation ($D_i + D_j$) is given by λ as indicated above. This value is assumed to be chain-length independent, although in principle a chain-length-dependent λ value could be simply incorporated into a model for FRP kinetics.

$$R_i + R_j \xrightarrow{k_t^{i,j}} D_i + D_j \text{ (or) } D_{i+j} \qquad \textbf{(1.8)}$$

Chain Transfer

Chain transfer reactions are so-called because they transfer the radical activity from one chemical species to another. Since the number of radicals in the system is unaffected by these reactions, they are akin to the propagation reaction, however the chain length of the growing radical is usually reduced rather than increased. This feature of chain transfer reactions can be used to control the chain length of the polymer: in such cases a chain transfer agent such as dodecanethiol is used. (eq. **(1.9)**)

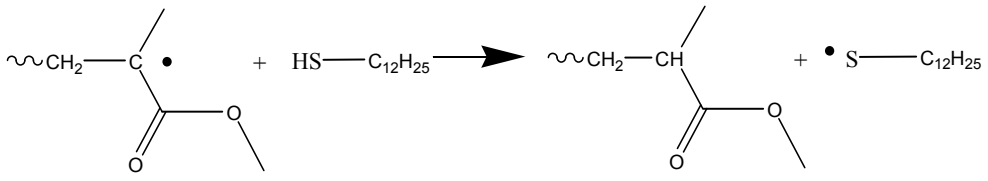

(1.9)

However, chain transfer often occurs without the specific addition of a chain transfer agent: chain transfer to monomer is shown for MMA[3] in eq. **(1.10)**. Chain transfer to polymer or initiator can also occur.

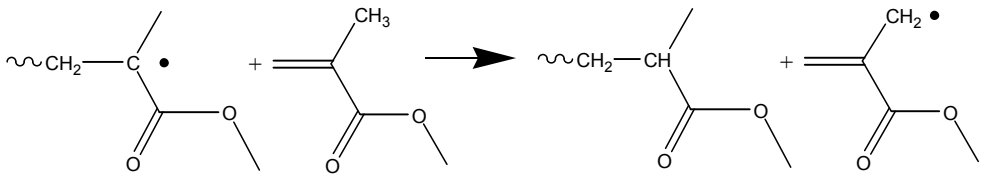

(1.10)

Chain transfer to polymer (eq. **(1.11)**) is an important process in some polymerisation systems, some of which represent an extremely significant fraction of industrial polymer production (for example ethylene polymerisation). If transfer to polymer is intramolecular, short branches are formed, while intermolecular transfer tends to form long branches. Since branching is rather complicated kinetically,[5,6] for simplicity it is not considered in the work of

this thesis, since the focus here is on understanding the kinetically fundamental polymerisation processes (*viz.* initiation, propagation and termination) in the absence of complicating factors as far as possible. However, it should be noted that if modelling of a polymerisation system in which chain transfer to polymer occurs to a signifcant extent were to be undertaken, branching should be incorporated into the model.

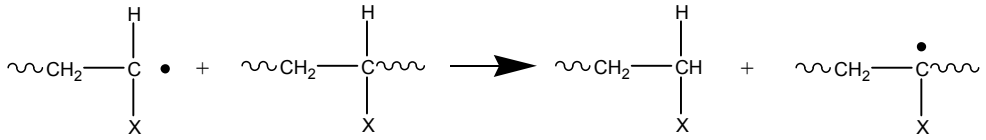

(1.11)

The following general reactions, given in eqs. **(1.12)** and **(1.13)**, for chain transfer suffice to describe the process for the purposes of this thesis. Reinitiation of the transfer-derived radical may proceed with a different rate coefficient ($k_{p,X}$) than other radicals.

$$R_i + X \xrightarrow{k_{tr,X}^{i}} D_i + X^{\bullet} \qquad \textbf{(1.12)}$$

$$X^{\bullet} + M \xrightarrow{k_{p,X}} R_1 \qquad \textbf{(1.13)}$$

1.3 Classical Kinetics

The standard scheme for analysis of RP data is referred to as classical (free) radical polymerisation kinetics. The most notable assumption in this scheme is that rate constants are assumed to be independent of chain length, *i*. There are several reasons for doing this. It greatly simplifies the mathematical complexity of the equations, and so simplifies analysis of data. Chain length dependence of kinetic parameters being incompletely understood, it is simple in another sense (in the absence of more detailed knowledge) to assume that there is no dependence. The occurrence of branching reactions is also ignored for similar reasons.

Initially, the scope of any theory of RP kinetics concerns the most basic and easily measured parameters of the process – the rate of conversion of monomer into polymer, and the molecular weight distribution (MWD) of the resulting polymer. These quantities are derived from a reaction scheme. Given the above, it is clear that the reaction scheme for classical RP kinetics comprises eqs. (**1.2**), **(1.5)**, **(1.8)** and **(1.12)**, with all notations of chain-length dependent rate coefficients expunged. In particular, $k_t^{i,j}$ becomes simply k_t. This results in the following expression for the rate of change of the total radical concentration, $[R] = \sum_{j=1}^{\infty} [R_j]$:

$$\frac{d[R]}{dt} = R_{init} - 2\, k_t\, [R]^2 \qquad \textbf{(1.14)}$$

In steady state, this gives

$$[R] = \left(\frac{R_{init}}{2k_t}\right)^{0.5} \qquad \textbf{(1.15)}$$

This result may be used to derive the rate law for polymerisation:

$$R_{pol} = -\frac{d[M]}{dt} = k_p\, [M]\, [R] = k_p\, [M] \left(\frac{R_{init}}{2k_t}\right)^{0.5} \qquad \textbf{(1.16)}$$

Introducing a new variable x, the fractional conversion of monomer into polymer, such that $[M] = [M]_{t=0}(1\text{-}x)$, leads to

$$\frac{d}{dt}(-\ln(1\text{-}x)) = k_p \left(\frac{R_{init}}{2k_t}\right)^{0.5} \qquad \textbf{(1.17)}$$

It is tempting to integrate this equation to obtain an expression for conversion in terms of time, however this is problematic as rate coefficients are conversion dependent. Analysis of rate data is most properly done by using eq. **(1.17)** to equate the slope of a plot of $-\ln(1\text{-}x)$ *vs.*

time with the appropriate ratio of rate coefficients. Of course, this should be done only for a range of conversion where the data indicates that this slope is constant. Perhaps surprisingly, most workers are lazy in this regard, and instead they either simply take the slope of a plot of [M] *vs.* t – even though eq. **(1.16)** shows that this value should never be constant – or else they take the slope of $-\ln(1-x)$ *vs.* t over a very large range of conversion. The perfectly avoidable error introduced by the former approach has recently been discussed elsewhere.[7]

Of more relevance for this thesis is that eq. **(1.16)** suggests that for a range of experiments, all else being equal, one should find that R_{pol} is proportional to $[M]^{1.0}$ and to $[I]^{0.5}$ (recall that $R_{init} = 2fk_d[I]$). Over the decades many experiments of this type have been carried out, for example[8] with bulk MMA monomer and varying amounts of AIBN initiator, and also with styrene monomer and varying amounts of ethyl benzene (this solvent in particular was chosen to effect the variation of monomer concentration while maintaining solution properties similar to those of styrene).

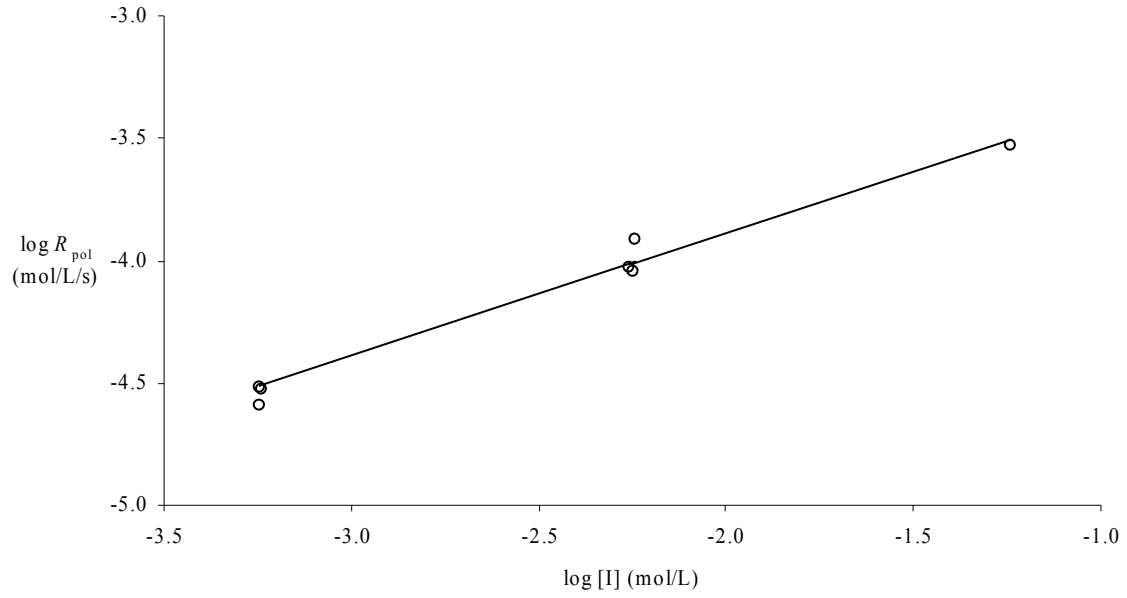

Fig. 1.1 Log Rate of polymerisation of bulk MMA at 50 °C *vs.* log concentration of AIBN initiator (points) and best fit line with a slope of 0.5.[8]

As is evident from *Fig. 1.1* and *Fig. 1.2*, this rate data is adequately described by the classical kinetics model. Evidently if classical kinetics is incorrect, data of this sort is not sensitive enough to demonstrate such a fact.

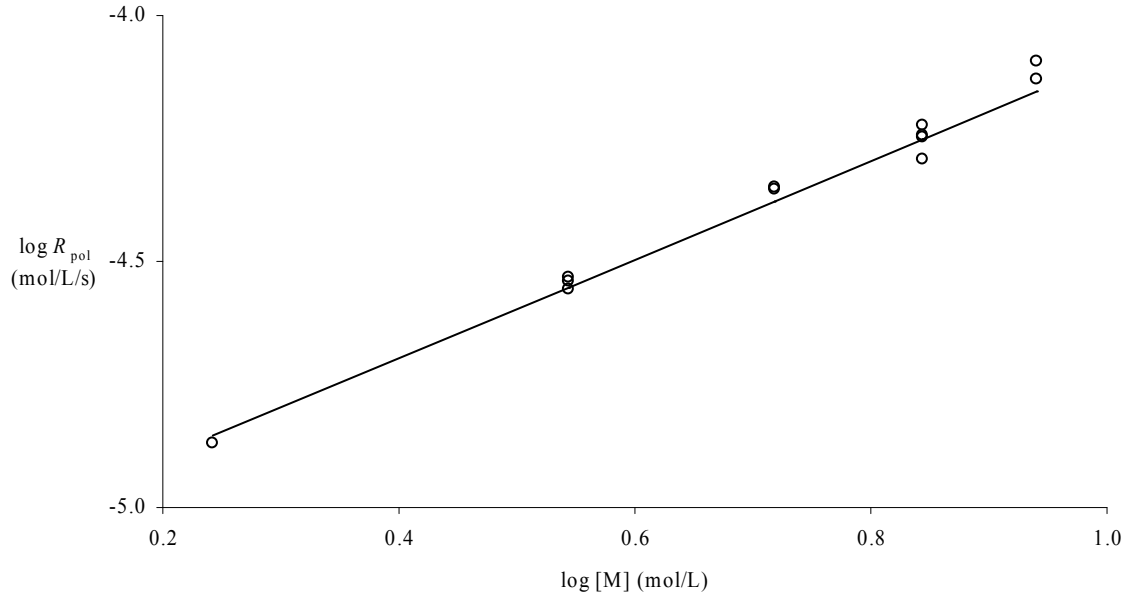

Fig. 1.2 Log Rate of polymerisation of styrene at 50 °C *vs.* log concentration of monomer (points) and best fit line with a slope of 1.0.[8]

Molecular weight distributions

Classical kinetics also predicts molecular weight distributions. Recall that the three reactions producing dead polymer are termination by disproportionation, termination by combination, and chain transfer. The instantaneous molecular weight distribution is therefore given by

$$\frac{d[D_i]}{dt} = k_{tr,X}\,[X]\,[R_i] + 2\lambda\, k_t\,[R_i]\,[R] + (1-\lambda)\, k_t \sum_{j=1}^{i-1} [R_j]\,[R_{i-j}]\,,\ i = 1, \infty \qquad \textbf{(1.18)}$$

As stated, eq. **(1.18)** requires knowledge of the radical chain length distribution (RCLD), $[R_i]$, for all chain lengths i. This is determined from eq. **(1.19)** in the steady state:

$$\frac{d[R_i]}{dt} = k_p [M] [R_{i-1}] - k_p [M] [R_i] - k_{tr,X} [X] [R_i] - 2k_t [R_i] [R] , \; i = 2, \infty \quad \textbf{(1.19)}$$

$$S = \frac{[R_i]}{[R_{i-1}]} = \frac{k_p [M]}{k_p [M] + k_{tr,X} [X] + 2k_t [R]} \quad \textbf{(1.20)}$$

Eq. **(1.20)** shows that S, the probability of radical propagation,[9] is a constant value independent of chain length. The RCLD is therefore given by eq. **(1.21)**:

$$[R_i] = [R_1] S^{i-1} = [R] (1 - S) S^{i-1} \quad \textbf{(1.21)}$$

Substituting eq. **(1.21)** into eq. **(1.18)**, one finds that

$$\frac{d[D_i]}{dt} = (k_{tr,X} [X] + 2\lambda k_t [R])[R](1 - S)S^{i-1} + (1-\lambda) k_t [R]^2(1 - S)^2(i-1)S^{i-2} \quad \textbf{(1.22)}$$

Daunting as eq. **(1.22)** may seem, it is possible to simplify it by defining the parameter F_n:

$$F_n = \frac{k_{tr,X} [X] + 2\lambda k_t [R]}{k_{tr,X} [X] + 2\lambda k_t [R] + (1-\lambda) k_t [R]} = \frac{k_{tr,X} [X] + 2\lambda k_t [R]}{k_{tr,X} [X] + (1+\lambda) k_t [R]} \quad \textbf{(1.23)}$$

The value of F_n must be between 0 and 1: for $F_n = 1$, the transfer and disproportionation terms on the left of eq. **(1.22)** dominate, whereas for $F_n = 0$ the combination term on the right of eq. **(1.22)** dominates. Specifically, F_n is the number fraction of chains formed by disproportionation and transfer. Eq. **(1.22)** now becomes

$$\frac{d[D_i]}{dt} \sim n(i) = F_n \frac{1-S}{S} S^i + (1-F_n) \left(\frac{1-S}{S}\right)^2 (i-1) S^i \quad \textbf{(1.24)}$$

As has been made clear here, $d[D_i]/dt$ is equivalent to the number distribution of chains, $n(i)$, for obvious reasons. Furthermore, eq. (**1.24**) is normalized. More familiar is the long-chain limit[9] of eq. (**1.24**):

$$n(i) = F_n \left(\frac{1}{v}\right)\exp\left(\frac{-i}{v}\right) + (1-F_n)\left(\frac{1}{v}\right)\left(\frac{i}{v}\right)\exp\left(\frac{-i}{v}\right) \qquad \textbf{(1.25)}$$

This equation is also normalized. The parameter v here is:

$$v = \frac{k_p\,[M]}{k_{tr,X}\,[X] + 2k_t\,[R]} = \frac{S}{1-S} \text{ or } S = \frac{1}{1+v^{-1}} \qquad \textbf{(1.26)}$$

Sometimes v is called the 'kinetic chain length', but this term is perhaps best avoided as there is some confusion over its precise meaning (others argue[9] that it should refer to the entire lifetime of a radical over all cycles of growth and transfer). Eq. **(1.25)** follows from eq. (**1.24**) using well-known series expansions for $1/(1+ v^{-1})$ and $\exp(-v^{-1})$. The historical motivation for deriving eq. **(1.25)** was the difficulty of evaluating the power terms in eq. (**1.24**). It is noted that this difficulty no longer exists – each equation is trivially evaluated using modern computer hardware in conjunction with spreadsheet software, and so there is no good reason to use the (ever so slightly) less accurate eq. **(1.25)**. Rather, what this form offers is more immediate appreciation of the nature of the MWD. This is that the parameter S (or, equivalently, v) dictates the *position* of the MWD while F_n (or, equivalently, F_w, see below) dictates the *shape*. This will be illustrated shortly. Implicit in this is that the whole MWD condenses down to two parameters only, even though there are many more kinetic parameters that go into the model. This is an important principle to understand, as it is recurrent throughout this thesis: the number of independent parameters in fitting RP data is usually much fewer than the total number of model kinetic parameters.

The most common form of MWD is not the number-MWD derived above (so-called because the distribution specifies the relative *number* of polymer chains of each chain length that are present), but rather is that delivered by size exclusion chromatography, the so-called SEC-MWD. If the number distribution is denoted $n(i)$, then the weight distribution (so-called because the distribution specifies the relative *weight* of polymer chains of each chain length that are present) is given by $w(i) \sim i\, n(i)$. Finally, the SEC-MWD is given by $w(\log_{10} i) = i\, w(i) \ln 10$, where the factor of ln10 is simply to preserve normalisation.

Rather than dealing with distributions, it is often convenient to characterise the MWD by an average chain length. This can be done in several ways, but the most frequently encountered are the number-average chain length $\overline{DP}_n$, and the weight-average chain length $\overline{DP}_w$. These are defined in terms of moments of their respective distributions:

$$\overline{DP}_n = \frac{\sum_{i=1}^{\infty} i\, n(i)}{\sum_{i=1}^{\infty} n(i)} \text{ and } \overline{DP}_w = \frac{\sum_{i=1}^{\infty} i\, w(i)}{\sum_{i=1}^{\infty} w(i)} = \frac{\sum_{i=1}^{\infty} i^2\, n(i)}{\sum_{i=1}^{\infty} i\, n(i)} \qquad \textbf{(1.27)}$$

From these two average chain lengths, the polydispersity index, PDI = $\overline{DP}_w/\overline{DP}_n$, is defined. A MWD with PDI = 1 is termed monodisperse, meaning that all polymer chains present are exactly the same chain length. Increasing PDI indicates an increasingly broad MWD. Characterising MWDs in this way may be seen as another approach to the observation noted above, that the MWD can be characterised by two parameters. This however is a purely statistical (as opposed to mechanistic) approach, with $\overline{DP}_n$ taking the place of S in indicating the position of the MWD, and PDI taking the place of F_n in indicating the shape of the MWD.

Returning to molecular weight distributions, after a little algebra it may be shown that eq. **(1.25)** leads to the following equation for the weight distribution:

$$w(i) = F_w \left(\frac{i}{\nu}\right)\exp\left(\frac{-i}{\nu}\right) + 0.5(1-F_w)\left(\frac{i}{\nu}\right)^2 \exp\left(\frac{-i}{\nu}\right) \qquad \textbf{(1.28)}$$

The only new term here is F_w, which replaces F_n:

$$F_w = \frac{F_n}{2-F_n} \qquad \textbf{(1.29)}$$

F_w is the weight fraction of chains formed by transfer and disproportionation, a number that is different to F_n because combination produces fewer chains than disproportionation but produces the same weight of chains. From eq. (**1.24**) it trivially follows that

$$w(\log_{10} i) \sim F_n \frac{1-S}{S} i^2 S^i + (1-F_n)\left(\frac{1-S}{S}\right)^2 (i-1)\, i^2\, S^i \qquad \textbf{(1.30)}$$

Four evaluations of this equation are given in *Fig. 1.3*. It is evident from the figure that variation of S affects only the position of the distribution on the chain length axis. At the same time, variation of F_n affects the position slightly (since combination forms longer chains than disproportionation or transfer), but more importantly, only variation of F_n affects the shape of the distribution.

Related to the issue of shape is that in classical kinetics the polydispersity index (PDI) must lie between 2 ($F_n = 1$; maximum broadness) and 1.5 ($F_n = 0$; minimum broadness). A feature of this thesis will be that chain-length-dependent reactivities significantly change this situation. Most significantly, chain-length-dependent termination (CLDT) always acts to *broaden* the MWD. For example, chain-length-dependent combination gives a MWD with a shape much like that from chain-length-independent disproportionation. When chain lengths

are relatively small, chain-length-dependent propagation can have a marked effect on broadness, making the MWD narrower. On top of these two effects is that of instrumental broadening due to SEC. This last effect will not be investigated in this thesis but it is noted that it may be accounted for using a 'reverse engineering' approach.[10,11]

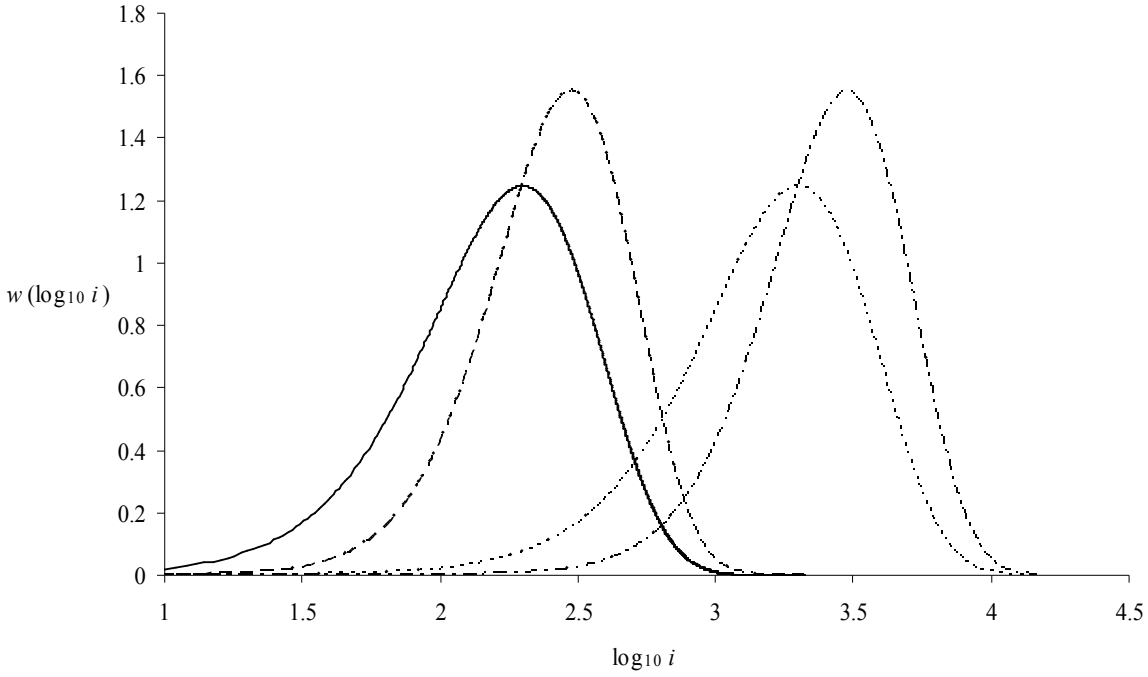

Fig. 1.3 Plots of $w(\log_{10} i)$ *vs.* $\log_{10} i$. Parameters used in eq. **(1.30)** were as follows. Solid line: $S = 0.99$, $F_n = 1$; Long dashed line: $S = 0.99$, $F_n = 0$; Short dashed line: $S = 0.999$, $F_n = 1$; Alternating short and long dashed line: $S = 0.999$, $F_n = 0$.

What the above discussion makes clear is the difficulty of extracting unambiguous kinetic information from a MWD, because the apparent broadness of a MWD is determined by all of SEC broadening, the extent of chain-length-dependent reactivities, and the natural balance between combination, disproportionation and transfer. There is much room here for false interpretation, and indeed many workers have erred in this regard, attributing broadening

effects to certain causes without considering alternatives. In order to avoid this problem as far as possible, it is recommended that rate and MWD data be used as a global data set for modeling: an approach that will be used in this thesis. This is because different causes of MWD broadening will have different effects on rate data.

Another important lesson to take from this section in going forward is that of the approach for understanding kinetics. Broadly speaking one may proceed either by using differential equations or probabilities. Of course the two approaches are equivalent, as has been mentioned here. Many people prefer the probability approach, as championed by the Olaj school.[12-15] In general this thesis will take the alternative route of differential equations, although at many points it will be seen that the probability approach gives the same results, as it always must. The advantage of the differential equation approach is that it is in fact most fundamentally related to kinetics, which of course defines rate coefficients in terms of differential equations for the concentrations of the relevant chemical species. Further, as more chain-length-dependent reactivities are introduced, the correctness of the results given by the probability approach become less-and-less self-evident. In contrast, derivations using differential equations do not become any harder conceptually, it is merely a matter of checking that all relevant gain and loss terms have been distinctly included in the equations.

1.4 Chain-length Dependent Reactions

Chain-length Dependent Termination

It has long been recognised that termination in RP is chain-length dependent, however at the same time investigation of the consequences of this fact has been limited. The effect known variously as the Trommsdorff[16]-Norrish[17] or gel effect, or autoacceleration, which was noted in the 1940s, was the first suggestion of the reality of chain-length dependent termination (CLDT). The effect is that at intermediate conversion of monomer into polymer, the rate of

many radical polymerisations increases, sometimes rather suddenly and dramatically.[3] Consideration of eq. **(1.16)** indicates that this effect is most reasonably explained by decreasing k_t, which could be caused by an increasing concentration of dead polymer chains raising the viscosity of the solution and slowing diffusion of terminating polymer radicals. It should be clear that this argument depends on k_t being diffusion controlled, rather than being activation controlled as most chemical reactions are. This is certainly plausible due to the high values of k_t (sometimes exceeding 10^8 L mol^{-1} s^{-1})[3,18] found for many polymerisation systems. CLDT is then an obvious further consequence of termination being diffusion controlled: diffusion of short polymeric radical chains is certain to be more rapid than diffusion of more massive and more entangled long chains. Pioneering investigations of CLDT were carried out in the 1960s.[19,20] However, progress was slow for many decades. While the reality of CLDT is strongly supported by the observation of the Trommsdorff effect, the evidence is indirect, and independent confirmation of the various effects leading to lowering of k_t was slow to come. In particular, a detailed mechanistic account of the diffusion process(es) that produce the Trommsdorff effect remains elusive.[21]

In recent years, however, the situation has changed. Direct evidence for the relationship between CLDT and diffusion has accumulated, experimental methods have improved so that the sometimes subtle effects of CLDT in RP can be observed, and the equations derived from RP kinetics models which include CLDT, historically considered intractable, have yielded some of their secrets due to the advent of modern computers. Regarding direct evidence, it has been shown that k_t varies with solution viscosity[22,23] and pressure[24,25] in a manner consistent with termination being diffusion controlled. Further, termination of small molecule radicals is well described by the Smoluchowski equation,[26] which strongly suggests that termination of slowly diffusing polymeric radicals must likewise be diffusion controlled. Also, diffusion has been shown to be chain-length dependent for long chains[27-30] and for short

chains.[31-33] Regarding experimental methods, perhaps the most important advance was the introduction of pulsed-laser initiated polymerisation (PLP), which can be used to investigate the kinetics of propagation[34,35] or termination[7] in isolation, in contrast to the situation with continuous initiation where only a ratio of rate coefficients can be determined (see eq. **(1.17)**). Incremental improvements in existing methods have also been made, for instance in SEC measurements.

Given that CLDT is a real phenomenon, the obvious next question is how to model it, that is, how does the chain-length dependent rate coefficient for termination, $k_t^{i,j}$, depend on the chain lengths i and j? The approach taken in this thesis, and in many previous investigations,[36,37] is to start with eq. **(1.31)**:

$$k_t^{i,i} = k_t^{1,1}\, i^{-e} \qquad \textbf{(1.31)}$$

In this equation, $k_t^{1,1}$ is the rate coefficient for termination between monomeric radicals, and e is an exponent which describes the degree of chain-length dependence. If e is set to zero, $k_t^{i,i}$ is independent of i and classical kinetics pertains; if instead e is greater than zero the physically realistic situation of $k_t^{i,i}$ decreasing with i is described. The power law form of eq. **(1.31)** is motivated by the observed dependence of diffusion coefficients on chain length being described by power laws.[27-33] Clearly, eq. **(1.31)** deals only with termination of two chains with identical chain lengths, or homotermination. A minimal model of CLDT must also describe cross-termination. Various models for this, which are introduced here, may be thought of as averaging functions:

$$k_t^{i,j} = k_t^{1,1}\,(ij)^{-e/2} = (k_t^{i,i}\,k_t^{j,j})^{0.5} \quad \text{(geometric mean)} \qquad \textbf{(1.32a)}$$

$$k_t^{i,j} = 0.5\,k_t^{1,1}\,(i^{-e} + j^{-e}) = 0.5(k_t^{i,i} + k_t^{j,j}) \quad \text{(diffusion mean)} \qquad \textbf{(1.32b)}$$

$$k_t^{i,j} = k_t^{1,1}\left(\frac{2ij}{i+j}\right)^{-e} \quad \text{(harmonic mean)} \qquad \textbf{(1.32c)}$$

A lot of ink can be spilled on trying to justify the employment of any of the above equations, but this will not be done here. This is because, as will be seen in this thesis, it turns out that RP kinetics are mostly only weakly dependent, if at all, on the actual cross-termination model. This is not to say that it is of no scientific interest which model is physically correct for any particular system, however this is not something of significant practical consequence. As an aside it is noted that one should logically expect eq. **(1.32b)** to hold for a diffusion-controlled process unless there is actual evidence to the contrary.

Chain-length Dependent Propagation

Similarly to chain-length-dependent termination, chain-length-dependent propagation (CLDP) has been somewhat neglected in kinetic models of RP. Perhaps this situation can be explained in part by the intuitive expectation that the observed variation of the rate coefficient for propagation, which takes place for only the first few addition steps,[38] would have an insignificant effect on the kinetics of RP systems where long polymer chains are formed. After all, while the Trommsdorff effect suggests CLDT, there is no such effect of similar magnitude that suggests CLDP, and propagation is certainly not diffusion controlled as termination is. Also, many of the points made above about the difficulties presented by investigation of CLDT also apply to CLDP. Notwithstanding this, it cannot be denied that CLDP occurs: studies of small-molecule radical kinetics,[39] studies of polymerising systems producing relatively short chain lengths,[12,40] and theoretical investigations[41] have all consistently supported this conclusion. Theory predicts an effect due to the (chemically controlled) rate coefficient for propagation having an Arrhenius frequency factor that decreases with chain length.[42] The following empirical equation is proposed to capture this behaviour, and will be used to model RP data in this thesis:

$$k_p^{\,i} = k_p^{\,\infty}\left(1 + C_1 \exp\left(\frac{-\ln(2)}{i_{½}}(i-1)\right)\right) \qquad \textbf{(1.33)}$$

In eq. **(1.33)**, $k_p^{\,\infty}$ denotes the value of $k_p^{\,i}$ pertaining to long chains, $C_1 = (k_p^{\,1} - k_p^{\,\infty})/k_p^{\,\infty}$ is the factor by which $k_p^{\,1}$ exceeds $k_p^{\,\infty}$, and $i_{½}$ dictates the magnitude of CLDP: the larger the value of $i_{½}$, the longer the chain length i at which the situation of $k_p^{\,i}$ significantly greater than $k_p^{\,\infty}$ persists.

1.5 Thesis Overview

To state the matter concisely, which is effectively just to integrate the work of the preceding two sections, the incorporation of chain-length-dependent termination and propagation means that the following equations are those that *properly* describe RP kinetics:

$$\frac{d[R_1]}{dt} = R_{init} + k_{tr}[X][R] - k_p^{\,1}[M][R_1] - k_{tr}[X][R_1] - f_t^{\,1}[R_1] \qquad \textbf{(1.34a)}$$

$$\frac{d[R_i]}{dt} = k_p^{\,i\text{-}1}[M][R_{i\text{-}1}] - k_p^{\,i}[M][R_i] - k_{tr}[X][R_i] - f_t^{\,i}[R_i] \quad , \quad i = 2, \infty \qquad \textbf{(1.34b)}$$

$$\frac{d[D_i]}{dt} = k_{tr}[X][R_i] + \lambda f_t^{\,i}[R_i] + (1\text{-}\lambda)\sum_{j=1}^{i\text{-}1} k_t^{\,j,i\text{-}j}[R_j][R_{i\text{-}j}] \quad , \quad i = 1, \infty \qquad \textbf{(1.34c)}$$

where the frequency of termination, $f_t^{\,i}$, is given by eq. **(1.35)**:

$$f_t^{\,i} = 2\sum_{j=1}^{\infty} k_t^{\,i,j}[R_j] \qquad \textbf{(1.35)}$$

Broadly speaking the aim of this work is to investigate the consequences of these equations, in particular the effects of CLDP and CLDT, and to compare the results with experimental data in order to build more mechanistically detailed and accurate models for RP kinetics. Of course this will not be the first work to do this, as many have previously grappled with chain-

length-dependencies in RP kinetics, especially chain-length-dependent termination. Pre-eminent in this regard is the Olaj school,[13,14,36,43-47] but of course there have been many others, *e.g.* Mahabadi,[37,48] Bamford,[49,50] de Kock *et al.*,[51,52] Moad,[53] Buback *et al.*[4,54] and Busch[4,5] (it is stressed that this is just a sample list, not a comprehensive one).

Needless to say it is impossible to investigate all aspects of the above equations, as the field is – literally! – as broad as that of RP kinetics. In general the focus in this thesis is on low conversion, bulk polymerisation systems with one type of monomer present (homopolymerisation). In chapter 2, a new model for termination is developed, building on eqs. **(1.31)** and **(1.32)**, and using eqs. **(1.34)** to simulate data. Chapter 3 seeks to apply the CLDT model developed in Chapter 2 for low-conversion, steady state polymerisation data, and also introduces CLDP (eq. **(1.33)**). The work of Chapter 4 is aimed at a reduced-variable, compact, 'universal' description of steady-state RP kinetics with CLDT. These endeavours owe a particular debt to the work of Olaj *et al.* It will be seen that it is possible to reduce computational time vastly. Chapter 5 will apply the notions of Chapter 4 to analyzing data, showing how the signature of CLDT can be elegantly and relatively simply observed in RP kinetics. Finally, in Chapter 6 there is an investigation of the impact of CLDT and CLDP on the kinetics of single-pulse pulsed-laser polymerisation experiments, which are regarded as the most potent experimental technique for investigating CLDT. A common theme in all the above is the complete confidence that all aspects of RP kinetics can be rigorously accounted for if chain-length-dependent reactivities are acknowledged and properly handled. No exceptions to this principle have been found.

While eqs. **(1.34)** underlie all of the investigations reported in this thesis, they are used in different ways. Broadly speaking there are steady state and non-steady state situations. The latter can only be handled by numerical solution of eqs. **(1.34)**. Therefore the next section

addresses this issue in general terms. Except for one particular situation (that of using the geometric mean, eq. **(1.32a)**), steady-state solutions of. eqs. **(1.34)** involve iterative solution of equations. This is outlined in general terms in Section 1.7.

1.6 Numerical Solution of Differential Equations

Mathematically speaking, eqs. **(1.34)** belong to the class of equations called Ordinary Differential Equations, since they contain derivatives with respect to one variable only (specifically, time t). Additionally, they are classed an Initial Value Problem,[55,56] with the typical initial conditions being that all radical and polymer concentrations are equal to zero at time $t = 0$.

Ideally an analytical solution would be available, however nature does not always cooperate in this regard, as is the case here: this is largely due to the fact that the equations are *coupled*, in other words the rate of change of (for instance) the concentration of radicals of chain length one ($d[R_1]/dt$) depends not only on $[R_1]$, but also depends on all other radical concentrations through the total radical concentration [R] and the termination frequency f_t^1, as can be seen by inspecting eq. **(1.34a)**. Such coupled systems of equations tend not to have analytical solutions. While analytical solutions have been obtained for certain models,[34,57,58] the specialised nature of these solutions, which usually apply only to the exact model the solution was derived for, have meant that analytical solutions have not seen wide application for solving eqs. **(1.34).**

However, the lack of an analytical solution is no impediment. Due to the historical importance of this class of equations in mathematics, science and engineering, a vast and sometimes bewildering armoury of approximate numerical methods has been assembled over many years, which have been very successful (when used appropriately) in providing accurate solutions to such problems.[56,59] A number of methods have been specifically applied

to solution of eqs. **(1.34)**, including Euler, Runge-Kutta, Gear,[53,60,61] Monte Carlo[62-65] and Galerkin[66,67] methods. Historically, the Gear method[55] has been popular, while the Galerkin method has enjoyed more recent popularity due to its employment in the simulation engine of the integrated RP kinetics modeling software package called "PREDICI" ©.[67]

A study undertaken by Rees[68] sought to evaluate various numerical methods with the specific application of pulsed-laser-initiated radical polymerisation (PLP) in mind. Because PLP is the form of RP in which radical concentrations are changing most strongly with time, one can assume that it provides the sternest and most meaningful test of numerical methods for their application in RP. Surprisingly, it was found[68] that the simple Euler method is no worse than any more complicated method: of course, more complicated methods offer the advantage of greater accuracy while using a larger *timestep* (see below),[68] but the advantage so gained was found to be no greater than the cost of greater computational time for the more complicated methods. In other words, even though one requires a smaller timestep to achieve high numerical accuracy with the simple Euler method, the fact that it is so computationally easy (see below) means that it is still competitively fast. For PLP it was found that as long as a timestep of $1/(k_p[M])$ is used, then the simple Euler method delivers results that can be regarded as exact.[68]

Given the above, this thesis only uses the simple Euler method for numerical solution of eqs. **(1.34)**. Therefore this method will now be outlined. In general, an initial-value problem is to be solved:

$$\frac{dx}{dt} = f(t,x)\,, \quad a \leq t \leq b\,, \quad x(a) = \alpha \qquad \textbf{(1.36)}$$

Using Taylor's Theorem, it is easy to show that

$$x(t+h) = x(t) + h\frac{\mathrm{d}}{\mathrm{d}t}(x(t)) + \frac{h^2}{2}\frac{\mathrm{d}^2}{\mathrm{d}t^2}(x(c)) \qquad \textbf{(1.37)}$$

where $t \leq c \leq t+h$. Euler's method consists of neglecting the final 'remainder' term in eq. **(1.37)**, and thereby obtaining a series of approximations w_n to the function $x(t)$ at time steps of h ($t_n = a + nh$, where n is a count of the number of time steps taken). One begins with the initial condition, so that $w_0 = x(a) = \alpha$, and then proceeds with eq. **(1.38)**:

$$w_{n+1} \approx x(t_n+h) = w_n + h f(t_n,w_n) \qquad \textbf{(1.38)}$$

Essentially what has been done here is to approximate a differential equation (eq. **(1.36)**) with a difference equation (eq. **(1.38)**), and approximate the unknown function $x(t)$ by making use of the known function $f(t,x)$. The *timestep*, h, is the interval between successive approximations, and determines the error associated with the approximation, as eq. **(1.37)** makes clear: the remainder term is proportional to h^2, so that the smaller the timestep, the smaller the error when the remainder term is neglected. For systems of equations, the method of solution is conceptually not much more complicated than for one equation: eq. **(1.38)** is applied for each distinct variable in turn at every timestep. For example, eq. **(1.39)** applies for all radicals with $i \geq 2$:

$$[\mathrm{R}_i](t_{n+1}) = [\mathrm{R}_i](t_n) + h\frac{\mathrm{d}[\mathrm{R}_i]}{\mathrm{d}t}(t_n) \qquad \textbf{(1.39)}$$

where $\mathrm{d}[\mathrm{R}_i]/\mathrm{d}t$ is given by eq. **(1.34b)**. Similar equations apply for all of the variables of eqs. **(1.34)**.

As part of this work, efficient numerical procedures were developed for numerical solution of. eqs. **(1.34)** for simulation of pulsed-laser polymerisation. Some details regarding these procedures are given in Chapter 8 of this thesis. It is noted that a PLP simulation was carried out using both the program of this work and PREDICI ©. For the chosen conditions,

PREDICI © was found to be far slower for the same level of accuracy. This emphasises the point above about the competitiveness of the simple Euler method. Where PREDICI © will come into its own is where chain lengths become very long, as the Galerkin method is specifically designed to reduce the number of equations to be solved in a large system of ODEs involving distributions. Of course, PREDICI is also indispensable for those not inclined to write their own code.

1.7 Iterative Solution of Equations

The steady-state solutions of eqs. **(1.34a)** and **(1.34b)** are:

$$[R_0] = \frac{R_{init} + k_{trX}[X][R]}{k_p^0[M]} \quad \textbf{(1.40a)}$$

$$[R_i] = [R_{i-1}]\frac{k_p^{i-1}[M]}{k_p^i[M] + k_{trX}[X] + f_t^i}, \; i = 1, \infty \quad \textbf{(1.40b)}$$

Note that $[R_0]$ is a notional concentration rather than the concentration of a particular real chemical species, and k_p^0 may be chosen arbitrarily as its value cancels out in evaluation of $[R_1]$. Upon some thought it can be seen that eqs. **(1.40)** lend themselves to iterative solution: given initial guesses for all $[R_i]$ (and hence also [R]), new values for all $[R_i]$ may be calculated, and this process may be repeated until there is convergence. Several immediate issues are raised here: (1) How to obtain initial guesses for all $[R_i]$? One convenient approach is just to guess [R], and then use classical kinetics in the form of eq. **(1.21)** to obtain all $[R_i]$. A more sophisticated approach is to use the geometric mean model, as will be seen in chapter 4. (2) How is 'convergence' best judged? In this work evaluation of the total radical concentration $[R] = \sum_{j=1}^{\infty}[R_j]$ is used, with iteration being carried out until [R] is accurate according to some suitable criterion.[69] (3) Equally important to evaluating these equations is

that values of $[R_i]$ must be calculated to a high enough chain length that numerical error associated with truncating the chain length distribution is suitably small.[69]

It should be pointed out that the dead-chain MWD, eq. **(1.34c)**, is not included in this iterative procedure, because it cannot be in steady-state, as it consists only of gain terms. Thus the steady-state solutions for the radical concentrations, once obtained by iterative solution, are simply used to evaluate eq. **(1.34c)**. This gives the instantaneous MWD. For steady-state this is also the cumulative MWD, as there is no change to the values eq. **(1.34c)** with time: this equation depends only on the (constant) $[R_i]$ values.

The first work that definitely solved eqs. **(1.34a)** and **(1.34b)** iteratively appeared in 1980.[70] It is possible that Benson and North, in their seminal 1962 paper,[20] did this, as they claim to have calculated the chain-length averaged rate coefficient for termination, $\langle k_t \rangle$, according to the well-known equation[19]

$$\langle k_t \rangle = \sum_{i=1}^{\infty} \sum_{j=1}^{\infty} k_t^{i,j} \frac{[R_i]}{[R]} \frac{[R_j]}{[R]} \qquad \textbf{(1.41)}$$

However they present no details as to how they obtained the $[R_i]$ for use in this equation, and it is unlikely that the computer power existed at the time to do so: more likely is that they used approximate closed equations. Olaj *et al.* are the first to have grappled seriously with the issue of iterative solution of eqs. **(1.34a)** and **(1.34b)**, presenting a comprehensive study in 1986.[47] They preferred to express the problem mathematically in terms of propagation probabilities rather than radical concentrations (a preference maintained by them to the present day). This approach emphasises the important point that the effect of CLDT is to make propagation probability a function of chain length (*c.f.* eqs. **(1.20)** and **(1.21)**). Russell[69] preferred the more transparent, although arguably less elegant, approach of using radical

concentrations, and explored issues such as those of truncation chain length (point (3) above) and coarse graining, showing (by comparison with exact numerical solutions) that it was possible to vastly reduce the number of equations to be solved but still obtain accuracy of better than 1%. It should be noted that the choice to derive equations in terms of propagation probabilities or radical concentrations does not affect the results from solution of the equations finally obtained for quantities of experimental interest such as $<k_t>$ and $\overline{DP}_n$: as such, the choice is essentially a stylistic one.

As part of this thesis, further improvements to the efficiency of numerical procedures were developed for iterative solution of. eqs. **(1.40)**. Some details regarding these procedures are given in Chapter 9.

For typical low-conversion polymerisation conditions, one needs to do about 50 iterations of eqs. **(1.34a)** and **(1.34b)** up to i of about 10,000 in order to obtain what may be regarded as exact numerical solutions. Just two decades ago, Olaj *et al.* required hours of time on a supercomputer to carry out such calculations.[47] By the early 1990s, Russell required about 60 minutes on a mainframe computer to do this.[69] Now this would require about 1 minute on a PC, which is no more time consuming than evaluating any classical kinetics equation using a hand-held calculator. Thus the only significant impediment to proper analysis of steady-state RP kinetics results is either obtaining or writing the code to do so.

References

(1) Roberts, R. M. *Serendipity: Accidental Discoveries in Science*; Stephen Kippur, 1989.

(2) Jenkins, A., Personal Communication.

(3) Rudin, A. *The Elements of Polymer Science and Engineering*; 1st ed.; Academic Press: Orlando and London, 1982.

(4) Buback, M.; Busch, M.; Kowollik, C. *Macromol. Theory Simul.* **2000**, *9*, 442-452.

(5) Busch, M. *Macromol. Theory Simul.* **2001**, *10*, 262-274.

(6) Hutchinson, R. A. *Macromol. Theory Simul.* **2001**, *10*, 144-157.

(7) Barner-Kowollik, C.; Buback, M.; Egorov, M.; Fukuda, T.; Goto, A.; Olaj, O. F.; Russell, G. T.; Vana, P.; Yamada, B.; Zetterlund, P. B. *Prog. Polym. Sci.* **2005**, *30*, 605-643.

(8) Taylor, D., B.Sc. (Hons) Report, University of Canterbury, 2001

(9) Russell, G. T. *Aust. J. Chem.* **2002**, *55*, 399-414.

(10) Buback, M.; Busch, M.; Lämmel, R. A. *Macromol. Theory Simul.* **1996**, *5*, 845-861.

(11) Castro, J. V.; van Berkel, K. Y.; Russell, G. T.; Gilbert, R. G. *Aust. J. Chem.* **2005**, *58*, 178-181.

(12) Olaj, O. F.; Vana, P.; Zoder, M.; Kornherr, A.; Zifferer, G. *Macromol. Rapid Commun.* **2000**, *21*, 913-920.

(13) Olaj, O. F.; Zifferer, G.; Gleixner, G. *Makromol. Chem., Rapid Commun.* **1985**, *6*, 773-784.

(14) Olaj, O. F.; Zifferer, G. *Macromolecules* **1987**, *20*, 850-861.

(15) Kornherr, A.; Zifferer, G.; Olaj, O. F. *Macromol. Theory Simul.* **1999**, *8*, 260-271.

(16) Trommsdorff, E.; Kohle, H.; Lagally, P. *Makromol. Chem.* **1948**, *1*, 169-198.

(17) Norrish, R. G. W.; Smith, R. R. *Nature (London)* **1942**, *150*, 336-337.

(18) Buback, M.; Egorov, M.; Gilbert, R. G.; Kaminsky, V.; Olaj, O. F.; Russell, G. T.; Vana, P.; Zifferer, G. *Macromol. Chem. Phys.* **2002**, *203*, 2570-2582.

(19) Allen, P. E. M.; Patrick, C. R. *Makromol. Chem.* **1961**, *47*, 154-167.

(20) Benson, S. W.; North, A. M. *J. Am. Chem. Soc.* **1962**, *84*, 935-940.

(21) O'Neil, G. A.; Wisnudel, M. B.; Torkelson, J. M. *Macromolecules* **1996**, *29*, 7477-7490.

(22) Fischer, J. P.; Mücke, G.; Schulz, G. V. *Ber. Bunsen-Ges. Phys. Chem.* **1969**, *73*, 154-163.

(23) Fischer, J. P.; Schulz, G. V. *Ber. Bunsen-Ges. Phys. Chem.* **1970**, *74*, 1077-1082.

(24) Ogo, Y.; Yokawa, M.; Imoto, T. *Makromol. Chem.* **1973**, *171*, 123-133.

(25) Buback, M.; Kuchta, F.-D. *Macromol. Chem. Phys.* **1997**, *198*, 1455-1480.

(26) Fischer, H.; Paul, H. *Acc. Chem. Res.* **1987**, *20*, 200-206.

(27) de Gennes, P. G.; Léger, L. *Ann. Rev. Phys. Chem.* **1982**, *33*, 49-61.

(28) Tirrell, M. *Rubber Chem. Technol.* **1984**, *57*, 523-556.

(29) Doi, M.; Edwards, S. F. *The Theory of Polymer Dynamics*; 1st ed.; Oxford University Press: New York, 1987.

(30) Freeman, B. D. In *Comprehensive Polymer Science: First Supplement*; Aggarwal, S. L., Russo, S., Eds.; Pergamon: Oxford, 1992; pp 167-198.

(31) Piton, M. C.; Gilbert, R. G.; Chapman, B. E.; Kuchel, P. W. *Macromolecules* **1993**, *26*, 4472.

(32) Griffiths, M. C.; Strauch, J.; Monteiro, M. J.; Gilbert, R. G. *Macromolecules* **1998**, *31*, 7835-7844.

(33) Strauch, J.; McDonald, J.; Chapman, B. E.; Kuchel, P. W.; Hawkett, B. S.; Roberts, G. E.; Tonge, M. P.; Gilbert, R. G. *J. Polym. Sci., Polym. Chem. Ed.* **2003**, *41*, 2491-2501.

(34) Olaj, O. F.; Bitai, I.; Hinkelmann, F. *Makromol. Chem.* **1987**, *188*, 1689-1702.

(35) Buback, M.; Gilbert, R. G.; Hutchinson, R. A.; Klumperman, B.; Kuchta, F.-D.; Manders, B. G.; O'Driscoll, K. F.; Russell, G. T.; Schweer, J. *Macromol. Chem. Phys.* **1995**, *196*, 3267-3280.

(36) Olaj, O. F.; Zifferer, G. *Makromol. Chem., Rapid Commun.* **1982**, *3*, 549-556.

(37) Mahabadi, H. K. *Macromolecules* **1985**, *18*, 1319-1324.

(38) Moad, G.; Solomon, D. H. *The Chemistry of Free Radical Polymerization*; 1st ed.; Pergamon: Oxford, 1995.

(39) Gridnev, A. A.; Ittel, S. D. *Macromolecules* **1996**, *29*, 5864-5874.

(40) Willemse, R. X. E.; Staal, B. B. P.; van Herk, A. M.; Pierik, S. C. J.; Klumperman, B. *Macromolecules* **2003**, *36*, 9797-9803.

(41) Heuts, J. P. A.; Gilbert, R. G.; Radom, L. *Macromolecules* **1995**, *28*, 8771-8781.

(42) Heuts, J. P. A.; Russell, G. T. *Eur. Polym. J.* **2006**, *42*, 3-20.

(43) Olaj, O. F.; Zifferer, G.; Gleixner, G. *Macromolecules* **1987**, *20*, 839-850.

(44) Olaj, O. F.; Kornherr, A.; Zifferer, G. *Macromol. Theory Simul.* **1997**, *6*, 655-666.

(45) Olaj, O. F.; Kornherr, A.; Zifferer, G. *Macromol. Theory Simul.* **1998**, *7*, 501-508.

(46) Olaj, O. F.; Kornherr, A.; Zifferer, G. *Macromol. Theory Simul.* **2001**, *10*, 881-890.

(47) Olaj, O. F.; Zifferer, G.; Gleixner, G. *Makromol. Chem.* **1986**, *187*, 977-994.

(48) Mahabadi, H. K. *Macromolecules* **1991**, *24*, 606-609.

(49) Bamford, C. H. *Eur. Polym. J.* **1989**, *25*, 683.

(50) Bamford, C. H. *Macromol. Symp.* **1996**, *111*, 171-181.

(51) de Kock, J. B. L.; Klumperman, B.; van Herk, A. M.; German, A. L. *Macromolecules* **1997**, *30*, 6743-6753.

(52) de Kock, J. B. L., Ph.D. Thesis, Technical University of Eindhoven, 1999

(53) Shipp, D. A.; Solomon, D. H.; Smith, T. A.; Moad, G. *Macromolecules* **2003**, *36*, 2032-2040.

(54) Buback, M.; Müller, E.; Russell, G. T. *J. Phys. Chem. A* **2006**, *110*, 3222-3230.

(55) Gear, C. W. *Numerical Initial-Value Problems in Ordinary Differential Equations*; Prentice Hall: Englewood Cliffs, N.J., 1971.

(56) Burden, R. L.; Faires, J. D. *Numerical Analysis*; 5th ed.; International Thomson Publishing, 1993.

(57) Aleksandrov, A. P.; Genkin, V. N.; Kitai, M. S.; Smirnova, I. M.; Sokolov, V. V. *Sov. J. Quantum Electron.* **1977**, *7*, 547-550.

(58) Evseev, A. V.; Nikitin, A. N. *Laser Chem.* **1995**, *16*, 83-99.

(59) Gear, C. W. *SIAM Review* **1981**, *23*, 10-24.

(60) Russell, G. T.; Gilbert, R. G.; Napper, D. H. *Macromolecules* **1993**, *26*, 3538-3552.

(61) Hutchinson, R. A.; Aronson, M. T.; Richards, J. R. *Macromolecules* **1993**, *26*, 6410-6415.

(62) O'Driscoll, K. F.; Kuindersma, M. E. *Macromol. Theory Simul.* **1994**, *3*, 469-478.

(63) He, J.; Zhang, H.; Chen, J.; Yang, Y. *Macromolecules* **1997**, *30*, 8010-8018.

(64) Lu, J.; Zhang, H.; Yang, Y. *Makromol. Chem., Theory Simul.* **1993**, *2*, 747-760.

(65) Manders, B. G.; van Herk, A. M.; German, A. L. *Macromol. Theory Simul.* **1995**, *4*, 325-333.

(66) Seeßelberg, M.; Thorn, M. *Macromol. Theory Simul.* **1994**, *3*, 825-843.

(67) Wulkow, M. *Macromol. Theory Simul.* **1996**, *5*, 393-416.

(68) Rees, M. T. L., Ph.D. Thesis, The University of Canterbury, 1999

(69) Russell, G. T. *Macromol. Theory Simul.* **1994**, *3*, 439-468.

(70) Yasukawa, T.; Murakami, K. *Polymer* **1980**, *21*, 1423-1426.

2 Termination in Dilute-Solution Free-Radical Polymerisation: A Composite Model

Abstract

Literature data are summarised for the chain-length-dependence of the termination rate coefficient in dilute solution free-radical polymerisations. In essence such experiments have yielded two parameter values: the rate coefficient for termination between monomeric free radicals, $k_t^{1,1}$, and a power-law exponent e quantifying how k_t values decrease with increasing chain length. All indications are that the value $e \approx 0.16$ in good solvent is accurate, however the values of $k_t^{1,1}$ which have been deduced are considerably lower than well-established values for small molecule radicals. This seeming impasse is resolved by putting forward a 'composite' model of termination: it is proposed that the value $e \approx 0.16$ holds only for long chains, with e being higher for small chains - the value 0.5 is used in this chapter, although it is not held to dogmatically. It is then investigated whether this model is consistent with experimental data. This is a non-trivial task, because although the experiments themselves and the ways in which they are analysed are elegant and not too complicated, the underlying theory is sophisticated, as is outlined. Simulations of steady-state polymerisation experiments are first of all carried out, and it is shown that the composite model of termination both recovers the e values which have been found and beautifully explains why these experiments considerably underestimate the true value of $k_t^{1,1}$. Simulations of pulsed-laser polymerisations find the same, although not quite so strikingly. It is therefore concluded that our new termination model, which retains the virtue of simplicity and in which all parameter values are physically reasonable, is consistent with experimental data. Taking a wider view, it seems likely that the situation of the exponent e varying with chain length will not just be the case in

dilute solution, but will be the norm for all conditions, which would give our model and our work a general relevance.

2.1 Introduction

Termination in free-radical polymerisation (FRP) is a fascinating phenomenon which is still widely debated.[1] Of particular interest are the chain-length dependence of the termination rate coefficient and the absolute values of these rate coefficients. In investigating this issue through analysis of FRP data it has been standard practice to use the following two-parameter equation:

$$k_t^{i,i} = k_t^{1,1}\, i^{-e} \qquad \textbf{(2.1)}$$

Here $k_t^{i,i}$ is the rate coefficient for termination between two polymerising radicals of degree of polymerisation i, and thus $k_t^{1,1}$ can be identified as the rate coefficient for termination between two monomeric free radicals while $e \geq 0$ is a power which quantifies the chain-length dependence of the termination rate coefficient: the higher its value, the stronger the decline of $k_t^{i,i}$ with increasing radical size. There is little doubt that the best data for $k_t^{1,1}$ and e has come from analysis[2-7] of experiments[3-5,8-11] on styrene and methyl methacrylate (MMA) systems at very low conversions. Such data is summarised in *Tab. 2.1*. The methods by which many of these values of e and $k_t^{1,1}$ were obtained will be discussed as appropriate in the course of this chapter. What is important for now is the remarkably consistent picture which emerges from *Tab. 2.1*: that $e \approx 0.2$ for both monomers while $k_t^{1,1} \approx 1\times10^8$ L·mol^{-1}·s^{-1} for styrene and is perhaps as much as 50% less than this for MMA.

Tab. 2.1 Values of the parameters $k_t^{1,1}$ and e, as defined in eq. **(2.1)**, from low-conversion polymerisation experiments. All systems were bulk polymerisations at ambient pressure unless otherwise indicated.

System	e	$\frac{k_t^{1,1}}{L \cdot mol^{-1} \cdot s^{-1}}$	Reference
Styrene, 30°C	0.24	0.99×10^{8} a)	2
Methyl methacrylate, 25°C	0.15	0.61×10^{8} a)	2
Styrene, 25°C	0.16-0.18	1.1×10^{8} a,b)	3
Methyl methacrylate, 25°C	0.16-0.17	0.5×10^{8} a,b)	4
Styrene, 25°C	≈ 0.2	- c)	5
Methyl methacrylate, 25°C	≈ 0.2	- c)	5
Styrene, 80°C, 2200 bar	0.16	0.7×10^{8}	6
Styrene, 50°C, in good solvent	0.26	- c)	7
Methyl methacrylate, 50°C, in good solvent	0.20	- c)	7

a) The literature value has been halved for consistency with the termination rate convention of this thesis (that the rate of termination equals $2\langle k_t \rangle [R]^2$).

b) Best estimate from given information in reference.

c) Values of $k_t^{1,1}$ were not reported.

Considering first the experimental values of e, they are in impressive agreement with what theory predicts for the case of the termination rate being controlled by the rate of chain-end encounter of overlapping macroradical coils: as has been pointed out,[12] regardless of whether the system is 'weakly reactive'[13,14] (*i.e.*, few chain-end encounters result in reaction) or 'strongly reactive'[12] (*i.e.*, all chain-end encounters result in reaction), $e \approx 0.16$ in good solvent is predicted.[12-14] This provides a persuasive argument for accepting this mechanism of - and with it this e value for - dilute solution termination between macroradical coils. Nevertheless,

one is entitled to wonder why this chain-length dependence has not been observed in studying processes which should mimic the termination reaction. For example, Wisnudel and Torkelson[15] have confirmed previous studies[16] in finding that $k_q \sim i^{-0.31}$ for phosphorescence quenching of benzil-capped polystyrene of chain length i by anthracene-capped polystyrene also of chain length i, where k_q denotes the rate coefficient for phosphorescence quenching and i ranged from 29 to 2015.[15] This of course suggests $e \approx 0.3$ for dilute solution termination. Interestingly, Buback *et al.* found $e = 0.32$ in applying their method to polymerisation of methyl acrylate at 40°C and 1000 bar.[6]

However one views the above situation, matters are much more serious in regard to the values of $k_t^{1,1}$, which in FRP experiments are not measured directly but are only deduced from the data. Direct and reliable measurements of termination rate coefficients, k_t, for a variety of small molecule radicals (*e.g. t*-butyl terminating with *t*-butyl) in a variety of solvents and over wide ranges of temperature have shown that in general one must have $k_t^{1,1} \approx 1\times10^9$ L·mol^{-1}·s^{-1} in FRP,[17] well in excess of all the values reported in *Tab. 2.1*. For example, $2k_t = 1.2\times10^9$ L·mol^{-1}·s^{-1} has been measured for cumyl radicals at 25°C in *t*-butylbenzene,[18] a value which strongly suggests that the $k_t^{1,1}$ values which have been deduced for styrene are non-physical. Recognising this, Olaj *et al.* recently concluded that their $k_t^{1,1}$ "has to be taken as characteristic of the reaction between two hypothetical radicals of unity degree of polymerisation with all the properties to be associated with a radical chain."[5] In other words, these workers are suggesting that FRP measurements of $k_t^{1,1}$ are not real values but are the values $k_t^{1,1}$ would be if monomeric radicals behaved as macroradical coils. This situation is perhaps unsatisfactory in that in an FRP experiment one has genuine monomeric free radicals rather than "hypothetical" ones, and so the genuine value of $k_t^{1,1}$ value should somehow be recoverable from data. Further, with the given interpretation it is hard to explain that Buback *et al.* measured the reasonable value of $k_t^{1,1} = 7\times10^8$ L·mol^{-1}·s^{-1} in their methyl

acrylate experiments.[6] In terms of the results of Fischer and Paul, whose small radical k_t were shown to be in excellent agreement with the Smoluchowski equation,[17] it is in fact impossible to explain the deduced values of $k_t^{1,1}$ being an order of magnitude different for methyl acrylate and styrene.[6] In fact it is easy to show that the Smoluchowski equation predicts $k_t^{1,1} \approx 10^9$ L·mol^{-1}·s^{-1} for dilute solution FRP.[19]

An obvious way around the problem outlined above would be to propose that $e = 0.16$ and $k_t^{1,1} \approx 1\times10^9$ L·mol^{-1}·s^{-1} for low conversion FRP of monomers such as styrene and MMA. But as will be seen in the calculations of this chapter, this gives overall termination rate coefficient, $\langle k_t \rangle$, values which are about an order of magnitude in excess of what is experimentally observed for such systems. Therefore this chapter proposes another solution, one which is more in line with experimental FRP data and at the same time retains the concepts of $e \approx 0.16$ for coils and $k_t^{1,1} \approx 10^9$ L·mol^{-1}·s^{-1}. Since dilute solution conditions are not of great technical importance, it may be wondered why so much effort is expended on trying to understand termination in such systems. The answer is that such systems are well suited to academic study, because they are at the very beginning of polymerisation when no polymer is present to complicate matters. Also, only by reaching an understanding of termination in very low conversion systems is one really in a position to go on to understand termination at intermediate and high conversions. Lastly, the model and methods of this chapter are applicable in general, not just for the specific polymerisation conditions we have in mind.

2.2 Termination Model

Homotermination rate coefficients

We propose that 'short' radicals terminate with each other according to the following standard functional form:

$$k_t^{i,i} = k_t^{1,1}\, i^{-e_S}, \quad i \le i_c \qquad \textbf{(2.2a)}$$

This $k_t^{1,1}$ should be the genuine rate coefficient for termination between monomeric free radicals (*c.f.* the interpretation of Olaj *et al.* quoted above[5]). From the discussion already given it is clear that $k_t^{1,1} = 1\times10^9$ L·mol^{-1}·s^{-1} is an appropriately representative value to use in calculations. Attention is thus focussed on the power e_S (where 'S' denotes 'short'). Since short chains are not coils, it is obvious that their rate of termination cannot be determined by the rate of chain-end encounter upon coil overlap. Rather, precisely because the concept of coil overlap has no relevance for short radicals, it is obvious to propose that their rate of termination is determined by centre-of-mass diffusion, exactly as is $k_t^{1,1}$.[17] Writing $D^i \sim i^{-e_D}$, where D^i denotes the diffusion coefficient of a species of chain length i, experiments have found $e_D \approx 0.5$[20] and 0.66[21] for oligomers (the notation e_D is used to distinguish these values from e for $k_t^{i,i}$: the two are not necessarily the same). It has also been pointed out[19] that diffusion[22] and intrinsic viscosity[23] data for polystyrene chains of length $i \approx 10$ to 100 imply $e_D \approx 0.5$. Since the Smoluchowski equation predicts $k_t^{i,i} \sim D^i$ if there is negligible variation of the capture radius for termination with i, all this data suggests $e_S \approx 0.5$. Evidence in support of this comes from the phosphorescence quenching experiments of Wisnudel and Torkelson, who found $k_q \sim (i^{-0.5} + 1)$ for quenching of benzil by anthracene-capped polystyrenes up to chain length $i \approx 330$.[15] As will be seen below (in discussing the 'diffusion mean' model), this strongly suggests $e_S \approx 0.5$. Hence $e_S = 0.5$ will be used in calculations.

For 'long' radicals we propose that

$$k_t^{i,i} = k_t^{1,1}\, (i_c)^{-e_S+e_L}\, i^{-e_L}, \quad i > i_c \qquad \textbf{(2.2b)}$$

The $k_t^{1,1}\, (i_c)^{-e_S+e_L}$ term in this equation gives continuity with Eq. **(2.2a)** at the 'crossover' chain length i_c. Considering all the experimental[2-7] and theoretical[12-14] evidence outlined above, one must conclude that for termination of long radicals $e_L \approx 0.16$ (corresponding to the best data

of *Tab. 2.1*), although we recognise that this value will depend somewhat on the monomer, temperature[24] and solvent quality.[25] Hence $e_L = 0.16$ will be used in the calculations of this chapter.

The value of i_c remains to be specified. Stukelj *et al.*[26] synthesised pyrene capped 100-mers of polystyrene and measured the rate of pyrene excimer formation in dilute solution. The pyrene encounter process, which should mimic the encounter process of the termination reaction, was found to be characterised by a diffusion coefficient which agreed exactly with an independently measured[22] value of the centre-of-mass diffusion coefficient of polystyrene 100-mers at identical conditions. This suggests $i_c \geq 100$. In fact, as has been outlined,[19] there is experimental evidence that $i_c \approx 100$. Further, this value appeals intuitively as the size at which a radical might start displaying long-chain behaviour with regard to termination. Therefore $i_c = 100$ will be used in the calculations of this chapter.

To summarise, in this chapter we propose and will use

$$k_t^{i,i} = 1\times10^9\ \mathrm{L\cdot mol^{-1}\cdot s^{-1}} \times \left\{ \begin{array}{c} i^{-0.5} \quad , \ i \leq 100 \\ 100^{-0.34}\ i^{-0.16} \quad , \ i > 100 \end{array} \right\} \qquad \textbf{(2.3)}$$

as a model for dilute solution (very low conversion) termination. Interestingly, $1\times10^9\ \mathrm{L\cdot mol^{-1}\cdot s^{-1}}\ (100)^{-0.34} = 2.1\times10^8\ \mathrm{L\cdot mol^{-1}\cdot s^{-1}}$ is encouragingly close in value to the apparent values of $k_t^{1,1}$ which have been deduced (see *Tab. 2.1*). This gives impetus to our model and perhaps vindicates the interpretation which Olaj *et al.*[5] have given to their $k_t^{1,1}$ values (see section 2.1).

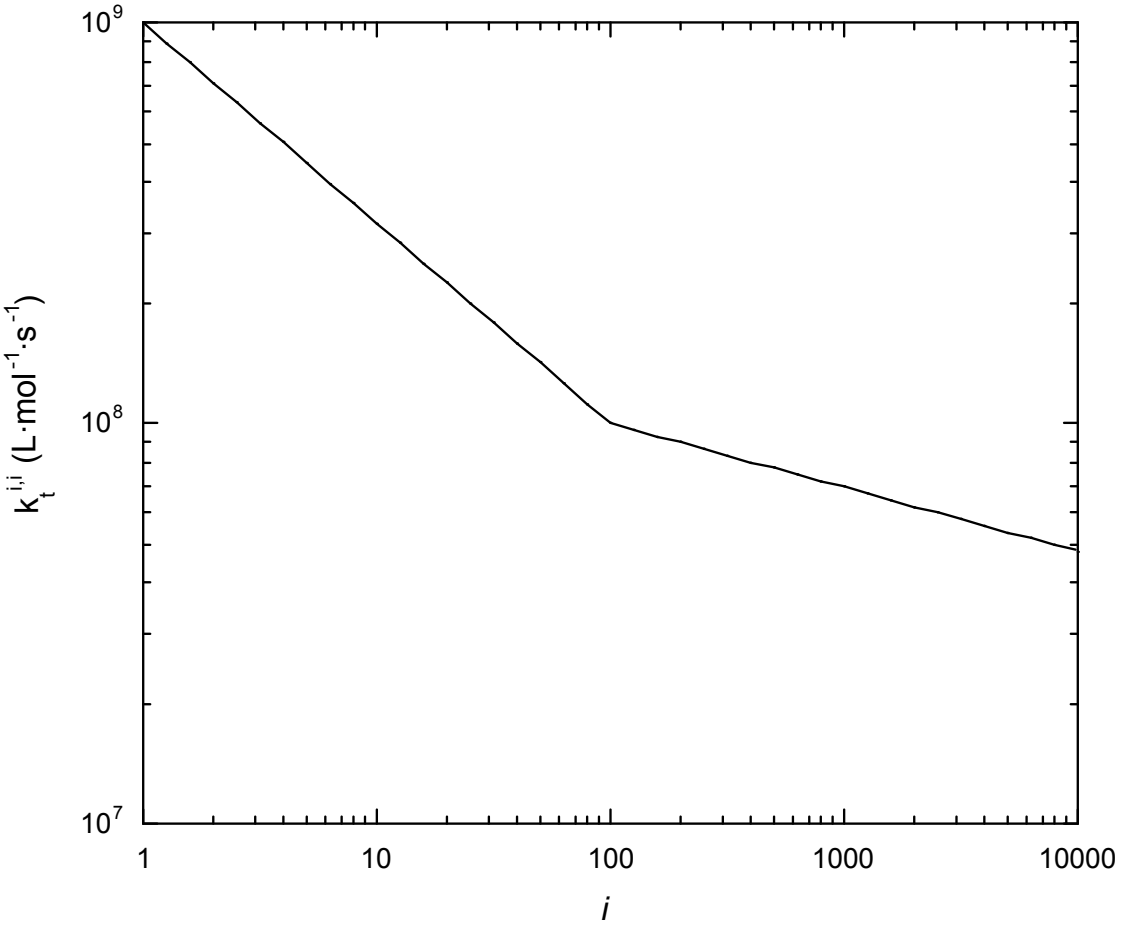

Fig. 2.1 Homotermination rate coefficient $k_t^{i,i}$ as a function of chain length i according to eq. **(2.3)**.

Eq. **(2.3)** is plotted in *Fig. 2.1*. The sharp change in behaviour at $i = i_c$ is evident, but in reality this crossover from short-chain behaviour to long-chain behaviour must be smooth, perhaps explaining that some experiments[6,15] have found $e \approx 0.3$ (results discussed above), intermediate between our e_S and e_L. In fact O'Driscoll has written[27] of his and Mahabadi's rather complicated theory[28,29] of dilute solution termination that (in the terminology of this chapter) "e is predicted to be 0.5 for short chain lengths (length *ca.* 100 or less) falling off to 0.1 for large chains (length > 1000)."[27] There is even some limited experimental evidence[5,30] for e varying continuously with i, with De Kock in fact claiming that acrylates have an intermediate regime in which $e \approx 1$.[30]

While the numerical methods of this chapter could be used to do calculations for any variation of e with i, for simplicity we will restrict ourselves to our "two-e" model. We do this for two reasons: (1) Because we feel that our model, which is a simple "composite" model in that it includes the ideas of both centre-of-mass diffusion[19,31] and chain-end encounter,[12-14] may capture the essence of the real situation, even if not the complete detail. In particular, it seems extremely likely to us that e is higher for small chains than for long chains. But it should be clear from this comment that the values of $k_t^{1,1}$, e_S, e_L and i_c which we use are just values which we consider the most sensible estimates currently available for dilute solution termination, not values which we insist are the final truth. (2) We wish to investigate systematically how the kinetics of FRP are affected by using a two-e model rather than just one value of e for all chain lengths, a situation which has been thoroughly investigated.[32,33] Although we use parameter values with low conversion termination in mind, some of our findings should be general, and should hold for different parameter sets applying at different conversions. This is another reason for using representative parameter values rather than ones which are necessarily as close as possible to those for a particular FRP system.

Cross-termination rate coefficients

We need also to specify values of the cross-termination rate coefficients $k_t^{i,j}$, where $i \neq j$. Three commonly used models are:[32-34]

$$k_t^{i,j}(\text{hm}) = k_t^{1,1}\left(\frac{2ij}{i+j}\right)^{-e} \qquad \textbf{(2.4)}$$

$$k_t^{i,j}(\text{dm}) = 0.5\, k_t^{1,1}\,(i^{-e} + j^{-e}) \qquad \textbf{(2.5a)}$$

$$k_t^{i,j}(\text{gm}) = k_t^{1,1}\,(\sqrt{ij})^{-e} = k_t^{1,1}\,(ij)^{-e/2} \qquad \textbf{(2.6a)}$$

These models are called the harmonic mean (hm), diffusion mean (dm) and geometric mean (gm) models, respectively. For $e < 1$ one has $k_t^{i,j}(\text{gm}) \le k_t^{i,j}(\text{dm}) \le k_t^{i,j}(\text{hm})$, *i.e.*, the dm value is between the other two. It is clear that the above are all "one-*e*" equations and that each reduces to the same expression for $k_t^{i,i}$, *viz.* $k_t^{1,1} i^{-e}$. Because the hm model is not factorisable there is no immediately obvious way of adapting it for use with the two-*e* $k_t^{i,i}$ model of this chapter. However the dm and gm models may more generally be expressed in terms of

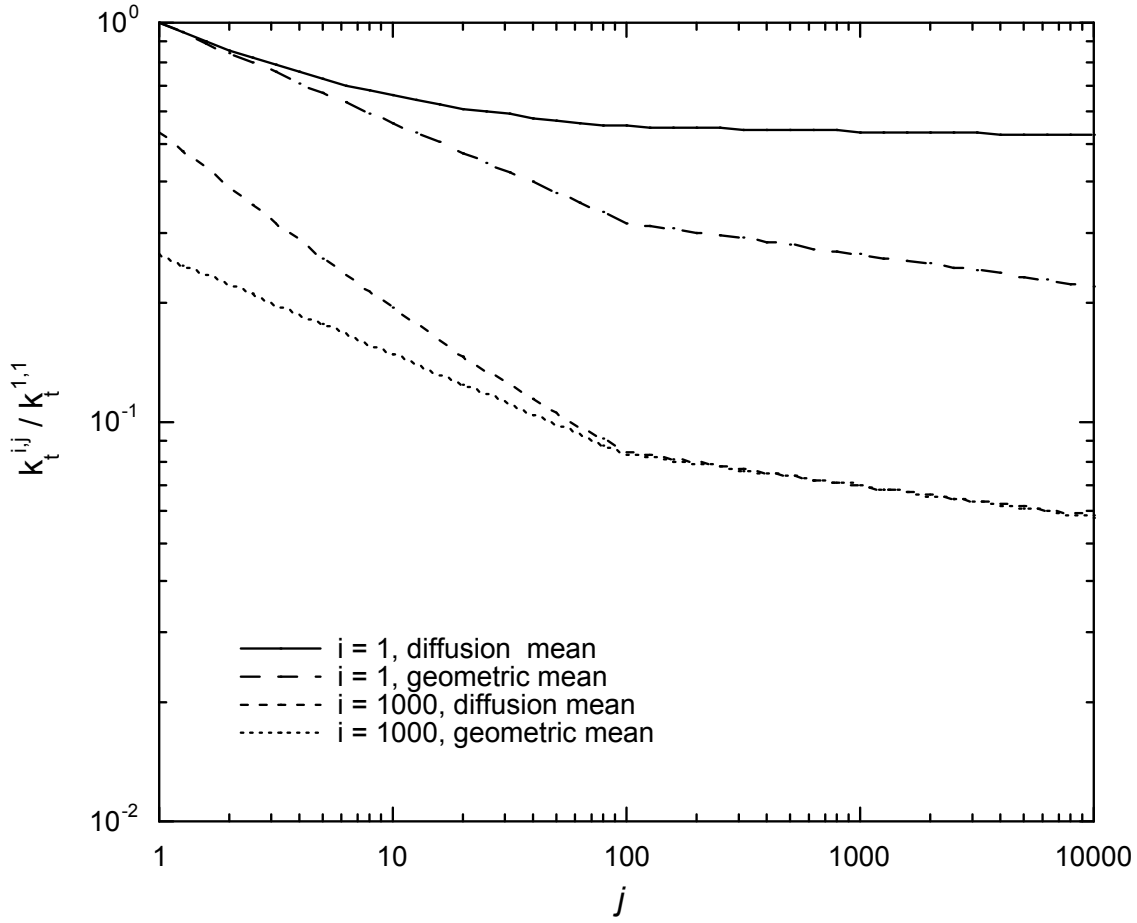

Fig. 2.2 Cross-termination rate coefficients $k_t^{i,j}$ as a function of chain length j for i =1 and i = 1000 evaluated according to the diffusion mean (eq. **(2.5b)**) and geometric mean (eq. **(2.6b)**) as indicated. Values are presented as $k_t^{i,j} / k_t^{1,1}$. The standard parameter values $e_S = 0.5$, $e_L = 0.16$ and $i_c = 100$ have been used.

separate components, as follows:

$$k_t^{i,j}(\text{dm}) = 0.5\,(k_t^{i,i} + k_t^{j,j}) \qquad \textbf{(2.5b)}$$

$$k_t^{i,j}(\text{gm}) = \sqrt{k_t^{i,i}\,k_t^{j,j}} \qquad \textbf{(2.6b)}$$

These expressions may obviously be used with any $k_t^{i,i}$ model, including the two-*e* model of this chapter. Therefore calculations will be carried out with both eqs. **(2.5b)** and **(2.6b)**. *Fig. 2.2* shows what these equations yield for $k_t^{1,j} / k_t^{1,1}$ and $k_t^{1000,j} / k_t^{1,1}$ when $k_t^{i,i}$ is as given by eq. **(2.3)**. It is evident that: (1) $k_t^{i,j}(\text{dm}) > k_t^{i,j}(\text{gm})$; (2) When i is small, $k_t^{i,j}(\text{dm})$ and $k_t^{i,j}(\text{gm})$ are similar for small j but diverge for large j; and (3) When i is large, $k_t^{i,j}(\text{dm})$ and $k_t^{i,j}(\text{gm})$ are different for small j but similar for large j.

It is fitting to consider the appropriateness of the above $k_t^{i,j}$ models for dilute solution termination as portrayed above. When at least one chain has $i \leq i_c$, one cannot really speak of coil-coil overlap occurring, and therefore it is unlikely that chain-end encounter upon coil overlap will control the rate of termination. Thus for 'short-short' and 'short-long' termination it seems physically reasonable to use the diffusion mean model, which is based on the Smoluchowski equation[34,35] and so should be appropriate for control of termination by centre-of-mass diffusion. Evidence for this is the already-mentioned phosphorescence quenching experiments of Wisnudel and Torkelson,[15] in which it was found that $k_q \sim (i^{-0.5} + 1)$ (*i.e.*, the diffusion mean with $j = 1$ and $e = 0.5$) provided a better fit of results than either a harmonic mean or geometric mean description. Turning now to 'long-long' termination in dilute solution, the harmonic mean model describes rates of chain-end encounter.[12-14] Therefore it would ideally be used for $k_t^{i,j}$ when $i, j > i_c$. While this could in principle be done (using $e = e_L$ and $k_t^{1,1}(i_c)^{-e_S+e_L}$ for $k_t^{1,1}$ in eq. (**2.4**)), for obvious reasons we prefer to use the one cross-termination model for all i and j rather than a mixture of models. Further, it is

easily shown that except for small *e* (say, well less than 0.5) the diffusion mean is at least a reasonable approximation for the harmonic mean,[34] with the two models in fact being the same for $e = 1$. All things considered it would therefore seem that the diffusion mean model is the most appropriate cross-termination model to use. Further recommending it is that the Smoluchowski equation is known to be an excellent description of diffusion-controlled reactions in general, and hence it can be argued that the diffusion mean should be preferred as a description of termination unless there is definite evidence that another model is superior.

Having said all the above, the geometric mean model will also be used in this chapter. Although it would seem to lack a physical basis for diffusion-controlled termination,[33,34] for small *e* it approximates well the harmonic mean model[13] (which does have a physical basis, see above), and it is of mechanistic relevance if termination is chemically (or perhaps if it is sterically) controlled.[34] Further, the geometric mean model is very amenable for calculations, as recently reviewed.[34] Previous work for both steady state[32,34] and non-steady state[33] polymerisation has shown that different cross-termination models nevertheless give extremely similar scaling behaviour for the one-*e* situation. Therefore it is of interest to see whether this also is so for the two-*e* situation. Hence calculations will be carried out with the two different cross-termination models, eqs. **(2.5b)** and **(2.6b)**. Although data analysis in this work always infers only $k_t^{i,i}$ values, it is stressed that cross-termination takes place as it should in all simulations which are carried out.

2.3 Population Balance Equations and Steady State Solutions

In the preceding section a model for $k_t^{i,j}$ was proposed. Ideally it would be possible to evaluate this model by direct comparison with free-radical polymerisation data. But unfortunately FRP data does not yield $k_t^{i,j}$ values directly. Rather, it yields quantities such as overall rates and average chain lengths. To learn about termination from this information, it

must be linked to the $k_t^{i,j}$ values. How this is done is outlined in this section, preparatory to presenting, in the following sections, results of FRP simulations using our termination model. In this way it can be critically evaluated whether our model is consistent with experimental observations.

Population balance equations

We use the following reaction scheme for conventional FRP:

$$\mathrm{I} \xrightarrow{R_{\mathrm{init}}} \mathrm{R}_1 \qquad \text{Initiation}$$

$$\mathrm{R}_i + \mathrm{M} \xrightarrow{k_\mathrm{p}} \mathrm{R}_{i+1} \qquad \text{Propagation}$$

$$\mathrm{R}_i + \mathrm{R}_j \xrightarrow{\lambda k_\mathrm{t}^{i,j}} \mathrm{D}_i + \mathrm{D}_j \qquad \text{Termination by disproportionation}$$

$$\mathrm{R}_i + \mathrm{R}_j \xrightarrow{(1-\lambda) k_\mathrm{t}^{i,j}} \mathrm{D}_{i+j} \qquad \text{Termination by combination}$$

$$\mathrm{R}_i + \mathrm{X} \xrightarrow{k_{\mathrm{trX}}} \mathrm{D}_i + \mathrm{R}_1 \qquad \text{Chain transfer}$$

Here I denotes initiator, M monomer, and R_i and D_i a living radical and a dead polymer molecule, respectively, of degree of polymerisation i. Rate coefficients, k, are as indicated, with R_{init} denoting the rate of initiation and λ the fraction of termination events which occur by disproportionation, assumed to be chain-length independent. We also neglect any chain-length dependence of the propagation and transfer reactions, although such dependencies can trivially be included in our equations if desired. It is assumed that reinitiation is relatively

rapid upon occurrence of transfer. If transfer to a variety of X species occurs, one just sums the individual transfer frequencies in the equations which follow.

The population balance equations which follow from the above reaction scheme are

$$\frac{d[R_1]}{dt} = R_{init} + f_{trX}[R] - f_p[R_1] - f_{trX}[R_1] - f_t^1[R_1] \quad \textbf{(2.7a)}$$

$$\frac{d[R_i]}{dt} = f_p([R_{i-1}] - [R_i]) - f_{trX}[R_i] - f_t^i[R_i] \quad , \qquad i = 2, \infty \quad \textbf{(2.7b)}$$

$$\frac{d[D_i]}{dt} = \lambda f_t^i[R_i] + (1 - \lambda)\sum_{j=1}^{i-1} k_t^{j,i-j}[R_j][R_{i-j}] + f_{trX}[R_i] \quad , \; i = 1, \infty \quad \textbf{(2.8)}$$

Here t is time,

$$[R] = \sum_{j=1}^{\infty}[R_j] \quad \textbf{(2.9)}$$

is the total free radical concentration and the f denote the various reaction frequencies: $f_p = k_p[M]$ is the frequency with which a radical undergoes propagation, $f_{trX} = k_{trX}[X]$ is the transfer frequency, and

$$f_t^i = 2\sum_{j=1}^{\infty} k_t^{i,j}[R_j] \quad \textbf{(2.10)}$$

is the frequency with which an R_i species terminates. Note that eq. **(2.10)** defines the rate law we use for termination, *i.e.*, with a factor of 2. For chain-length-independent termination (all $k_t^{i,j}$ equal to the one value, k_t), eq. **(2.10)** becomes $f_t^i = 2k_t[R]$, *i.e.*, there is no dependence on chain length, which greatly simplifies matters. But whenever termination is chain-length dependent, f_t^i is a function of chain length, and thus the kinetics of FRP is greatly

complicated. That said, eq. **(2.10)** can be significantly simplified when the cross-termination models introduced above are used. Considering first the diffusion mean model, it is easy to show that when eq. **(2.5b)** is substituted into eq. **(2.10)** one obtains

$$f_t^i(\mathrm{dm}) = k_t^{i,i}[\mathrm{R}] + \sum_{j=1}^{\infty} k_t^{i,j}[\mathrm{R}_j] \qquad \textbf{(2.11a)}$$

This result, which has been noted or implicitly recognised by others,[32,36,37] holds regardless of the functional form of $k_t^{i,i}$. It means that only one summation needs to be carried out in order to evaluate all f_t^i, as opposed to needing to carry out a different summation for every f_t^i (compare eqs. **(2.10)** and **(2.11a)**). This speeds up computation times enormously. Similarly for the geometric mean, eq. **(2.6b)**, which gives

$$f_t^i(\mathrm{gm}) = 2\,(k_t^{i,i})^{0.5} \sum_{j=1}^{\infty} (k_t^{j,j})^{0.5}[\mathrm{R}_j]) \qquad \textbf{(2.12a)}$$

Again, this result is implicit in the work of others.[2,38] It is noted that no simplification of f_t^i is possible with the harmonic mean model, meaning that computation times are much longer when it is used.

In general eqs. **(2.7a)**, **(2.7b)** and **(2.8)** must be solved numerically. The $[\mathrm{R}_i]$ at any instant may be used to evaluate

$$\langle k_t \rangle = \sum_{i=1}^{\infty}\sum_{j=1}^{\infty} k_t^{i,j} \frac{[\mathrm{R}_i]}{[\mathrm{R}]}\frac{[\mathrm{R}_j]}{[\mathrm{R}]} \qquad \textbf{(2.13)}$$

This is the overall rate coefficient for termination - the termination rate coefficient observed in an FRP experiment - at any instant.[34,39] As this statement implies, eq. **(2.13)** is not restricted to steady states. Rather, it always holds, but in non-steady states it results in $\langle k_t \rangle$

varying with time. The values of $[D_i]$ from integrating eq. **(2.8)** may be used to evaluate the number- and weight-average degrees of polymerisation of dead polymer, denoted $\overline{DP}_n$ and $\overline{DP}_w$ respectively:

$$\overline{DP}_n = \frac{\sum_{i=1}^{\infty} i\,[D_i]}{\sum_{i=1}^{\infty} [D_i]} \qquad \textbf{(2.14)}$$

$$\overline{DP}_w = \frac{\sum_{i=1}^{\infty} i^2\,[D_i]}{\sum_{i=1}^{\infty} i\,[D_i]} \qquad \textbf{(2.15)}$$

Both these expressions will be used in the course of this work.

Steady state solutions

Standard, continuously initiated FRP experiments take place to good approximation in a steady state. Therefore it is common procedure to consider steady state solutions of the kinetic equations for FRP. This means setting $d[R_i]/dt = 0$ for all i. eqs. **(2.7a)** and **(2.7b)** now become:

$$[R_0] = \frac{R_{init} + f_{trX}\,[R]}{f_p} \qquad \textbf{(2.16a)}$$

$$[R_i] = [R_{i-1}]\frac{1}{1 + \frac{f_{trX}}{f_p} + \frac{f_t^i}{f_p}} = [R_0]\prod_{j=1}^{i}\left(1 + \frac{f_{trX}}{f_p} + \frac{f_t^j}{f_p}\right)^{-1}, \quad i = 1, \infty \qquad \textbf{(2.16b)}$$

Here $[R_0]$ is a dummy concentration which can be considered as being the overall concentration (from both initiation and transfer) of initiating radicals. Because steady state $[R_i]$ are by definition constant, it follows that all $d[D_i]/dt$ are constant. This means that $[D_i] \sim d[D_i]/dt$, and thus one uses $d[D_i]/dt$ for $[D_i]$ in eqs. (**2.14**) and (**2.15**) in order to evaluate the steady state $\overline{DP}_n$ and $\overline{DP}_w$ respectively.

The above equations hold for any model for $k_t^{i,j}$. However their evaluation can be simplified for the two $k_t^{i,j}$ models of this chapter. Considering first the diffusion mean, substituting eq. **(2.5b)** into the condition of steady state gives that

$$R_{init} = \sum_{i=1}^{\infty}\sum_{j=1}^{\infty} 2\, k_t^{i,j}\,[R_i]\,[R_j] = 2\,[R]\sum_{i=1}^{\infty} k_t^{i,i}\,[R_i] \qquad \textbf{(2.17)}$$

Eq. **(2.11a)** now simplifies to

$$f_t^i(dm,SS) = k_t^{i,i}\,[R] + \frac{R_{init}}{2[R]} \qquad \textbf{(2.11b)}$$

where 'SS' denotes steady state. This equation means that a single value of [R] is sufficient to evaluate all f_t^i, and hence all $[R_i]$. So the only summation which needs to be carried out in iterating eqs. **(2.16)** until convergence[40,41] is that of eq. **(2.9)** after each new evaluation of the $[R_i]$. This makes computation extremely rapid.

Turning now to the geometric mean model, eq. **(2.6b)**, it results in the following steady state condition:

$$R_{init} = \sum_{i=1}^{\infty}\sum_{j=1}^{\infty} 2\, k_t^{i,j}\,[R_i]\,[R_j] = 2\left(\sum_{i=1}^{\infty} (k_t^{i,i})^{0.5}\,[R_i]\right)^2 \qquad \textbf{(2.18)}$$

Eq. **(2.12a)** now simplifies to

$$f_t^i(\mathrm{gm,SS}) \;=\; (2\,k_t^{i,i}\,R_{\mathrm{init}})^{0.5} \qquad \textbf{(2.12b)}$$

Although expressed differently, this result is present in earlier work.[2,38,40] It means that all $[R_i]/[R_0]$ can be evaluated straight off and without iteration, making for facile computation of these values.

It turns out that further progress can be made with eq. **(2.12b)**, as follows.[2,38] The quite general approximation

$$\left(1+\frac{f_{\mathrm{trX}}}{f_p}+\frac{f_t^j}{f_p}\right)^{-1} \;\approx\; \exp\left(-\frac{f_{\mathrm{trX}}}{f_p}-\frac{f_t^j}{f_p}\right) \qquad \textbf{(2.19)}$$

is the 'long chain approximation' (LCA) in that it becomes exactly true in the limit of infinitely long chains. Using this approximation, eq. **(2.16b)** becomes

$$\frac{[R_i]}{[R_0]} \;\approx\; \exp\left(-i\frac{f_{\mathrm{trX}}}{f_p}\right)\exp\left(\sum_{j=1}^{i}\frac{-f_t^j}{f_p}\right) \;\approx\; \exp\left(-i\frac{f_{\mathrm{trX}}}{f_p}\right)\exp\left(\int_0^i\frac{-f_t^j}{f_p}\,\mathrm{d}j\right) \qquad \textbf{(2.20)}$$

These equations are general but are only of use if the f_t^j are known in value, as is the case with eq. **(2.12b)**. Substituting this equation into eq. **(2.20)**, then using eqs. **(2.2a)** and **(2.2b)** for $k_t^{j,j}$, and then evaluating the integral, one obtains

$$\frac{[R_i]}{[R_0]} \approx \exp\left(-i\frac{f_{\mathrm{trX}}}{f_p}\right)\times\left\{\begin{array}{cc}\exp(-C_S\,i^{E_S}) & ,\; i\le i_c\\ \exp(-C_S\,i_c^{E_S}+I_c\,C_L\,i_c^{E_L}-I_c\,C_L\,i^{E_L}) & ,\; i>i_c\end{array}\right\} \qquad \textbf{(2.21)}$$

Here $E_S = (2\text{-}e_S)/2$, $C_S = (2R_{\mathrm{init}}k_t^{1,1})^{0.5}/(f_pE_S)$, $E_L = (2\text{-}e_L)/2$, $C_L = (2R_{\mathrm{init}}k_t^{1,1})^{0.5}/(f_pE_L)$ and $I_c = (i_c)^{-e_S+e_L}$. In the case of $f_{\mathrm{trX}} = 0$ (no transfer) and $e_S = e_L$ (one-e model), closed expressions for the moments of the above distribution are available, and thus one can obtain closed expressions for quantities such as $\langle k_t\rangle$,[2] $\overline{DP}_n$ and $\overline{DP}_w$.[38,42] Some of these results will be quoted below. In fact they provide the motivation for deriving eqs. **(2.21)** here: that closed

expressions for $\langle k_t \rangle$, $\overline{DP}_n$ and $\overline{DP}_w$ might also exist for the case of a multiple-*e* model. Unfortunately the moments of the above $[R_i]/[R_0]$ do not appear to be available when $e_S \neq e_L$. So although these approximate values of $[R_i]/[R_0]$ can be easily evaluated (and might, for example, be compared with the exact values from the easily computed eq. **(2.16b)**), $\langle k_t \rangle$, $\overline{DP}_n$ and $\overline{DP}_w$ can still only be obtained by carrying out the appropriate summations. Thus at this stage it would seem there is no real advantage to be gained from eqs. **(2.21)**.

2.4 Steady State Calculations

Data from steady-state (SS) polymerisation have been used to make deductions about the chain-length dependence of termination.[7,34,43] With this in mind, in this section we present the results of steady state calculations which mimic the experimental investigations. The calculations are carried out as follows. eq. **(2.16b)** is evaluated using eq. **(2.11b)** (diffusion mean) or eq. **(2.12b)** (geometric mean) as appropriate. In the dm case one needs to guess a starting value of [R] and iteratively evaluate eq. **(2.16b)** until [R] (eq. **(2.9)**) converges.[40,41] From these $[R_i]$, $\langle k_t \rangle$ (= $R_{init}/(2[R]^2)$ for SS polymerisation) and $d[D_i]/dt$ (eq. **(2.8)**) can be evaluated, and from the latter $\overline{DP}_n$ can then be obtained (eq. (**2.14**), using $d[D_i]/dt$ for $[D_i]$, as explained above. A technical detail here is that $[R_i]$ cannot be computed up to infinite *i*, as in principle is required in order to calculate $\langle k_t \rangle$ and $\overline{DP}_n$. In practice one considers all radicals beyond a certain very large size as a single group and one computes a sufficiently large number of individual $[R_i]$ - perhaps as many as 10,000 or more - that quantities such as [R] and $\langle k_t \rangle$ show no variation if an even larger number of individual $[R_i]$ are computed and individually included in the sums.[41]

For steady state (continuously initiated) polymerisation, $R_{init} = 2fk_d[I]$, where this f is the initiator efficiency (not a reaction frequency), k_d is the initiator decomposition rate coefficient, and [I] the initiator concentration. *Tab. 2.2* lists the values of these and all other parameter values which are used at all times in this chapter, unless otherwise stated. Notwithstanding that rounded parameter values have been used, they have in mind bulk polymerisation of MMA at 25°C, this being an archetypal experimental system (see the *Tab. 2.1*). Styrene at 25°C will be similar, except in that k_p will be about half the value[44,45] and dead chain formation will be predominantly by combination ($\lambda = 0$) (note that the latter does

Tab. 2.2 Standard parameter values used in steady state calculations ('SS value') and pulsed-laser polymerisation simulations ('PLP value').

Parameter	Symbol	SS value	PLP value
Effective rate coefficient for radical generation	fk_d	2.5×10^{-8} s^{-1}	–
Initiator concentration	[I]	1×10^{-2} mol·L^{-1}	–
Radical concentration generated per laser pulse	ρ	–	5×10^{-8} mol·L^{-1}
Time between laser pulses	t_d	–	0.1 s
Propagation rate coefficient	k_p	200 L·mol^{-1}·s^{-1}	200 L·mol^{-1}·s^{-1}
Monomer concentration	[M]	10 mol·L^{-1}	10 mol·L^{-1}
Transfer rate coefficient	k_{trX}	0	0
Homotermination rate coefficients	$k_t^{i,i}$	Eq. **(2.3)**	Eq. **(2.3)**
Cross-termination rate coefficients	$k_t^{i,j}$	Eqs. **(2.5b)** or **(2.6b)**	Eq. **(2.5b)**
Fraction of termination by disproportionation	λ	1	1

not affect $<k_t>$). *Tab. 2.2* gives individual parameter values, even though it will be evident from the preceding section that results actually only depend on various products and ratios of individual parameter values, *e.g.* $[R_i]/[R_0]$ is a function of only $(2R_{init}k_t^{1,1})^{0.5}/(k_p[M])$[40,46] and $k_{trX}[X]/(k_p[M])$. The *Tab. 2.2* approach with parameter values is taken because it gives a better feel for the real-world conditions in mind in performing sets of calculations.

All sets of calculations are carried out with three lots of e values: (1) $e_S = e_L = 0.16$, results denoted $<k_t>(e = 0.16)$; (2) $e_S = 0.5$ and $e_L = 0.16$, giving $<k_t>(e_S = 0.5, e_L = 0.16)$ values; and (3) $e_S = e_L = 0.5$, $<k_t>(e = 0.5)$. This is done because although it is the two-e case which is specifically of interest in this chapter, its results should obviously be compared with those of the two corresponding one-e cases. Thus the graphs of this section each present six lots of results: the three lots of e values, each used with both the dm and gm. Fig. 2.3 shows how $<k_t>$ varies with [I], all other parameter values being held constant at their Tab. 2.2 values. These results thus mimic a set of experiments in which $<k_t>$ is measured for different initiator concentrations. Fig. 2.4 shows how $<k_t>$ varies with [M] when all other parameter values are held constant. This would correspond to measuring $<k_t>$ as a function of solvent amount while holding $k_t^{1,1}$ constant. Fig. 2.5 presents $<k_t>$ as a function of $k_t^{1,1}$, for example using solvents of different viscosity while holding all else constant. Because these calculations obviously have solution polymerisation in mind, [M] = 2 mol·L^{-1} rather than the Tab. 2.2 value is used. Finally, the variations of $<k_t>$ with $\overline{DP}_n$ from the calculations of *Fig. 2.3* and *Fig. 2.4* are presented in Fig. 2.6. For reasons which will become obvious in the discussion which follows, all results have been presented as log-log plots.

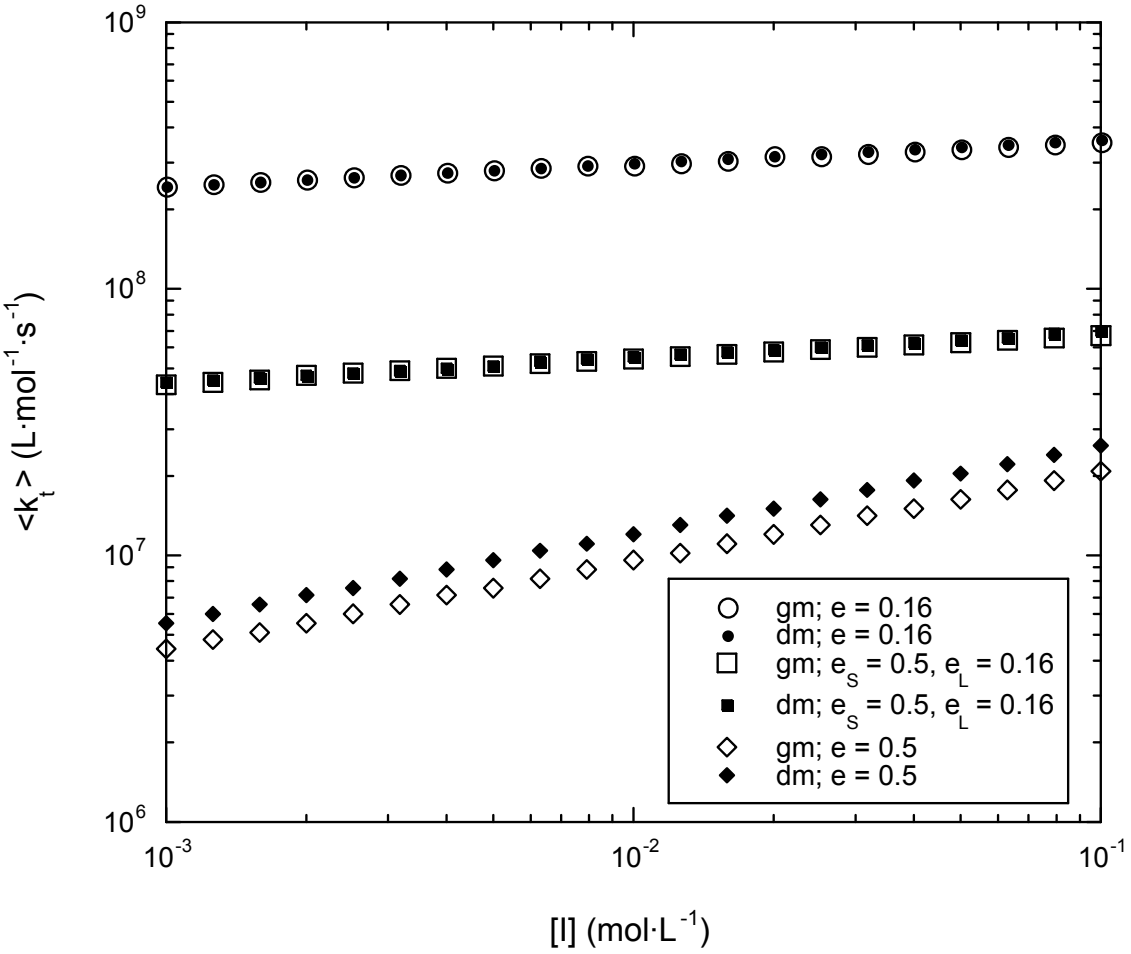

Fig. 2.3 Overall termination rate coefficient $<k_t>$ versus initiator concentration [I], as calculated using steady state parameter values of *Tab. 2.2*. Results are presented for three different lots of *e* values with each of the geometric mean (gm) and diffusion mean (dm) for $k_t^{i,j}$, as indicated.

Some points to note immediately about the results are: (1) $<k_t>(e = 0.16) > <k_t>(e_S = 0.5, e_L = 0.16) > <k_t>(e = 0.5)$ is always observed because of the $k_t^{i,i}$ values being in this same order. (2) The $<k_t>$ values obtained using $e = 0.16$ are much higher than $<k_t>$ values obtained experimentally, the latter typically being 10^7-10^8 L mol^{-1} s^{-1} for styrene and MMA. This evidences the point made in section 2.1 that with $k_t^{1,1} \approx 1\times10^9$ L·mol^{-1}·s^{-1} and $e = 0.16$ one cannot explain the magnitude of experimentally observed values of $<k_t>$. (3) On the other

hand, the values of $\langle k_t \rangle$ obtained with eq. **(2.3)** are much closer in magnitude to what is experimentally observed, while the values with $e = 0.5$ are probably too low. (4) The figures show that $\langle k_t \rangle$ increases with increasing [I], $\langle k_t \rangle$ decreases with increasing [M], and that $\langle k_t \rangle$ has a stronger than first-order dependence on $k_t^{1,1}$. These are all well-known qualitative effects of chain-length-dependent termination.[43] (5) $\langle k_t \rangle$(dm) > $\langle k_t \rangle$(gm), because $k_t^{i,j}$(dm) >

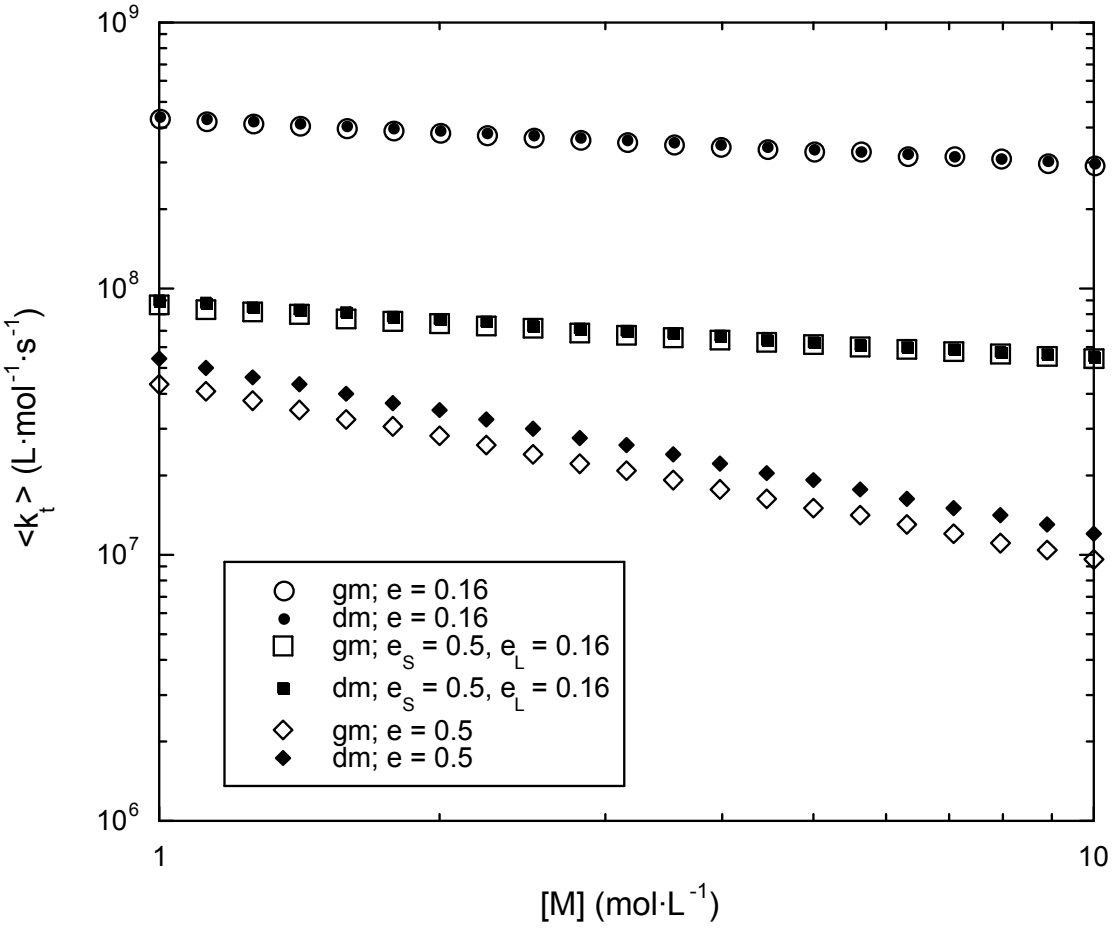

Fig. 2.4 Overall termination rate coefficient $\langle k_t \rangle$ versus monomer concentration [M], as calculated using steady state parameter values of *Tab. 2.2*. Results are presented for three different lots of e values with each of the geometric mean (gm) and diffusion mean (dm) for $k_t^{i,j}$, as indicated.

$k_t^{i,j}$(gm) (see *Fig. 2.2*). (6) Although the dm and gm models give $\langle k_t \rangle$ values which are different in magnitude, it is evident that $\langle k_t \rangle$(dm) and $\langle k_t \rangle$(gm) both show nearly identical *variation* with [I], [M] and $k_t^{1,1}$. In other words, the scaling behaviour of $\langle k_t \rangle$ is essentially unaffected by $k_t^{i,j}$ for the present values of *e*. This is already known for one-*e* models,[32,34] but

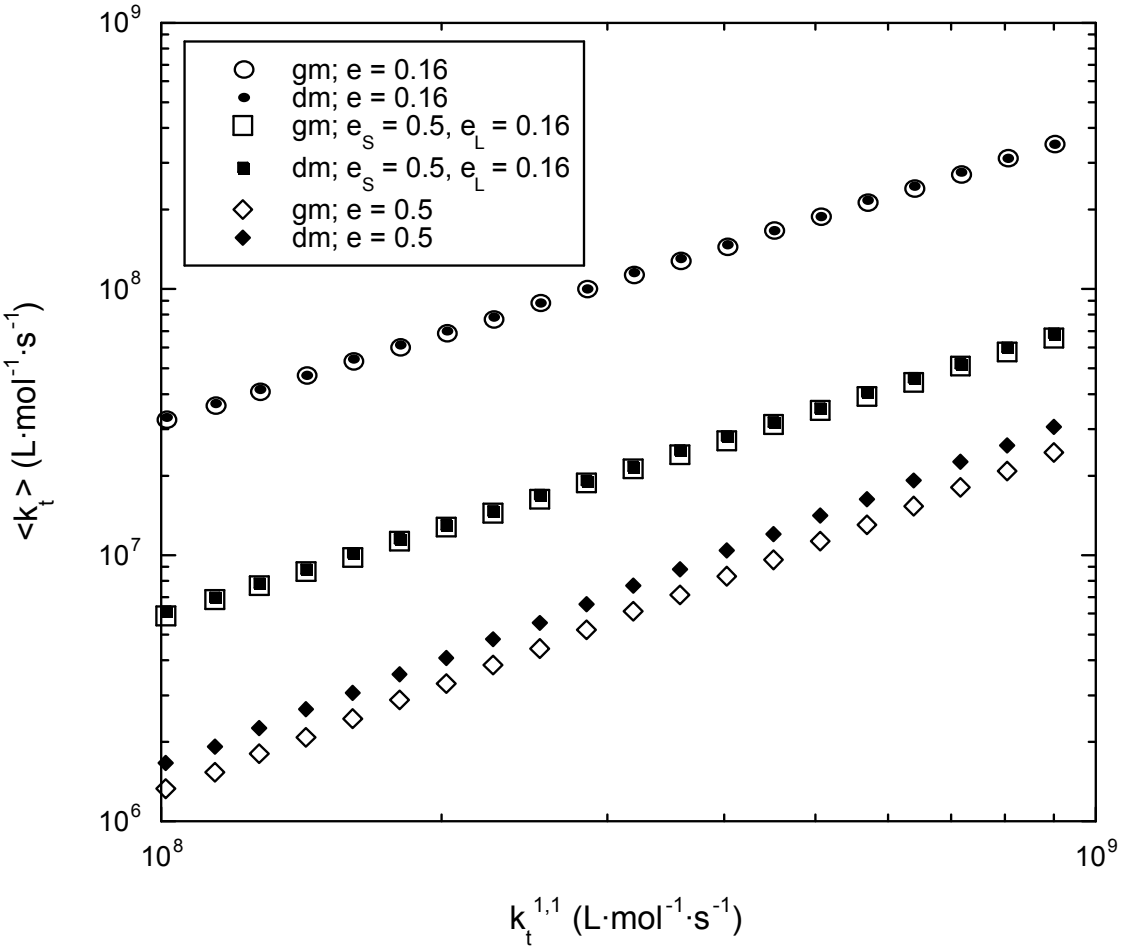

Fig. 2.5 Overall termination rate coefficient $\langle k_t \rangle$ versus rate coefficient for termination between monomeric free radicals, $k_t^{1,1}$. Calculations used steady state parameter values of *Tab. 2.2* except for [M] = 2 mol·L^{-1}. Results are presented for three different lots of *e* values with each of the geometric mean (gm) and diffusion mean (dm) for $k_t^{i,j}$, as indicated.

here we show it for a two-*e* model for the first time.

Quantitative aspects of the results of *Fig. 2.3*, *Fig. 2.4* and *Fig. 2.5* will now be considered. It is evident from these figures that for all three sets of *e* values the results are excellently described by

$$\langle k_t \rangle \sim [\mathrm{I}]^a [\mathrm{M}]^{-b} (k_t^{1,1})^c \qquad \textbf{(2.22)}$$

This means that *a* denotes the slope of a log-log plot of $\langle k_t \rangle$ versus [I], *e.g. Fig. 2.3*; likewise for -*b* and *c*. It can be shown that eqs. **(2.21)** with $e_S = e_L$ and $f_{trX} = 0$ result in[2] (the working once again involves summations being approximated by integrals)

$$\langle k_t \rangle(\mathrm{gm,LCA}) = k_t^{1,1} \left[\Gamma\left(\frac{2}{2\text{-}e}\right) \right]^{-2} \left[\frac{(2R_{init}\, k_t^{1,1})^{0.5}}{f_p} \left(\frac{2}{2\text{-}e}\right) \right]^{2e/(2\text{-}e)} \qquad \textbf{(2.23a)}$$

Here LCA denotes 'long chain approximation' and $\Gamma()$ the gamma function. Comparing eqs. **(2.22)** and **(2.23a)** one easily sees that

$$a(\mathrm{gm,LCA}) = \frac{e}{2\text{-}e}, \quad b(\mathrm{gm,LCA}) = \frac{2e}{2\text{-}e}, \quad c(\mathrm{gm,LCA}) = 1 + \frac{e}{2\text{-}e} \qquad \textbf{(2.24)}$$

It is stressed that eqs. **(2.23a)** and **(2.24)** hold only in the absence of transfer (and for a steady state). The predictions of eq. **(2.24)** may be compared with the actual values from the calculations of this work (in which, as required, $f_{trX} = 0$ was used). This is done in *Tab. 2.3*. Some points which emerge: (1) The 'gm' values of *a*, *b* and *c* are not exactly equal to the 'gm,LCA' values, because the latter are only exact in the limit of infinitely long chains. Nevertheless it is evident that the LCA is essentially exact for the conditions of *Tab. 2.2*, meaning *a*(gm) ≈ *a*(gm,LCA), and similarly for *b* and *c*. (2) Not only this, it is clear *a*(dm) ≈ *a*(gm,LCA), and similarly for *b* and *c*, meaning the 'gm' and 'dm' values of *a*, *b* and *c* are in all cases very similar. This formalises the point made above about the two different $k_t^{i,j}$

models resulting in very much the same scaling behaviour. (3) *Tab. 2.3* formally shows what is very much evident from the figures: that the scaling with [I], [M] and $k_t^{1,1}$ of the $<k_t>(e_S$ = 0.5, e_L = 0.16) values is determined predominantly by e_L (= 0.16) and hardly at all by e_S (= 0.5).

Tab. 2.3 Values of parameters from power law variations of the overall termination rate coefficient $<k_t>$ for steady state polymerisation. The parameters *a*, *b* and *c* are defined by eq. **(2.22)**, the parameters *g* and *G* by eq. **(2.25)**. The abbreviations 'dm' and 'gm' denote values from calculations with the diffusion mean and geometric mean respectively, while 'gm,LCA' denotes geometric mean values in the limit of infinitely long chains.

Parameter	Obtained from	e = 0.16	e_S = 0.5, e_L = 0.16	e = 0.5
a(dm)	*Fig. 2.3*	0.087	0.094	0.331
a(gm)	*Fig. 2.3*	0.087	0.091	0.333
a(gm,LCA)	Eq. **(2.24)**	0.087	–	0.333
b(dm)	*Fig. 2.4*	0.173	0.214	0.656
b(gm)	*Fig. 2.4*	0.173	0.199	0.664
b(gm,LCA)	Eq. **(2.24)**	0.174	–	0.667
c(dm)	*Fig. 2.5*	1.086	1.104	1.328
c(gm)	*Fig. 2.5*	1.087	1.097	1.332
c(gm,LCA)	Eq. **(2.24)**	1.087	–	1.333
g(dm)	*Fig. 2.6*	0.159	0.183	0.496
g(gm)	*Fig. 2.6*	0.160	0.174	0.499
g(gm,LCA)	Eq. **(2.26)**	0.160	–	0.500
G(dm)	*Fig. 2.6*	1.106	0.290	1.556
G(gm)	*Fig. 2.6*	1.095	0.263	1.355
G(gm,LCA)	Eq. **(2.26)**	1.099	–	1.368

The relevance of all this is as follows: for a steady-state system in which negligible transfer occurs, measurement of a, b or c yields e, *via* eq. **(2.24)**. There is no requirement to know the cross-termination model which applies, as for $e \leq 0.5$ (at least) the relationships of eq. **(2.24)**

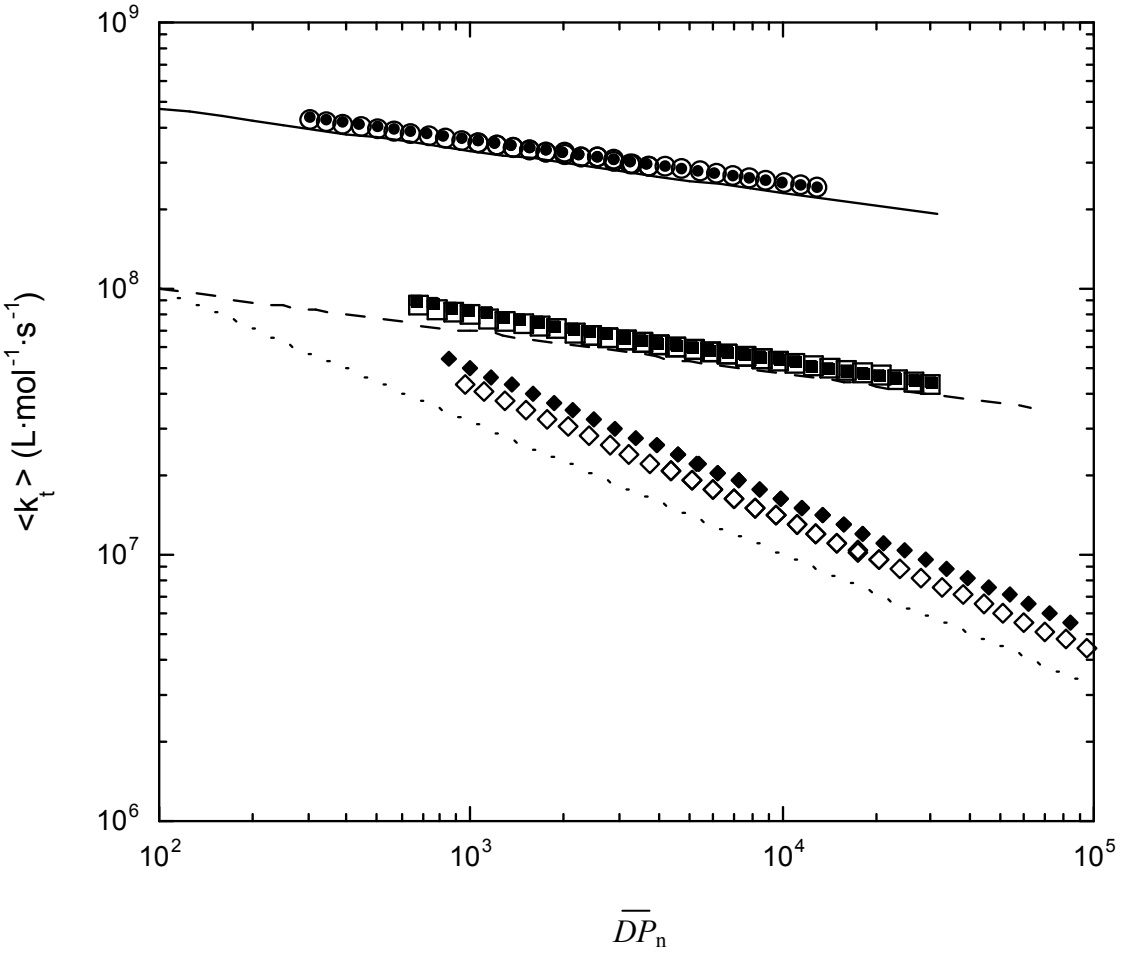

Fig. 2.6 Overall termination rate coefficient $<k_t>$ versus number-average degree of polymerisation of dead chains, $\overline{DP}_n$. Values are from the calculations of *Fig. 2.3* and *Fig. 2.4*, with the same symbols being used (points). The lines are the values of $k_t^{i,i}$ used in the three sets of calculations: $e_S = e_L = 0.16$ (upper, unbroken line), $e_S = 0.5$ and $e_L = 0.16$ (middle, dashed line), and $e_S = e_L = 0.5$ (lower, dotted line).

hold independent of the functional form of $k_t^{i,j}$. Thus one has a simple, elegant route to determining the power describing the chain-length dependence of termination. As has been summarised,[34,43] careful investigations have typically found $a \approx 0.1$. Values of b quite a bit higher than $2a$ (see eq. **(2.24)**) have typically been found, however these values cannot be taken at face value, because in varying [M] the solution viscosity has also usually been varied, thereby violating the requirement of a constant $k_t^{1,1}$ (compare eqs. **(2.22)** and **(2.23a)**). Measurements of $<k_t>$ purely as a function of $k_t^{1,1}$ (by varying solvent viscosity while keeping solvent power constant so that e does not vary) are consistent with $c \approx 1$.[47,48] Considering all this information, one can say that steady state polymerisation data is consistent with $e \approx 0.2$ or less, consistent with the e values of *Tab. 2.1*. What the present calculations have shown is that this does not mean that e is this small in value for all lengths of chains. Specifically - and this is the really important point - our $e_S = 0.5$, $e_L = 0.16$ model is fully consistent with experiment. However, what the experimental data for a, b and c does preclude is the possibility[19] of $e_L \approx 0.5$ for low-conversion systems.

Now we consider the results of *Fig. 2.6*. When termination is chain-length independent ($e = 0$), $<k_t>$ is independent of variations of $\overline{DP}_n$ as [I] and [M] are varied. Thus a plot of $<k_t>$ versus $\overline{DP}_n$ will be a flat line. *Fig. 2.6* reveals that this is no longer the case when termination is chain-length dependent: $<k_t>$ decreases as $\overline{DP}_n$ increases. This is to be qualitatively understood by realising that a larger $\overline{DP}_n$ reflects a radical chain length distribution that must be more weighted toward long chain lengths, which means a lower $<k_t>$. For obvious reasons it is desirable to quantify this intuitive idea. It is evident that the data of *Fig. 2.6* are very well described by

$$<k_t> \;=\; k_t^{1,1}\, G\, (\overline{DP}_n)^{-g} \qquad \textbf{(2.25)}$$

Using eq. **(2.23a)** and expressions given by Olaj *et al.*[38,42] for $\overline{DP}_n$(gm,LCA), the geometric mean value of $\overline{DP}_n$ in the long-chain limit and in the absence of transfer, one can show that

$$<k_t>(\text{gm,LCA}) = k_t^{1,1}\left(\Gamma\left(\frac{2}{2\text{-}e}\right)\right)^{e\text{-}2}\left(\frac{2}{(2\text{-}e)}\frac{2}{(1+\lambda)}\right)^{e}\left(\overline{DP}_n(\text{gm,LCA})\right)^{-e} \qquad \textbf{(2.23b)}$$

Hence one sees that

$$g(\text{gm,LCA}) = e\,,\quad G(\text{gm,LCA}) = \left(\Gamma\left(\frac{2}{2\text{-}e}\right)\right)^{e\text{-}2}\left(\frac{2}{(2\text{-}e)}\frac{2}{(1+\lambda)}\right)^{e} \qquad \textbf{(2.26)}$$

Note that both Mahabadi papers[2,7] unfortunately give incorrect expressions for G(gm,LCA). *Tab. 2.3* also compares the predictions of eq. **(2.26)** with the actual values from the calculations of this work. (1) As with a, b and c it is evident that g(gm,LCA) ≈ g(gm) ≈ g(dm), meaning once again that the scaling behavior does not discriminate between the two models. (2) Not surprisingly the value of G(gm,LCA) is accurate for the gm at both e = 0.16 and 0.5, but for the dm it is only accurate for the lower e value: by e = 0.5 the absolute values of $<k_t>$ with the dm are significantly above the corresponding gm values. (3) As is also the case with a, b and c values (see above), the scaling behaviour (g values) of the $<k_t>$(e_S = 0.5, e_L = 0.16) results is determined predominantly by e_L (= 0.16) and hardly at all by e_S (= 0.5). (4) G for the $<k_t>$(e_S = 0.5, e_L = 0.16) results is very much less than might be expected. That this is very significant will soon become clear.

Now it should be evident why the present calculations have been carried out: because they mimic a way in which e and $k_t^{1,1}$ have been estimated from experimental data. (1) e can very simply be determined as the slope of a log-log plot of $<k_t>$ versus $\overline{DP}_n$ values from steady state experiments. It was in this way that Mahabadi[2,7] determined e (see *Tab. 2.1*) (notwithstanding that in the first instance[2] he actually used non-steady state data, a procedure

only subsequently shown to be legitimate[33], see below). The significance of the present simulations is that they show that Mahabadi's findings of $e \approx 0.15$ - 0.25 are fully consistent with the actual value of e for small chains being much higher - see the $\langle k_t \rangle (e_S = 0.5, e_L = 0.16)$ results for g in *Tab. 2.3*. (2) The value of $k_t^{1,1}$ is obtained from the intercept of a plot of $\log\langle k_t \rangle$ versus $\log\overline{DP}_n$. Because G is close in value to 1, to first approximation one can use intercept $\approx k_t^{1,1}$. A more refined estimate can be obtained by using the experimentally obtained e value to calculate G with eq. **(2.26)**, and then evaluating $k_t^{1,1}$ = intercept / G, as done by Mahabadi.[2] A really significant result from the present calculations is that this procedure underestimates the value of $k_t^{1,1}$ by almost an order of magnitude with the $e_S = 0.5$, $e_L = 0.16$ model, because the actual G is almost an order of magnitude less than the G one would expect on the basis of g. This immediately explains one of the problems which motivated this work, that values of $k_t^{1,1}$ deduced from FRP experiments are about an order of magnitude lower in value than they should be (see section 2.1). Thus our model seems to be consistent both with the results of steady state experiments and what is independently known about $k_t^{1,1}$.

Regarding the above method of determining $k_t^{1,1}$ and e, a nice thing about it is that one can use any data as long as $k_t^{1,1}$ doesn't vary. Thus one can use results from experiments in which both [I] and [M] are varied (cf. measurement of a and b), however one cannot use data in which viscosity is varied. This is why values of $\overline{DP}_n$ from the calculations behind *Fig. 2.5* have not been included in *Fig. 2.6*. Nevertheless, eq. **(2.23b)** makes clear how $\langle k_t \rangle / k_t^{1,1}$ varies with $\overline{DP}_n$ due to variation of $k_t^{1,1}$. So if one was confident of the relationship between $k_t^{1,1}$ and viscosity (say $k_t^{1,1} \sim \eta^{-1}$), one could use appropriately scaled values of $\langle k_t \rangle$ to determine e and the value of $k_t^{1,1}$ at a reference viscosity.

Finally, we return to the intuitive idea that pairs of $\langle k_t \rangle$-$\overline{DP}_n$ values might directly reveal something about $k_t^{i,i}$. To this end, the three lots of $k_t^{i,i}$ values used in calculations ($e = 0.16$; $e_S = 0.5$, $e_L = 0.16$; and $e = 0.5$) have all been included in *Fig. 2.6*. It is evident that $\langle k_t \rangle$-$\overline{DP}_n$ points mirror very well the $k_t^{i,i}$-i used to generate them. This of course follows from the results of *Tab. 2.3*: when $g = e$ and $G \approx 1$, as has been seen is the case for the one-e calculations, eq. **(2.25)** becomes $\langle k_t \rangle \approx k_t^{1,1}(\overline{DP}_n)^{-e}$. The closer G is to 1, the more exact this relationship becomes. Even for the two-e model, in which the values of g and G are not so directly interpretable, it is evident that $\langle k_t \rangle$-$\overline{DP}_n$ pairs approximate very well the underlying $k_t^{i,i}$. While this has obvious advantages, it also implies the danger of extrapolating $\langle k_t \rangle$ values into regions of $\overline{DP}_n$ where no measurements have been carried out. For example, the $\langle k_t \rangle$($e_S = 0.5$, $e_L = 0.16$) versus $\overline{DP}_n$ data that is presented here underestimate $k_t^{1,1}$ when extrapolated to small i. This is a neat explanation for the much-discussed underestimation of $k_t^{1,1}$ by FRP experiments. Out of interest we calculated $\langle k_t \rangle$($e_S = 0.5$, $e_L = 0.16$) for very small $\overline{DP}_n$ (results not presented). As would be expected we found that the $\langle k_t \rangle$ values started to curve upward toward a much higher intercept. It was observed that the scaling behaviour (a, b, c and g) of the $\langle k_t \rangle$($e_S = 0.5$, $e_L = 0.16$) results presented here is a consequence of them having $\overline{DP}_n$ well in excess of the value $i_c = 100$ used in calculations. This is fully justified in that the $\overline{DP}_n$ of our presented calculations correspond to those observed in SS experiments. This leads to an obvious experimental suggestion for trying to observe if e_S really equals 0.5 for short chains. The problem with implementing this suggestion is that transfer agents are the best way of bringing about very small $\overline{DP}_n$, but then one has transfer-controlled kinetics, whereas the work of this chapter has assumed negligible transfer.

2.5 Pulsed-Laser Polymerisation Simulations

Pulsed-laser polymerisation (PLP) data[3-6] were used to determine the majority of values of $k_t^{1,1}$ and e given in *Tab. 2.1*. Therefore PLP simulations with our termination model will be carried out in this section. Technical details regarding our PLP simulation program have been given elsewhere.[49] Briefly, simulations involve carrying out numerical integration of eqs. **(2.7a)**, **(2.7b)** and **(2.8)**. This is necessary because a steady state never prevails as a consequence of laser pulses inducing periodic bursts of extremely rapid initiation, between which there is negligible creation of new radicals. This is simulated by having $R_{init} = 0$ but increasing $[R_1]$ by an amount ρ at intervals t_d of time. The simulation is carried out until a pseudo-steady state is reached, *i.e.*, the radical loss between laser pulses exactly matches the radical gain as a result of a laser pulse. The simulation is then carried out for one further time period t_d, and the results from this time period only are saved, as it corresponds most closely to the results of an actual PLP lasting hundreds or even thousands of laser pulses. The values of $[D_i]$ from this single time period of pseudo-steady state polymerisation are used to calculate $\overline{DP}_n$ and $\overline{DP}_w$ (eqs. (**2.14**) and (**2.15**) respectively). Calculating a representative $\langle k_t \rangle$ is not as clear-cut, because it is changing constantly with time as a result of the $[R_i]$ changing constantly with time. Olaj *et al.* have recommended[33,50,51] and used[3,4,24,25] the following two ways for obtaining a $\langle k_t \rangle$ which is representative of the termination occurring in a PLP:

$$\overline{DP}_w \langle R_{pol} \rangle = \frac{k_p^{\,2}}{2\langle k_t \rangle_a} [M]^2 (3 - \lambda) \qquad \textbf{(2.27a)}$$

$$\langle R_{pol} \rangle = \frac{1}{t_d} \frac{k_p[M]}{2\langle k_t \rangle_b} \ln\left\{1 + \rho \langle k_t \rangle_b t_d \left[1 + \left(1 + \frac{2}{\rho \langle k_t \rangle_b t_d}\right)^{0.5}\right]\right\} \qquad \textbf{(2.27b)}$$

These will be referred to as methods a and b as indicated. The quantity $<R_{pol}>$ is the average rate of polymerisation over one period of pseudo-steady state polymerisation, determined experimentally from the average conversion per pulse and accessible from simulations as

$$<R_{pol}> \;=\; \frac{1}{t_d}\int_{t'}^{t'+t_d} k_p[M][R]\,dt \;\approx\; \frac{k_p[M]}{t_d}\int_{t'}^{t'+t_d}[R]\,dt \qquad \textbf{(2.28)}$$

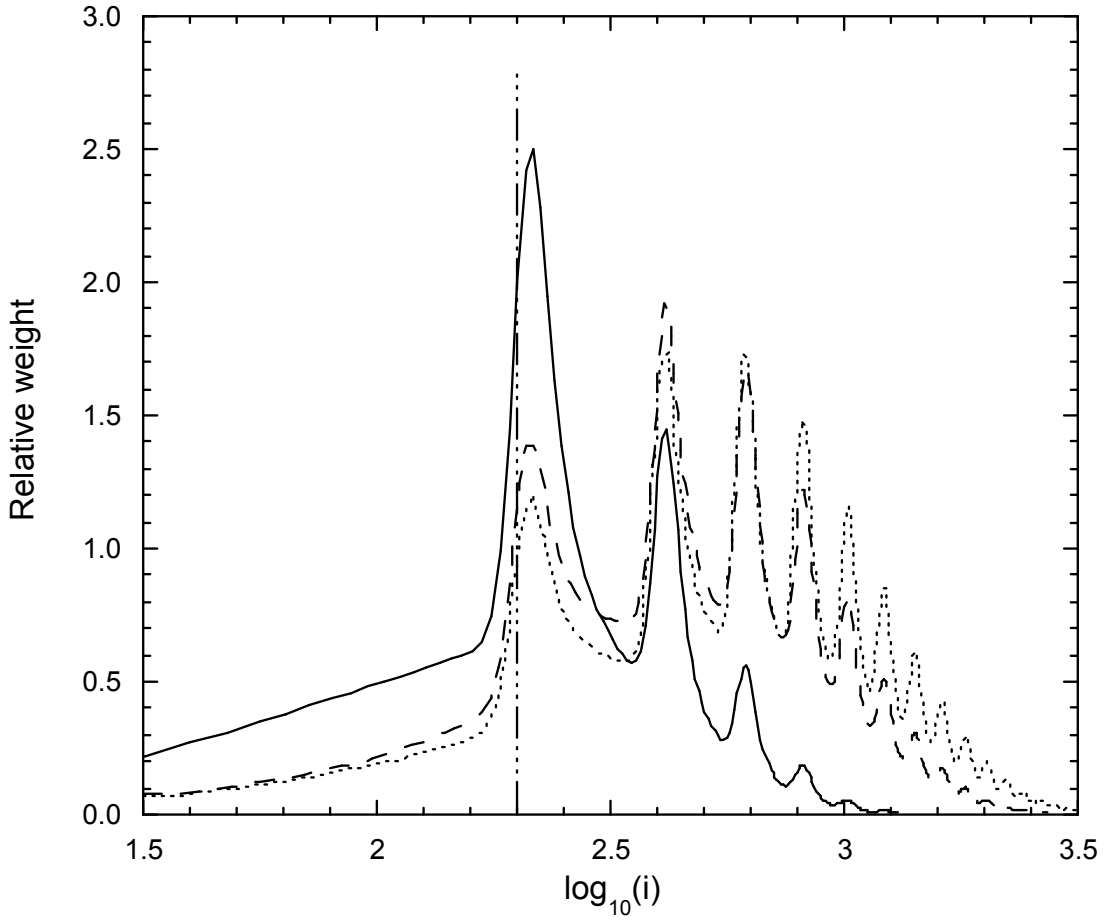

Fig. 2.7 Normalised chain length distributions from PLP simulations using parameter values of *Tab. 2.2*. Results are presented as $w(\log_{10} i)$, where w denotes relative weight and i chain length. Unbroken line: results from simulation with $e_S = e_L = 0.16$; dashed line: $e_S = 0.5$ and $e_L = 0.16$; dotted line: $e_S = e_L = 0.5$. The dot-dashed vertical line denotes the value $k_p[M]t_d$ (see text).

Here t' is any time after attainment of pseudo-steady state. The integral of eq. **(2.28)** is evaluated numerically from simulation data. As indicated, for simplicity our simulations assume that [M] decreases negligibly during a PLP (although if desired it would be no problem to solve d[M]/dt numerically). The value of $\langle k_t \rangle_a$ is found by rearrangement of eq. **(2.27a)**, however the value of $\langle k_t \rangle_b$ can only be obtained by iterative solution of eq. **(2.27b)**.

Standard parameter values for our PLP simulations are as given in *Tab. 2.2*. As in the previous section, and once again for the purpose of comparison, we carry out simulations for three different $k_t^{i,i}$, *viz.* $e = 0.16$; $e_S = 0.5$, $e_L = 0.16$; and $e = 0.5$. However in this section we carry out simulations only with the diffusion mean for $k_t^{i,j}$. In a comprehensive study it has been shown by Olaj *et al.*[33] that, as with steady state polymerisation, the geometric mean gives essentially the same results for PLP as the diffusion mean (this has also been shown for rotating sector polymerisation[52]). Therefore there is no need to carry out simulations with both models.

First of all we present in *Fig. 2.7* the chain length distributions (CLDs) obtained from PLP simulations with the parameter values of *Tab. 2.2*. Qualitatively similar results can be found in the literature.[53] Although it is apparent that each lot of e values results in a different CLD (because termination is different in each case), it is also clear that each CLD has the characteristic structure associated with PLP. Further, it is evident that each CLD affords an accurate estimate of the value of k_p, as can be seen by the position of the chain length $k_p[M]t_d$ in *Fig. 2.7*.[45,54] This is mentioned because in the literature surprisingly few simulations have been presented confirming the validity of the PLP-CLD method for determining k_p in the event of termination being chain length dependent. This said, the focus of this chapter is termination, not k_p.

How can PLP-obtained values of $\langle k_t \rangle$ be used to learn about the chain-length dependence of termination? It turns out the above procedure involving pairs of $\langle k_t \rangle$ and $\overline{DP}_n$ values also works well for PLP in which there is negligible transfer,[33] even though this procedure only has an *a priori* basis for steady state polymerisation. In other words, one plots $\log\langle k_t \rangle$ versus $\log\overline{DP}_n$, and to good approximation the slope is equal to $-e$ while the intercept is close in value to $k_t^{1,1}$. In this way[3,4,24,25] PLP has been used to obtain some of the styrene[3] and MMA[4] values of $k_t^{1,1}$ and e quoted in *Tab. 2.1*. $\overline{DP}_n$ may be experimentally varied by altering either t_d or ρ. In practice both were varied in order to keep $t_d\rho$ approximately constant in value,[3,4] as is recommended from theory.[33] The same approach was therefore taken in this chapter: (1) for simulations with $e_S = e_L = 0.16$, t_d and ρ were varied such that the parameter[33] value $2k_t^{1,1}\rho t_d \approx 5$ was maintained; (2) for $e_S = 0.5$, $e_L = 0.16$ simulations we used $2k_t^{1,1}\rho t_d \approx 10$; while (3) for $e_S = e_L = 0.5$ we used $2k_t^{1,1}\rho t_d \approx 30$. These values were used because they give $\overline{DP}_n$ values traversing much the same range as those in the experiments[3,4] we have in mind. We have reported these values of $2k_t^{1,1}\rho t_d$ because results for the variation of $\langle k_t \rangle$ with $\overline{DP}_n$ do depend on it (both the value itself and whether or not it is held constant) to a small but noticeable extent.

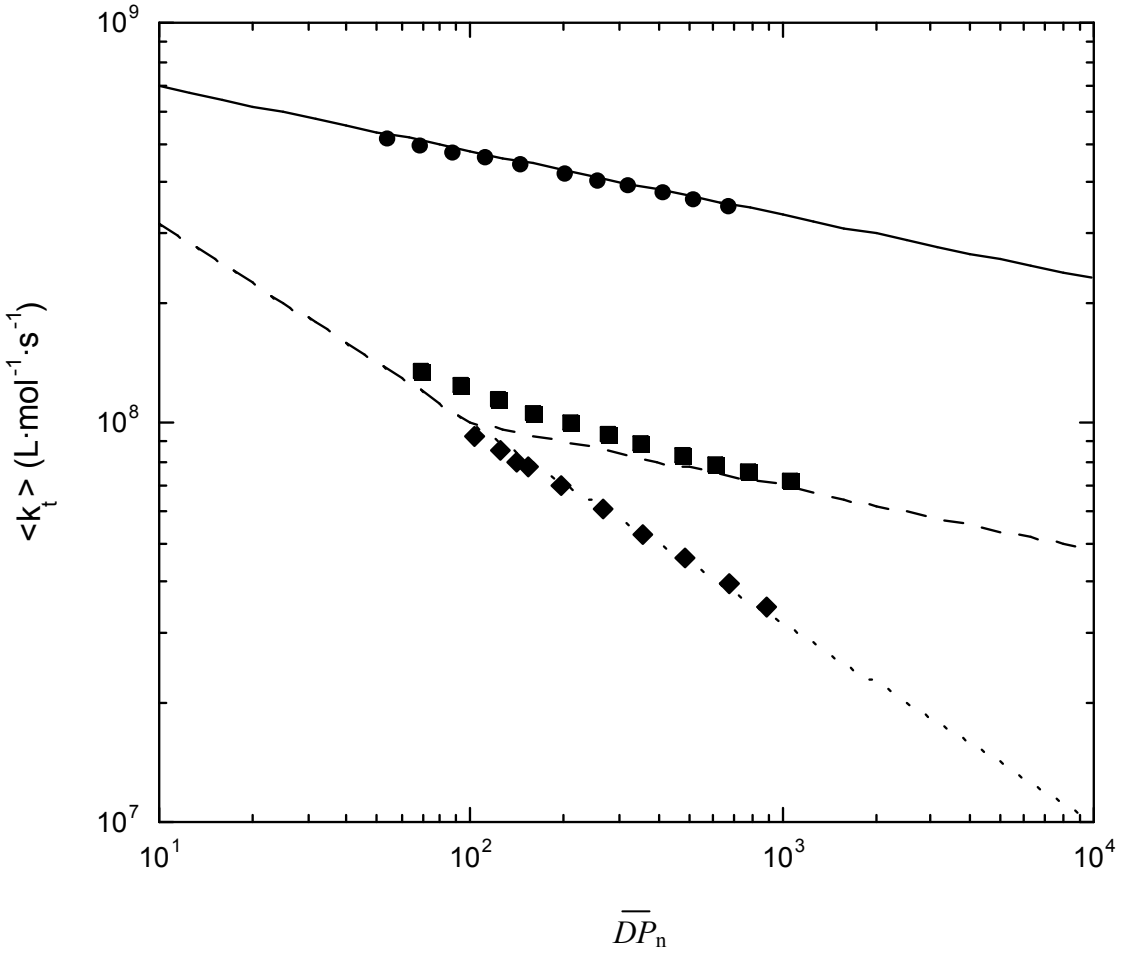

Fig. 2.8 Overall termination rate coefficient $<k_t>$, as evaluated using eq. **(2.27a)**, versus number-average degree of polymerisation of dead chains, $\overline{DP}_n$, from PLP simulations carried out with the parameter values of *Tab. 2.2* and $0.05 \leq t_d$ / s ≤ 0.5 and $7\times10^{-9} \leq \rho$ / mol·L^{-1} $\leq 1\times10^{-7}$ (see text). Circles: results from simulations with $e_S = e_L = 0.16$; squares: $e_S = 0.5$ and $e_L = 0.16$; diamonds: $e_S = e_L = 0.5$. The lines are the values of $k_t^{i,i}$ used in the three sets of simulations: $e_S = e_L = 0.16$ (upper, unbroken line), $e_S = 0.5$ and $e_L = 0.16$ (middle, dashed line), and $e_S = e_L = 0.5$ (lower, dotted line).

For each simulation the values of $<k_t>_a$, $<k_t>_b$ and $\overline{DP}_n$ were obtained. *Fig. 2.8* presents

simulation results as $\log\langle k_t\rangle_a$ versus $\log\overline{DP}_n$, *Fig. 2.9* as $\log\langle k_t\rangle_b$ versus $\log\overline{DP}_n$. (A technical point is that one should not use the actual $\overline{DP}_n$ but rather the $\overline{DP}_n$ one would get if all

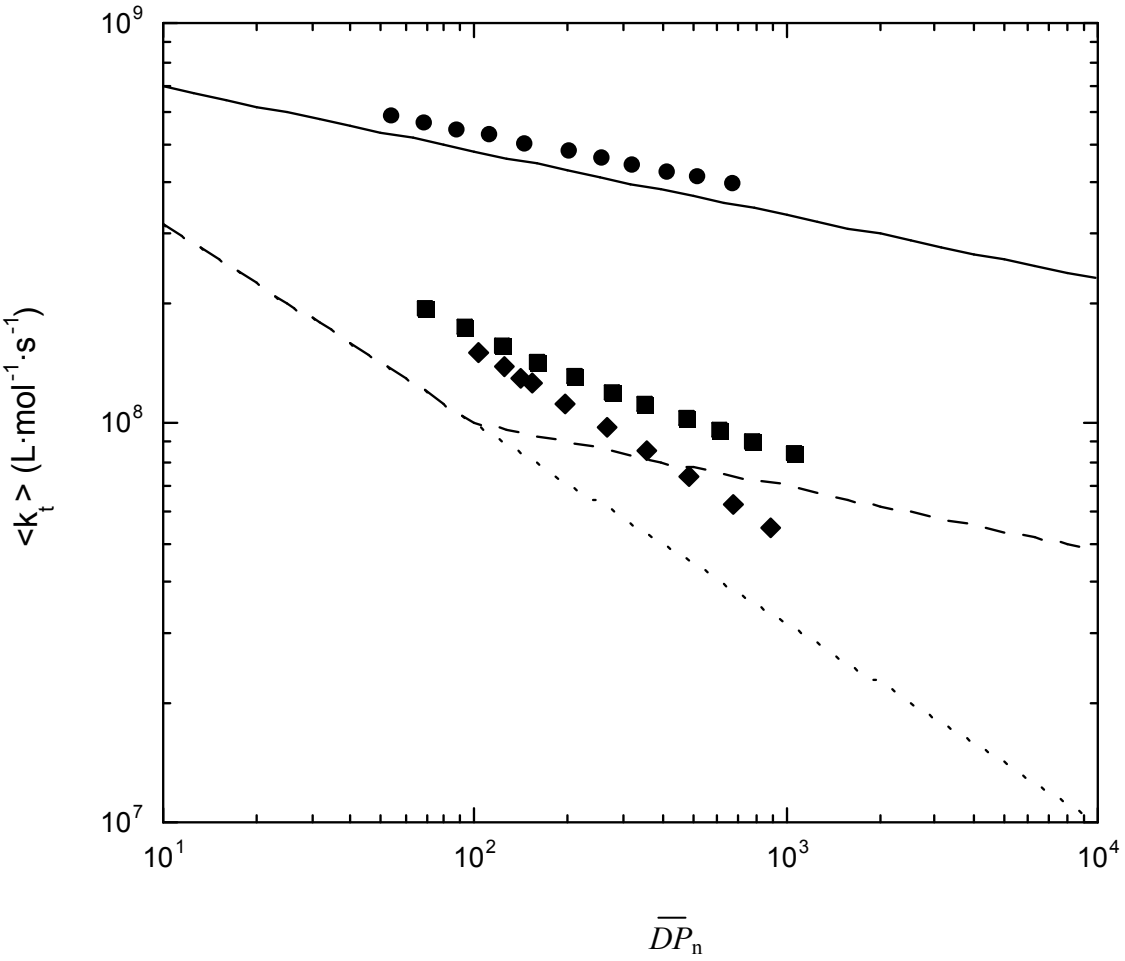

Fig. 2.9 Overall termination rate coefficient $\langle k_t\rangle$, as evaluated using eq. **(2.27b)**, versus number-average degree of polymerisation of dead chains, $\overline{DP}_n$, from PLP simulations carried out with the parameter values of Tab. 2.2 and $0.05 \leq t_d$ / s ≤ 0.5 and $7\times10^{-9} \leq \rho$ / mol·L^{-1} $\leq 1\times10^{-7}$ (see text). Circles: results from simulations with $e_S = e_L = 0.16$; squares: $e_S = 0.5$ and $e_L = 0.16$; diamonds: $e_S = e_L = 0.5$. The lines are the values of $k_t^{i,i}$ used in the three sets of simulations: $e_S = e_L = 0.16$ (upper, unbroken line), $e_S = 0.5$ and $e_L = 0.16$ (middle, dashed line), and $e_S = e_L = 0.5$ (lower, dotted line).

termination was by disproportionation.[3] But in the present case $\lambda = 1$, and so the two values are equal.) Again using the notation of eq. **(2.25)**, the slopes, g, and intercepts relative to $k_t^{1,1}$, G, of the data in *Fig. 2.8* and *Fig. 2.9* are listed in *Tab. 2.4*. Also given are the eq. **(2.26)** values, even though these have no *a priori* basis for PLP results.

The following predominantly technical comments can be made regarding the results of *Fig. 2.8* and *Fig. 2.9*: (1) In several cases where we used the same parameter values as had been used in ref.[33] we established that both lots of simulations gave very close agreement for both $\langle k_t \rangle_a$ and $\langle k_t \rangle_b$. This endorses the different numerical methods employed in each work. (2) Our $\langle k_t \rangle_b$ exceed our $\langle k_t \rangle_a$ by 10-20% for $e = 0.16$ (consistent with experiment[3,4]) and by more for higher e, as also found in the simulations of ref.[33] (3) *Tab. 2.4* shows that $g \approx e$ for

Tab. 2.4 Values of parameters from power law variation of the overall termination rate coefficient $\langle k_t \rangle$ for pulsed-laser polymerisation. The parameters g and G are defined by eq. **(2.25)** and are for $\langle k_t \rangle_a$ and $\langle k_t \rangle_b$ values as indicated. The abbreviation 'gm,LCA' denotes steady-state geometric mean values in the limit of infinitely long chains.

Parameter	Obtained from	$e = 0.16$	$e_S = 0.5$, $e_L = 0.16$	$e = 0.5$
$g(\langle k_t \rangle_a)$	Fig. 2.8	0.154	0.232	0.449
$g(\langle k_t \rangle_b)$	Fig. 2.9	0.155	0.304	0.463
g(gm,LCA)	Eq. **(2.26)**	0.160	–	0.500
$G(\langle k_t \rangle_a)$	Fig. 2.8	0.957	0.350	0.738
$G(\langle k_t \rangle_b)$	Fig. 2.9	1.096	0.678	1.288
G(gm,LCA)	Eq. **(2.26)**	1.099	–	1.368

the one-*e* results. This was established previously for $e = 0.16$[33] but is shown here for the first time for *e* as high as 0.5. (4) Values of *G* obtained from $\langle k_t \rangle_b$ are surprisingly close in value to *G*(gm,LCA) values. This presents an avenue for estimating $k_t^{1,1}$ (as the intercept divided by *G*(gm,LCA), as in the previous section). (5) Alternatively, one might estimate $k_t^{1,1}$ by using $\langle k_t \rangle_a$ values and assuming $G = 1$. This is evident from the remarkable coincidence of $\langle k_t \rangle_a$ and $k_t^{i,i}$ values in *Fig. 2.8*. On the other hand, it is evident from *Fig. 2.9* that $\langle k_t \rangle_b$ results should not be expected to equal $k_t^{i,i}$, which should be remembered in interpreting experimental results. These findings are intriguing in view of the fact that $\langle k_t \rangle_b$ is regarded as the better estimate of the 'true' value of $\langle k_t \rangle$ for a PLP.[33]

Now we consider the results of *Fig. 2.8* and *Fig. 2.9* in relation to actual experimental results.[3,4] (1) Perhaps surprisingly, the experimentally obtained $\langle k_t \rangle_a$ and $\langle k_t \rangle_b$ are closest in absolute value to the simulation results obtained here with $e_S = e_L = 0.5$ (importantly, recall that both lots of results are for similar $\overline{DP}_n$). That said, there is no question that the $e_S = e_L = 0.5$ simulation results show scaling behaviour very different to that observed experimentally (compare *g* of *Tab. 2.4* with *e* of *Tab. 2.1*). (2) Of more importance is that the $e_S = 0.5$, $e_L = 0.16$ simulation results give *g* values which are in encouraging agreement with the experimental *g* of 0.16-0.18 (see *Tab. 2.1*), found for both $\langle k_t \rangle_a$ and $\langle k_t \rangle_b$. This is especially so for the $\langle k_t \rangle_a$ values ($g = 0.23$), even if the $\langle k_t \rangle_b$ value ($g = 0.30$) is rather high. Nevertheless, what is clear from the figures is that *g* values appreciably above $e_L = 0.16$ in value have been found because simulations giving $\overline{DP}_n < i_c = 100$ were carried out. The data of refs.[3,4] does not extend down to $\overline{DP}_n$ this low, and instead extends to $\overline{DP}_n$ above 1000. Because of these larger $\overline{DP}_n$, the experiments will yield an *e* value pertaining to longer chain lengths, whereas in the present simulation results the short-chain value $e_S = 0.5$ is already starting to exert influence. The PLP results we present and the steady-state results above

make it clear what would be observed if PLP simulations with very high $\overline{DP}_n$ were carried out (such simulations are extremely time consuming). (3) Also of importance is that extrapolation of the e_S = 0.5, e_L = 0.16 results will lead to significant underestimation of $k_t^{1,1}$ (see the figures and the *G* values of *Tab. 2.4*). Admittedly the inferred $k_t^{1,1}$ will not be as low as the experimentally obtained values[3,4] (see *Tab. 2.4*). Nevertheless, it is clear that if simulations used a slightly lower $k_t^{1,1}$ than 1×10^9 L·mol^{-1}·s^{-1}, as is justifiable,[17] and if they were carried out to higher $\overline{DP}_n$, then the e_S = 0.5, e_L = 0.16 model would yield $\langle k_t\rangle_a$ and $\langle k_t\rangle_b$ values very much in accord with those obtained experimentally. Of course the $e_S = e_L$ = 0.16 model is also in accord with the PLP data for $\langle k_t\rangle$, it's just that it also requires an uncomfortably low $k_t^{1,1}$ value.

It is evident from the above that the PLP-based methods of deducing $k_t^{1,1}$ and *e* are exactly analogous to one of the steady-state methods which has been examined: in one case one uses $\langle k_t\rangle$ and $\overline{DP}_n$ values from PLP, in the other $\langle k_t\rangle$ and $\overline{DP}_n$ from steady state polymerisation. Further, it would seem that both methods can be misleading in the same way about $k_t^{1,1}$ and e_S. Given that SS experiments are much easier to carry out, why perform PLP in this way to learn about termination? The main advantage would seem to be the more precise control over conversion. However the PLP approach has disadvantages, including: (1) The sharper features of CLDs from PLP make them more subject to distortion by size exclusion chromatography (SEC) broadening. This introduces error into values of $\overline{DP}_n$ and $\overline{DP}_w$, which are both used in deducing $k_t^{1,1}$ and *e*. (It is noted that the effect of SEC broadening on k_p[55] and another method of $\langle k_t\rangle$ determination[56] by PLP have received some investigation.) (2) PLP results in much larger numbers of very small chains than does steady state polymerisation. This also results in inaccuracy in $\overline{DP}_n$ and $\overline{DP}_w$ as determined by SEC. For these reasons one might suggest that careful SS polymerisation should be just as accurate as PLP for

determining $k_t^{1,1}$ and e. At the very least it would be interesting to analyse the one system in both ways and to see if consistent values of $k_t^{1,1}$ and e were obtained. In fact, in a first effort in this regard, SS results for MMA-styrene copolymerisation have recently been reported.[57]

Next we note that the third method developed by Olaj, Vana *et al.*[5] for $k_t^{i,i}$ determination directly gives e at a particular i (as opposed to the two methods investigated above, which give $k_t^{i,i}$ indirectly). Thus there is no need to test this third method with the model of eq. **(2.3)**, because, when applied to simulation results, this method must give $e = e_S$ for $i \leq i_c$ and $e = e_L$ for $i > i_c$. Indeed, applying this third method to actual PLP data suggests that e decreases with i,[5] although the limited precision of the data makes this finding tentative at best. Nevertheless, it is fully consistent with the ideas of this chapter. Related to the above, mention should be made of the pioneering PLP-based method for $k_t^{i,i}$ determination.[58] This method involves time-resolved determination of the rate of polymerisation subsequent to a single laser pulse, and thus, identically to the method of ref.[5], it must recover $k_t^{i,i}$ exactly, as indeed has been established in simulations[59] (interestingly, de Kock *et al.*[59] also propose a method for determining cross-termination rate coefficients from PLP experiments). While the time-resolved PLP method[58] is regarded as being extremely promising for $k_t^{i,i}$ determination, thus far it has not been widely used in this capacity, and in particular it has not been used for styrene and MMA, hence it not being given more attention in this chapter. One limitation of the time-resolved PLP method and indeed of all the methods for $k_t^{i,i}$ determination presented in this chapter is that they assume negligible chain transfer. This is a major limitation which perhaps prevents the widespread application of these methods, for with many monomers the occurrence of significant chain transfer is unavoidable. In this event there is no alternative but to carry out full modeling of rate and/or MWD data (using the appropriate equations in this chapter which include chain transfer). Nevertheless insofar as transfer can be ignored, the

methods of this chapter are general and can be used for any monomer, subject only to experimental realisation.

2.6 Conclusion

The one-*e* model for $k_t^{i,i}$, eq. **(2.1)**, is very simple and contains only the two parameters *e* and $k_t^{1,1}$. Ultimately this model leads to elegant and simple ways of analysing experimental $\langle k_t \rangle$ values to obtain $k_t^{1,1}$ and *e*. Nevertheless the details of how $k_t^{i,i}$ is related to $\langle k_t \rangle$ are complex, and it is necessary to understand these details if one is really to understand what is obtained in experiments. Hence this chapter started with a simple idea but ended up telling a complicated story. Specifically, we were motivated to try and understand how careful FRP experiments have yielded $k_t^{1,1}$ values which are much lower than is to be expected on the basis of small molecule k_t values. We also wanted to see if the value $e \approx 0.2$ from FRP experiments necessarily means that *e* is this small for small chains as well, which is also hard to reconcile with independent data. Hence we proposed a two-*e* model of termination, eqs. **(2.2a)** and **(2.2b)**, not because we adamantly hold that it is a fully correct model for termination, but because it is the simplest model which can incorporate ideas which we feel are likely to be correct, *viz.* $k_t^{1,1} \approx 10^9$ L·mol^{-1}·s^{-1}, $e_S \approx 0.5$ and $e_L \approx 0.2$ (for dilute solution termination of MMA and styrene). This was the simple part. The exhaustive part was showing that this model for $k_t^{i,i}$ is consistent with the best experimental results for $\langle k_t \rangle$. We have not considered all such data here (*e.g.* the Buback / Kowollik approach[6,10] is certainly worth mention), because to do so would be impractical. However we feel we have investigated a broad spectrum of experimental methods. It has emerged that steady-state experimental $\langle k_t \rangle$ data is spectacularly consistent with eq. **(2.3)**. The agreement with PLP data is not so spectacular, but we feel it is still very encouraging. It is hoped that with this chapter, a contribution has been made toward the understanding of dilute solution termination

in particular (the values of e_S, e_L and $k_t^{1,1}$) and termination in FRP in general (the two-*e* model). Further, it is recognised that in both regards there is still a long way to go. Termination in FRP remains a fascinating, elusive phenomenon.

2.7 Postscript

The above chapter was published in its entirety as Smith, G. B.; Russell, G. T.; Heuts, J. P. A. *Macromol. Theory Simul.* **2003**, *12*, 299-314. Since that time, the ideas presented here have been spectacularly verified in various careful and independent experiments of a sophisticated nature. The first such study[60] used Buback's new technique of SP-PLP-ESR, which will be the subject of Chapter 6 of this thesis. For dodecyl methacrylate at 0 °C it was found that e_S = 0.5, e_L = 0.16, and $i_c \approx 100$.[60] Using the same technique, essentially the same values were found a short time later to hold also for dibutyl itaconate.[61] Next, and as a result of the work of Chapter 6, a more refined analysis of the original dodecyl methacrylate data was carried out, together with analysis of new data for benzyl methacrylate and cyclohexyl methacrylate.[62] For all three monomers the composite termination model was found to hold, with the only nuances being that e_S seems to be slightly higher for dodecyl methacrylate (0.65) while i_c seems to be slightly lower (of order 50) for the two systems with cyclic pendant groups on the polymer chain. It is stressed that these findings are not the result of taking the composite termination model and insisting that it be fitted to the experimental data; rather the data genuinely suggests that there are two termination regimes, exactly as postulated in this chapter. Less clear-cut in this regard is the data from Barner-Kowollik's so-called RAFT-CLD-T technique,[63] which is essentially just a living radical polymerisation analogue of SP-PLP.[64] When this technique came to be applied to methyl methacrylate,[65] it was found that the slope of a plot of $\log k_t^{i,i}$ *vs.* log*i* seems to gradually become less negative. At the same time, it was also found that a plot of $\log k_t^{i,i}$ *vs.* log*i* was well described by e_S =

0.65, $e_L = 0.16$, $i_c = 100$, and $k_t^{1,1} \approx 10^9$ L mol^{-1} s^{-1}, despite the aforementioned curvature of the plot. Thus, this data also confirms the composite termination model, which by now can be regarded as an accepted model for CLDT.

References

(1) Buback, M.; Egorov, M.; Gilbert, R. G.; Kaminsky, V.; Olaj, O. F.; Russell, G. T.; Vana, P.; Zifferer, G. *Macromol. Chem. Phys.* **2002**, *203*, 2570-2582.

(2) Mahabadi, H. K. *Macromolecules* **1985**, *18*, 1319-1324.

(3) Olaj, O. F.; Vana, P. *Macromol. Rapid Commun.* **1998**, *19*, 433-439.

(4) Olaj, O. F.; Vana, P. *Macromol. Rapid Commun.* **1998**, *19*, 533-538.

(5) Olaj, O. F.; Vana, P.; Kornherr, A.; Zifferer, G. *Macromol. Chem. Phys.* **1999**, *200*, 2031-2039.

(6) Buback, M.; Busch, M.; Kowollik, C. *Macromol. Theory Simul.* **2000**, *9*, 442-452.

(7) Mahabadi, H. K. *Macromolecules* **1991**, *24*, 606-609.

(8) O'Driscoll, K. F.; Mahabadi, H. K. *J. Polym. Sci., Polym. Chem. Ed.* **1976**, *14*, 869-881.

(9) Mahabadi, H. K.; O'Driscoll, K. F. *J. Macromol. Sci., Chem.* **1977**, *A11*, 967-976.

(10) Buback, M.; Kowollik, C.; Kurz, C.; Wahl, A. *Macromol. Chem. Phys.* **2000**, *201*, 464-469.

(11) Ito, K. *J. Polym. Sci., Polym. Chem. Ed.* **1974**, *12*, 2581-2593.

(12) Friedman, B.; O'Shaughnessy, B. *Macromolecules* **1993**, *26*, 5726-5739.

(13) Olaj, O. F.; Zifferer, G. *Makromol. Chem., Rapid Commun.* **1982**, *3*, 549-556.

(14) Khokhlov, A. R. *Makromol. Chem., Rapid Commun.* **1981**, *2*, 633-636.

(15) Wisnudel, M. B.; Torkelson, J. M. *J. Polym. Sci., Polym. Phys. Ed.* **1996**, *34*, 2999-3008.

(16) Mita, I.; Horie, K. *J. Macromol. Sci., Rev. Macromol. Chem. Phys.* **1987**, *C27*, 91-169.

(17) Fischer, H.; Paul, H. *Acc. Chem. Res.* **1987**, *20*, 200-206.

(18) Kothe, T.; Marque, S.; Martschke, R.; Popov, M.; Fischer, H. *J. Chem. Soc., Perkin Trans. 2* **1998**, 1553-1559.

(19) Russell, G. T. *Macromol. Theory Simul.* **1995**, *4*, 497-517.

(20) Piton, M. C.; Gilbert, R. G.; Chapman, B. E.; Kuchel, P. W. *Macromolecules* **1993**, *26*, 4472.

(21) Griffiths, M. C.; Strauch, J.; Monteiro, M. J.; Gilbert, R. G. *Macromolecules* **1998**, *31*, 7835-7844.

(22) Huber, K.; Bantle, S.; Lutz, P.; Burchard, W. *Macromolecules* **1985**, *18*, 1461-1467.

(23) Amin Sanayei, R.; O'Driscoll, K. F. *J. Macromol. Sci., Chem.* **1991**, *A28*, 987-1000.

(24) Olaj, O. F.; Vana, P. *J. Polym. Sci., Polym. Chem. Ed.* **2000**, *38*, 697-705.

(25) Olaj, O. F.; Zoder, M.; Vana, P. *Macromolecules* **2001**, *34*, 441-446.

(26) Stukelj, M.; Martinho, J. M. G.; Winnik, M. A.; Quirk, R. P. *Macromolecules* **1991**, *24*, 2488-2492.

(27) O'Driscoll, K. F. In *Chain Polymerization I*; Eastwood, G. C., Ledwith, A., Russo, S., Sigwalt, P., Eds.; Pergamon: Oxford, 1989; Vol. 3, pp 161-170.

(28) Mahabadi, H. K.; O'Driscoll, K. F. *Macromolecules* **1977**, *10*, 55-58.

(29) Mahabadi, H. K.; O'Driscoll, K. F. *J. Polym. Sci., Polym. Chem. Ed.* **1977**, *15*, 283-300.

(30) de Kock, J. B. L., Ph.D. Thesis, Technical University of Eindhoven, 1999

(31) Clay, P. A.; Gilbert, R. G.; Russell, G. T. *Macromolecules* **1997**, *30*, 1935-1946.

(32) Olaj, O. F.; Zifferer, G. *Macromolecules* **1987**, *20*, 850-861.

(33) Olaj, O. F.; Kornherr, A.; Zifferer, G. *Macromol. Theory Simul.* **1998**, *7*, 501-508.

(34) Russell, G. T. *Aust. J. Chem.* **2002**, *55*, 399-414.

(35) Russell, G. T.; Gilbert, R. G.; Napper, D. H. *Macromolecules* **1993**, *26*, 3538-3552.

(36) Clay, P. A.; Gilbert, R. G. *Macromolecules* **1995**, *28*, 552-569.

(37) Soh, S. K.; Sundberg, D. C. *J. Polym. Sci., Polym. Chem. Ed.* **1982**, *20*, 1299-1313.

(38) Olaj, O. F.; Zifferer, G.; Gleixner, G. *Makromol. Chem., Rapid Commun.* **1985**, *6*, 773-784.

(39) Allen, P. E. M.; Patrick, C. R. *Makromol. Chem.* **1961**, *47*, 154-167.

(40) Olaj, O. F.; Zifferer, G.; Gleixner, G. *Makromol. Chem.* **1986**, *187*, 977-994.

(41) Russell, G. T. *Macromol. Theory Simul.* **1994**, *3*, 439-468.

(42) Olaj, O. F.; Zifferer, G.; Gleixner, G. *Macromolecules* **1987**, *20*, 839-850.

(43) Russell, G. T. *Macromol. Theory Simul.* **1995**, *4*, 519-548.

(44) Beuermann, S.; Buback, M.; Davis, T. P.; Gilbert, R. G.; Hutchinson, R. A.; Olaj, O. F.; Russell, G. T.; Schweer, J.; van Herk, A. M. *Macromol. Chem. Phys.* **1997**, *198*, 1545-1560.

(45) Buback, M.; Gilbert, R. G.; Hutchinson, R. A.; Klumperman, B.; Kuchta, F.-D.; Manders, B. G.; O'Driscoll, K. F.; Russell, G. T.; Schweer, J. *Macromol. Chem. Phys.* **1995**, *196*, 3267-3280.

(46) Olaj, O. F.; Zifferer, G.; Gleixner, G.; Stickler, M. *Eur. Polym. J.* **1986**, *22*, 585-595.

(47) Fischer, J. P.; Mücke, G.; Schulz, G. V. *Ber. Bunsen-Ges. Phys. Chem.* **1969**, *73*, 154-163.

(48) Fischer, J. P.; Schulz, G. V. *Ber. Bunsen-Ges. Phys. Chem.* **1970**, *74*, 1077-1082.

(49) Tanaka, K.; Yamada, B.; Fellows, C. M.; Gilbert, R. G.; Davis, T. P.; Yee, L. H.; Smith, G. B.; Rees, M. T. L.; Russell, G. T. *J. Polym. Sci., Polym. Chem. Ed.* **2001**, *39*, 3902-3915.

(50) Olaj, O. F.; Kornherr, A.; Zifferer, G. *Macromol. Rapid Commun.* **1997**, *18*, 997-1007.

(51) Olaj, O. F.; Kornherr, A.; Zifferer, G. *Macromol. Rapid Commun.* **1998**, *19*, 89-96.

(52) Olaj, O. F.; Kornherr, A.; Zifferer, G. *Macromolecules* **1999**, *32*, 8800-8806.

(53) Buback, M.; Busch, M.; Lämmel, R. *DECHEMA Monogr.* **1995**, *131*, 569-577.

(54) Olaj, O. F.; Bitai, I.; Hinkelmann, F. *Makromol. Chem.* **1987**, *188*, 1689-1702.

(55) Buback, M.; Busch, M.; Lämmel, R. A. *Macromol. Theory Simul.* **1996**, *5*, 845-861.

(56) Buback, M.; Lämmel, R. A. *Macromol. Theory Simul.* **1998**, *7*, 197-202.

(57) Olaj, O. F.; Kornherr, A.; Vana, P.; Zoder, M.; Zifferer, G. *Macromol. Symp.* **2002**, *182*, 15-30.

(58) Buback, M.; Schweer, J. *Z. Phys. Chem. (Munich)* **1989**, *161*, 153-165.

(59) de Kock, J. B. L.; Klumperman, B.; van Herk, A. M.; German, A. L. *Macromolecules* **1997**, *30*, 6743-6753.

(60) Buback, M.; Egorov, M.; Junkers, T.; Panchenko, E. *Macromol. Rapid Commun.* **2004**, *25*, 1004-1009.

(61) Buback, M.; Egorov, M.; Junkers, T.; Panchenko, E. *Macromol. Chem. Phys.* **2005**, *206*, 333-341.

(62) Buback, M.; Müller, E.; Russell, G. T. *J. Phys. Chem. A* **2006**, *110*, 3222-3230.

(63) Vana, P.; Davis, T. P.; Barner-Kowollik, C. *Macromol. Rapid Commun.* **2002**, *23*, 952-956.

(64) Barner-Kowollik, C.; Buback, M.; Egorov, M.; Fukuda, T.; Goto, A.; Olaj, O. F.; Russell, G. T.; Vana, P.; Yamada, B.; Zetterlund, P. B. *Prog. Polym. Sci.* **2005**, *30*, 605-643.

(65) Johnston-Hall, G.; Theis, A.; Monteiro, M. J.; Davis, T. P.; Stenzel, M. H.; Barner-Kowollik, C. *Macromol. Chem. Phys.* **2005**, *206*, 2047-2053.

3 Testing a Composite Model for Termination in Free Radical Polymerisation at Low Chain-Lengths

Abstract

In this chapter, the composite termination model proposed in Chapter 2 is tested by simultaneously modeling experimental rate and molecular weight distribution data for the continuously initiated free radical polymerisation of methyl methacrylate at 60°C. Very high concentrations of dodecanethiol chain transfer agent are added so as to produce short chains, in order to investigate the appropriateness of the composite termination model at short chain-lengths. It is found that inclusion of chain-length dependent propagation leads to excellent modeling results, and also helps to explain some puzzling features of the experimental data.

3.1 Introduction

The last 2 decades have seen a great revival of free-radical polymerisation (FRP) kinetics, mainly due to the advent of pulsed-laser polymerisation (PLP) and the general availability of more sophisticated molecular weight analysis instrumentation. Although, because of these developments we can state that we are well underway in measuring and understanding the magnitudes of propagation rate coefficients, there is still considerable debate about the termination rate coefficient. It has been well-established for several decades that the termination rate coefficient is chain-length dependent and is governed by the rate of several different diffusion processes. This means that there is no such thing as *the* termination rate coefficient of a given monomer at a given temperature, but that it is a function of many different factors such as chain length, viscosity (and hence monomer conversion), monomer and temperature.

Several different research groups over the past few decades have put a considerable effort into measuring termination rate coefficients as a function of these factors and have come up with (often complicated mathematical) models to describe the termination process. Although the relatively complicated nature of the problem has often limited the research of termination reactions to the more theoretically inclined kineticists, the basic kinetic problem is still a very simple one. One of the most important process parameters is the rate of polymerisation, R_{pol}, which is determined by an average termination rate coefficient, $\langle k_t \rangle$. This is not a constant, but a complicated function of the factors already mentioned above:

$$R_{pol} = \langle k_p \rangle [M] \sqrt{\frac{f k_d [I]}{\langle k_t \rangle}} \qquad \textbf{(3.1)}$$

In this expression $\langle k_p \rangle$ is the (chain-length-averaged) propagation rate coefficient, [M] the monomer concentration, f the initiator efficiency, k_d the initiator decomposition rate coefficient, and [I] the initiator concentration.

$$\langle k_t \rangle = \sum_{i=1}^{\infty} \sum_{j=1}^{\infty} k_t^{i,j} \frac{[R_i]}{[R]} \frac{[R_j]}{[R]} \qquad \textbf{(3.2)}$$

The average termination rate coefficient is given by eq. **(3.2)**, from which it can be seen that it is an average of all possible termination reaction rates between radicals R of chain lengths i and j. In this equation, [R] is the total radical concentration, and $k_t^{i,j}$ is the termination rate coefficient between two radicals R_i and R_j; $k_t^{i,j}$ depends on the monomer type, temperature and viscosity. Much theoretical work focuses on finding an adequate description for $k_t^{i,j}$, with the following power law standardly being used:

$$k_t^{i,i} = k_t^{1,1} \, i^{-e} \qquad \textbf{(3.3)}$$

In this equation, e is an exponent that describes the strength of the chain-length dependence of termination and $k_t^{1,1}$ is the rate coefficient for termination between radicals of degree of polymerisation 1. Recently,[1] in the work in chapter 2, it was proposed that it is unreasonable to expect e to be independent of chain length in reality. As a first effort in doing away with this assumption, the following 'two-e' model was proposed:

$$k_t^{i,i} = k_t^{1,1}\, i^{-e_S}, \quad i \le i_c \qquad \textbf{(3.4a)}$$

$$k_t^{i,i} = k_t^{1,1}\, (i_c)^{-e_S+e_L}\, i^{-e_L}, \quad i > i_c \qquad \textbf{(3.4b)}$$

As is evident from eqs. **(3.4)**, two types of chains are recognised, short and long, each having their own value of e: e_S for short chains and e_L for long chains. The basic motivation for this model is that termination is diffusion controlled, and diffusion coefficients are well known to display different behaviour depending on chain length.[2,3] Further, this model allows the recovery from FRP data of a value of $k_t^{1,1}$ that is more in line with experimental measurements[4] than what is obtained when eq. **(3.3)** is used.[5-7] At the time this was the primary driving force for the proposal of the above model, with only limited experimental data existing that suggested that e can vary with chain length.[8,9] However subsequently there has emerged further evidence in this regard.[10,11] Perhaps the more interesting of these studies was the one in which time-resolved EPR spectroscopy was used to *directly* follow the free radical concentration consequent upon a irradiation of a FRP system by a single laser pulse.[11] Rather remarkably, it was found that the data were best fitted by $e_S \approx 0.2$, $e_L \approx 0.5$ and $i_c \approx 100$, exactly as proposed.[1] Of course more complicated variations of e with chain length can be envisaged, but especially in view of the EPR experiments[11] it seems sensible to adopt the above model in further tests of the basic concept of chain-length dependent e values.

In the current work we present our own experimental investigations into the model of eqs. **(3.4)**. Of course this model focuses attention on the termination kinetics of very short chains,

therefore it makes sense to carry out experiments involving relatively high amounts of very short chains. This can be achieved using a chain transfer agent (CTA; prohibitively high initiator concentrations would be required to effect the reduction of average chain length desired here). Hence we measure the rate and molecular weight distribution (MWD) of polymerisations of methyl methacrylate (MMA) in bulk at 60°C in which the chain length is regulated up to high concentrations of dodecanethiol (DDM). We then model these results, seeking confirmation of the correctness of our termination model.

Notwithstanding that the present work was conceived and carried out independently of the other recent investigations[10,11] into chain-length-dependent termination (CLDT), our work is distinguishable from these efforts in the following important ways: (1) Our experiments are steady-state (rather than non-steady state[11]) and involve conventional FRP (rather than living FRP[10]). In other words, a different means of modulating the chain length is used. (2) Both rate and MWD data are simultaneously evaluated rather than just kinetic data alone. (3) Genuine modeling of the data is carried out. (4) Not only is chain-length-dependent propagation (CLDP) recognised in addition to CLDT, but it is concluded that CLDP is pivotal in explaining the data.

3.2 Experimental

The experimental work discussed here was carried out by Ming (Henry) Yin, under the supervision of Dr. Johan P. A. Heuts at the University of New South Wales, Sydney, Australia.

Polymerisation reactions were carried out with methyl methacrylate (MMA) monomer, dodecanethiol (DDM) as chain transfer agent, and 2,2'-azobis(isobutyronitrile) (AIBN) as radical initiator, at a temperature of 60°C.

Conversion of MMA was measured by ^{1}H-NMR, using deuterated DMSO as NMR solvent. The signal ratio, ϕ, of the vinyl protons (δ = 6 - 7 ppm) and the ester methyl group protons (δ = 4.1 – 5 ppm) is related to the fractional conversion, x, by eq. **(3.5)**

$$x = 1 - \frac{3}{2}\phi \qquad \textbf{(3.5)}$$

MWDs were measured by gel permeation chromatography (GPC).

3.3 Experimental Results and Preliminary Analysis

Concentrations of monomer and chain transfer agent

Normally in FRP the level of chain transfer agent (X, DDM) is sufficiently low that the effect of its addition on the concentration of monomer (M, MMA) can be ignored without incursion of significant error. However, due to the desire to generate extremely short chains, such high levels of DDM - up to 13 mol % - were used in this work that this usual assumption cannot be justified, and so the reduction of [MMA] due to addition of DDM had to be taken into account in data analysis and modeling. Assuming ideal mixing, the concentrations of monomer and chain transfer agent are given, quite generally, by eqs. **(3.6)**:

$$[\mathrm{M}] = \frac{1-f_\mathrm{X}}{f_\mathrm{X} V_\mathrm{X} + (1-f_\mathrm{X}) V_\mathrm{M}} \qquad \textbf{(3.6a)}$$

$$[\mathrm{X}] = \frac{f_\mathrm{X}}{f_\mathrm{X} V_\mathrm{X} + (1-f_\mathrm{X}) V_\mathrm{M}} \qquad \textbf{(3.6b)}$$

For this experimental system, f_X is the mole fraction of DDM, and V_M and V_X are the molar volumes of MMA and DDM respectively. We calculate f_X from the experimental quantity [X]/[M] (see *Tab. 3.2*) using

$$f_X = \frac{[X]/[M]}{1 + [X]/[M]} \quad \textbf{(3.7)}$$

The values of V_M and V_X we used can be found in *Tab. 3.1*. The value of V_M at 60°C was easily obtained from the known temperature dependence of the density of MMA:[12]

$$\rho(\text{MMA}) / (\text{g mL}^{-1}) = (1.025934 + 0.001494 \times \text{T} / (°\text{C}))^{-1} \quad \textbf{(3.8)}$$

However, the value of V_X is problematic because we only have available the density of DDM[13] at 25°C, *viz.* 0.846 g mL^{-1}. To estimate its value at 60°C, we make the assumption that the volume fraction of DDM in the mixture is temperature independent.

$$\phi_X = \frac{w_X/\rho_X}{w_X/\rho_X + (1-w_X)/\rho_M} \quad \textbf{(3.9)}$$

Eq. **(3.9)** gives a general expression for the volume fraction (ϕ) of X in terms of the mass fraction (w) of X and the densities (ρ) of X and M. For ϕ_X to be temperature independent clearly requires the relationship expressed in eq. **(3.10)**, where the dash (‘) indicates a value at a different temperature.

$$\rho'_X = \frac{\rho'_M}{\rho_M}\rho_X \quad \textbf{(3.10)}$$

Using this equation in conjunction with known densities gives us an estimate for the density of DDM at 60°C of 0.8063 g mL^{-1}. The molar volumes given in *Tab. 3.1* are then trivially given by eq. **(3.11)**, where M is molar mass and ρ is in g mL^{-1}:

$$V = \frac{M}{1000 \text{ mL L}^{-1} \times \rho} \quad \textbf{(3.11)}$$

Tab. 3.1 Summary of parameter values used in data analysis.

Parameter	Value	Units
fk_d	6.1×10^{-6}	s^{-1}
V_{MMA}	0.1117	L mol^{-1}
V_{DDM}	0.2510	L mol^{-1}
k_p^{∞}	833.77	L mol^{-1} s^{-1}

Rate and MWD results

Typical rate data are shown in *Fig. 3.1*. From the figure it is apparent that the data are adequately described by a single parameter, namely the slope of the line when the data are presented as $-\ln(1-x)$ *vs.* t, where t is time. This indicates that the steady state approximation is applicable over the whole dataset, so that the data should be exactly described by eq. **(3.12)**, the integrated rate law written in terms of conversion, where [R] is the overall radical concentration. In particular, no 'induction time' is evident (a period of negligible polymerisation that is sometimes observed in FRP due to consumption of initiator by various impurities). Also, the observations are limited to low conversion, so that the rate acceleration phenomenon variously known as the gel effect, the Tromsdorff effect, or autoacceleration, is not seen.

$$-\ln(1-x) = \langle k_p \rangle [R]\, t = \langle k_p \rangle \sqrt{\frac{fk_d[I]}{\langle k_t \rangle}}\, t \qquad \textbf{(3.12)}$$

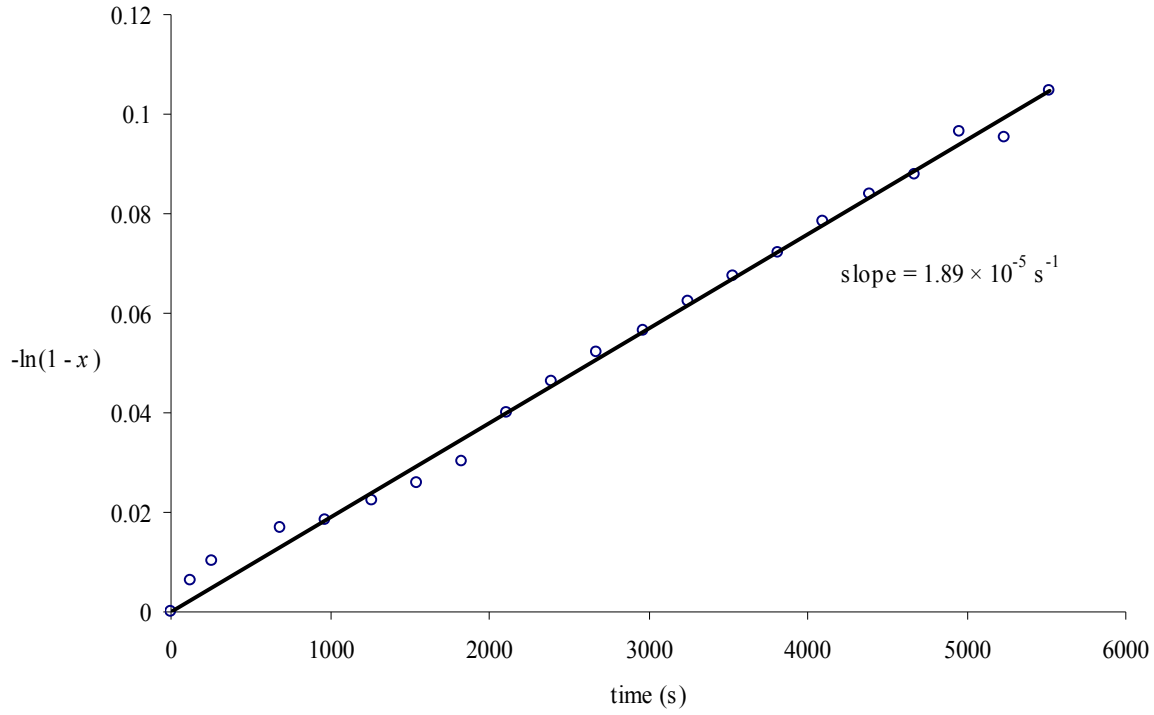

Fig. 3.1 A typical pseudo-first order plot of conversion (x, plotted as $-\ln(1-x)$) *vs.* time (for experiment 61-1 of *Tab. 3.2*) (open circles), with the best fit according to eq. **(3.12)** (line). The slope of the best fit line is indicated.

The rate of initiation can be determined from the known concentration of AIBN (*Tab. 3.2*) and the value[14] $fk_d = 6.1\times10^{-6}$ s^{-1}, so that for each experiment at a particular DDM concentration we can determine the ratio of average rate coefficients $\langle k_p\rangle/\langle k_t\rangle^{0.5}$. For the data presented in *Fig. 3.1*, this ratio is 0.108 $(L\ mol^{-1}\ s^{-1})^{0.5}$.

After determining the ratio $\langle k_p\rangle/\langle k_t\rangle^{0.5}$ for each experiment, the results are presented in *Fig. 3.2*. The dotted line represents the predictions of the classical FRP kinetics model, where the rate coefficients k_p and k_t are assumed to be chain-length independent. Accordingly, the dotted line is simply the mean of the $\langle k_p\rangle/\langle k_t\rangle^{0.5}$ values. Using the measured long-chain

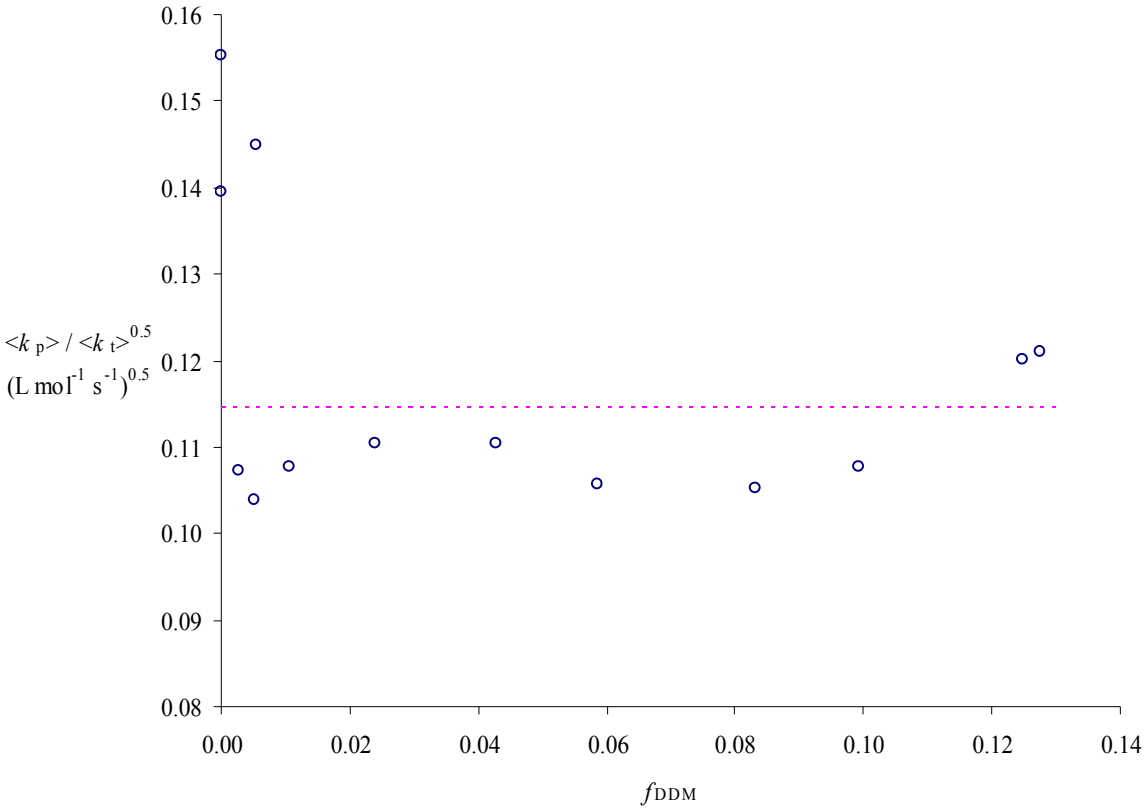

Fig. 3.2 The ratio $\langle k_p \rangle / \langle k_t \rangle^{0.5}$ *vs.* mole fraction of DDM in the polymerisation mixture, f_{DDM} (open circles), and the average value of this ratio (dotted line).

value of k_p,[15] as given in *Tab. 3.1*, the rate coefficient for termination, k_t, is determined to be 5.0×10^7 L mol^{-1} s^{-1}. This is a typical value obtained when assuming classical kinetics. However the trends evident in the data, particularly the higher values of the ratio $\langle k_p \rangle / \langle k_t \rangle^{0.5}$ for low concentrations of DDM, cannot be adequately reproduced by the classical kinetics model, as expected.

Having established some of the kinetic parameters that can be extracted from the rate data, we turn to the molecular weight data.

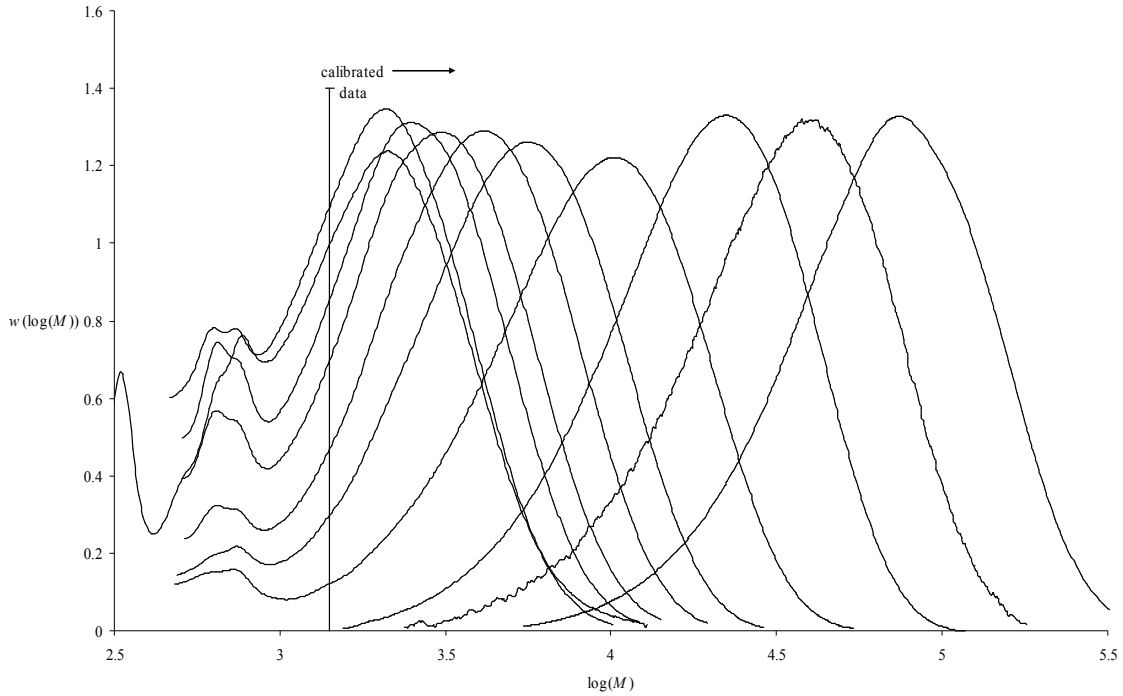

Fig. 3.3 GPC MWD data, plotted as relative weight of polymer, $w(\log(M))$, *vs.* logarithmic molecular weight, $\log(M)$. The vertical line indicates the lower limit of calibration (see discussion in text).

All of the molecular weight distributions obtained for this work are presented in *Fig. 3.3*. As is apparent from the figure, addition of increasing amounts of DDM (moving to the left on the figure) decreased the average molecular weight of the distributions, as was intended.

One subtlety of the gel-permeation chromatography (GPC) technique used to measure these MWDs is that a calibration must be performed with polymer standards of known molecular weight. The region for which the calibration curve is valid is indicated on the graph. Data measured for molecular weights below this point is not only uncalibrated, but also subject to well-known difficulties in measuring the relative amounts of oligomers with GPC. Normally this is not a problem, as GPC distributions tend to be more like those on the right-hand side

of *Fig. 3.3*. In this case however, we need to make allowance for the fact that a significant portion of the low end of the molecular weight distributions can not be measured accurately.

Experimental parameters and a summary of results are shown in *Tab. 3.2*.

Tab. 3.2 Experimental parameters and results.

Exp. Code	$\frac{[DDM]}{[MMA]}$	[AIBN] ($mol \cdot L^{-1} \times 10^{-3}$)	$\langle k_p \rangle [R]$ [a] ($s^{-1} \times 10^{-5}$)	M_{peak} [b] ($g \cdot mol^{-1}$)	$\bar{M}_w$ ($g \cdot mol^{-1}$)	$\bar{M}_n$ ($g \cdot mol^{-1}$)
61-4	1.46×10^{-1}	4.88	2.09	2071	2228	1456
51-1	1.42×10^{-1}	5.26	2.16	2114	2198	1214
51-2	1.10×10^{-1}	5.16	1.92	2484	2782	1750
51-4	9.06×10^{-2}	5.09	1.86	3060	3337	2029
51-5	6.22×10^{-2}	4.99	1.85	4092	4527	2693
51-6	4.47×10^{-2}	4.92	1.92	5608	6117	3454
51-7	2.46×10^{-2}	4.83	1.90	10277	10739	5317
61-1	1.06×10^{-2}	5.03	1.89	22301	23195	14538
61-2	5.45×10^{-3}	5.04	2.55	-	40500	24800
61-6	5.21×10^{-3}	4.86	1.79	37721	40835	24793
61-3	2.62×10^{-3}	5.04	1.89	73758	80151	49320
51-3	0.00	4.72	2.37	-	737000	453000
61-5	0.00	5.05	2.73	-	558000	335000

a) The slope of a plot of $-\ln(1-x)$ *vs.* t - see eq. **(3.12)**.

b) The molar mass corresponding to the peak of the GPC MWD - see *Fig. 3.3*.

The value of the chain transfer constant

We use the Mayo method to determine the value of the chain transfer constant, $C_{trX} = k_{trX}/k_p$ (where k_{trX} refers to transfer to DDM). Normally this involves using the following equation:[16]

$$\left(\overline{DP}_n\right)^{-1} = \left(\overline{DP}_n^{\,0}\right)^{-1} + C_{trX}\frac{[X]}{[M]} \qquad \textbf{(3.13a)}$$

Here $\overline{DP}_n$ is the number-average degree of polymerisation, and thus $\overline{DP}_n^{\,0}$ is the value in the absence of chain transfer agent. This equation makes the long-chain approximation (LCA), which in the present context is dangerous because of the extremely short chain lengths in some experiments. It is not too difficult to show that when the LCA is not made, the following equation is instead obtained when termination is exclusively by disproportionation:

$$\left(\overline{DP}_n - 1\right)^{-1} = \left(\overline{DP}_n^{\,0}\right)^{-1} + C_{trX}\frac{[X]}{[M]} \qquad \textbf{(3.13b)}$$

The $\overline{DP}_n^{\,0}$ here in fact has the same value, in terms of rate coefficients, as in eq. **(3.13a)**. The physical interpretation of this equation is that an additional monomer is incorporated into a chain by the reaction that starts it (whether transfer or initiation), and so it must be subtracted from the measured $\overline{DP}_n$ in using the Mayo equation. Eq. **(3.13b)** will be used here.

Using eq. **(3.13b)**, we can construct *Fig. 3.4*. As noted, the open circles are derived by using values of $\overline{DP}_n$ directly, and the value of C_{trX} thus determined is 0.56 (by comparison, 0.52 is obtained if eq. **(3.13a)** is used to analyse data; this plot is not presented). A better estimate may be obtained by assuming that the polydispersity index, $PDI = \overline{DP}_w / \overline{DP}_n$, is equal to 2, where $\overline{DP}_w$ is the weight-average degree of polymerisation. $PDI = 2$ is the case for classical kinetics in the absence of combination, and should be a good approximation here given the

transfer-dominated nature of most experiments (that said, *PDI* will not exactly equal 2 because the LCA will not hold exactly, as explained above). We can then estimate the value of $\overline{DP}_n$ from the value of M_w, which can be more accurately determined due to the decreased emphasis the weight average places on (inaccurately determined) oligomeric species (see eqs. **(3.23)**). As we would expect from these arguments, the fit in *Fig. 3.4* of the solid line to the filled circles is noticeably better than the fit based on direct use of eq. **(3.13b)**; the value of C_{trX} thus determined is 0.69 (0.63 if eq. **(3.13a)** is used instead).

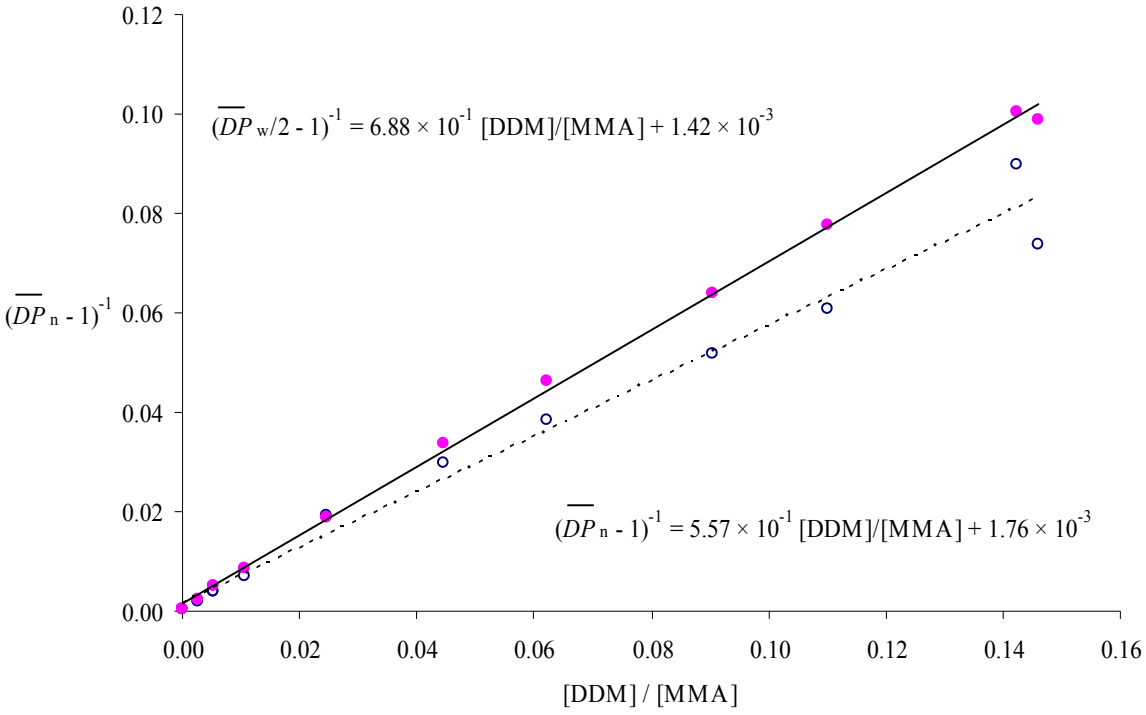

Fig. 3.4 Mayo plot for the data of *Tab. 3.2*, showing values of eq. **(3.13b)** using $\overline{DP}_n$ directly (open circles) with best fit (dotted line), and values of eq. **(3.13b)** using $\overline{DP}_n = \overline{DP}_w/2$ (closed circles) with best fit (solid line). Best fit parameters obtained are as indicated.

The above values for C_{trX} may be compared with literature values for the same quantity (of course for DDM/MMA at 60°C, exactly as here): (1) Heuts *et al.*[17] found $0.97 \leq C_{trX} \leq 1.51$ using $\overline{DP}_n$ values and $1.06 \leq C_{trX} \leq 1.27$ using $\overline{DP}_w$ / 2 values. While eq. **(3.13a)** rather than eq. **(3.13b)** was used, the error thus introduced should have been negligible, as the chains were considerably longer than in the present study. The difference from the present estimates is therefore curious, as the experiments were of the same nature, and in fact were analysed in the same lab. (2) On the other hand, Hutchinson *et al.*[13] used a different type of experiment (PLP) and analysed their data in a different way (using the slope of the high molecular-weight region of the number-MWD[18]), and yet they found the temperature independent value of $C_{trX} = 0.68 \pm 0.02$ over 20 – 80°C, essentially identical to what has been found here. These comparisons suggest that a reliable value of C_{trX} has been found in the present work, but at the same time they also give some idea of the error inherent in determining the value of this parameter.

Finally, it is noted that a better estimate of C_{trX} will emerge in the course of the modeling that follows. To a small extent this is a consequence of the inclusion of chain-length-dependent propagation (the above Mayo approach implicitly assumes chain-length-independent propagation), but mostly it is a result of the use of what we believe is a more accurate index for characterising an MWD (in the present context) than are $\overline{DP}_n$ and $\overline{DP}_w$. The best estimate that is finally obtained is $C_{trX} = 0.82$ (which, it is interesting to note, is a move closer to the values obtained by Heuts *et al.*[17]).

3.4 Kinetic Equations

The reaction scheme used in the modeling of this work is as follows:

$$I \xrightarrow{R_{init}} R_1 \qquad \text{Initiation}$$

$$R_i + M \xrightarrow{k_p^{\,i}} R_{i+1} \qquad \text{Propagation}$$

$$R_i + X \xrightarrow{k_{trX}} D_i + R_1 \qquad \text{Chain transfer}$$

$$R_i + R_j \xrightarrow{k_{td}^{\,i,j}} D_i + D_j \qquad \text{Termination (by disproportionation)}$$

$$R_i + R_j \xrightarrow{k_{tc}^{\,i,j}} D_{i+j} \qquad \text{Termination (by combination)}$$

Here $R_{init} = 2fk_d[I]$ is the rate of initiation. For all calculations in this work we use $fk_d = 6.1\times10^{-6}$ s^{-1} (as in *Tab. 3.1*) and $[I] = 5.0\times10^{-3}$ mol L^{-1}, representative of all the experiments (see *Tab. 3.2*): although there is slight variation of [I] from experiment to experiment, this is inconsequential in modeling because of the transfer-dominated nature of the systems. The above scheme considers chain transfer only to chain transfer agent, X, as this will usually be present in high concentrations, and thus dominate over transfer to monomer or other species. We use $k_t^{\,i,j} = k_{tc}^{\,i,j} + k_{td}^{\,i,j}$ and $\lambda = k_{td}^{\,i,j}/k_t^{\,i,j}$, the number fraction of termination that occurs by disproportionation, assumed to be chain length independent, rather than using the rate coefficients for combination and disproportionation individually. In the calculations of this work we will use $\lambda = 1$, the limit most appropriate for MMA,[19-21] unless otherwise stated. It is recognised that in fact $\lambda \approx 0.7$. Note that an important feature of the above scheme is that both termination and propagation are dependent on the chain-lengths of the radicals involved in the reaction.

We now re-present the equations from chapter 2 that will again be used in this chapter of work, updating them as necessary for the new feature of CLDP. The mass balance differential equations that are derived from the above reaction scheme are as follows:

$$\frac{d[R_1]}{dt} = R_{init} + f_{trX}[R] - f_p^1[R_1] - f_{trX}[R_1] - f_t^1[R_1] \quad \textbf{(3.14a)}$$

$$\frac{d[R_i]}{dt} = f_p^{i-1}[R_{i-1}] - f_p^i[R_i] - f_{trX}[R_i] - f_t^i[R_i], \qquad i = 2, \infty \quad \textbf{(3.14b)}$$

Here t is time,

$$[R] = \sum_{j=1}^{\infty}[R_j] \quad \textbf{(3.15)}$$

is the total free radical concentration and the f denote reaction frequencies with respect to radicals: $f_{trX} = k_{trX}[X]$ is the transfer frequency, and $f_p^i = k_p^i[M]$ and

$$f_t^i = 2\sum_{j=1}^{\infty} k_t^{i,j}[R_j] \quad \textbf{(3.16)}$$

are the frequencies with which an R_i species propagates and terminates respectively. Note that eq. **(3.16)** defines implicitly the rate law we use for termination, *i.e.*, with a factor of 2. Also note that radicals are not differentiated according to whether they originate from CTA (*i.e.* DDM in the present case) or initiator (AIBN).

For chain-length-independent termination (all $k_t^{i,j}$ equal to the one value, k_t), eq. **(3.16)** becomes $f_t^i = 2k_t[R]$, *i.e.*, there is no dependence on chain length, which greatly simplifies calculations. But whenever termination is chain-length dependent, f_t^i is a function of chain length, and thus the kinetics of FRP is greatly complicated. That said, eq. **(3.16)** can be significantly simplified when the geometric mean model for cross-termination is used:

$$k_t^{i,j} = (k_t^{i,i} \times k_t^{j,j})^{0.5} \quad \textbf{(3.17)}$$

This leads to the following equation for the termination frequencies:

$$f_t^i = 2\,(k_t^{i,i})^{0.5} \sum_{j=1}^{\infty} (k_t^{j,j})^{0.5}\,[R_j] \qquad \textbf{(3.18)}$$

Although the rectitude of the geometric mean model is questionable, it is well established that it gives the same *trends* as other cross-termination models, and so it is justified to cash in on the computational celerity it provides. Hence eq. **(3.18)** will be used in all modeling results presented in this work. Note that in some instances modeling was also carried out using the diffusion mean model (*e.g.* see chapter 2), and it always resulted in identical conclusions.

Because the experiments of this work were continuously initiated, it is legitimate to model the results using steady-state solutions of eqs. **(3.14)**. These are:

$$[R_0] = \frac{R_{init} + f_{trX}\,[R]}{f_p^0} \qquad \textbf{(3.19a)}$$

$$[R_i] = [R_{i\text{-}1}]\,\frac{f_p^{i\text{-}1}}{f_p^i + f_{trX} + f_t^i} = [R_0] \prod_{j=1}^{i} \left(\frac{f_p^{j\text{-}1}}{f_p^j + f_{trX} + f_t^j} \right) ,\ i = 1, \infty \qquad \textbf{(3.19b)}$$

Note that any value may be used for the (non-physical) quantity f_p^0, as it cancels out in evaluating $[R_1]$, so that the following equation (which is convenient for calculations) is obtained:

$$[R_i] = \frac{R_{init} + f_{trX}\,[R]}{f_p^i} \prod_{j=1}^{i} \left(\frac{f_p^j}{f_p^j + f_{trX} + f_t^j} \right) ,\ i = 1, \infty \qquad \textbf{(3.20)}$$

These equations will be solved numerically in the usual way: as was done in the work of chapter 2, the numerical solution of eq. **(3.20)** consists of iteration (repeated evaluation of the equations) and truncation (inclusion in calculations of sufficiently large chain lengths, i) such that the solution obtained meets specified precision tolerances.

Comparing modeled results with experimental data

In this work various quantities will be calculated from the radical chain length distribution (RCLD), which results from the complete solution of eq. **(3.20)**. Eq. **(3.2)** for the overall rate coefficient for termination has already been given. In an entirely similar fashion, the overall rate coefficient for propagation, $\langle k_p \rangle$, may be evaluated:

$$\langle k_p \rangle = \sum_{i=1}^{\infty} \left(k_p{}^{i} \frac{[R_i]}{[R]} \right) \qquad \textbf{(3.21)}$$

The instantaneous dead chain-length distribution (DCLD) is given by

$$\frac{d[D_i]}{dt} = \lambda f_t^i [R_i] + (1 - \lambda) \sum_{j=1}^{i-1} k_t^{j,i-j} [R_j] [R_{i-j}] + f_{trX} [R_i] \quad , \; i = 1, \infty \qquad \textbf{(3.22)}$$

The three terms in eq. **(3.22)** account for formation of dead chains by termination by disproportionation and combination, and by transfer, respectively. For the experiments presently under consideration, the distribution calculated from eq. **(3.22)** is proportional to the observed cumulative DCLD, as a steady-state prevails and the traversed conversion range is sufficiently small that there is negligible change in reactant concentrations and in rate coefficients over the course of a given experiment. Hence experimental values of the number- and weight-average degrees of polymerisation of dead polymer, denoted $\overline{DP}_n$ and $\overline{DP}_w$ respectively, may be compared with the following modeling values:

$$\overline{DP}_n = \frac{\sum_{i=1}^{\infty} i \frac{d[D_i]}{dt}}{\sum_{i=1}^{\infty} \frac{d[D_i]}{dt}} \qquad \textbf{(3.23a)}$$

$$\overline{DP}_w = \frac{\sum_{i=1}^{\infty} i^2 \frac{d[D_i]}{dt}}{\sum_{i=1}^{\infty} i \frac{d[D_i]}{dt}} \qquad \textbf{(3.23b)}$$

3.5 Modeling Results and Discussion

As described above, we have obtained rate and molecular weight data for the polymerisation of MMA at 60°C. A series of experiments were performed where the concentration of chain transfer agent DDM was varied, in order to produce shorter chains and probe the applicability of a 'composite' termination model to this system. In this section we will describe our efforts to find a match between the experimental data and modeling predictions, as obtained using the equations and procedures given in the preceding section.

Data and strategy

In this work we will seek modeling parameter sets which reproduce both rate and MWD data simultaneously. In fact it is rare for FRP modeling to be this stringent (usually either rate or molecular weight information is modeled, not both), although of course it should be standard practice. However there remains the issue of what form of the data to model. For rate data this is quite easy: as there is no doubt about the rate of initiation, modeling should seek to reproduce the experimental values of $<k_p>/<k_t>^{0.5}$ (see *Tab. 3.2*). However the most appropriate way to model MWD data is more subjective. Clearly, attempting to match model to experiment at the level of detail of MWDs (*Fig. 3.3*) would be laborious. Equally problematic is to use an average degree of polymerisation, for example a Mayo-type approach (*Fig. 3.4*), since we know that some of our distributions are not complete. For these reasons, and after much thought and some trial and error, we concluded that the most appropriate MWD parameter to model is the experimental value of i_{peak}, the chain length of

the *peak* of a molecular weight distribution. Not only is i_{peak} the most distinguishable feature of an experimental MWD, but its only error should be GPC calibration error, and even this should be minimal, as i_{peak} is always well inside the calibrated part of the MWD. Baseline subtraction should not introduce significant error (as the largest magnitude value will naturally be least affected by this), and similarly column broadening (which should only enlarge the width of a symmetric GPC MWD curve, see *Fig. 3.3*, not move the location of its peak). Of course correctly reproducing the value of i_{peak} does not of itself reproduce the whole MWD, however this is a matter over which one has no control: modeling of a transfer-dominated MWD results in a particular width, and if the experimental MWD has a different width, then there is nothing that modeling can do to simulate this. In other words, the best modeling can do is to correctly locate the peak of the MWD, which is precisely why we use i_{peak} as a modeling index. Besides, it will be seen that more often than not our modeling does do a good job, all things considered, of reproducing MWD width and shape as well.

A technical note is that because i_{peak} is taken from the maximum of the experimental GPC MWD, the simulated value of i_{peak} is the i at which $i^2\, d[D_i]/dt$ (calculated using eq. **(3.22)**) is a maximum.

In terms of modeling strategy, our modus operandi was as follows. Although it may seem as though a lot of modeling parameters have been introduced, in fact this is not the case: only $k_t^{1,1}$ and C_{trX} were taken as unknown in value for each modeling exercise (for which particular CLDT and CLDP models were assumed in turn). In principle it would be best practice to carry out global modeling of all $\langle k_p \rangle / \langle k_t \rangle^{0.5}$ and i_{peak} values in order to determine best-fit values of $k_t^{1,1}$ and C_{trX}. However this turned out not to be necessary, as in transfer-dominated MWDs, i_{peak} values are largely insensitive to the values of $k_t^{i,j}$ that are used. Thus C_{trX} could first be obtained by fitting the i_{peak} data (for example using the Mayo plot value as

a first guess for C_{trX}), without having to worry about the appropriateness of $k_t^{i,j}$ values for the rate data. Having obtained C_{trX}, the set of $\langle k_p \rangle / \langle k_t \rangle^{0.5}$ data were then modeled to obtain the best-fit value of $k_t^{1,1}$ (note that because C_{trX} plays a role in determining the RCLD, see eq. **(3.20)**, it does affect the value of $\langle k_p \rangle / \langle k_t \rangle^{0.5}$). At the end of this procedure it was of course checked that the best-fit value of $k_t^{1,1}$ still gave a *best*-fit to the i_{peak} data with the original value of C_{trX}.

Finally, each modeling exercise involved two CLDT models: (1) The composite model, eqs. **(3.4)**, with $e_S = 0.5$, $e_L = 0.16$, $i_c = 100$, and with $k_t^{1,1}$ to be fitted. This model is used because the whole point of this work is to test the validity of this model. Of course these values of e_S, e_L and i_c are not to be taken as exact, however they are appropriate for ascertaining whether the composite model is, in a general sense, consistent with data. (2) Eq. **(3.3)** with $e = 0.16$ and $k_t^{1,1}$ to be fitted. This model is used as it represents the most commonly espoused CLDT model.

Modeling with chain-length-independent propagation

First of all we model our data using[15] $k_p^{\,i} = 834$ L mol^{-1} s^{-1} for all i (see *Tab. 3.2*). The best fit of i_{peak} values was obtained using $C_{trX} = 0.82$ (both CLDT models) and is depicted in *Fig. 3.5*. It is evident that the experimental data could hardly be better reproduced. The only concern might be over the apparent trend in the residuals – predicted i_{peak} values are a little high at low values of f_{DDM}, and a little low at high f_{DDM}. The magnitude of the trend is very small, however, and so it will not be considered further. It is noted that this new (and better) estimate of C_{trX} is different to that from the Mayo approach because of the use of a different (and better) MWD index, *viz*. i_{peak} rather than $\overline{DP}_n$ or $\overline{DP}_w$.

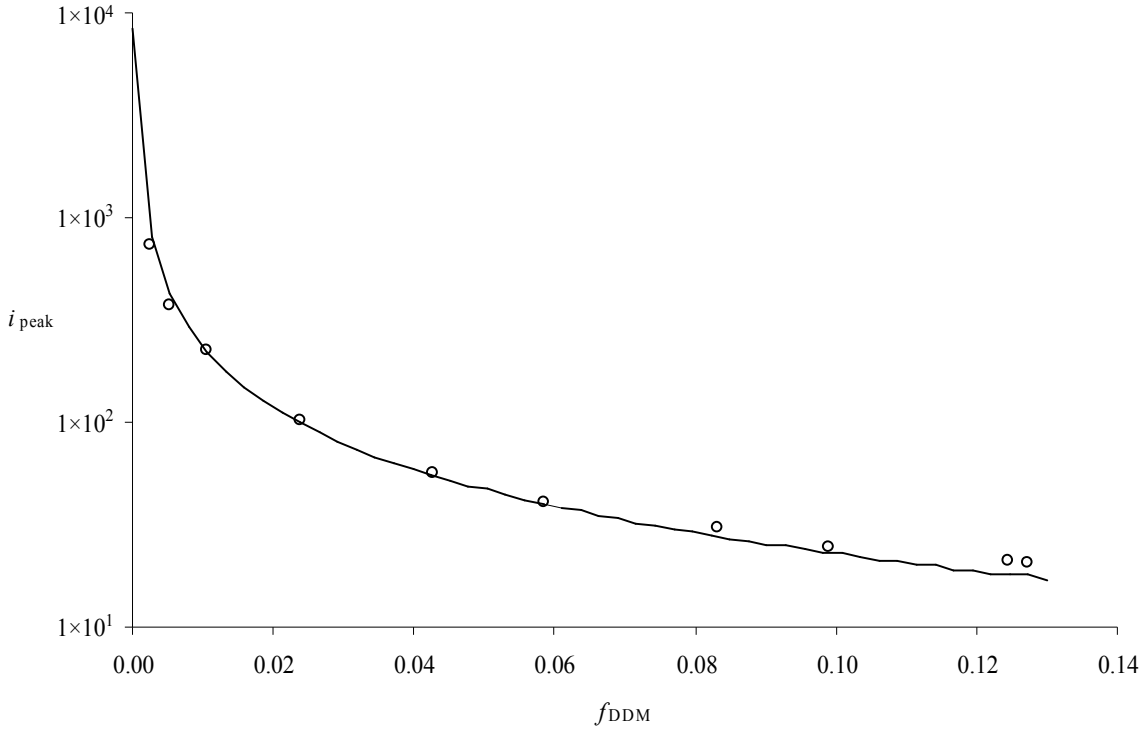

Fig. 3.5 Plot of the chain length of the peak in the GPC distribution, i_{peak}, *vs.* the mole fraction of DDM in the polymerisation mixture, f_{DDM}, for experiments (points) and model results (line) with CLD termination and no CLDP. The line was generated using C_{trX} = 0.82 and represents the best fit to the experimental data.

We now turn our attention to the rate data and the effect of a chain-length dependent termination model. The results are shown in *Fig. 3.6*. The composite termination model gives a best-fit value of $k_t^{1,1}$ of 3.50×10^8 L mol^{-1} s^{-1}, while the single-*e* model gives a $k_t^{1,1}$ of 9.97×10^7 L mol^{-1} s^{-1}.

At first glance, it is disappointing to note that the single-*e* model gives a better quality of fit than the composite model. However, the value $k_t^{1,1} = 9.97\times10^7$ L mol^{-1} s^{-1} from the single-*e* model is unphysically low[1,4] (as will be discussed in due course), and further, it is evident that both termination models display an important *qualitative* failure: neither reproduces the slight

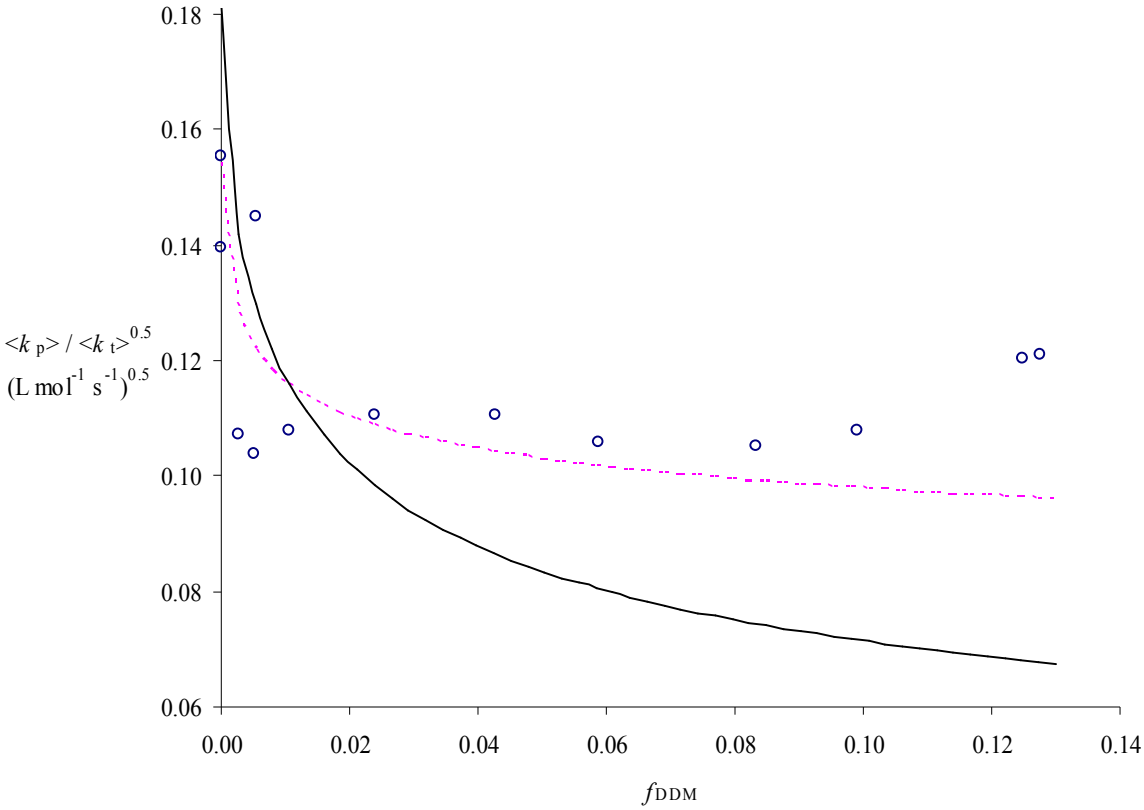

Fig. 3.6 Plot of rate data as the ratio $\langle k_p \rangle / \langle k_t \rangle^{0.5}$, *vs.* mole fraction of DDM in the polymerisation mixture, f_{DDM}. Datasets are experimental (points), composite termination model with parameters as indicated in the text (solid line) and single-*e* model with parameters as indicated in the text (dotted line).

increase of $\langle k_p \rangle / \langle k_t \rangle^{0.5}$ at large values of f_{DDM}. Upon reflection it becomes evident that this trend is extremely unusual: as the DDM level increases and more short chains are generated, any *reasonable* termination model must predict an increasing $\langle k_t \rangle$, and therefore a decreasing value of $\langle k_p \rangle / \langle k_t \rangle^{0.5}$. The qualifier 'reasonable' is used here because a model in which $k_t^{i,i}$ increased with increasing chain length could of course explain the observed trend, however it is physically nonsensical to suggest that chains diffuse faster as they get longer. In fact the best one can do in the present context is to posit chain-length-independent termination, which would of course result in $\langle k_p \rangle / \langle k_t \rangle^{0.5}$ being independent of f_{DDM}, as in *Fig. 3.2*. While *Fig.*

3.2 reveals a reasonable 'fit' to the data obtained in the presence of DDM, it is also evident that a constant $\langle k_t \rangle$ singularly fails to describe the rate in the absence of DDM. Further, it is obviously unsatisfactory to suggest that termination under these conditions is truly chain length independent in rate, for it is well established that it is not.

The most obvious step to take to resolve the above conundrum is to introduce chain-length-dependent propagation, which must play some sort of role in systems in which radical chain lengths are very small. As is evident from eq. **(3.21)**, as the radical CLD becomes weighted towards smaller chain lengths, the value of $\langle k_p \rangle$ must increase (this is because of k_p^i increasing as i decreases, as will shortly be discussed). Hence $\langle k_p \rangle$ must increase as f_{DDM} increases, which introduces the possibility of explaining the highly unusual trend in rate data that has been noted above.

Modeling with chain-length-dependent propagation

To incorporate CLDP into modeling, the first thing that is needed is appropriate values for k_p^i. There is no doubt that propagation is faster for very small chains than for long chains.[19] Further, the theoretical reasons for this have even been established.[22] However there is very little concrete data on k_p^i for actual FRP systems. The best *direct* data that we know of for MMA is that of Gridnev and Ittel.[23] They were able to measure the rate coefficients for the first two propagation steps of MMA at 60°C using cobalt-based catalytic chain transfer agents. In order to use this information, we fitted their data with our own equation for CLDP:

$$k_p^i = k_p^\infty \left(1 + C_1 \exp\left(\frac{-\ln(2)}{i_{½}} (i-1)\right)\right) \qquad \textbf{(3.24)}$$

In eq. **(3.24)**, k_p^∞ is the long-chain value of the propagation rate coefficient. The parameter C_1 is equal to $(k_p^1 - k_p^\infty) / k_p^\infty$, *i.e.*, it is the factor by which k_p^1 exceeds k_p^∞ in value, for example $C_1 = 1$ means that k_p^1 is double the long-chain value of k_p. So C_1 determines the model value

of k_p^1, and by setting C_1 equal to zero, the model collapses to the case of chain-length independent propagation. The third and last model parameter in eq. **(3.24)** is the 'half chain-length', $i_{½}$, so denoted because it is the change in i necessary for $k_p^i - k_p^\infty$ to halve in value (in other words, $i_{½}$ is analogous to the familiar 'half-life' of first-order reaction kinetics). Clearly $i_{½}$ reflects the degree of chain length dependence of the propagation rate coefficient: the larger is $i_{½}$, the greater the chain lengths to which the CLDP persists. The above model, which it is stressed is purely utilitarian, has been chosen to be able to reproduce the essential features of experimentally observed CLDP – an initially large value 'decaying' to a final low value.

In this work we will always use the recommended[15] value of k_p^∞ = 834 L mol^{-1} s^{-1} at 60°C. *Fig. 3.7* shows the fit of eq. **(3.24)** to the data of Gridnev and Ittel.[23] At 60°C they measured k_p^1 = 14000 L mol^{-1} s^{-1}, which leads to C_1 = 15.8, and k_p^2 = 3600 L mol^{-1} s^{-1}, leading to $i_{½}$ = 0.44. Because no k_p^i for higher i were measured, the fit to the data is exactly determined (3 points and 3 unknowns), so too much confidence should not be placed in the obtained parameter values, which – see *Fig. 3.7* – suggest that k_p^i very quickly decays to its long-chain value (*e.g.* the fit gives k_p^4 = 956 L mol^{-1} s^{-1}).

We will now examine the effect of including CLDP in our model. An important point in this regard is that C_{trX} now represents k_{trX}/k_p^∞, from which k_{trX} is calculated for use in all the equations of Section 3.4.

First of all the i_{peak} data were modeled, and it was found that C_{trX} = 0.82 gave a best fit to the data. Not surprisingly the fit was essentially identical to that of *Fig. 3.5*, and hence the results are not presented again (in fact, this comment applies to all subsequent i_{peak} fitting). However what is surprising is that even though CLDP has been introduced, the best-fit value of C_{trX} is

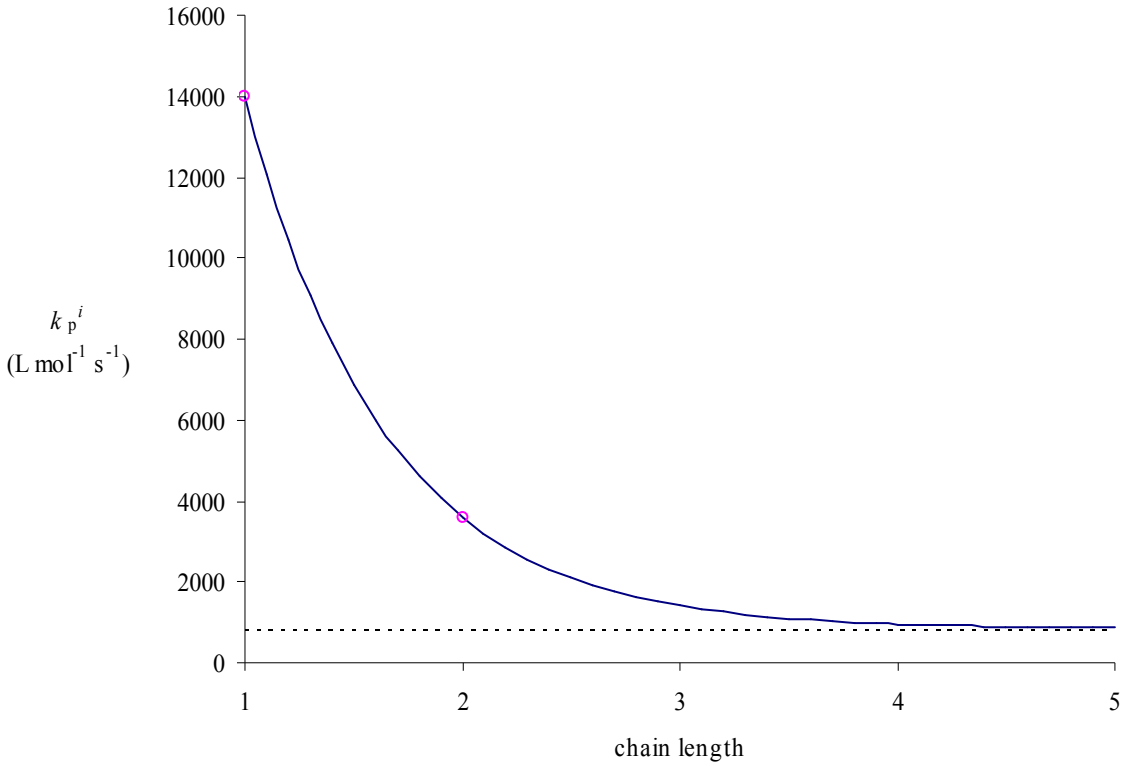

Fig. 3.7 The rate coefficient for propagation, k_p^i, as a function of chain length. Experiments[23] (points), best fit to experimental data, with parameters as indicated in the text (line), and long-chain value (*Tab. 3.1*) (dotted line).

not affected. This is a surprise because modeled molecular weight distributions, and hence values of $\overline{DP}_n$ and $\overline{DP}_w$, are certainly affected by CLDP. On reflection though it makes sense that i_{peak} is not significantly affected by the introduction of CLDP. The reason for this is that CLDP only affects the RCLD at the very short chain lengths for which the CLDP is operative. Beyond these short chain lengths one still has, for transfer-dominated systems, a Schulz-Flory (*i.e.*, exponential-like) distribution for the RCLD, and it is in this region of the RCLD that the value of i_{peak} is located. Of course there is slight variation of i_{peak} as the CLDP is varied (because the RCLD is not exactly the same in the Schulz-Flory region), however this variation only affects the best-fit value of C_{trX} to the third decimal place, which is not significant.

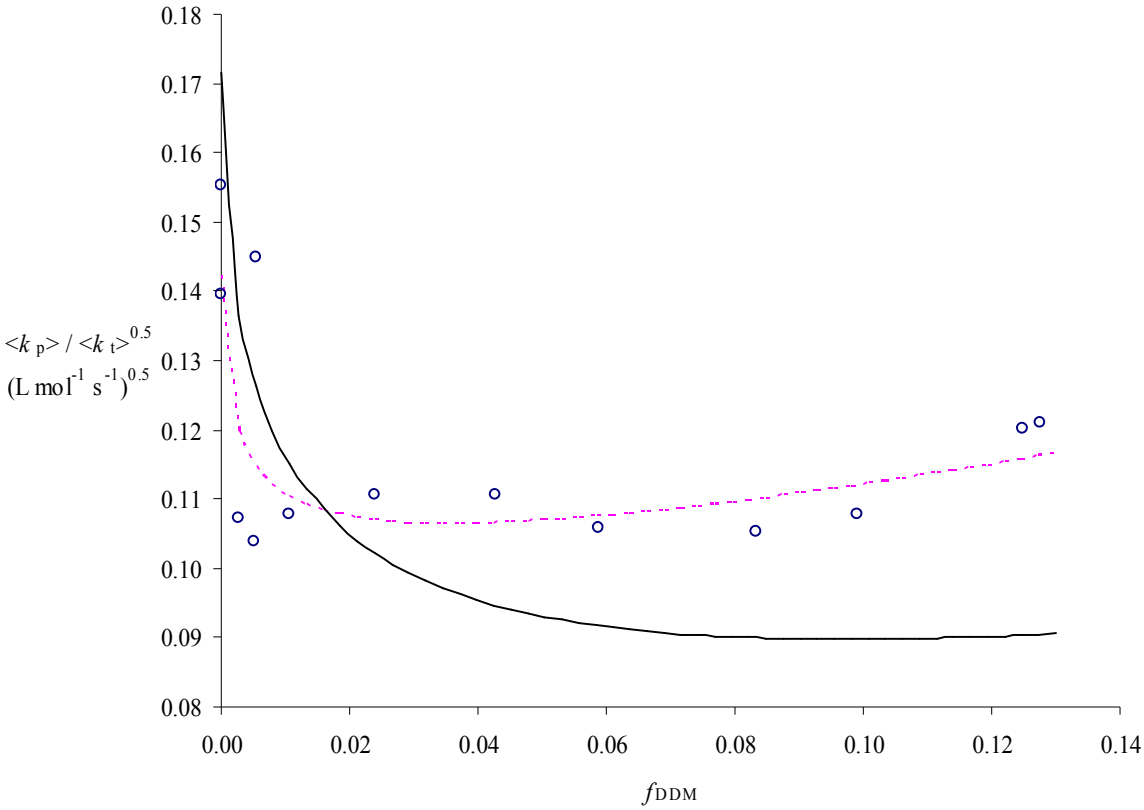

Fig. 3.8 As for *Fig. 3.6*, with CLDP parameters derived from *Fig. 3.7* (see text).

We present in *Fig. 3.8* the results of fitting the rate data by varying $k_t^{1,1}$, as was done for *Fig. 3.6*. Although the composite model is now a better description of the data, once again we see that the data are better fitted by the single-*e* model, in fact an excellent fit is obtained. However, exactly as before, the value of $k_t^{1,1}$ is too low: the best fit for the single-*e* model is produced with $k_t^{1,1} = 1.16\times10^8$ L mol^{-1} s^{-1}, whereas the composite termination model yields $k_t^{1,1} = 3.90\times10^8$ L mol^{-1} s^{-1}.

It is worth discussing the issue of the value of $k_t^{1,1}$ at this point, because in fact this is the only problem with the single-*e* model at this stage. From actual measurements of the termination rate coefficients of small radicals,[4] one would expect $k_t^{1,1} \approx 10^9$ L mol^{-1} s^{-1} for polymerising systems. In the present case most chains are started by the radical derived from DDM, *viz*.

$C_{12}H_{25}S^{\bullet}$, and because of the relatively large size of this species one can justify $k_t^{1,1}$ being somewhat lower than 10^9 L mol^{-1} s^{-1}. Thus a value around 5×10^8 L mol^{-1} s^{-1} is reasonable, however 1×10^8 L mol^{-1} s^{-1} remains too low to be realistic. This is an important point in assessing whether a termination model is reasonable.

Although the above modeling has thrown up some interesting results, it is unsatisfactory in two regards: firstly, the composite termination model, which in other respects had looked as though it provided a promising description of data,[1] has not fared so well; second, and more objectively, it must be said that the CLDP parameters used above are somewhat tenuous. It is therefore of interest to seek out further data on the chain-length-dependence of MMA propagation. This topic was recently investigated by Willemse *et al.*[24] They used the now-standard pulsed-laser polymerisation (PLP) method to determine $\langle k_p \rangle$,[15,25,26] but with molecular weight distributions determined by matrix-assisted laser desorption ionisation time-of-flight mass spectrometry (MALDI-TOF-MS), as this eliminates some of the weaknesses of GPC, ones we have also encountered in this work. The value of $\langle k_p \rangle$ that is determined from PLP, which we here denote $\langle k_p \rangle_{PLP}$, is related to the microscopic, chain-length-dependent k_p values by eq. **(3.25)**:

$$\left(\langle k_p \rangle_{PLP}\right)^{-1} = \frac{1}{L}\sum_{i=1}^{L}\frac{1}{k_p^{\,i}} \qquad \textbf{(3.25)}$$

In this equation, L is the chain length used to determine $\langle k_p \rangle_{PLP}$, *i.e.*, the (average) chain length grown between pulses. It is important to realise that $\langle k_p \rangle_{PLP}$ is an average not only with respect to chain length, but also with respect to time, so that it is quite distinct from the value in eq. **(3.21)**, which applies at a particular instant in time, and is merely chain-length averaged (hence the different notation). Specifically, $\langle k_p \rangle_{PLP}$ is the time-averaged value of $\langle k_p \rangle$ over any whole number of initiation pulse periods.

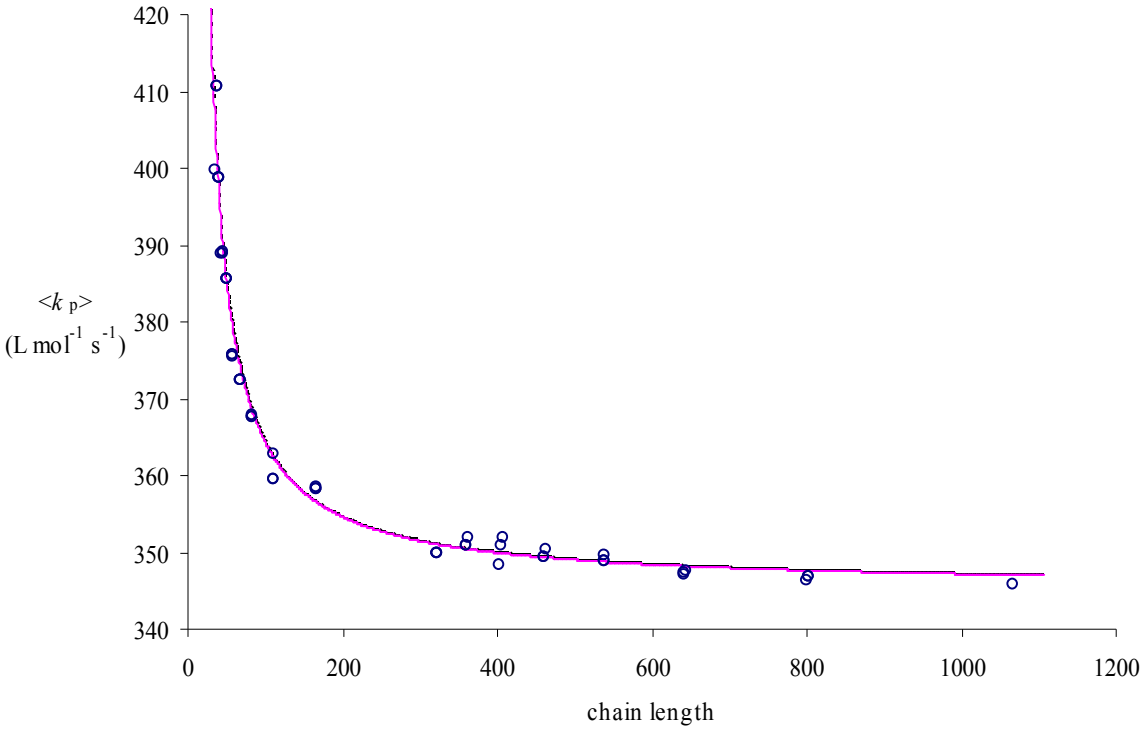

Fig. 3.9 Chain-length averaged propagation rate coefficient, $\langle k_p \rangle$, as determined by PLP/MALDI-TOF-MS[4], *vs.* chain length at which the PLP peak was measured (points), and two (visually almost identical) fits to the data using eqs. **(3.24)** and **(3.25)**. Fitted parameter values are given in the text.

It is important to understand that in contrast to the measurements of Gridnev and Ittel,[23] values of $\langle k_p \rangle_{PLP}$ do not yield k_p^i *directly*. Rather, all one can do is use eq. **(3.25)** to see if a set of k_p^i values is consistent with the PLP results. Willemse *et al.*[24] used a simple model in which k_p^i is infinity below a certain chain length and the long-chain value above it. We carried out our own fitting of their data using our more realistic function for CLDP, eq. **(3.24)**. This was necessary because in our modeling it is obviously undesirable to use $k_p^i = \infty$ for very small chain lengths, as this would impede the ability of the termination model to affect the result of simulations. Results of this fitting, for the 25°C data set, are depicted in *Fig. 3.9*. It was found that the data allow a range of $i_{½}$ and C_1 values to give the same quality

of fit – these two parameters are coupled. One can choose a value for C_1 within a certain range, and obtain a best-fit value for $i_{½}$. For example, the solid line depicted in *Fig. 3.9* arises from a CLDP model where $i_{½}$ = 1.16 and C_1 = 15.8. Sharp-eyed readers may be able to observe the dotted line, obtained with the model parameters $i_{½}$ = 1.42 and C_1 = 9.0. For the relatively high chain lengths (compared to our work) that the data are measured at, we cannot individually determine these parameters. These data therefore allow a range of CLDP parameters to be used, which may or may not lead to different predicted rate and MWD data. This issue will be investigated shortly.

Willemse *et al.*[24] measured $\langle k_p \rangle_{PLP}$ for MMA at –18°C, 1°C and 25°C. We fitted all three datasets, as in *Fig. 3.9*, and it was found that for a given C_1 the value of $i_{½}$ was essentially independent of temperature. The results of this fitting are presented in *Tab. 3.3*.

Tab. 3.3 Results from fitting all Willemse *et al.*[24] MMA datasets.

T / °C	$i_{½}$	
	C_1 = 9.0	C_1 = 15.8
24.7	1.423	1.156
0.7	1.282	1.042
-18.3	1.455	1.172
mean	1.387	1.123

What is immediately interesting about the results of *Fig. 3.9* and *Tab. 3.3* is that they reveal a CLDP which persists out to longer chain lengths than previously suspected, because (for the same C_1 = 15.8) the value of $i_{½}$ is larger: 1.12 here as opposed to 0.44 in *Fig. 3.7*. This may seem a minor difference, but in fact it will be seen in *Fig. 3.10* that it represents a major effect on k_p^i, and further, it will also be seen that it is enough to have a major effect on

predicted rate data. The above said, the CLDP represented by $i_{½}$ = 1.12 does not extend out to nearly the chain lengths suggested by Olaj *et al.*,[27] whose reanalysis of $\langle k_p \rangle_{PLP}$ data led them to speculate that f_p^i might be chain length dependent out to chain lengths in the hundreds (kinetically it does not matter if the variation is due to k_p or [M]). However, in tandem with very large values of $i_{½}$, the modeling of Olaj *et al.* used very low C_1 (using here the parlance of this work), something called into question by the more precise $\langle k_p \rangle_{PLP}$ data subsequently obtained by Willemse *et al.*[24] as a result of using MALDI-TOF-MS rather than GPC.

Tab. 3.4 Calculated Arrhenius frequency factors for the addition of hydrocarbon radicals to ethylene.[22]

Radical	Radical 'chain length' i	Frequency factor A^i / (L mol^{-1} s^{-1})
Ethyl	1	1.7×10^8
Propyl	1.5	8.7×10^7
Butyl	2	9.8×10^7
Pentyl	2.5	7.9×10^7
Hexyl	3	6.3×10^7
Heptyl	3.5	5.0×10^7
Macroradical	∞	$(1.0–1.7) \times 10^7$

Before carrying out any modeling, we consider whether the k_p^i we have deduced from the data of Willemse *et al.*[24] are reasonable. A window onto this is provided by the use of *ab initio* molecular orbital calculations and transition state theory (TST) to understand the propagation reaction.[22] Arrhenius frequency factors, A^i, for the gas-phase reaction of ethylene with various small hydrocarbon radicals (of 'chain length' i) have been calculated, and are presented in *Tab. 3.4*. The predicted variation of the frequency factor with chain length is primarily due to the "degree to which the internal rotations of the transition state are

hindered"[22]. The activation energy, in contrast, should not be significantly affected by the length of the hydrocarbon radical. We therefore expect the variation of k_p^i with chain length to be similar to the variation of the frequency factor with radical size. Given this, one may say that $A^i/A^1 \approx k_p^i/k_p^1$, so that $k_p^i = A^i\,(k_p^1/A^1)$ may be estimated from the A^i values in *Tab. 3.4*, scaled according to the ratio k_p^1/A^1. Two values of k_p^1 were chosen, *viz*. those corresponding to the values C_1 = 15.8 and 9.0 used in the analysis of the Willemse *et al.*[24] data above. When used with the known value of k_p^∞ (= 834 L mol^{-1} s^{-1}), both k_p^1 values pass the 'consistency test' of giving a value of $A^\infty = k_p^\infty\,(A^1/k_p^1)$ that is within the range given in *Tab. 3.4*.

The two sets of estimated k_p^i are presented as points in *Fig. 3.10*, where they are compared with the corresponding k_p^i used to fit the Willemse *et al.* data, presented as lines. It is evident that the best-fit k_p^i from the $\langle k_p \rangle_{PLP}$ data vary with chain length exactly as theory predicts. While one should not become overly enthusiastic about this agreement – after all, gas phase ethylene cannot be an exact model for fluid phase MMA – it is nevertheless an encouraging result in two ways: (1) it indicates that eq. **(3.24)** is a justifiably pragmatic functional form for k_p^i, and (2) it gives confidence in our parameter values from fitting the Willemse *et al.* data. Specifically, one can feel confident that C_1 is of order 10-15, *i.e.*, that k_p^1 is of order 11-16 times larger than k_p^∞, as also found by Gridnev and Ittel.[23] However *Fig. 3.10* shows that the $i_{½}$ implied by the Gridnev and Ittel[23] data is at variance with what TST predicts. Specifically, TST predicts a CLDP which persists to higher chain length. Although the investigation of Willemse *et al.*[24] did not generate k_p^i values directly, in view of the (likely) precision and accuracy of the large $\langle k_p \rangle_{PLP}$ data set they gathered, and its concord with TST predictions, we feel it is justified to regard the k_p^i we have deduced from their data as being the best currently available for MMA. Certainly the measurements of Gridnev and Ittel[23] should in principle be superior in that they were direct, however their data set was very limited (k_p^1 and

k_p^2 only) and their methodology was difficult. Besides, it is clear that these values are not inconsistent with the new values deduced above, but they lack information about k_p^i for the range $i \approx 3$-10. As will now be seen, these values of k_p^i can be crucial.

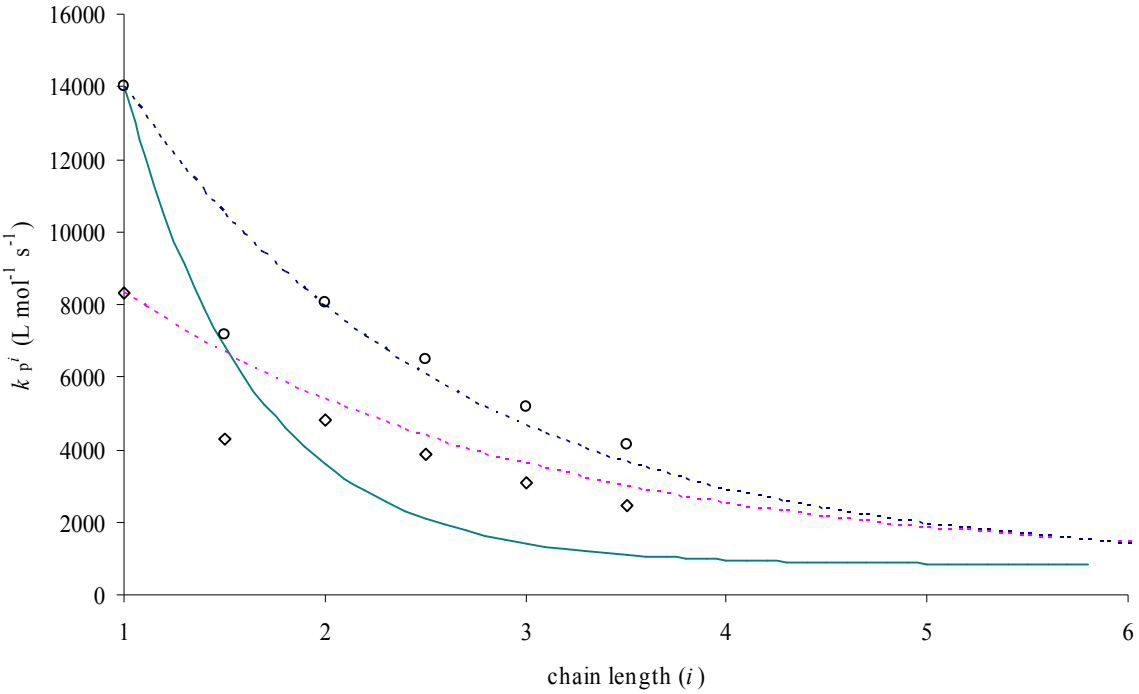

Fig. 3.10 Variations of k_p^i with i discussed in this work: solid line – fit of Gridnev and Ittel[23] data (as in *Fig. 3.7*); dashed lines – best fits of the data of Willemse *et al.*[24] (upper: C_1 = 15.8, $i_{½}$ = 1.12; lower: C_1 = 9.0, $i_{½}$ = 1.39); points – estimates from theoretical predictions of Heuts *et al.*[22] (upper [circles]: using $k_p^1 = 1.40\times10^4$ L mol^{-1} s^{-1}; lower [diamonds]: using $k_p^1 = 8.34\times10^3$ L mol^{-1} s^{-1}).

It would seem most appropriate to use the C_1 values and mean values of $i_{½}$ from *Tab. 3.3* for modeling our own 60°C data. First of all the i_{peak} data were modeled, and it was once again found that $C_{trX} = 0.82$ gave the best fit (see earlier discussion). Results of fitting the rate data are presented in *Fig. 3.11*.

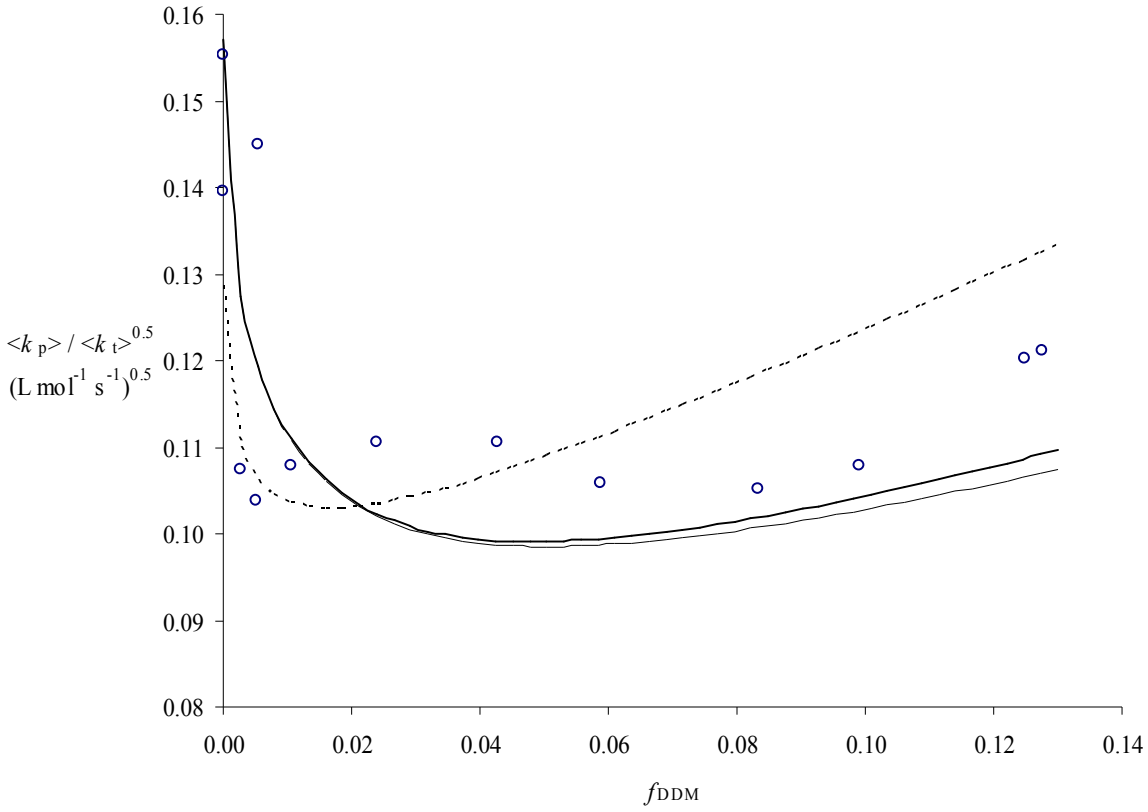

Fig. 3.11 As for *Fig. 3.6*, but with $C_1 = 15.8$ and $i_{½} = 1.12$ used for calculating k_p^i (see text). The extra line (long dashes) for the composite termination model results used $C_1 = 9.0$ and $i_{½} = 1.39$ for calculating k_p^i.

Several things can be said about *Fig. 3.11*. Firstly, it is evident that with these CLDP parameters, the composite termination model provides an excellent description of the rate data. In particular, it reproduces – and thus makes sense of – the increase of rate with f_{DDM}, which was at first mystifying. Second, the composite termination model now provides a better fit of the data than does the single-*e* model. With the latter model, the weaker CLDT in tandem with the stronger CLDP produces values of the ratio $\langle k_p \rangle / \langle k_t \rangle^{0.5}$ that are too high at higher fractions of DDM. In contrast, the composite termination model provides very good agreement with the experimental data. Third, the two sets of CLDP model parameters lead to almost identical predicted rate data, even though the actual k_p^i are different. Therefore, the

concern raised above, that our inability to individually determine the CLDP parameters $i_{½}$ and C_1 from the available experimental data could lead to a range of model predictions, is assuaged: the higher k_p^1 of one k_p^i fit is offset by the CLDP not extending to chain lengths as high. Fourth, the $k_t^{1,1}$ values from the fitting of *Fig. 3.11* are as follows: 4.6×10^8 L mol^{-1} s^{-1} for the composite model (both CLDP parameter sets giving the same best-fit value to 2 significant figures), and 1.4×10^8 L mol^{-1} s^{-1} for the single-*e* model. So once again the composite model gives a physically reasonable value whereas the single-*e* model does not.

All in all it must be said that the modeling of this chapter has ultimately been impressively successful: a kinetic model as microscopically correct as possible has been used, the very best available values of rate parameters have been employed, rate and MWD data have been simultaneously reproduced to high accuracy, highly plausible values for the only two fitted parameters have been obtained, and a mysterious trend in experimental rate data has been explained. It is therefore worth looking at some of our modeling results in more detail. In what follows the presented results will always be for the best-fit composite termination model of *Fig. 3.11*.

The variation of the overall rate coefficient for propagation

The variation of $\langle k_p \rangle$ with f_{DDM} from modeling is presented in *Fig. 3.12*. The strong increase of $\langle k_p \rangle$ with f_{DDM} is evident. It is this increase which is responsible for the unusual increase of rate with f_{DDM}: although $\langle k_t \rangle$ is increasing as chain lengths get shorter, as is implicit in the results of *Fig. 3.6*, this is overridden by the increase of $\langle k_p \rangle$. Of course it is important to be aware that rate varies as $\langle k_p \rangle / \langle k_t \rangle^{0.5}$, so that one gets more pronounced effects from changes in $\langle k_p \rangle$ compared with changes in $\langle k_t \rangle$.

Also presented in *Fig. 3.12* are values of $\langle k_p \rangle$ calculated according to:

$$\langle k_p \rangle = \sum_{i=1}^{\infty} k_p^{\,i} \left(\frac{f_{trX}}{f_p^{\,i}} \prod_{j=1}^{i} \frac{f_p^{\,j}}{f_p^{\,j} + f_{trX}} \right) = k_{trX} \frac{[X]}{[M]} \sum_{i=1}^{\infty} \prod_{j=1}^{i} \left(1 + \frac{k_{trX}}{k_p^{\,j}} \frac{[X]}{[M]} \right)^{-1} \qquad \textbf{(3.26)}$$

Eq. **(3.26)** is obtained by substituting the transfer-control limit ($f_{trX}[R] \gg R_{init}$ and $f_{trX} \gg f_t^{\,i}$) of eq. **(3.20)** for $[R_i]/[R]$ into eq. **(3.21)**. Note that at the crucial low chain lengths where $k_p^{\,i}$ is significantly greater than $k_p^{\,\infty}$, $[R_i]/[R]$ is not an exponential-like distribution (due to the $f_p^{\,i}$ term in the first form of eq. **(3.26)**), so one cannot make the standard assumption (for transfer control) of an exponential RCLD for evaluating $\langle k_p \rangle$. Although eq. **(3.26)** may look inhospitable, in fact it is very amenable to spreadsheet evaluation, with the sum simply being calculated for increasing *i* until convergence is evident (for the calculations presented in *Fig.*

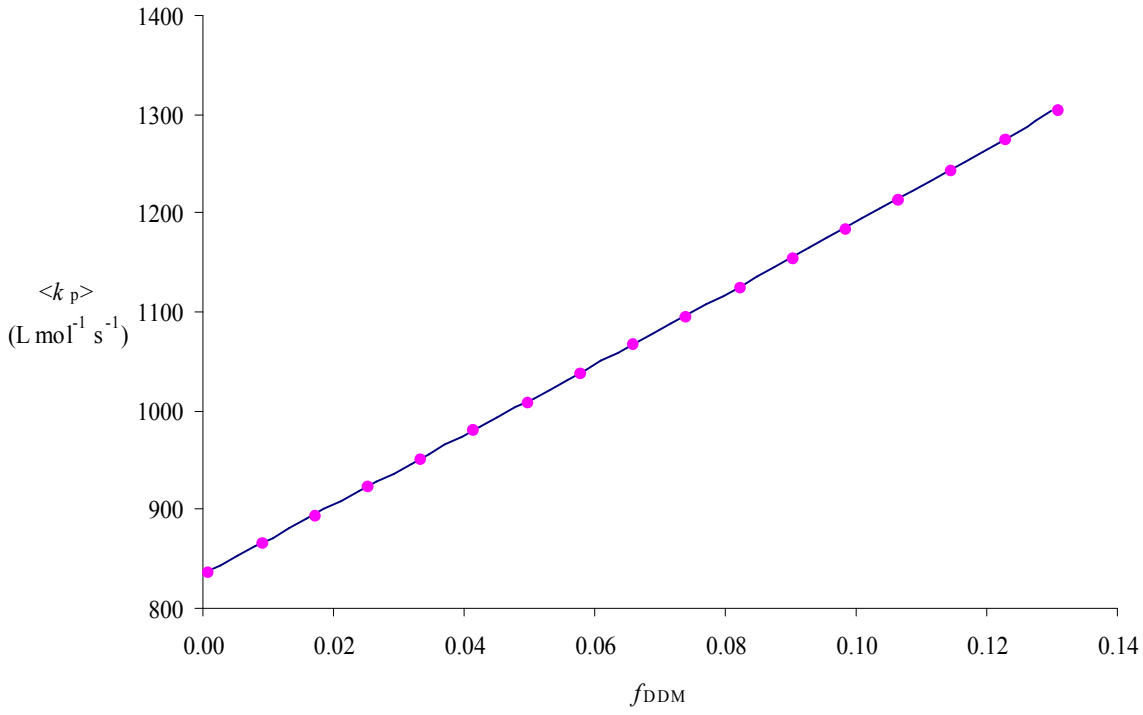

Fig. 3.12 The average rate coefficient for propagation, $\langle k_p \rangle$, *vs.* mole fraction of DDM in the polymerisation mixture, f_{DDM}, from simulations (line) and calculated using eq. **(3.26)** (points).

3.12 it was found that summing up to i = 1100 was sufficient to yield convergence to 3 significant figures).

The stunning accuracy of eq. **(3.26)** is evident from *Fig. 3.12*. It is therefore clear that the assumptions behind eq. **(3.26)** are good ones, for this system. Specifically, these assumptions are that all dead chain formation is by transfer, and that transfer is chain-length independent in rate (the latter assumption is noted because an analogue of eq. **(3.26)** for the case of chain-length-dependent transfer cannot be derived, much as one may be tempted to attempt it). Of course at high f_{DDM} it is expected that the RCLD is completely determined by transfer, explaining the accuracy of eq. **(3.26)** under these circumstances. However, it might be wondered why eq. **(3.26)** is so highly accurate even down to low values of f_{DDM}, where termination must also play a role in shaping the RCLD. This accuracy must be due to the deviation of $<k_p>$ from k_p^{∞} being so small that the precise details of the RCLD do not matter: as long as the distribution extends out to high chain lengths (where $k_p^i \approx k_p^{\infty}$), which the transfer limit RCLD will do at low f_{DDM}, an accurate value of $<k_p>$ will be obtained. Note however that for $f_{DDM} = 0$, the sum in eq. **(3.26)** does not converge, and so, of course, the equation cannot be used in the limit of no transfer.

The near-linearity of the values of eq. **(3.26)** presented in *Fig. 3.12* leads one to wonder if a simplified expression may be derived. Progress can be made by considering the very simple CLDP model used by Willemse *et al.*,[24] which is restated here:

$$k_p^i = \infty \quad , i \leq i_{min} \qquad \textbf{(3.27a)}$$

$$k_p^i = k_p^{\infty} \quad , i > i_{min} \qquad \textbf{(3.27b)}$$

In eqs. **(3.27)**, the parameter i_{min} determines the degree of CLDP, somewhat analogously to $i_{½}$ (eq. **(3.24)**): here the transition from high short-chain k_p^i values to the long-chain value is sharp rather than smooth. When this CLDP model is substituted into eq. **(3.26)**, one obtains:

$$<k_p> = k_{trX}\frac{[X]}{[M]}\left(i_{min} + \sum_{i=1}^{\infty}\prod_{j=1}^{i}\left(1 + C_{trX}\frac{[X]}{[M]}\right)^{-1}\right) \qquad \textbf{(3.28)}$$

Note that in eq. **(3.28)**, the product and sum would properly begin at a chain length of (i_{min} + 1), but since the upper bound of the sum is infinity and the argument is independent of chain length, the lower bounds may be transformed. Also, the term i_{min} enters because the propagation probabilities are 1 up until this chain length, and thus their product up until this chain length is also 1. When i_{min} such products are summed, of course one obtains the value i_{min}. Further, upon realising that the sum is a sum to infinity of a geometric series, for which the formula $\sum_{i=1}^{\infty}\prod_{j=1}^{i}(r) = \frac{r}{1 - r}$ may be used, the following equation is obtained:

$$<k_p> = k_{trX}\frac{[X]}{[M]}\left(i_{min} + \left(C_{trX}\frac{[X]}{[M]}\right)^{-1}\right) = k_p^{\infty}\left(C_{trX}\frac{[X]}{[M]}\,i_{min} + 1\right) \qquad \textbf{(3.29)}$$

Turning now to our own CLDP model (eq. **(3.24)**), it seems likely that a functional form similar to eq. **(3.29)** may approximate the results of *Fig. 3.12*. Examining eq. **(3.26)** more closely, we consider the dependence of the product on chain length in *Fig. 3.13*.

It is clear from the figure that the product in eq. **(3.26)** is well approximated by a sharp transition from a constant to an exponential function. Noting then the analogous relationship between $i_{½}$ and i_{min}, the following equation is formulated:

$$<k_p> \approx k_p^{\infty}\left(C_{trX}\frac{[X]}{[M]}(n \times i_{½}) + 1\right) \qquad \textbf{(3.30)}$$

In this equation, n is the multiple of $i_{½}$ at which the smooth decay of eq. **(3.24)** may be approximated by a sharp decrease (as in eqs. **(3.27))**. It should now be clear that eq. **(3.30)** would give an excellent description of the curve in *Fig. 3.12*, bearing in mind that the abscissa in *Fig. 3.12* is f_{DDM} , which approximates [X]/[M] (refer to eq. **(3.7)**). Indeed, fitting modeled values of $\langle k_p \rangle$ with eq. **(3.30)** yields n = 4.1, a value which is concordant with what one might expect, referring to *Fig. 3.13*.

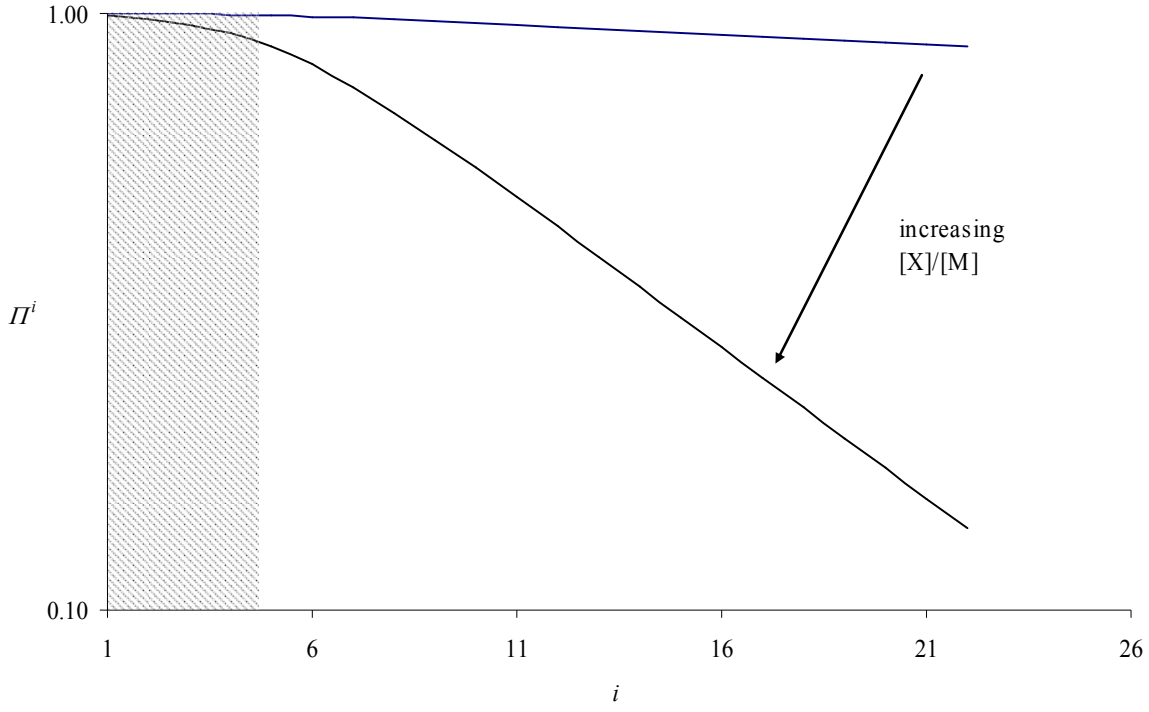

Fig. 3.13 The logarithmic dependence of $\Pi^i = \prod_{j=1}^{i} \left(1 + \frac{k_{trX}}{k_p^j} \frac{[X]}{[M]}\right)^{-1}$ (see eq. **(3.26)**) on chain length, i. Eq. **(3.24)** with C_1 = 15.8 and $i_{½}$ = 1.12 were used for calculating k_p^i. Representative values of [X]/[M] used were 9×10^{-3} (top) and 0.15 (bottom), with the direction of increasing [X]/[M] also indicated. The right-hand border of the shaded box corresponds to the value of $n\times i_{½}$ subsequently determined (see text).

In principle the only sure way to calculate $\langle k_p \rangle$ is *via* iterative evaluation of eq. **(3.20)**, as has been done throughout this work. However it is evident from *Fig. 3.12* and the ensuing discussion that eq. **(3.26)** (or eq. **(3.30)** if appropriate) can be considered a thoroughly acceptable alternative, provided only that it is transfer (and not, for example, an extremely high initiator concentration) that is driving $\langle k_p \rangle$ to deviate from its long-chain value. This will almost always be the case.

Molecular weight distributions

Fig. 3.14 presents a comparison of a selection of experimental MWDs with the corresponding modeling predictions. It is stressed that there is a sense in which the modeling results are predictions, for it has only been i_{peak} values which are fitted. It is evident that the model does an excellent job of reproducing the entire MWDs. Some differences are evident, however.

In *Fig. 3.14*, the trend that was evident in *Fig. 3.5* is even more clear – in the rightmost distribution (lowest f_{DDM}), the experimental peak position is at a noticeably lower value of log(M) than the simulated peak position, and in the leftmost distribution (highest f_{DDM}) the opposite situation applies. A second feature is particularly apparent in the two right-hand distributions: on the low molecular weight side of the distributions, simulations predict that more polymer should be present than is measured. If these trends are real then they are difficult to explain, but most likely these trends just reflect systematic GPC error.

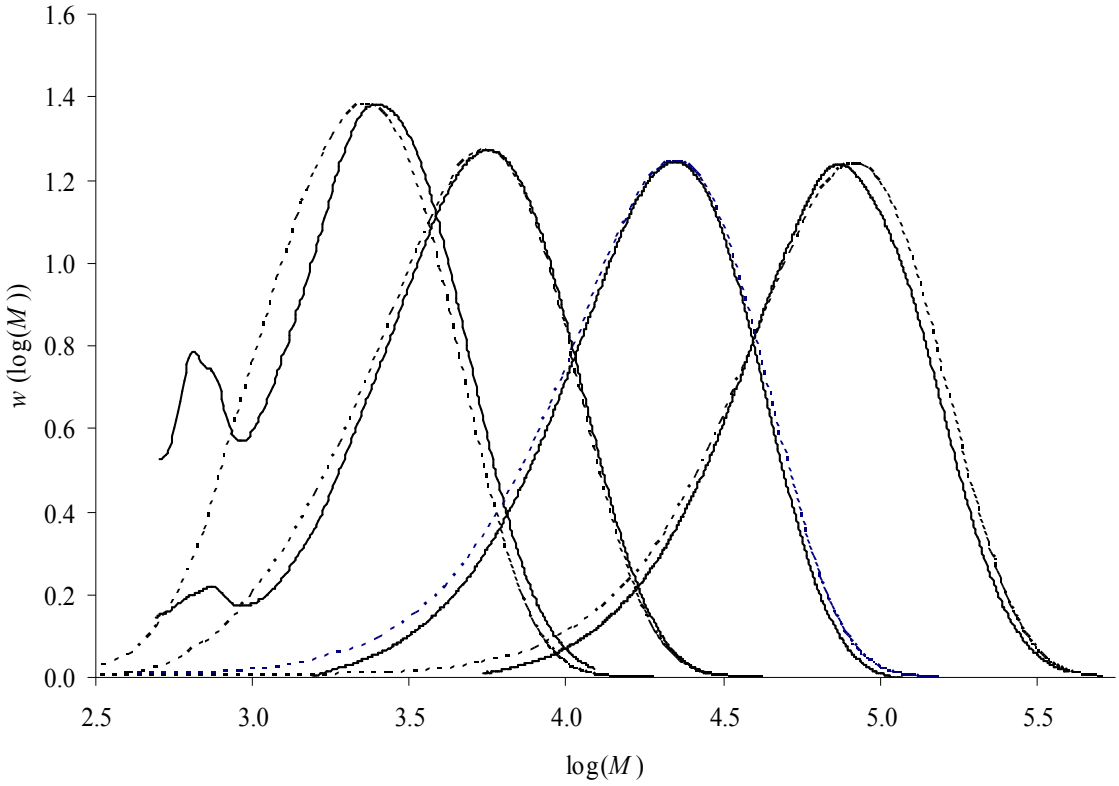

Fig. 3.14 MWD curves, plotted as relative weight of polymer, $w(\log(M))$, *vs.* logarithmic molecular weight, $\log(M)$. Selected experimental distributions (solid lines), from left to right, are from datasets 51-2, 51-6, 61-1 and 61-3 of *Tab. 3.2*. Also presented are the corresponding simulated distributions (dotted lines), obtained by fitting i_{peak} values (see *Fig. 3.5*). Experimental distributions have been scaled so as to have the same peak heights as the corresponding simulated distributions.

Values of average degrees of polymerisation

It is of interest to compare predicted and experimental values of $\overline{DP}_n$ and $\overline{DP}_w$. This is done in *Fig. 3.15*. The reason this comparison is of interest is because the modeling values of $\overline{DP}_n$ and $\overline{DP}_w$ are not fitted, but are just those that follow from the fitting of the rate and i_{peak} data.

It is evident that the experimental values of $\overline{DP}_n$ and $\overline{DP}_w$ are very well reproduced. The fact that the modeling values are generally a bit low is acceptable in view of the probable inflation of the experimental values due to the lack of calibration of GPC data at lowest molecular weights (as discussed in Section 3.3). A more resounding vote of confidence in the modeling comes from the $\overline{DP}_n$ and $\overline{DP}_w$ values in the experiments without DDM. In this case the modeling values are effectively *a priori* predictions, because i_{peak} values from these experiments were not part of the fitting procedure (refer to $f_{DDM} = 0$ in *Fig. 3.5*). So what *Fig. 3.15* is showing at $f_{DDM} = 0$ is that the termination model used to reproduce the rate data also reproduces very well, without any parameter value manipulation, the values of $\overline{DP}_n$ and $\overline{DP}_w$

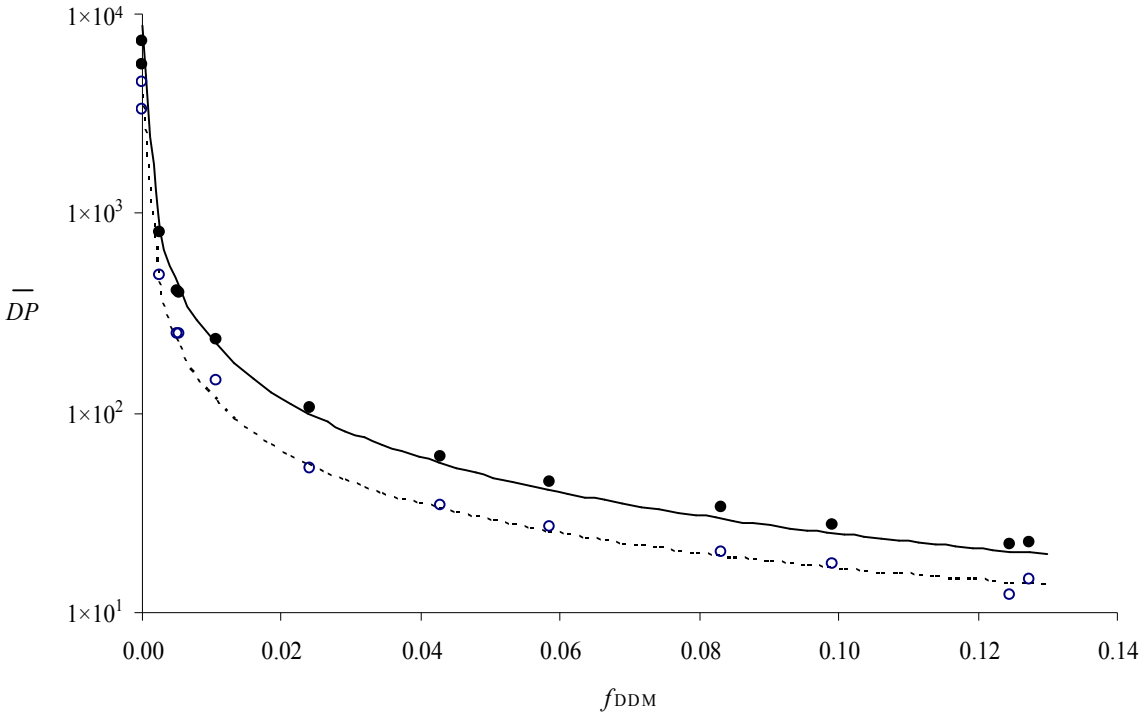

Fig. 3.15 Logarithmic MWD averages calculated from the experimental data of *Tab. 3.2* (points – $\overline{DP}_w$: filled; $\overline{DP}_n$: hollow), and from modeling (lines – $\overline{DP}_w$: unbroken; $\overline{DP}_n$: dashed).

when dead chain formation is exclusively by termination. Specifically, simulations predict $\overline{DP}_n$ = 3020 and $\overline{DP}_w$ = 6030, which compare favourably with values calculated from the data of *Tab. 3.2*.

In relation to *Fig. 3.15* it should also be mentioned that modeling values of $\overline{DP}_n$ and $\overline{DP}_w$ are significantly affected by CLDP parameters: as the extent of CLDP becomes greater, values of $\overline{DP}_n$ and $\overline{DP}_w$ increase, because small chains are propagating more quickly, and thus larger chains are produced. If one attempts to fit $\overline{DP}_n$ and $\overline{DP}_w$ values, this necessitates that C_{trX} be increased in order to offset this effect. Alternatively, for a particular CLDP model one can shift values of $\overline{DP}_n$ and $\overline{DP}_w$ up or down by decreasing or increasing (respectively) C_{trX}. For example, one could decrease C_{trX} in order to obtain better agreement in *Fig. 3.15*. However this approach is unsatisfactory in that then the entire MWD is shifted, and so agreement is lost between the central peak position of experimental and simulated MWDs. This is one reason why we concluded that the superior modeling procedure is to fit experimental i_{peak} values.

Polydispersity index

Discussion of $\overline{DP}_n$ and $\overline{DP}_w$ leads naturally into discussion of the polydispersity index, *PDI* = $\overline{DP}_w/\overline{DP}_n$, experimental and model values for which are presented in *Fig. 3.16*. *PDI* is discussed separately here because a novel result emerges, as is immediately evident from *Fig. 3.16*: there is a steady decrease in *PDI* with increasing f_{DDM}, with values being reached that are well below 2, the classical value for transfer control. This is clearly evident in the simulated data of *Fig. 3.16*. This trend is also responsible for the increasing MWD peak height with increasing f_{DDM} in *Fig. 3.14* – since the (simulated) distributions are normalised

so that they have the same area, decreasing *PDI* decreases the width of the distributions so that the height must increase.

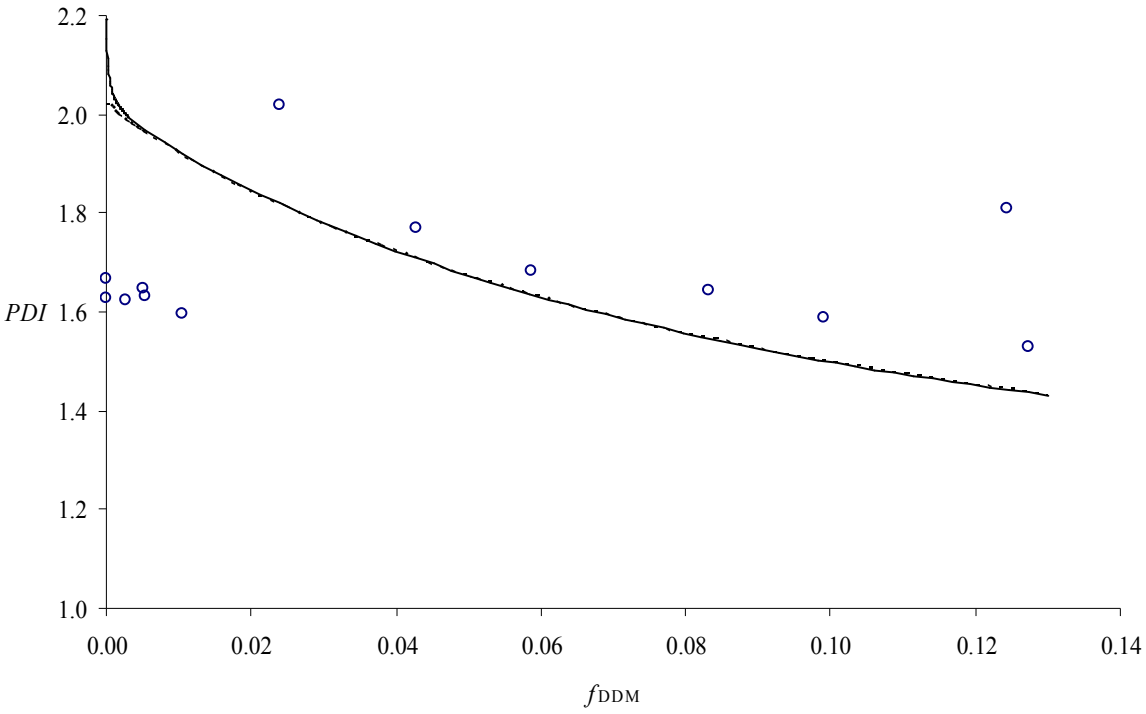

Fig. 3.16 Polydispersity index ($PDI = \overline{DP}_w/\overline{DP}_n$) calculated from the experimental data of *Tab. 3.2* (points) and from simulations (lines – full: $\lambda = 1$; dotted: $\lambda = 0.5$).

The first thing to understand is the origin of this result. It is that CLDP causes small chains to propagate faster, and thus fewer dead chains of these sizes are formed. This means that there is narrowing of the dead-chain CLD, and thus *PDI* is reduced. Having realised this, it is obvious that the stronger the CLDP, the greater this effect. Equally, the higher the frequency of transfer, the higher the proportion of small chains that experience CLDP, and thus the greater the reduction of *PDI*. It is the latter that is observed in *Fig. 3.16*, with, perhaps remarkably, *PDI* as low as 1.4 being predicted at the highest DDM level.

The next issue to consider is whether this remarkable trend is present in the experimental data. It seems to be, with the experimental values of *PDI* steadily decreasing for $f_{DDM} \geq 0.02$. Further, these experimental *PDI* are only slightly above the modeling predictions, exactly as one would expect due to GPC broadening (which of course is not accounted for in the modeling procedure). On the other hand, PDI may be underestimated due to error associated with GPC baseline subtraction.[28] In fact one would have to say that our modeling has helped us to understand what would otherwise be inexplicable experimental results, *viz.* the *PDI* being well less than 2 in transfer-dominated systems. This is a classic example of how modeling can advance the understanding of FRP by making sense of unexpected results.

Notwithstanding the above triumph, there is the issue of what is happening at low DDM levels – specifically, $f_{DDM} < 0.02$ – where the experimental *PDI* are all less than the values from modeling. In this regard it can firstly be confirmed that the modeled *PDI* are correct, for from the work of Olaj *et al.*[29] one can derive the following equation for *PDI* as a function of λ and e:

$$PDI = \frac{1+\lambda}{2}\left(\frac{\Gamma\left(\frac{6-e}{2-e}\right)}{\left(\Gamma\left(\frac{4-e}{2-e}\right)\right)^2} + 1 - \lambda\right) \qquad \textbf{(3.31)}$$

This equation (where $\Gamma()$ is the gamma function) is derived making the long-chain assumption, and holds only in the absence of transfer. The geometric mean model for termination is also used, however it has been shown that switching to other models is of negligible consequence.[30] For $\lambda = 1$, eq. **(3.31)** gives *PDI* = 2.18 and 2.83 for $e = 0.16$ and 0.5 respectively. Although the composite termination model, which employs both these values of e, has been used to generate the modeling results of *Fig. 3.16*, it is evident the obtained *PDI* of 2.19 at $f_{DDM} = 0$ is essentially identical to the expected $e = 0.16$ value. This makes sense,

because in the absence of DDM the chains will be long, meaning that the long-chain value of e (*i.e.*, 0.16) dominates the termination kinetics.[1]

In view of the disagreement between model and experimental *PDI* at low f_{DDM}, we decided to introduce some termination by combination into our simulations, knowing that this would reduce the obtained *PDI*. This is reasonable in view of the fact that it is now definitively established that termination in MMA is not exclusively by disproportionation.[20,21] Equally, these studies have confirmed that termination is predominantly by disproportionation, so we used $\lambda = 0.5$ as a lower bound value (in fact λ for MMA will not be this low[20,21]). The results are shown in *Fig. 3.16*. Only at the very lowest f_{DDM} is there an effect, because otherwise dead chain formation is predominantly by transfer, so that the particulars of the termination mechanism are unimportant. Near $f_{DDM} = 0$ it is indeed observed that introducing combination does lower the value of *PDI* – the value obtained from the calculations presented in *Fig. 3.16* is *PDI* = 2.02. Further, the effect is astonishingly accurately predicted by eq. **(3.31)**, which gives *PDI* = 2.01 for $e = 0.16$. However this reduction is not enough to explain the experimental *PDI* data of between 1.6 and 1.7, which are too low to be explained by any FRP model in which termination is predominantly by disproportionation (because that must lead to *PDI* of 2 or greater).

An inspection of the modeling and experimental MWDs at low f_{DDM} – see *Fig. 3.14* – reveals that the origin of the *PDI* discrepancy is at chain lengths below i_{peak}, where in the experiments not quite as much polymer was observed as modeling would predict, with the MWDs otherwise being in good agreement. Beyond this one can only speculate, although it is worth making the general point that *PDI* is difficult to determine to high precision, as indeed is implicit in the slight difference between experimental and model MWDs in *Fig. 3.14* giving rise to a relatively large difference in *PDI*. We realise that this lack of (perfect) agreement

between model and experimental *PDI* data at low f_{DDM} calls into question the accuracy of all experimental *PDI* values, and therefore raises the issue of whether the agreement at high f_{DDM} is just a fortuitous accident. However we feel that this agreement is sufficiently remarkable and unexpected that it cannot just be a coincidence.

Combined use of termination rate coefficients and number-average chain length

A relationship sometimes used to analyse FRP data in order to determine the chain-length-dependence of termination is

$$\langle k_t \rangle \approx k_t^{1,1} (\overline{DP}_n)^{-e} \qquad \textbf{(3.32)}$$

Although originally derived for steady-state data,[5,30] this equation has also been shown to hold for PLP[31-33] and even rotating sector[34] data. As indicated the constant of proportionality in eq. **(3.32)** is only approximately equal to $k_t^{1,1}$,[1,5] however it is close enough that a log-log plot of $\langle k_t \rangle$ *vs.* $\overline{DP}_n$ gives a good estimate of $k_t^{1,1}$ as the intercept; further, the slope of such a plot gives *e* accurately. Therefore in *Fig. 3.17* we have plotted our experimental data in this way, where the $\langle k_t \rangle$ values are those obtained from the experimental $\langle k_p \rangle / \langle k_t \rangle^{0.5}$ values assuming, as an experimental worker might, a constant $\langle k_p \rangle$ (= 834 L mol^{-1} s^{-1} in this case). These are the open circles of *Fig. 3.17*, with the dotted line being the best fit of them.

The dotted line in *Fig. 3.17* has slope of -0.084 and intercept of 7.4×10^7 L mol^{-1} s^{-1}. According to eq. **(3.32)** one would conclude from this that $e = 0.084$ and $k_t^{1,1} \approx 7.4\times10^7$ L mol^{-1} s^{-1}. Not only is this value of $k_t^{1,1}$ non-physically low, but in the context of the rest of this work it is now clear that both values are misleading because of the assumption that $\langle k_p \rangle$ is constant. Indeed, if one were to ignore the two data points from the experiments without DDM, the rest of the data would have a (very slight) positive slope, leading to $e < 0$, which is ridiculous in that it suggests that termination becomes faster as chains become longer.

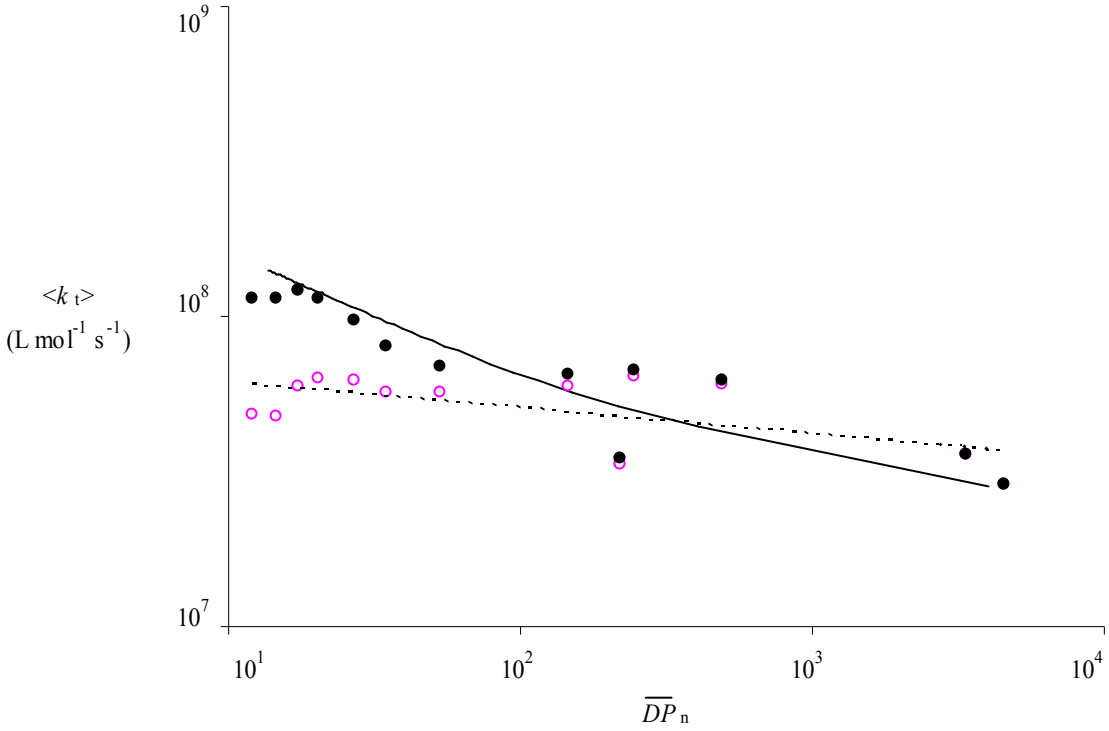

Fig. 3.17 Double logarithmic plot of data as $<k_t>$ *vs.* $\overline{DP}_n$. Points: experimental values assuming constant $<k_p>$ (open circles) and using $<k_p>$ from modeling (filled circles); dotted line: best fit to open circles; unbroken curve: modeling values. Note that for the rightmost two points, the open and closed circles coincide.

In view of the above, it is evident that if one wishes to plot values of $\log<k_t>$ *vs.* $\log \overline{DP}_n$, then any variation of $<k_p>$ has to be allowed for in deducing $<k_t>$ from measured rates. To illustrate this, we have used $<k_p>$ values from modeling to calculate $<k_t>$ from the measured rates. This leads to the filled circles of *Fig. 3.17*. Superimposed on these (as an unbroken line) are the best-fit values from our modeling (*i.e.*, composite termination model results of *Fig. 3.11*). It is evident that 'experiment' and theory are now in agreement. Further, if one were to fit the modeling results, one would conclude from the slope of the fit at high chain

lengths that $e_L \approx 0.16$, from the slope of the fit at low chain lengths that $e_S \approx 0.5$, and from the intercept (*i.e.*, value of $\langle k_t \rangle$ at $\overline{DP}_n = 1$) that $k_t^{1,1} \approx 5 \times 10^8$ L mol^{-1} s^{-1}. All of these conclusions would be correct of course, confirming that this method of data analysis can be rigorous – provided that one uses genuine values of $\langle k_t \rangle$ (as opposed to values obtained assuming a constant $\langle k_p \rangle$).

Apart from the obvious difficulty of obtaining experimental data that are sufficiently precise to make such conclusions (refer to the scatter of the filled circles about the unbroken line), there is also the difficulty of how $\langle k_p \rangle$ varies. In principle this is best addressed by carrying out full modeling, however the success of eq. **(3.26)** suggests that it is valid to put faith in this equation, and use it to calculate the way in which $\langle k_p \rangle$ must be varying. Thus one may determine $\langle k_t \rangle$ values that may, for example, be used to plot $\log\langle k_t \rangle$ *vs.* $\log \overline{DP}_n$.

At least two studies in the literature[35,36] have determined e as above for transfer-dominated systems with relatively short chain lengths (although not quite as short as here). Both analyses assumed constant $\langle k_p \rangle$. It is thus now clear that the obtained values of e (both about 0.2) must be lower bounds for the true values, which could be better estimated by use of eq. **(3.26)** to reanalyse the rate data. Because of the possibility of CLDP, in general the $\log\langle k_t \rangle$ *vs.* $\log \overline{DP}_n$ procedure should be used with caution to determine e – insofar as it is accurate when a constant $\langle k_p \rangle$ has been assumed, it will be in yielding values of e_L, because for long-chain systems $\langle k_p \rangle$ will be invariant. A further point worth mentioning is that values of $\overline{DP}_n$ obtained from GPC are somewhat inaccurate. By contrast, this work has proposed a more accurate way of using GPC data (*i.e.*, i_{peak} modeling) for investigating kinetics.

Other considerations

A number of factors cannot be taken into account with the current state of our knowledge about this system. It seems likely however that they are of minor importance, although in combination they may alter our conclusions somewhat.

In our kinetic scheme we do not distinguish between initiator-derived monomeric radicals and transfer-derived monomeric radicals (R_1). Therefore we have implicitly assumed that rate of addition of monomer to DDM derived radicals (*i.e.* 'reinitiation' of transfer-derived radicals) is the same as the rate of propagation of initiator-derived radicals. Clearly these are chemically distinct species ($C_9H_{17}O_2^{\bullet}$ for the AIBN-derived radical and $C_{12}H_{25}S^{\bullet}$ for the DDM-derived radical), and it seems likely that their reaction rates will be different. In systems where the reinitiation step is particularly slow, the rate of polymerisation is adversely affected (retardation) or stopped until the chain transfer agent is consumed (inhibition). There is no indication that the rate of polymerisation is so adversely affected by the addition of chain transfer agent in this system, so for simplicity we have made the assumption outlined above. Note also that in calculations where CLD propagation is used, the value of k_p^1 is rather high, which probably exacerbates the problem.

We have made use of the idea that propagation is chain-length dependent to explain this data. At the same time, we use a chain-length independent model for chain transfer. In this work best results were obtained with chain-length independent transfer (eq. **(3.20)** is easily adapted to the case of CLD transfer), but the actual CLD of transfer is unknown.

3.6 Conclusion

It is hard to think of another work in which modeling of FRP data has been carried out as rigorously and as successfully as here. We have shown that the composite CLDT model, in

conjunction with reasonable CLDP parameters, can provide a consistent explanation for the data we have obtained. Of course this does not guarantee rectitude, as one cannot dispel the possibility that another model might do as well, or even better, in reproducing data. Indeed, we have demonstrated in this work that other models can also fit our data. However, these other models do fail to explain some of the observed details of termination and propagation kinetics, so it would seem that more sophisticated models such as the composite termination model are necessary. It is interesting that when propagation is assumed to be chain length independent, using $e = 0.16$ for all termination gives superior agreement with the data. This suggests that the traditional approach of ignoring CLDP in analysing data has had the effect of masking that termination has a stronger chain length dependence at short chain lengths (recognising here that few would dispute that $e \approx 0.2$ for 'long' chains at low conversion). In fact CLDP has interesting effects on the kinetics of FRP, for example the narrowing of the MWD that has been discussed above. Simulations will be used to demonstrate these effects in a paper that is currently in preparation. In general it is recommended that whenever polymerisations produce very short chains, CLDP as well as CLDT must be incorporated into modeling of the data, otherwise false conclusions will be reached. Of course this can make modeling a sophisticated exercise, as has been seen. However this is preferable to oversimplifying the analysis and arriving at incorrect conclusions.

The most obvious additional work suggested by the present endeavours would be that all FRP data be analysed with the rigour employed here. Obviously it would be of interest to do as we have here but for experimental systems with different monomers and/or different chain transfer agents, *e.g.* catalytic chain transfer agents.[35-37] In particular it is recommended that both rate and MWD data be measured and modeled.

3.7 Postscript

A summary of the major results of this chapter has been published as Smith, G. B.; Russell, G. T.; Yin, M.; Heuts, J. P. A. *Eur. Polym. J.* **2005**, *41*, 225. Some further results from this chapter were published in Smith, G. B.; Heuts, J. P. A.; Russell, G. T. *Macromol. Symp.* **2005**, *226*, 133-146.

References

(1) Smith, G. B.; Russell, G. T.; Heuts, J. P. A. *Macromol. Theory Simul.* **2003**, *12*, 299-314.

(2) Tirrell, M. *Rubber Chem. Technol.* **1984**, *57*, 523-556.

(3) Fujita, H. *Polymer Solutions*; Elsevier: Amsterdam, 1990.

(4) Fischer, H.; Paul, H. *Acc. Chem. Res.* **1987**, *20*, 200-206.

(5) Mahabadi, H. K. *Macromolecules* **1985**, *18*, 1319-1324.

(6) Olaj, O. F.; Vana, P. *Macromol. Rapid Commun.* **1998**, *19*, 433-439.

(7) Olaj, O. F.; Vana, P. *Macromol. Rapid Commun.* **1998**, *19*, 533-538.

(8) de Kock, J. B. L., Ph.D. Thesis, Technical University of Eindhoven, 1999

(9) de Kock, J. B. L.; van Herk, A. M.; German, A. L. *J. Macromol. Sci., Polym. Rev.* **2001**, *C41*, 199-252.

(10) Vana, P.; Davis, T. P.; Barner-Kowollik, C. *Macromol. Rapid Commun.* **2002**, *23*, 952-956.

(11) Buback, M.; Egorov, M.; Junkers, T.; Panchenko, E. *Macromol. Rapid Commun.* **2004**, *25*, 1004-1009.

(12) Eastmond, G. C. *Makromol. Chem., Macromol. Symp.* **1987**, *10/11*, 71-87.

(13) Hutchinson, R. A.; Paquet, D. A., Jr.; McMinn, J. H. *Macromolecules* **1995**, *28*, 5655-5663.

(14) Berger, K. C. *Makromol. Chem.* **1975**, *176*, 3575-3592.

(15) Beuermann, S.; Buback, M.; Davis, T. P.; Gilbert, R. G.; Hutchinson, R. A.; Olaj, O. F.; Russell, G. T.; Schweer, J.; van Herk, A. M. *Macromol. Chem. Phys.* **1997**, *198*, 1545-1560.

(16) Barson, C. A. In *Chain Polymerization I*; Eastwood, G. C., Ledwith, A., Russo, S., Sigwalt, P., Eds.; Pergamon: Oxford, 1989; Vol. 3, pp 171-183.

(17) Heuts, J. P. A.; Davis, T. P.; Russell, G. T. *Macromolecules* **1999**, *32*, 6019-6030.

(18) Clay, P. A.; Gilbert, R. G. *Macromolecules* **1995**, *28*, 552-569.

(19) Moad, G.; Solomon, D. H. *The Chemistry of Free Radical Polymerization*; 1st ed.; Pergamon: Oxford, 1995.

(20) Zammit, M. D.; Davis, T. P.; Haddleton, D. M.; Suddaby, K. G. *Macromolecules* **1997**, *30*, 1915-1920.

(21) Zammit, M. D.; Davis, T. P.; Haddleton, D. M. *Macromolecules* **1996**, *29*, 492-494.

(22) Heuts, J. P. A.; Gilbert, R. G.; Radom, L. *Macromolecules* **1995**, *28*, 8771-8781.

(23) Gridnev, A. A.; Ittel, S. D. *Macromolecules* **1996**, *29*, 5864-5874.

(24) Willemse, R. X. E.; Staal, B. B. P.; van Herk, A. M.; Pierik, S. C. J.; Klumperman, B. *Macromolecules* **2003**, *36*, 9797-9803.

(25) Olaj, O. F.; Bitai, I.; Hinkelmann, F. *Makromol. Chem.* **1987**, *188*, 1689-1702.

(26) Buback, M.; Gilbert, R. G.; Hutchinson, R. A.; Klumperman, B.; Kuchta, F.-D.; Manders, B. G.; O'Driscoll, K. F.; Russell, G. T.; Schweer, J. *Macromol. Chem. Phys.* **1995**, *196*, 3267-3280.

(27) Olaj, O. F.; Vana, P.; Zoder, M.; Kornherr, A.; Zifferer, G. *Macromol. Rapid Commun.* **2000**, *21*, 913-920.

(28) Moad, G.; Moad, C. L. *Macromolecules* **1996**, *29*, 7727-7733.

(29) Olaj, O. F.; Zifferer, G.; Gleixner, G. *Macromolecules* **1987**, *20*, 839-850.

(30) Olaj, O. F.; Zifferer, G. *Macromolecules* **1987**, *20*, 850-861.

(31) Olaj, O. F.; Kornherr, A.; Zifferer, G. *Macromol. Rapid Commun.* **1997**, *18*, 997-1007.

(32) Olaj, O. F.; Kornherr, A.; Zifferer, G. *Macromol. Rapid Commun.* **1998**, *19*, 89-96.

(33) Olaj, O. F.; Kornherr, A.; Zifferer, G. *Macromol. Theory Simul.* **1998**, *7*, 501-508.

(34) Olaj, O. F.; Kornherr, A.; Zifferer, G. *Macromolecules* **1999**, *32*, 8800-8806.

(35) Suddaby, K. G.; Maloney, D. R.; Haddleton, D. M. *Macromolecules* **1997**, *30*, 702-713.

(36) Kukulj, D.; Davis, T. P. *Macromol. Chem. Phys.* **1998**, *199*, 1697-1708.

(37) Heuts, J. P. A.; Roberts, G. E.; Biasutti, J. D. *Aust. J. Chem.* **2002**, *55*, 381-398.

4 An Analysis of Steady-State Free-Radical Polymerisation Kinetics with Chain-length-dependent Termination: Theoretical Aspects

Abstract

A general description of steady state free radical polymerisation incorporating chain-length-dependent termination and propagation is presented and analysed. Results obtained by previous workers are discussed. A convenient framework for analysis of the model and comparison with experimental data is described herein.

4.1 Introduction

Although for many years it has been understood that the termination reaction in free radical polymerisation (FRP) must be chain length dependent,[1,2] analysis of experimental data is usually performed using the 'classical kinetics' model, which assumes chain-length-independent (CLI) termination. Indeed, it is often found that the classical model provides at least a superficially adequate description of data,[3] an example of which is provided in Chapter 3. However, advances in experimental techniques, including measurement of individual (propagation or termination) rate coefficients by (for example) pulsed laser polymerisation (PLP), have improved the sensitivity of experimental data to the point where the effects of chain-length dependent termination (CLDT) may often be reliably detected. The work of Chapter 3 also evidences that chain-length-dependent propagation (CLDP) often needs to be included too. It is timely therefore to investigate the effects of CLDT and CLDP from a modeling standpoint. The issue of CLDT of course has been investigated previously for steady-state polymerisation,[4-15] with the work of Olaj *et al.*[5] providing the impetus and foundation for the present investigation. Not only is this work progressed here, but CLDP is

introduced for the first time, it turns out at the cost of essentially no additional complexity. It is noted that Olaj *et al.* have also recently published an impressive mountain of work on the consequences that CLDT has on intermittently initiated polymerisation.[16-26] While this work is of enormous relevance for these types of experiment, they are beyond the scope of the present work, in which only steady-state polymerisation is considered.

As will soon become apparent, the introduction of chain-length-dependent reactivities into the FRP scheme in principle results in an enorrmous multiplication of complexity. However it will be shown that not all this complexity is necessary. The motivation for the present work is to develop a theoretical framework that is relatively easy to use, compared with full numerical calculations, for analysis of experimental data. We deal with a general model incorporating CLD termination and propagation, and MWDs as well as kinetics are discussed. We are aware that one of the virtues of classical free-radical polymerisation kinetics is simplicity, which is why most experimental workers continue to adopt this approach even in the face of the overwhelming evidence that it is physically flawed.[2,3] Therefore we strive to minimise the complications introduced by CLD termination and propagation.

4.2 Free Radical Polymerisation Model

Reaction scheme

We consider the usual reactions of free radical polymerisation in the following kinetic scheme:

$$\mathrm{I} \xrightarrow{R_{\mathrm{init}}} \mathrm{R}_1 \qquad \text{Initiation}$$

$$R_i + M \xrightarrow{k_p^i} R_{i+1} \qquad \text{Propagation}$$

$$R_i + X_n \xrightarrow{k_{tr}^{X_n}} D_i + R_1 \qquad \text{Chain transfer}$$

$$R_i + R_j \xrightarrow{\lambda k_t^{i,j}} D_i + D_j \qquad \text{Termination by disproportionation}$$

$$R_i + R_j \xrightarrow{(1-\lambda) k_t^{i,j}} D_{i+j} \qquad \text{Termination by combination}$$

Free radical initiator, monomer and chain transfer agent(s) are denoted by I, M and X_n respectively, where n is an index enumerating distinct chain transfer agents. Radicals and dead polymer are denoted by R_i and D_i respectively, where i is the chain-length (in monomer units) of the species. The aforementioned chain length distributions are subsequently referred to as the radical chain-length distribution (RCLD) and dead polymer chain-length distribution (DCLD), respectively. The rate of initiation is denoted by R_{init}, and rate coefficients k are as indicated. The number fraction of termination that occurs by disproportionation is denoted λ. Note that propagation and termination rate coefficients are dependent on the chain-lengths (i, j) of the radical(s) involved, whereas all previous workers[4-15] considered only chain-length dependent termination in their analysis of steady-state kinetics. The concept of chain-length dependent termination is central to this chapter and will now be examined in more detail.

Termination models

In this work, we consider three commonly used models for the chain-length dependence of the termination rate coefficient k_t. For termination of two radical chains of equal length (homotermination), all three models are equivalent:

$$k_t^{i,i} = k_t^{1,1}\, i^{-e} \qquad \textbf{(4.1)}$$

In eq. **(4.1)**, i is the chain length of the terminating radicals, $k_t^{1,1}$ is the rate coefficient for termination of two chain-length one (monomeric) radicals, and the parameter e determines the rate of decrease of $k_t^{i,i}$ with chain length. When $e = 0$, k_t is the same value for all chain lengths, and so-called classical kinetics apply. In Chapter 2 we advanced a composite termination model, wherein the parameter e varied with chain length. Here we consider long chains, and also the limit of infinitely long chains, where the short-chain phenomenon that the composite termination model deals with is of minor importance. On the other hand, solutions will be presented in such a way that such models can be easily incorporated.

The models differ from each other in their description of termination of radicals of different chain lengths. Each model involves a substitution of a different 'mean' of the chain lengths i and j of the terminating radicals in place of the chain length i in equation **(4.1)**. Eqs. **(4.2)**, **(4.3)** and **(4.4)** are for the harmonic mean (hm), diffusion mean (dm) and geometric mean (gm) respectively.

$$k_t^{i,j}\,(\text{hm}) = k_t^{1,1}\left(\frac{2ij}{i+j}\right)^{-e} \qquad \textbf{(4.2)}$$

$$k_t^{i,j}\,(\text{dm}) = k_t^{1,1}\,(i^{-e} + j^{-e})/2 \qquad \textbf{(4.3)}$$

$$k_t^{i,j}\,(\text{gm}) = k_t^{1,1}\,(i\,j)^{-e/2} \qquad \textbf{(4.4)}$$

The physical meaning of these models has been discussed elsewhere.[3] To summarize, the hm describes the situation in which segmental rearrangements control the rate of termination[4,27] while the dm describes the (more common) situation of center-of-mass diffusion controlling the rate of termination.[13,28-30]

It is convenient to adopt the approach of Olaj *et al.*[5] and define the general form of these equations:

$$k_t^{i,j} = k_t^{1,1} M(i,j) \quad \textbf{(4.5)}$$

In eq. **(4.5)**, $M(i,j)$ stands for one of the functional forms of eqs. **(4.2)**, **(4.3)** and **(4.4)**. Whereas the harmonic and geometric means are standardly defined means, the so-called[5] diffusion mean has its origin in the Smoluchowski equation for diffusion-controlled reactions. Note that when $e = 1$, the harmonic and diffusion mean models are equal. In the event of chain-length-independent termination, we simply have $M(i,j) \equiv 1$ so that $k_t^{i,j} = k_t^{1,1} = k_t$. Furthermore, it is possible to generalise the expressions for the diffusion and geometric mean models so that they only describe heterotermination:

$$M(i,j)\,(\mathrm{dm}) = (M(i,i) + M(j,j))/2 \quad \textbf{(4.6)}$$

$$M(i,j)\,(\mathrm{gm}) = \sqrt{M(i,i)\,M(j,j)} \quad \textbf{(4.7)}$$

This leaves one free to choose a model for homotermination (*i.e.*, $M(i,i)$ values) other than eq. **(4.1)**, for instance the composite termination model advanced in chapter 3. Note however that no such factorisation is possible for the harmonic mean termination model.

As noted above, the propagation reaction is also chain-length dependent. This is acknowledged for completeness, considering the conclusions about the importance of CLDP reached in chapter 3. However, the investigations of subsequent chapters focus on the behavior of the model at long chain lengths (where CLDP is of minor importance), and so we will also give results with CLI propagation. Following the approach of eq. **(4.5)**, the general form of a model for chain-length dependent propagation (CLDP) is

$$k_p^{\,i} = k_p^{\,\infty} N(i) \quad \textbf{(4.8)}$$

In this equation the chain-length dependence is defined relative to k_p^{∞}, the long-chain value of the propagation rate coefficient, as all but the shortest chains will grow with this value of k_p. In the event of CLI propagation, we simply have $N(i) \equiv 1$ so that $k_p^{i} = k_p^{\infty} = k_p$.

4.3 Analysis of the Model

Microscopic model equations

Regardless of whatever further approximations are made, the presence of chain-length dependent rate coefficients in the above kinetic scheme demands that a fully microscopic set of equations (*i.e.* recognising each chain length as a separate entity) be derived and solved.

From the above kinetic scheme, the following differential equations are derived. For polymerising radicals:

$$\frac{d[R_1]}{dt} = R_{init} + f_{tr}[R] - f_p^1[R_1] - f_{tr}[R_1] - f_t^1[R_1] \qquad \textbf{(4.9a)}$$

$$\frac{d[R_i]}{dt} = f_p^{i-1}[R_{i-1}] - f_p^i[R_i] - f_{tr}[R_i] - f_t^i[R_i] \quad , \quad i = 2, \infty \qquad \textbf{(4.9b)}$$

And now for dead polymer:

$$\frac{d[D_i]}{dt} = f_{tr}[R_i] + \lambda f_t^i[R_i] + (1-\lambda)\sum_{j=1}^{i-1} k_t^{j,i-j}[R_j][R_{i-j}] \quad , \quad i = 1, \infty \qquad \textbf{(4.10a)}$$

In eqs. **(4.9)** and **(4.10a)**, t is time; [R] is the total radical concentration; and f_{tr}, f_p^i and f_t^i are the frequencies with respect to radicals of the transfer, propagation and termination reactions respectively:

$$[R] = \sum_{j=1}^{\infty}[R_j] \qquad \textbf{(4.11a)}$$

$$f_{\mathrm{tr}} = \sum_{n} k_{\mathrm{tr}}^{\mathrm{X}_n} [\mathrm{X}_n] \qquad \textbf{(4.12)}$$

$$f_{\mathrm{p}}^{\,i} = k_{\mathrm{p}}^{\,i} [\mathrm{M}] \qquad \textbf{(4.13)}$$

$$f_{\mathrm{t}}^{i} = 2 \sum_{j=1}^{\infty} k_{\mathrm{t}}^{i,j} [\mathrm{R}_j] \qquad \textbf{(4.14a)}$$

For completeness it is noted that chain-length-dependent transfer (CLDTr) could very easily be included in the above model. Indeed, given that propagation is now established[31,32] as being chain-length dependent, it follows that transfer must also be chain-length dependent.[33] However essentially nothing is established about CLDTr, so it is justified not to include it. Further, it turns out that CLDTr has an undesirably complicating effect on the present results.

Steady-state chain-length distributions

We consider here continuously initiated polymerisations at low conversion, so that it is appropriate to make the steady state assumption (SSA) for radical species:

$$\frac{\mathrm{d}[\mathrm{R}_i]}{\mathrm{d}t} = 0 \qquad \textbf{(4.15)}$$

Using eq. **(4.15)**, eqs. **(4.9)** may be solved to give eq. **(4.16a)**:

$$[\mathrm{R}_i] = \frac{R_{\mathrm{init}} + f_{\mathrm{tr}} [\mathrm{R}]}{f_{\mathrm{p}}^{0}} \prod_{j=1}^{i} \frac{f_{\mathrm{p}}^{j\text{-}1}}{f_{\mathrm{p}}^{j} + f_{\mathrm{tr}} + f_{\mathrm{t}}^{j}} \qquad \textbf{(4.16a)}$$

In this equation, $f_{\mathrm{p}}^{0} = N(0)\ k_{\mathrm{p}}^{\infty}\ [\mathrm{M}]$ may be chosen arbitrarily, as it cancels out when the expression is evaluated. For convenience of derivation, we set $N(0) = 1$, so that $f_{\mathrm{p}}^{0} = f_{\mathrm{p}}^{\infty}$. The form of eq. **(4.16a)** invites the following definitions:

$$[\mathrm{R}_0] = \frac{R_{\mathrm{init}} + f_{\mathrm{tr}}\,[\mathrm{R}]}{f_{\mathrm{p}}^{\infty}} \qquad \textbf{(4.17a)}$$

$$P_i = \prod_{j=1}^{i} \frac{f_{\mathrm{p}}^{j\text{-}1}}{f_{\mathrm{p}}^{j} + f_{\mathrm{tr}} + f_{\mathrm{t}}^{j}} = \prod_{j=1}^{i} \frac{f_{\mathrm{p}}^{j\text{-}1}}{f_{\mathrm{p}}^{j}} \prod_{j=1}^{i} \alpha_j \qquad \textbf{(4.18a)}$$

It is noted that in the event of CLDTr, the transfer gain term in the numerator of eq. **(4.17a)** becomes a sum over all chain lengths. Although this may seem an innocuous change, in fact it has profound effects on both numerical procedures and analytic simplification. These results are presented here, but it is noted at this point that most of the important results that now follow do not hold in the event of CLDTr.

The quantity P_i has not previously been defined; as will emerge here, it is an extremely convenient quantity with which to work. This can be seen immediately: eq. **(4.16a)** may be written in the shorter form

$$[\mathrm{R}_i] = [\mathrm{R}_0]\, P_i \qquad \textbf{(4.16b)}$$

While the reason for introducing eq. **(4.16b)** may not at first be apparent, this form of the RCLD is rather convenient – the parameter $[\mathrm{R}_0]$ does not depend on chain length (explicitly, at least), and P_i is chain-length dependent. It is worth noting however, that the index of zero as used in the above equations (*i.e.* $N(0)$ and $[\mathrm{R}_0]$) has no physical meaning, and in particular it does not refer to primary radicals. The above definitions may be contrasted with those of Olaj *et al.*[5]: the parameter $[\mathrm{R}_0]$ defined here is identical, while P_i is related to the "propagation probability", $\alpha_i = (1 + f_{\mathrm{tr}} + f_{\mathrm{t}}^{i} / f_{\mathrm{p}}^{i})^{-1}$ used by Olaj *et al.*,[8,10] by the rightmost form of eq. **(4.18a)**. It is clear from this equation that α_i corresponds to the true propagation probability, which is $f_{\mathrm{p}}^{i\text{-}1} / (f_{\mathrm{p}}^{i} + f_{\mathrm{tr}} + f_{\mathrm{t}}^{i})$, only in the event of CLI propagation. This means that the results of Olaj *et al.*[5,8,10-12] hold only in this event. In essence Olaj *et al.*[5,8,10-12] make the

conceptual omission of failing to recognise the population balance equations, eqs. **(4.9),** and thus they never arrive at the true propagation probability.

We henceforth refer to P_i as the 'reduced' RCLD (rRCLD), since it will be seen that it is possible to obtain a solution for it with a reduced number of input parameters, compared to the number of input parameters required to solve eq. **(4.16a)**. This reduction in the number of parameters allows for a simpler analysis of the model's characteristics. The general approach of the derivation (see section 4.7) is to replace $[R_i]$ with the expression on the righthand side of eq. **(4.16b)**, and similarly replace $k_p^{\,i}$ and $k_t^{\,i,j}$ with expressions from eq. **(4.8)** and eq. **(4.5)**, respectively. Note that this reduction in the number of parameters is due to the use of the SSA, which, when applied to the *total* radical concentration, yields eq. (**4.19a**):

$$\frac{\mathrm{d}[R]}{\mathrm{d}t} = 0 = R_{\mathrm{init}} - \sum_{i=1}^{\infty} f_t^i\,[R_i] = R_{\mathrm{init}} - 2\sum_{i=1}^{\infty}\sum_{j=1}^{\infty} k_t^{\,i,j}\,[R_i]\,[R_j] \qquad \textbf{(4.19a)}$$

Combining this equation with eq. **(4.17a)**, it can be shown (see section 4.7) that[11]

$$r_t\,S_t + r_{tr}\,S_r = 1 \qquad \textbf{(4.20)}$$

with the definitions

$$r_t = \frac{\sqrt{2\,k_t^{\,1,1}\,R_{\mathrm{init}}}}{f_p^{\,\infty}} \qquad \textbf{(4.21)}$$

$$r_{tr} = \frac{f_{tr}}{f_p^{\,\infty}} \qquad \textbf{(4.22)}$$

$$(S_t)^2 = \sum_{i=1}^{\infty}\sum_{j=1}^{\infty} M(i,j)\,P_i\,P_j \qquad \textbf{(4.23a)}$$

$$S_r = \sum_{i=1}^{\infty} P_i \qquad \textbf{(4.24)}$$

The parameters[6,7] r_t and r_{tr} are comprised of rate parameters and are so named because they contain the parameters for termination and transfer respectively: S_t and S_r are the (weighted) sums of the rRCLD which appear in expressions for the rate of termination and the total radical concentration respectively. Eq. **(4.20)** establishes a correlation between these two sums, which will prove useful later on. In the case of CLI termination (classical kinetics), $S_t = S_r$, and S_r is given by eq. **(4.25)**.

$$S_r = \frac{1}{r_t + r_{tr}} \qquad \textbf{(4.25)}$$

As the CLDT parameter e increases, the extent to which $S_t < S_r$ will increase.

With the above definitions established, it is possible to show that eq. **(4.18a)** yields

$$\frac{P_i}{P_{i\text{-}1}} = \frac{N(i\text{-}1)}{N(i) + r_{tr} + \frac{r_t}{S_t}\sum_{j=1}^{\infty} M(i,j)\, P_j} \qquad \textbf{(4.18b)}$$

It is evident from eq. **(4.18b)** that the rRCLD (*i.e.* P_i for all chain lengths i) depends on the CLDP model $N(i)$, the CLDT model $M(i,j)$, and the two aggregate parameters r_t and r_{tr}. Further, in this general case (without considering the characteristics of the CLDT model $M(i,j)$), in order to evaluate the rRCLD one must start with an initial guess and iterate eq. **(4.18b)** until a convergence criterion is reached. It is worth noting that S_t in eq. **(4.18b)** need not be calculated directly from eq. **(4.23a)**, but may instead be far more cheaply calculated from eq. **(4.20)**, knowing the value of S_r – in other words, the calculation of a one-dimensional sum (S_r) replaces the calculation of a two-dimensional sum (S_t). Further, once a

solution for all P_i values has been obtained, the following equation, which is derived by eliminating the term $\sum_{j=1}^{\infty} M(i,j)\, P_j$ from eqs. **(4.23a)** and **(4.18b)**, may be used:

$$S_t = \frac{1}{r_t} \sum_{i=1}^{\infty} N(i\text{-}1)\, P_{i\text{-}1} - N(i)\, P_i - r_{tr}\, P_i \qquad \textbf{(4.23b)}$$

With chain-length-independent propagation, eq. **(4.23b)** becomes eq. **(4.23c)**, in which S_t is equivalent to the variable S_1 defined by Olaj *et al.*[5].

$$S_t = \frac{1}{r_t} \sum_{i=1}^{\infty} P_{i\text{-}1} - P_i - r_{tr}\, P_i \qquad \textbf{(4.23c)}$$

The RCLD may be recovered by using eq. **(4.16b)**, first calculating $[R_0]$ according to eq. **(4.17b)**. Note how some of the components of r_t must be individually defined in order to calculate the RCLD.

$$[R_0] = \sqrt{\frac{R_{init}}{2\, k_t^{1,1}}} / S_t \qquad \textbf{(4.17b)}$$

Considering now the dead polymer chain-length distribution, it can be shown that by using the approach of the previous section, eq. **(4.10a)** leads to eq. **(4.26)**.

$$[D_i] \sim r_{tr}\, P_i + \lambda\, (N(i\text{-}1)\, P_{i\text{-}1} - N(i)\, P_i - r_{tr}\, P_i) + \frac{1\text{-}\,\lambda}{2} \frac{r_t}{S_t} \sum_{j=1}^{i\text{-}1} M(i\text{-}j,j)\, P_{i\text{-}j}\, P_j \qquad \textbf{(4.26)}$$

In eq. **(4.26)**, the three terms are due to transfer, disproportionation, and combination respectively (see section 4.7). Contrary to the first two terms, evaluation of the term due to combination requires significant additional calculations in general.

Predicting experimental quantities – polymerisation rate and average molecular weight

Typically, FRP data do not allow direct comparison with the results of the equations given above. Commonly measured data are the overall rate of polymerisation, R_{pol}, and the number average degree of polymerisation, $\overline{DP}_n$.

$$R_{pol} = \frac{-d[M]}{dt} = \sum_{j=1}^{\infty} k_p^{\,i} [M] [R_j] \qquad \textbf{(4.27a)}$$

Eq. **(4.27a)** is generally applicable. With the SSA and CLI propagation ($N(i) \equiv 1$ and $k_p^{\,i} \equiv k_p$), the following equation applies:

$$R_{pol} = k_p [M] [R] = f_p \sqrt{\frac{R_{init}}{2\langle k_t \rangle}} \qquad \textbf{(4.27b)}$$

In the above equation, $f_p = k_p [M]$ and $\langle k_t \rangle$ is the chain-length averaged rate coefficient for termination, defined by eq. **(4.28a)**:[11]

$$\langle k_t \rangle = \sum_{i=1}^{\infty} \sum_{j=1}^{\infty} k_t^{\,i,j} \frac{[R_i]}{[R]} \frac{[R_j]}{[R]} = k_t^{\,1,1} \left(\frac{S_t}{S_r} \right)^2 \qquad \textbf{(4.28a)}$$

Alternatively, R_{pol} may be expressed in terms of S_r and S_t directly:[11]

$$R_{pol} = \frac{R_{init} S_r}{r_t S_t} \qquad \textbf{(4.27c)}$$

The number average molecular weight is defined by eq. **(4.29a)**:

$$\overline{DP}_n = \frac{\sum_{i=1}^{\infty} i \frac{d[D_i]}{dt}}{\sum_{i=1}^{\infty} \frac{d[D_i]}{dt}} \qquad \textbf{(4.29a)}$$

In section 4.7 it is shown that the distribution of eq. **(4.26)**, with CLI propagation, gives the following convenient equation (previously only presented in an obscure form[5]) for $\overline{DP}_n$:

$$\overline{DP}_n = \frac{1 + S_r}{r_{tr} S_r + \frac{1+\lambda}{2}(1 - r_{tr} S_r)} \qquad \textbf{(4.29b)}$$

It is worth noting about the above equation that when $\lambda = 1$ (*i.e.* all termination is by the disproportionation mechanism), $\overline{DP}_n = 1+S_r$, and thus is (approximately) equal to S_r.

From the above, it is clear that in order to compare model results with experimental data, it is necessary to know S_t and S_r, but that for these purposes the details of the calculations may be ignored. Therefore, in analysing the characteristics of the model, one should focus on the dependence of S_t and S_r on the model input parameters.

Results with geometric and diffusion mean termination models

Certain termination models lead to simplification of the equations for the steady state CLDs presented above. With the geometric mean model, eq. **(4.7)**, the expression for S_t, eq. **(4.23a)**, becomes[11]

$$S_t = \sum_{i=1}^{\infty} \sqrt{M(i,i)}\, P_i \qquad \textbf{(4.30)}$$

which in turn leads to the following equation for the rRCLD (previously presented in a different form and only for CLI propagation[11]):

$$\frac{P_i}{P_{i\text{-}1}} = \frac{N(i\text{-}1)}{N(i) + r_{tr} + r_t\sqrt{M(i,i)}} \qquad \textbf{(4.31)}$$

In contrast to the case with a general CLDT model (see eq. **(4.18b)**), eq. **(4.31)** may be evaluated without iteration. With CLI propagation, this equation is equivalent to the one given by Olaj *et al.*[12]

Similarly, the diffusion mean model, eq. **(4.6)**, leads to

$$(S_t)^2 = S_r \sum_{i=1}^{\infty} M(i,i)\, P_i \qquad \textbf{(4.32)}$$

and the rRCLD is given by

$$\frac{P_i}{P_{i\text{-}1}} = \frac{N(i\text{-}1)}{N(i) + \dfrac{S_r^{-1} + r_{tr}}{2} + M(i,i)\dfrac{r_t^2}{2\,(S_r^{-1} - r_{tr})}} \qquad \textbf{(4.33)}$$

The above equation makes use of eqs. **(4.20)** and **(4.32)** to arrive at an expression that includes only one unknown parameter, S_r. The equation must therefore be evaluated iteratively until convergence in S_r is achieved, so that it is more expensive to evaluate than the analogous expression for the geometric mean, eq. **(4.31)**. However, it is still far less expensive than the general case, where it is necessary to calculate a sum for each chain length i (see eq. **(4.18b)**) – this necessity greatly increases computation time, particularly for large chain lengths.

With the above in mind, it is clear that if computational expense is an issue, it is preferable to use either the geometric or diffusion mean termination model. Further, of the two, the diffusion mean model is physically more realistic, although slightly more computationally expensive.

The limits of dead chain formation by termination and transfer

Two limiting cases of the above solution can be identified, where dead chain formation occurs exclusively by termination, or by transfer. The limits can be defined with reference to eq. **(4.20)**. In the termination limit, $r_{tr} = 0$, so that $S_t = r_t^{-1}$ and S_r is also determined by r_t, although the rRCLD must be calculated to determine the latter dependency. Similarly, in the

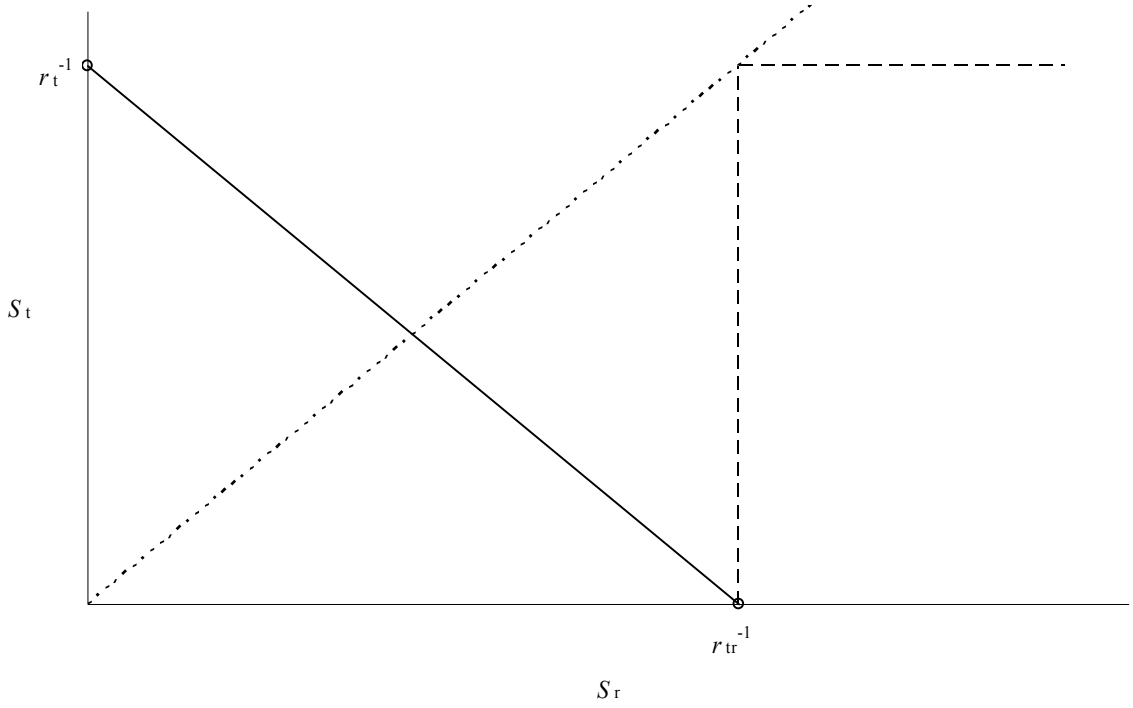

Fig. 4.1 Diagram of S_t *vs.* S_r, showing how eq. **(4.20)** (solid line) leads to the definition of the termination (long-dashed horizontal line) and transfer (long-dashed vertical line) limits. The case of CLI termination (short-dashed line), where $S_t = S_r$, is also shown.

transfer limit we can set $r_t = 0$, so that $S_r = r_{tr}^{-1}$, and calculation of the rRCLD is necessary to determine how S_t varies with r_{tr}. The situation is represented graphically in *Fig. 4.1*. If r_t and r_{tr} are both nonzero, eq. **(4.20)** dictates that solutions to **(4.18b)** must lead to values of S_t and S_r that fall upon the solid line. This has been verified by Olaj *et al.*[5] in simulations, although it

must be said that their presentation is difficult to follow, meaning that this remarkable result is obscured. In the termination limit, S_t is determined by r_t, and S_r must lie on the horizontal long-dashed line. Similarly in the transfer limit, S_r is determined by r_{tr}, and S_t must lie on the vertical long-dashed line. Also, as noted previously, the termination models used here all lead to $S_t \leq S_r$, so that all solutions lie below the short-dashed line.

There are slight differences in the nature of the two limits. The termination limit may be imagined as representing an actual physical system, where no transfer agent has been added and care has been taken to exclude the transfer reactions. However, the transfer limit is a limit in the sense of a mathematical ideal that can only be approached by physical systems, since there must always be some termination to balance initiation in order to have a steady state concentration of radicals. But the relevant comparison is between r_t and r_{tr} – as r_{tr} increases, the transfer limit is approached. In contrast to the physical situation, there are no difficulties with the above equations in setting $r_t = 0$, since eq. **(4.18b)** simply gives

$$P_i = \left(\frac{1}{1 + r_{tr}}\right)^i \qquad \textbf{(4.34)}$$

It must be noted that in the transfer limit, eq. **(4.23b)** cannot be used to calculate S_t, due to the assumptions made in its derivation being incompatible with the transfer limit; instead eq. **(4.23a)** for a general termination model or the equations for the geometric and diffusion means introduced in the previous section must be used.

4.4 Analytic solutions with the long chain assumption

In this section we will discuss the analytic solutions to the model equations that can be derived for certain special cases. For some years it has been known[6-9,12] that an analytic solution is available for the geometric mean model, eq. **(4.4)**, in the termination limit ($r_{tr} = 0$). Similar solutions are available in the transfer limit[5,6] ($r_t = 0$), but these are even less well-

known, perhaps due to less experimental interest in such conditions. Although the computational expense of the alternative, numerical solutions is no longer a really compelling reason to use these solutions, they point the way to general relationships that can be used to analyse model results calculated numerically. These solutions make the long chain assumption (LCA), in that sums are approximated with integrals.

In the case of the geometric mean termination model in the termination limit, the following equation can be derived:

$$S_r\,(\mathrm{gm}, r_{tr}=0, \mathrm{LCA}) = \Gamma(2/(2-e))\,(1-e/2)^{e/(2-e)}\,(r_t)^{-2/(2-e)} \qquad \textbf{(4.35)}$$

In the transfer limit, analytic expressions may be derived for both the geometric and diffusion mean termination models. In both cases, eq. **(4.36)** is used to approximate the sums.

$$\sum_{i=1}^{\infty} i^n \left(\frac{1}{1+r}\right)^i = \Gamma(1+n)\, r^{-(1+n)} \qquad \textbf{(4.36)}$$

With the geometric mean, eq. **(4.30)** leads to eq. **(4.37)**, and with the diffusion mean, eq. **(4.32)** leads to eq. **(4.38)**:

$$S_t\,(\mathrm{gm}, r_t=0, \mathrm{LCA}) = \Gamma(1-e/2)\, r_{tr}^{-(1-e/2)} \qquad \textbf{(4.37)}$$

$$\frac{S_t^2}{S_r}\,(\mathrm{dm}, r_t=0, \mathrm{LCA}) = \Gamma(1-e)\, r_{tr}^{-(1-e)} \qquad \textbf{(4.38)}$$

Given the above, it turns out to be convenient to examine the dependence of S_t on S_r. Eqs.**(4.35)**, **(4.37)** and **(4.38)** are all described by eq. **(4.39)**, with only the parameter A, given in subsequent equations, varying for each case.

$$S_t = A\,(S_r)^{1-e/2} \qquad \textbf{(4.39)}$$

$$A\,(\text{gm}, r_{tr}=0, \text{LCA}) = [\Gamma((4-e)/(2-e))]^{e/2}\,\Gamma(2/(2-e))^{-1} \quad \textbf{(4.40)}$$

$$A\,(\text{gm}, r_{t}=0, \text{LCA}) = \Gamma(1 - e/2) \quad \textbf{(4.41)}$$

$$A\,(\text{dm}, r_{t}=0, \text{LCA}) = \Gamma(1 - e)^{1/2} \quad \textbf{(4.42)}$$

Eq. **(4.39)**, in concert with eq. **(4.28a)** may be used to write an expression for $\langle k_t \rangle$:

$$\langle k_t \rangle = k_t^{1,1}\,A^2\,(S_r)^{-e} \quad \textbf{(4.28b)}$$

As was noted in the discussion following eq. **(4.29b)**, $S_r \approx \overline{DP}_n$, so that eq. **(4.28b)** may be summarised as $\langle k_t \rangle \sim (\overline{DP}_n)^{-e}$. Comparing with eq. **(4.1)**, it is evident that (at least with the long chain assumption), the chain-length averaged quantities ($\langle k_t \rangle$ and $\overline{DP}_n$) are related by the same power law parameter, e, as the microscopic quantities ($k_t^{i,i}$ and chain length i). This intuitively appealing and striking concept has been noted by previous workers.[5,6]

4.5 Techniques and Issues for Numerical Steady-State Solutions

In this section the strategy used to generate the numerical solutions presented in this thesis is discussed. For additional details, see Chapter 9. In principle, the chain length distribution generated by eq. **(4.18b)** is infinite. In contrast to the analytic solutions presented above, numerical calculations necessarily deal with finite quantities, therefore we have to truncate the calculation at some chain length. It is desirable therefore to have some measure of the error introduced by this truncation, so that it may be reduced to acceptable levels. This is done by introducing a notional reaction into the scheme, wherein radicals of chain length z, which is termed the truncation chain-length, do not propagate further:

$$R_{z-1} + M \xrightarrow{k_p^{\infty}} R_z$$

The differential equation for $[R_z]$ can be solved to give eq. **(4.43)**, or equivalently in terms of the rRCLD, eq. **(4.44)**.

$$[R_z] = \frac{f_p^{\infty}\,[R_{z-1}]}{f_{tr} + f_t^z} \qquad \textbf{(4.43)}$$

$$\frac{P_z}{P_{z-1}} = \left(r_{tr} + \frac{r_t}{S_t} \sum_{j=1}^{\infty} M(z,j)\, P_j \right)^{-1} \qquad \textbf{(4.44)}$$

Noting the similarity of eq. **(4.44)** to eq. **(4.18b)**, it makes sense to evaluate both equations in parallel, which allows us to evaluate ε_z, the relative error in S_r (refer to eq. **(4.24)**) associated with truncation at chain length z, according to eq. **(4.45)**.

$$\varepsilon_z = \frac{P_z}{\sum_{i=1}^{z-1} P_i + P_z} \qquad \textbf{(4.45)}$$

Calculations involve evaluation of eq. **(4.18b)** (or the equivalent expressions for the geometric or diffusion mean models) for increasing chain length i, until ε_z is sufficiently low. Typically we use $\varepsilon_z = 10^{-6}$.

When the geometric mean model is used, the rRCLD is given by eq. **(4.31)**, and as noted above, this may be evaluated without iteration. The same is also true in the transfer limit, where eq. **(4.34)** applies. In all other cases, an initial guess is made for S_r. Depending on circumstances, this value of S_r is either the result of calculations using a different termination model, but with all other parameters identical, or calculated from eq. **(4.25)**.

$$\varepsilon_{it} = \frac{S_r(\text{old}) - S_r}{S_r(\text{old})} \qquad \textbf{(4.46)}$$

Eq. **(4.46)** is the measure used for the error associated with iteration, where S_r(old) is the value of S_r obtained in the previous iteration. Typically we use $\varepsilon_{it} = 10^{-7}$.

Preliminary calculations indicate that when using eq. **(4.18b)** with the harmonic mean termination model, eq. **(4.2)**, the values of S_r obtained in each iteration oscillate above and below the eventual converged value of S_r, and convergence is relatively slow. The oscillatory behaviour is eliminated and convergence made more rapid by using the value of S_r given by eq. **(4.47)** (where S_r(new) denotes the value of S_r obtained for the iteration just completed) to calculate the next iteration.

$$S_r = \sqrt{S_r(\text{new})\, S_r(\text{old})} \qquad \textbf{(4.47)}$$

At this stage it is appropriate to comment in more detail on the computational expense involved in the calculations described above. Evaluation of the rRCLD in the general case, according to eq. **(4.18b)**, involves a number of floating point operations proportional to z^2, where z is the truncation chain length. Evaluation of the relative DCLD according to **(4.26)** also involves z^2 operations, mainly due to the evaluation of the termination by combination term (if required). In contrast, if only the number average chain length $\overline{DP}_n$ is required, evaluation of eq. **(4.29b)** is essentially free, even with combination. Evaluation of the rRCLD with the geometic mean according to eq. **(4.31)**, or the diffusion mean according to eq. **(4.33)**, involves only z operations, which allows rapid calculations (minutes of CPU time) up to very large chain lengths ($\overline{DP}_n \approx 10^5$).

Given the above discussion, in some circumstances it may be considered worthwhile to sacrifice some accuracy for faster calculations. In evaluating the rRCLD in the general case with eq. **(4.18b)**, it is clear that the sum need not be calculated for each i – especially for longer chain lengths, the sum should change relatively slowly. A scheme can be developed to

describe the chain lengths for which the sum will be calculated, and the ranges of chain lengths for which these calculated sums will be used in place of the fully accurate choice of calculating the sum for each i.

4.6 Conclusion

The incorporation of CLDP and CLDT into FRP kinetics results in these kinetics being greatly complicated. Broadly, two methods have been described in this chapter to solve these kinetics, namely analytic and numerical methods. Even where numeric methods are used, it has been made clear that their evaluation can be greatly sped up by employing the analytic results as part of the computation procedure. For example, where the FRP kinetic scheme with CLDT and CLDP is in general a two-dimensional iterative procedure, and is how it must be employed for the harmonic mean model, in the case of the geometric mean it has been shown that calculations reduce to a one-dimensional, non-iterative procedure. Further, it has been shown that the analytic results give a much clearer picture of the effects of CLDT than is possible when the defining population balance equations are used in an un-distilled form. Indeed, to impart understanding and facilitate faster computation are motivations that fully justify the present work. It is clear that these aims have been fulfilled.

In the Chapter 5 the work of the present chapter will be exploited in seeking to understand better the kinetics of FRP. To be considered are systems with termination only (what has been referred to here as the termination limit), systems with mixed termination and transfer, and finally the situation of the transfer limit. This last situation will be treated separately because the transfer limit has been largely ignored by workers to date, but it is felt to be of great potential significance. Importantly, comparisons with experimental data will be made. Although Chapter 5 will not include CLD propagation, an important result of the present

chapter is that it may be incorporated into numerical calculations with no additional complications.

4.7 Addendum: Derivations

In order to retain some narrative flow in the text of this chapter, many derivations were not included as part of it, but are instead presented in what follows. Keen followers of the work of Olaj *et al.*[5,8,10-12] will recognise much of what follows, and this body of work should be taken as a general reference for the following results and derivations. However it is stressed that the inclusion of CLDP is new, and as a result of this the ambiguity with regard to the concept of 'propagation probability' (see earlier comment) is ironed out. Further, some equations are felt to be given in a neater form here, and of course it is hoped that greater clarity has been achieved.

The steady state radical chain length distribution

The steady state assumption, eq. **(4.15)**, applied to eqs. **(4.9)** leads to eqs. **(4.48)** and **(4.49a)**, which are summarised in eq. **(4.16a)**.

$$[\mathrm{R}_1] = \frac{R_{\mathrm{init}} + f_{\mathrm{tr}}\,[\mathrm{R}]}{f_{\mathrm{p}}^{\,1} + f_{\mathrm{tr}} + f_{\mathrm{t}}^{\,1}} \qquad \textbf{(4.48)}$$

$$[\mathrm{R}_i] = [\mathrm{R}_{i\text{-}1}]\,\frac{f_{\mathrm{p}}^{\,i\text{-}1}}{f_{\mathrm{p}}^{\,i} + f_{\mathrm{tr}} + f_{\mathrm{t}}^{\,i}} \qquad \textbf{(4.49a)}$$

The correlation between the sums S_{r} and S_{t}

As noted in the text, we proceed by substituting eq. **(4.16b)** for $[\mathrm{R}_i]$, eq. **(4.5)** for $k_{\mathrm{t}}^{\,i,j}$, and eq. **(4.8)** for $k_{\mathrm{p}}^{\,i}$ into the model equations. Eqs. **(4.11a)** and (**4.19a**) are transformed accordingly, at which point it is convenient to introduce the sums S_{r} and S_{t}, according to eqs. **(4.23a)** and **(4.24)**.

$$[\mathrm{R}] \;=\; [\mathrm{R}_0] \sum_{i=1}^{\infty} P_i \;=\; [\mathrm{R}_0]\, S_\mathrm{r} \qquad \textbf{(4.11b)}$$

$$R_\mathrm{init} \;=\; 2\, k_\mathrm{t}^{1,1}\, [\mathrm{R}_0]^2 \sum_{i=1}^{\infty} \sum_{j=1}^{\infty} M(i,j)\, P_i\, P_j \;=\; 2\, k_\mathrm{t}^{1,1}\, ([\mathrm{R}_0]\, S_\mathrm{t})^2 \qquad \textbf{(4.19b)}$$

Upon substituting the RHSs of eqs. **(4.11b)** and **(4.19b)** into **(4.17a)** and dividing by $[\mathrm{R}_0]$, eq. **(4.50)** is obtained.

$$1 \;=\; \frac{2\, k_\mathrm{t}^{1,1}}{f_\mathrm{p}^{\infty}}\, [\mathrm{R}_0]\, (S_\mathrm{t})^2 + \frac{f_\mathrm{tr}}{f_\mathrm{p}}\, S_\mathrm{r} \qquad \textbf{(4.50)}$$

Eq. **(4.19b)** may be rearranged to eq. **(4.19c)**, which when substituted into eq. **(4.50)** yields eq. **(4.51)**. Defining r_t and r_tr according to eqs. **(4.21)** and **(4.22)** finally gives eq. **(4.20)**.

$$[\mathrm{R}_0]\, S_\mathrm{t} \;=\; \sqrt{\frac{R_\mathrm{init}}{2\, k_\mathrm{t}^{1,1}}} \qquad \textbf{(4.19c)}$$

$$1 \;=\; \frac{\sqrt{2\, k_\mathrm{t}^{1,1}\, R_\mathrm{init}}}{f_\mathrm{p}^{\infty}}\, S_\mathrm{t} + \frac{f_\mathrm{tr}}{f_\mathrm{p}}\, S_\mathrm{r} \qquad \textbf{(4.51)}$$

Further rearrangement of eq. **(4.19c)** leads to the expression for $[\mathrm{R}_0]$, eq. **(4.17b)**, given in the text.

The reduced radical chain length distribution

As in the previous section, we substitute eq. **(4.16b)** for $[\mathrm{R}_i]$, eq. **(4.5)** for $k_\mathrm{t}^{i,j}$, and eq. **(4.8)** for $k_\mathrm{p}^{\,i}$ into the model equations. Eq. **(4.49a)**, after dividing both the numerator and denominator of the fraction by f_p^{∞}, leads to **(4.49b)**, and eq. **(4.14a)** yields eq. **(4.14b)**.

$$\frac{P_i}{P_{i\text{-}1}} \;=\; \frac{N(i\text{-}1)}{N(i) + \dfrac{f_\mathrm{tr}}{f_\mathrm{p}^{\infty}} + \dfrac{f_\mathrm{t}^{i}}{f_\mathrm{p}^{\infty}}} \qquad \textbf{(4.49b)}$$

$$f_t^i = 2\, k_t^{1,1}\, [R_0] \sum_{j=1}^{\infty} M(i,j)\, P_j \qquad \textbf{(4.14b)}$$

Substitution of eqs. **(4.14b)** for f_t^i and **(4.17b)** for $[R_0]$, and using the definitions of r_{tr} and r_t given in eqs. **(4.22)** and **(4.21)**, finally leads to eq. **(4.18b)**.

The relative dead chain length distribution

The usual substitutions transform eq. **(4.10a)** into eq. **(4.10b)**. Upon dividing by $f_p^{\infty}\, [R_0]$ and substituting eq. **(4.17b)** for $[R_0]$, we obtain eq. **(4.10c)**.

$$\frac{d[D_i]}{dt} = f_{tr}\, [R_0]\, P_i + \lambda\, 2\, k_t^{1,1}\, [R_0]^2\, P_i \sum_{j=1}^{\infty} M(i,j)\, P_j$$

$$+ (1-\lambda)\, k_t^{1,1}\, [R_0]^2 \sum_{j=1}^{i-1} M(i-j,j)\, P_{i-j}\, P_j \qquad \textbf{(4.10b)}$$

$$[D_i] \sim r_{tr}\, P_i + \lambda \frac{r_t}{S_t} P_i \sum_{j=1}^{\infty} M(i,j)\, P_j + \frac{1-\lambda}{2} \frac{r_t}{S_t} \sum_{j=1}^{i-1} M(i-j,j)\, P_{i-j}\, P_j \qquad \textbf{(4.10c)}$$

Rearranging eq. **(4.18b)** gives eq. **(4.18c)**, which when substituted into eq. **(4.10c)** yields the result given in the text, eq. **(4.26)**.

$$\frac{r_t}{S_t} \sum_{j=1}^{\infty} M(i,j)\, P_j = N(i\text{-}1) \frac{P_{i-1}}{P_i} - N(i) - r_{tr} \qquad \textbf{(4.18c)}$$

Number average chain length of dead polymer

The moments of the dead polymer chain-length distribution given by eq. **(4.10c)** are given by eq. **(4.52)**, with termwise moments $S_r^{(k)}$, $S_t^{(k)}$ and $S_c^{(k)}$ subsequently defined.

$$\sum_{i=1}^{\infty} i^k \,[\mathrm{D}_i] \;=\; r_{\mathrm{tr}}\, S_{\mathrm{r}}^{(k)} + \lambda\, r_{\mathrm{t}}\, S_{\mathrm{t}}^{(k)} + \frac{1-\lambda}{2}\, r_{\mathrm{t}}\, S_{\mathrm{c}}^{(k)} \qquad \textbf{(4.52)}$$

$$S_{\mathrm{r}}^{(k)} \;=\; \sum_{i=1}^{\infty} i^k\, P_i \qquad \textbf{(4.53)}$$

$$S_{\mathrm{t}}^{(k)} \;=\; \sum_{i=1}^{\infty} i^k \frac{1}{S_{\mathrm{t}}} P_i \sum_{j=1}^{\infty} M(i,j)\, P_j \qquad \textbf{(4.54a)}$$

$$S_{\mathrm{c}}^{(k)} \;=\; \sum_{i=1}^{\infty} i^k \frac{1}{S_{\mathrm{t}}} \sum_{j=1}^{i-1} M(i\text{-}j,j)\, P_{i-j}\, P_j \qquad \textbf{(4.55a)}$$

Substituting **(4.18c)** into **(4.54a)** gives eq. **(4.54b)**.

$$S_{\mathrm{t}}^{(k)} \;=\; \frac{1}{r_{\mathrm{t}}} \sum_{i=1}^{\infty} i^k \left(P_{i\text{-}1}\, N(i\text{-}1) - N(i)\, P_i - r_{\mathrm{tr}}\, P_i\right) \qquad \textbf{(4.54b)}$$

Given the above equation, it follows that when all termination is by the disproportionation mechanism (λ = 1), eq. **(4.52)** leads to eq. **(4.56)**. The second form of this equation is obtained by transforming the index variable for the first term (i-1 becomes i), and noting that $P_0 = 1$ (refer to eq. **(4.18a)**).

$$\sum_{i=1}^{\infty} i^k \,[\mathrm{D}_i] \;=\; \sum_{i=1}^{\infty} i^k \left(N(i\text{-}1)\, P_{i\text{-}1} - N(i)\, P_i\right) \;=\; 1 + \sum_{i=1}^{\infty} \left[(i+1)^k - i^k\right] N(i)\, P_i \qquad \textbf{(4.56)}$$

Lower order moments $S_{\mathrm{c}}^{(k)}$ are obtained by subtituting $x = i\text{-}j$ in eq. **(4.55a)**, which gives eq. **(4.55b)**.

$$S_{\mathrm{c}}^{(k)} \;=\; \frac{1}{S_{\mathrm{t}}} \sum_{x=1}^{\infty} \sum_{j=1}^{\infty} (x+j)^k\, M(x,j)\, P_x\, P_j \qquad \textbf{(4.55b)}$$

Examination of this equation for k=0 and k=1 shows that $S_c^{(0)} = S_t$ (compare with eq. **(4.23a)**) and $S_c^{(1)} = 2\ S_t^{(1)}$ (compare with eq. **(4.54a)**). Also, eq. **(4.55b)** allows simplified expressions to be derived for the geometric mean case[5] although this is not possible in general.

We now have all the information necessary to find an expression for the number average chain length, $\overline{DP}_n$. Eq. **(4.52)** with k=0 and k=1 give eqs. **(4.57)** and **(4.58)**. The second form of eq. **(4.58)** shows that this moment is independent of λ, and thus eq. **(4.56)** with k=1 may be used to evaluate it. With CLI propagation, $\overline{DP}_n$ is therefore finally given by eq. **(4.29b)**.

$$\sum_{i=1}^{\infty} [D_i] = r_{tr} S_r + \lambda r_t S_t + \frac{1 - \lambda}{2} r_t S_t = r_{tr} S_r + \frac{1 + \lambda}{2}(1 - r_{tr} S_r) \qquad \textbf{(4.57)}$$

$$\sum_{i=1}^{\infty} i\,[D_i] = r_{tr} S_r^{(1)} + \lambda r_t S_t^{(1)} + (1- \lambda) r_t S_t^{(1)} = r_{tr} S_r^{(1)} + r_t S_t^{(1)} \qquad \textbf{(4.58)}$$

Analytic solutions with the long chain assumption

Eq. **(4.31)** gives the rRCLD with the geometric mean termination model. With CLI propagation in the termination limit (r_{tr}=0), eq. **(4.24)** for S_r becomes eq. **(4.59a)**. Upon replacing sums with integrals and solving the innermost integral, eq. **(4.59b)** is obtained.

$$S_r = \sum_{i=1}^{\infty} \prod_{j=1}^{i} (1 + r_t j^{-e/2})^{-1} \approx \sum_{i=1}^{\infty} \prod_{j=1}^{i} \exp(-r_t j^{-e/2}) = \sum_{i=1}^{\infty} \exp(-r_t \sum_{j=1}^{i} j^{-e/2}) \qquad \textbf{(4.59a)}$$

$$S_r \approx \int_{i=0}^{\infty} \exp(-r_t \int_{j=0}^{i} j^{-e/2}\, dj)di = \int_{i=0}^{\infty} \exp(-r_t \frac{i^{1-e/2}}{1 - e/2})\, di \qquad \textbf{(4.59b)}$$

Substituting x from eq. **(4.60a)** and dx from eq. **(4.60b)** results in eq. **(4.59c)**.

$$x = r_t \frac{i^{1-e/2}}{1 - e/2} \qquad \textbf{(4.60a)}$$

$$dx = r_t\, i^{-e/2}\, di \qquad \textbf{(4.60b)}$$

$$S_r \approx (r_t)^{-1} \int_{x=0}^{\infty} i^{e/2} \exp(-x)\, dx \qquad \textbf{(4.59c)}$$

Rearranging eq. **(4.60a)** gives eq. **(4.60c)**, which, when substituted into eq. **(4.59c)**, results in eq. **(4.59d)**. The integral is then given by the gamma function, eq. **(4.61)**, and finally eq. **(4.35)** is obtained.

$$i = (x\,(1 - e/2) / r_t)^{1/(1-e/2)} \qquad \textbf{(4.60c)}$$

$$S_r \approx (1 - e/2)^{e/(2-e)}\, (r_t)^{-2/(2-e)} \int_{x=0}^{\infty} x^{e/(2-e)} \exp(-x)\, dx \qquad \textbf{(4.59d)}$$

$$\Gamma(n + 1) = \int_{i=0}^{\infty} i^n\, e^{-i}\, di \qquad \textbf{(4.61)}$$

Eq. **(4.36)** is derived in a similar fashion. Approximating sums with integrals leads to the intermediate form of eq. **(4.62)**, and the substitution $x = ri$ yields the final form. Substituting the integral for the gamma function completes eq. **(4.36)**.

$$\sum_{i=1}^{\infty} i^n \left(\frac{1}{1 + r}\right)^i \approx \int_{i=0}^{\infty} i^n\, e^{-ri}\, di = r^{-(n+1)} \int_{x=0}^{\infty} x^n\, e^{-x}\, dx \qquad \textbf{(4.62)}$$

References

(1) Benson, S. W.; North, A. M. *J. Am. Chem. Soc.* **1962**, *84*, 935-940.

(2) Buback, M.; Egorov, M.; Gilbert, R. G.; Kaminsky, V.; Olaj, O. F.; Russell, G. T.; Vana, P.; Zifferer, G. *Macromol. Chem. Phys.* **2002**, *203*, 2570-2582.

(3) Russell, G. T. *Aust. J. Chem.* **2002**, *55*, 399-414.

(4) Olaj, O. F.; Zifferer, G. *Makromol. Chem., Rapid Commun.* **1982**, *3*, 549-556.

(5) Olaj, O. F.; Zifferer, G. *Macromolecules* **1987**, *20*, 850-861.

(6) Mahabadi, H. K. *Macromolecules* **1985**, *18*, 1319-1324.

(7) Mahabadi, H. K. *Macromolecules* **1991**, *24*, 606-609.

(8) Olaj, O. F.; Zifferer, G.; Gleixner, G. *Makromol. Chem., Rapid Commun.* **1985**, *6*, 773-784.

(9) Bamford, C. H. *Macromol. Symp.* **1996**, *111*, 171-181.

(10) Olaj, O. F.; Zifferer, G.; Gleixner, G. *Makromol. Chem.* **1986**, *187*, 977-994.

(11) Olaj, O. F.; Zifferer, G.; Gleixner, G.; Stickler, M. *Eur. Polym. J.* **1986**, *22*, 585-595.

(12) Olaj, O. F.; Zifferer, G.; Gleixner, G. *Macromolecules* **1987**, *20*, 839-850.

(13) Russell, G. T.; Gilbert, R. G.; Napper, D. H. *Macromolecules* **1992**, *25*, 2459-2469.

(14) Russell, G. T. *Macromol. Theory Simul.* **1994**, *3*, 439-468.

(15) Smith, G. B.; Russell, G. T.; Heuts, J. P. A. *Macromol. Theory Simul.* **2003**, *12*, 299-314.

(16) Olaj, O. F.; Kornherr, A.; Zifferer, G. *Macromol. Theory Simul.* **1997**, *6*, 655-666.

(17) Olaj, O. F.; Kornherr, A.; Zifferer, G. *Macromol. Rapid Commun.* **1997**, *18*, 997-1007.

(18) Olaj, O. F.; Kornherr, A.; Zifferer, G. *Macromol. Rapid Commun.* **1998**, *19*, 89-96.

(19) Olaj, O. F.; Kornherr, A.; Zifferer, G. *Macromol. Theory Simul.* **1998**, *7*, 501-508.

(20) Olaj, O. F.; Vana, P. *Macromol. Rapid Commun.* **1998**, *19*, 433-439.

(21) Olaj, O. F.; Vana, P. *Macromol. Rapid Commun.* **1998**, *19*, 533-538.

(22) Olaj, O. F.; Vana, P.; Kornherr, A.; Zifferer, G. *Macromol. Chem. Phys.* **1999**, *200*, 2031-2039.

(23) Olaj, O. F.; Vana, P. *J. Polym. Sci., Polym. Chem. Ed.* **2000**, *38*, 697-705.

(24) Olaj, O. F.; Zoder, M.; Vana, P. *Macromolecules* **2001**, *34*, 441-446.

(25) Olaj, O. F.; Kornherr, A.; Zifferer, G. *Macromol. Theory Simul.* **1999**, *8*, 561-570.

(26) Olaj, O. F.; Kornherr, A.; Zifferer, G. *Macromolecules* **1999**, *32*, 8800-8806.

(27) Friedman, B.; O'Shaughnessy, B. *Macromolecules* **1993**, *26*, 5726-5739.

(28) Russell, G. T. *Macromol. Theory Simul.* **1995**, *4*, 497-517.

(29) Russell, G. T. *Macromol. Theory Simul.* **1995**, *4*, 519-548.

(30) Russell, G. T. *Macromol. Theory Simul.* **1995**, *4*, 549-576.

(31) Willemse, R. X. E.; Staal, B. B. P.; van Herk, A. M.; Pierik, S. C. J.; Klumperman, B. *Macromolecules* **2003**, *36*, 9797-9803.

(32) Moad, G.; Solomon, D. H. *The Chemistry of Free Radical Polymerization*; 1st ed.; Pergamon: Oxford, 1995.

(33) Heuts, J. P. A.; Sudarko; Gilbert, R. G. *Macromol. Symp.* **1996**, *111*, 147-157.

5 An Analysis of Steady-State Free-Radical Polymerisation Kinetics with Chain-length-dependent Termination: Model Properties and Analysis of Experimental Data

Abstract

In this chapter, the properties of the model presented in Chapter 4 are investigated. The applicability of power law relationships between S_r and S_t suggested by the analytical results of Chapter 4 is found to be quite general, justifying the analysis of experimental steady-state radical polymerisation data using these analytical results.

5.1 Introduction

In chapter 4, we presented a kinetic scheme for free-radical polymerisation (FRP) incorporating chain-length-dependent (CLD) termination and propagation. The steady-state solution to this kinetic scheme was found to depend on two aggregate parameters, one including termination rate parameters (r_t, eq. **(4.21)**) and one including transfer rate parameters (r_{tr}, eq. **(4.22)**), as well as the CLD termination and propagation model parameters. These solutions are obtained numerically, however we also described analytic solutions obtained with the long-chain approximation (LCA). In this chapter, we will use the results obtained in chapter 4 to investigate the properties of the obtained solutions, and also show how they may be used to analyse experimental FRP data to obtain CLD termination parameters.

In this chapter, we will compare results calculated with different one-*e* termination models – the geometric mean (gm), diffusion mean (dm) and harmonic mean (hm) - with a view to model discrimination. We will focus at first on results obtained in the two limits of

termination (r_{tr}=0) and transfer (r_t=0), and then consider mixed kinetics. We will investigate the validity of the analytic LCA solutions eqs. **(4.35)**, **(4.37)** and **(4.38)** by comparison with numerical solutions of eq. **(4.18b)**. Further, we consider how changing the CLD termination parameter e (eq. **(4.3)**) affects the above. Finally we analyse experimental FRP rate and molecular weight distribution (MWD) data using this model, and attempt to recover CLD termination model parameters.

5.2 Investigation of Model Properties

The data considered in this section were generated by methods described in section 4.5. Where applicable, tolerances of $\varepsilon_z = 10^{-6}$ (truncation tolerance) and $\varepsilon_{it} = 10^{-8}$ (iteration tolerance) were used. Recall that many kinetic data of interest (*e.g.* the rate of polymerisation, the number average degree of polymerisation, *etc.*) may be compared with results of simulations in the form of the sums S_r and S_t only; accordingly these values were calculated and recorded. Eq. **(4.20)**, which relates the two sums, was found to hold to approximately the same accuracy as the tolerances specified above. In chapter 4 it was established that the number average molecular weight $\overline{DP}_n$ is approximately equal to S_r, which is a direct result of calculations; see eq. **(4.29b)**. A reasonable upper bound is $\overline{DP}_n = 10^5$, and accordingly input parameters were chosen such that $S_r < 10^5$. For the more computationally demanding harmonic mean model however, an upper bound of 10^3 was chosen. The lower bound for S_r is 100, which corresponds to the value in chapter 2 chosen for the boundary between short and long chain lengths in the composite termination model. Modeling data at chain lengths lower than this would seem unnecessary with this simplified termination model. Calculations were performed with each termination model (gm, dm and hm) and for a range of e values between 0.1 and 2.0. While e is unlikely to be higher than 0.5-0.6 at low conversion, e values of 2 or

even higher have been suggested for high conversion conditions[1], so that these calculations have some relevance to FRP.

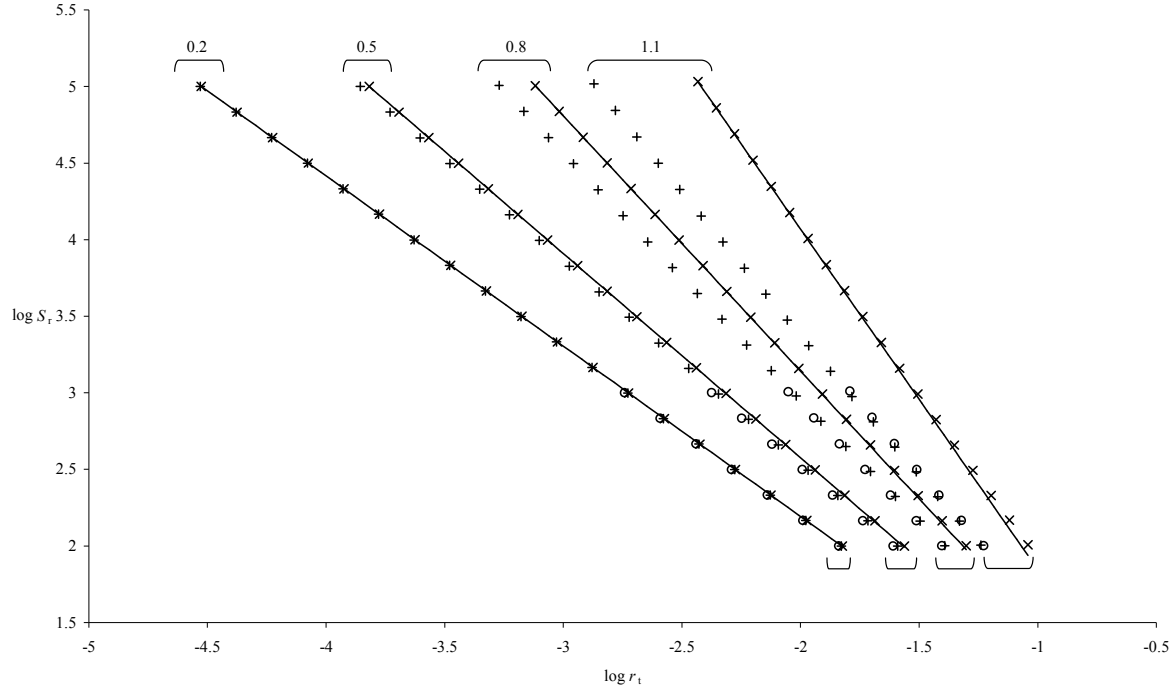

Fig. 5.1 Plot of (decimal) log S_r calculated in the termination limit ($r_{tr} = 0$) *vs.* log r_t. Data represented by lines are calculated using the gm LCA expression (eq. **(4.35)**), and symbols are calculated using methods described in section 4.5, and indicate the type of mean used: diagonal crosses (gm), vertical/horizontal crosses (dm) and circles (hm). Sets of data, from left to right, use values of *e* of 0.2, 0.5, 0.8 and 1.1, as indicated.

The limits of dead chain formation by termination and transfer were discussed in chapter 4. Recall that in the termination limit, variation of r_t leads to variation of S_r, with S_t simply given by r_t^{-1}. Therefore, selected data calculated in the termination limit are presented in *Fig. 5.1* as S_r *vs.* r_t. Firstly, agreement between analytic and numerical calculations with the gm termination model is excellent, at least for r_t approximately less than 10^{-2}. Of course, the

divergence of the values as r_t (or equivalently, e) increases is due to the breakdown of the LCA. As e increases, it is clear that the dm and hm values diverge from the gm ones, while remaining quite similar to each other. However it can also be seen that these models still obey a power law (albeit with different parameters) due to the linearity of the data series.

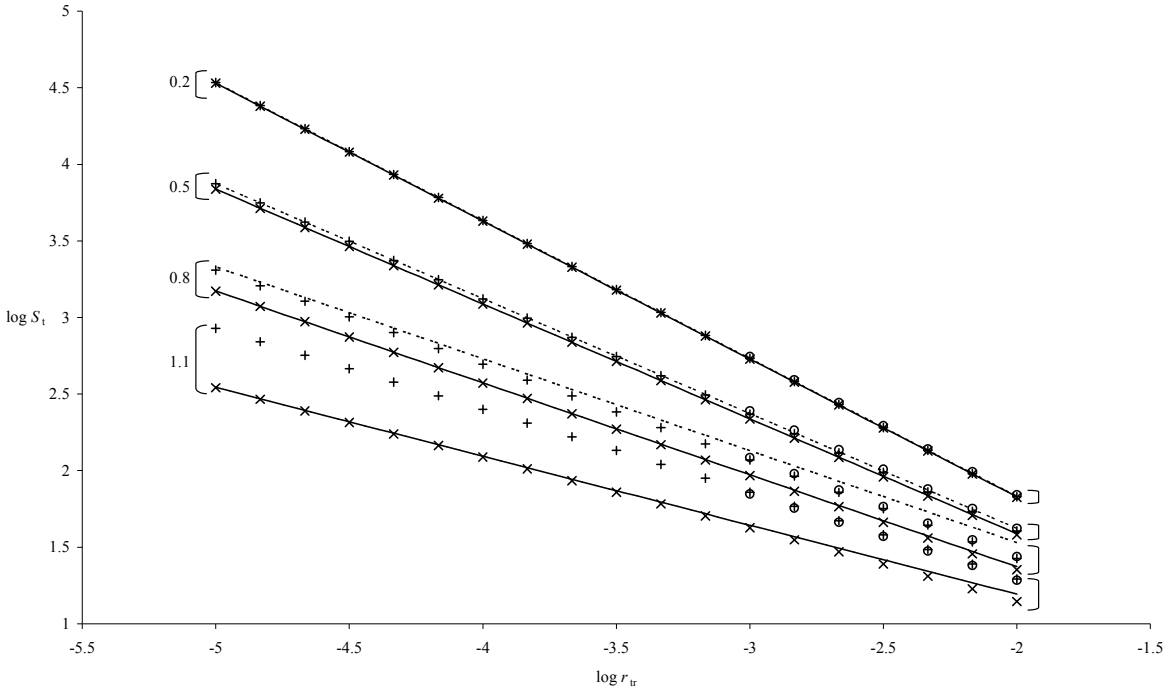

Fig. 5.2 Plot of log S_t calculated in the transfer limit (r_t = 0) *vs.* log r_{tr}. Data represented by lines are calculated from LCA expressions: solid line (gm), dashed line (dm); and symbols are calculated using methods described in section 4.5: diagonal crosses (gm), vertical/horizontal crosses (dm) and circles (hm). Sets of data, from top to bottom, use values of e of 0.2, 0.5, 0.8 and 1.1.

Turning now to the transfer limit, recall that under these conditions the inverse situation applies compared to the termination limit discussed above: variation of r_{tr} leads to variation

of S_t, with S_r simply given by r_{tr}^{-1}. Accordingly, selected data calculated in the transfer limit are plotted in *Fig. 5.2* as S_t *vs.* r_{tr}. While the LCA solutions are fairly accurate for low e values, they perform less well for higher e values than the LCA solutions did in the termination limit. In fact, due to the nature of the gamma function, eq. **(4.61)**, the LCA solution for the dm cannot be evaluated for $e \geq 1$. In other ways, the behaviour mirrors the behaviour found in the termination limit: initially at low e values, results for each termination model are similar and as e increases, the dm and hm results diverge from the gm results, but remain similar to each other. As before, all of the data series shown in the graph would be

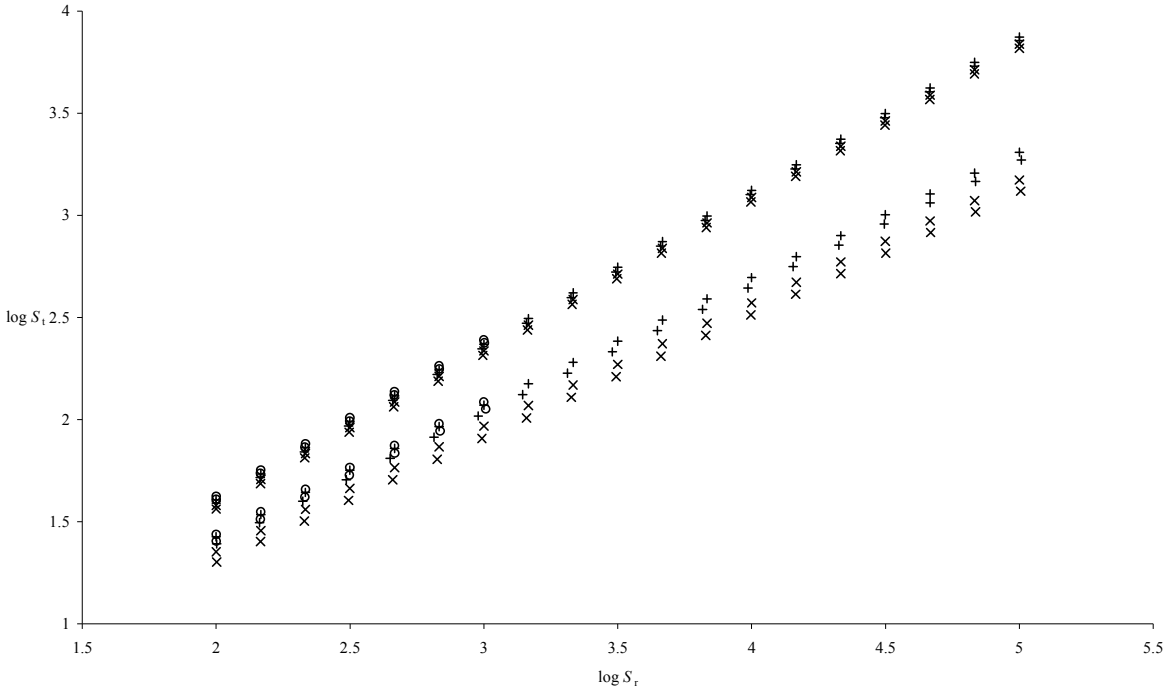

Fig. 5.3 Selected data previously discussed, in both the transfer and termination limits, plotted as log S_t *vs.* log S_r. Symbols have the same meaning as in previous figures. The upper set of data was generated with e=0.5, while the lower set used e=0.8. Within each dataset consisting of identical symbols, the upper series were calculated in the transfer limit, while the lower series were calculated in the termination limit.

reasonably well described by power laws.

Having considered data calculated in the limits of dead chain formation by termination and transfer separately, we now consider results from the transfer and termination limits side by side. This is a first step towards consideration of 'mixed' kinetics, *i.e.* data in which r_t and r_{tr} both vary. This is done in *Fig. 5.3* by plotting S_t *vs.* S_r. This form of presentation is used to delineate the range of solutions that arise with mixed kinetics, although the presentation necessarily obscures the input parameters (*i.e.* r_t and r_{tr}) used in the calculations. In other words, regardless of input parameters, any solution must lie inside the narrow band in (S_r, S_t) space bounded above by the transfer limit results, and below by the termination limit results. Furthermore, it is apparent from the figure that numerically, the two limits are perhaps surprisingly close: note that changing the termination model actually accounts for a larger variation than the variation between the limits. As with many previously identified trends, it is noted that the extent of variation between the termination and transfer limits increases with the parameter *e*.

$$S_t = A\,(S_r)^a \qquad \textbf{(5.1)}$$

Consideration of *Fig. 5.3* suggests the method of calculation of a data series between two S_r values. This was specified earlier in the initial description of the data, and the method can now be detailed. Firstly, calculations are made in the transfer limit, where the required input parameters are easily determined, since $S_r = r_{tr}^{-1}$ in this limit. Secondly, the series of transfer limit data is fit to the power law eq. **(5.1)**. This function was chosen since it was observed that the power law describing the LCA solutions, eq. **(4.39)**, is not obeyed strictly by all numerical solutions, but that a generalised power law does apply. On further inspection of the figure, it seems reasonable to assume that the series of termination limit data also follows a

power law, with the same value of a (slope) as was found in the transfer limit. Picking a reasonable input value of r_t and calculating the resulting (S_r, S_t) values, the parameter A for the termination limit data series can be estimated. Using the estimated power law parameters,

Tab. 5.1 Power law (eq. **(5.1)**) parameters fitted to data calculated with the geometric mean termination model, and calculated with LCA results.

e	Termination limit			Transfer limit			a (LCA) [a]
	A	A (LCA)	a	A	A (LCA)	a	
0.1	1.028	1.030	0.950	1.029	1.031	0.950	0.950
0.2	1.057	1.061	0.900	1.064	1.069	0.900	0.900
0.3	1.087	1.095	0.851	1.103	1.112	0.851	0.850
0.4	1.118	1.131	0.801	1.149	1.164	0.801	0.800
0.5	1.151	1.170	0.752	1.202	1.225	0.752	0.750
0.6	1.184	1.211	0.702	1.262	1.298	0.703	0.700
0.7	1.218	1.256	0.653	1.330	1.385	0.654	0.650
0.8	1.252	1.304	0.604	1.408	1.489	0.605	0.600
0.9	1.285	1.357	0.555	1.496	1.616	0.557	0.550
1.0	1.313	1.414	0.507	1.594	1.772	0.510	0.500
1.1	1.336	1.477	0.460	1.703	1.968	0.464	0.450
1.2	1.344	1.546	0.414	1.822	2.218	0.418	0.400
1.3	1.338	1.623	0.370	1.951	2.546	0.374	0.350
1.4	1.316	1.710	0.327	2.085	2.992	0.331	0.300
1.5	1.258	1.807	0.289	2.222	3.626	0.291	0.250
1.6	1.171	1.919	0.254	2.357	4.591	0.253	0.200
1.7	[b]	2.050	[b]	2.483	6.220	0.217	0.150
1.8	[b]	2.208	[b]	2.593	9.514	0.185	0.100
1.9	[b]	2.408	[b]	2.680	19.470	0.155	0.050
2.0	[b]	[c]	[b]	2.739	[c]	0.129	[c]

[a] Values of a (LCA) are the same for both limits.

[b] Calculations failed, since the truncation chain length ε_z was exceeded.

[c] LCA result cannot be evaluated for $e = 2$.

the values of S_t corresponding to the desired limits of S_r can be found, and the appropriate input parameters r_t can be determined, since in the termination limit $S_t = r_t^{-1}$. Inspection of *Fig. 5.3* shows that this method works well, since despite there being no strictly accurate way of predicting S_r based on the input value of r_t, the extreme values of the calculated data series are always very close to the desired values (*viz.* log S_r between 2 and 5).

The data described above has been analysed using eq. **(5.1)**, and the fitted parameters are listed in *Tab. 5.1* (gm results) and *Tab. 5.2* (dm and hm results). The variation of the fitted parameters with the value of *e* is shown in *Fig. 5.4* (pre-factor *A*) and *Fig. 5.5* (slope *a*). The observation made above, that the line in (S_r, S_t) space described by transfer limit data is always above the line described by the termination limit data, can be confirmed by comparing values of *A* found in the two limits. It is not obvious why this should be so, but it is seen in all of the calculations made here. Also, it is clear from the tables and from *Fig. 5.5* that the values of the parameter *a* in the two limits are if not identical, then very close to each other in all of the conditions examined here. It should be mentioned that despite the mathematical necessity that the dm and hm results are equal when $e = 1$ (and in fact results of calculations with both means are equal for equal input parameters), the parameters fitted to the power law are not the same. This serves to illustrate that the fitted parameters depend somewhat on the range of S_r that the fitted data covers; recall that dm data was calculated up to $S_r=10^5$, whereas for hm data it was practical to calculate only up to $S_r=10^3$. By limiting the range of data fitted, it becomes clear that eq. **(5.1)** is more exactly satisfied at higher S_r (longer chain lengths). This trend was noted by Olaj *et al.*.[2] However, rather than attempt to pursue this elusive mathematical ideal, we limit ourselves to physically reasonable chain lengths in order that the derived parameters *A* and *a* retain physical meaning.

Another interesting feature of the results of *Tab. 5.1* and *Tab. 5.2* is in the tendency of the value of a as e increases. While the gm results closely follow the LCA result, *viz.* $a = 1 - e/2$, the dm and hm results tend to $a = 0.5$ as e increases. This accounts for a large part of the

Tab. 5.2 Power law (eq. **(5.1)**) parameters fitted to data calculated with the diffusion and harmonic mean termination models.

e	Diffusion mean				Harmonic mean			
	Termination limit		Transfer limit		Termination limit		Transfer limit	
	A	a	A	a	A	a	A	a
0.1	1.030	0.950	1.031	0.950	1.039	0.951	1.040	0.951
0.2	1.065	0.901	1.072	0.901	1.080	0.903	1.085	0.903
0.3	1.108	0.851	1.123	0.851	1.124	0.855	1.136	0.856
0.4	1.159	0.802	1.187	0.803	1.169	0.809	1.190	0.810
0.5	1.219	0.755	1.263	0.755	1.214	0.764	1.247	0.765
0.6	1.287	0.708	1.350	0.709	1.256	0.720	1.303	0.723
0.7	1.359	0.664	1.444	0.666	1.292	0.680	1.355	0.683
0.8	1.426	0.624	1.535	0.626	1.317	0.643	1.399	0.647
0.9	1.476	0.589	1.610	0.592	1.328	0.610	1.430	0.615
1.0	1.496	0.561	1.655	0.565	1.321	0.582	1.445	0.587
1.1	1.482	0.540	1.664	0.544	1.296	0.559	1.442	0.564
1.2	1.437	0.526	1.640	0.529	1.254	0.540	1.422	0.545
1.3	1.376	0.516	1.594	0.519	1.199	0.525	1.387	0.529
1.4	1.308	0.510	1.538	0.513	1.137	0.515	1.341	0.517
1.5	1.242	0.507	1.480	0.508	1.071	0.507	1.288	0.508
1.6	1.182	0.505	1.425	0.506	1.005	0.501	1.232	0.500
1.7	1.129	0.503	1.375	0.504	0.942	0.497	1.174	0.495
1.8	1.083	0.502	1.331	0.503	0.883	0.494	1.118	0.491
1.9	1.043	0.502	1.293	0.502	0.828	0.492	1.064	0.488
2.0	1.008	0.501	1.260	0.502	0.778	0.490	1.013	0.485

differences between the means noted earlier, that is to say that A values for all three means are quite similar. The quality of the fits is good ($R^2 > 0.99$ in all cases) but some trends are evident. For the gm, the quality of fit decreases steadily as e increases. With reference to *Fig. 5.1* and *Fig. 5.2*, it is clear that this trend is due to deviation from the LCA results at short chain lengths, as previously discussed. Curiously, the behaviour of the dm and hm results is somewhat different: the quality of fit drops initially, is a minimum at roughly $e = 1$, and finally increases at higher e. This corresponds with the transition of both means from concurrence with the gm LCA value of $a = 1\text{-}e/2$, to the high-e limit of $a = 0.5$. It should be noted that, as a matter of convenience, curve fitting was done by fitting a linear relationship

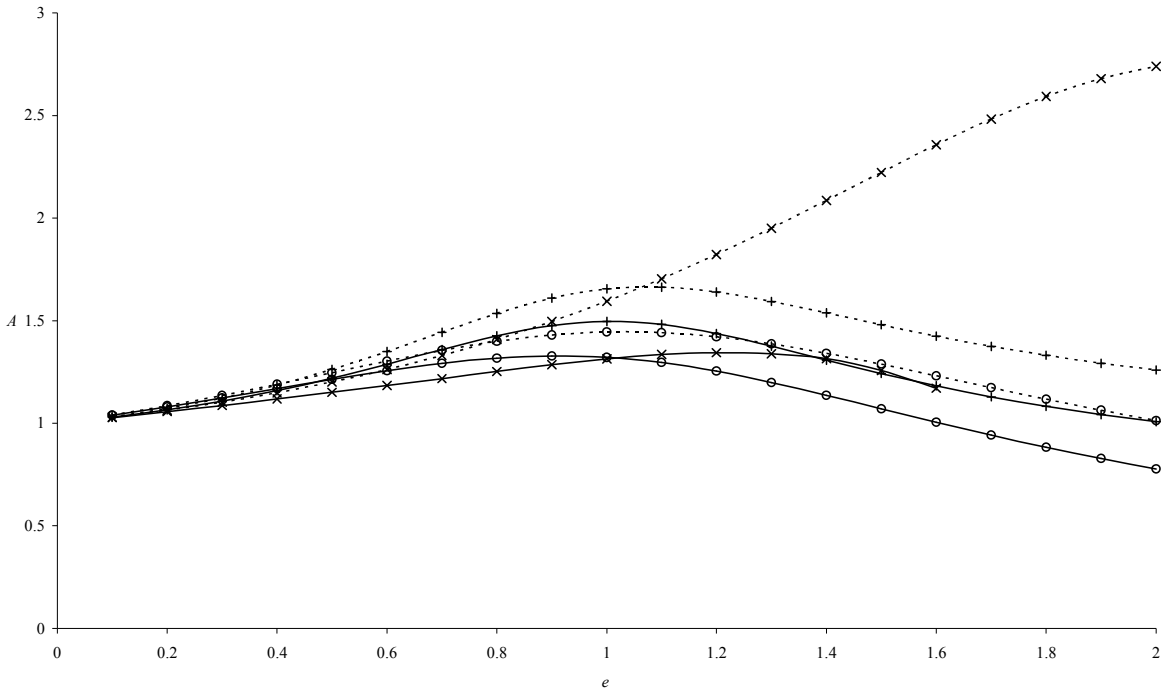

Fig. 5.4 Plot of A vs. e from *Tab. 5.1* and *Tab. 5.2*. Symbols denote the type of mean used in the termination model as in previous figures. The lines joining the symbols indicate the limit that applies to the data: solid line indicates termination limit, dashed line indicates transfer limit.

to log S_t *vs.* log S_r data, rather than the more statistically correct method of non-linear least squares fitting eq. **(5.1)** directly to the data. To ascertain the effect of this simplified method, data for the geometric mean in the termination limit with $e = 0.2$ was analysed by nonlinear least squares fitting. The fitted values of a and A were identical to those given in *Tab. 5.1*, showing that the method of analysis used is perfectly adequate in this case.

It is important to be mindful of the relationship between the quantities under discussion in the previous section - namely the aggregate rate parameters r_t and r_{tr}, and the resultant sums S_r and S_t, which are natural modeling input and output variables respectively – and the quantities that are naturally discussed in an experimental context. These relationships were discussed in section 4.3, and may be summarised by saying that independent experimental quantities (*e.g.* initiator concentration) are components of the input modeling parameters,

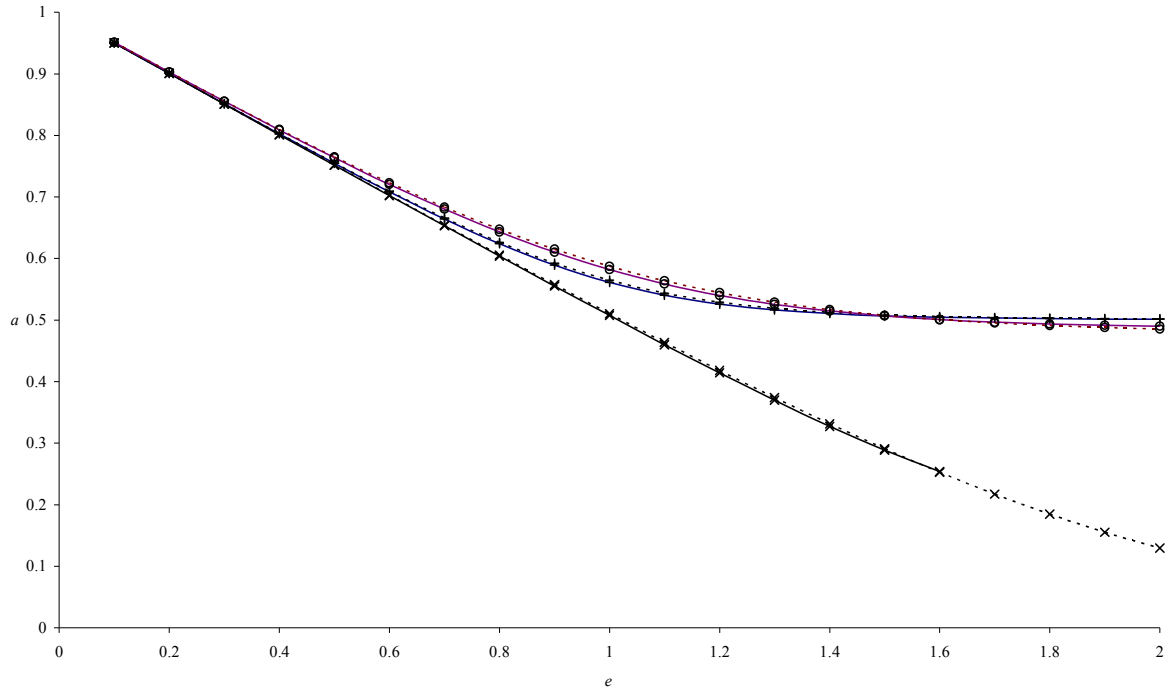

Fig. 5.5 Plot of a vs. e from *Tab. 5.1* and *Tab. 5.2*. Lines and symbols are as for *Fig. 5.4*.

while dependent experimental quantities (*e.g.* the chain-length-averaged rate coefficient for termination, $\langle k_t \rangle$) are combinations of the output modeling variables. Thus relationships between the modeling variables explored in the previous section have numerous experimental consequences, which are all traceable to the above results. For instance, examination of the dependences of $\langle k_t \rangle$ on R_{init}, [M] and $k_t^{1,1}$ in the termination limit[3] reveal similarities, which are all traceable to the relationship between r_t and S_r. This issue will be examined in more detail later in the chapter.

Following on from the above, the relationship between $\langle k_t \rangle$ and $\overline{DP}_n$ is of particular interest, as was mentioned in section 4.4. Eq. **(4.28a)** combined with eq. **(5.1)** (rather than the LCA expression used in section 4.4) gives eq. **(5.2)** for $\langle k_t \rangle$:

$$\langle k_t \rangle = k_t^{1,1} A^2 (S_r)^{2(a-1)} \qquad \textbf{(5.2)}$$

The previously given expression for $\overline{DP}_n$, eq. **(4.29b)**, can be rearranged to give S_r in terms of $\overline{DP}_n$, and then inserted into eq. **(5.2)**. The existence of power law relationships between S_t and S_r in the termination and transfer limits implies power law relationships between $\langle k_t \rangle$ and $\overline{DP}_n$ in these limits. In an experimental context, this requires variation of experimental parameters such that limiting conditions are maintained. Nevertheless, at moderately low e, the differences between the A values in the two limits may be difficult to resolve experimentally, so that a power law provides a reasonable fit to FRP data even if it is not in one of the limits, and also provides a reasonable estimate of the value of e.

$$S_r (r_{tr} = 0) = \frac{1+\lambda}{2} \overline{DP}_n - 1 \qquad \textbf{(5.3)}$$

$$S_r (r_t = 0) = \overline{DP}_n - 1 \qquad \textbf{(5.4)}$$

The above equations show that the occurrence of combination does not qualitatively change the relationship between $<k_t>$ and $\overline{DP}_n$; a power law still applies (neglecting the subtraction of one, which is insignificant here as we have $S_r > 100$). Also the well-known[4] transfer limit result that $\overline{DP}_n \approx r_{tr}^{-1}$ is recovered when eq. **(5.4)** is combined with eq. **(4.20)**. Eq. **(5.2)** of course is similar to eq. **(4.28b)**, which was derived for the gm termination model with the LCA. The interesting result of the latter equation, that the exponent of $\overline{DP}_n$ is $-e$ (analogous to the microscopic termination model eq. **(4.1)**), still holds with eq. **(5.2)** and the gm termination model (since the LCA results were found to be closely followed for this termination model). However for the dm and hm termination models it was found that a has a limiting value of 0.5 as e increases, so that the exponent of $\overline{DP}_n$ tends to -1. The occurrence of combination will act to increase the apparent value of the power law pre-factor in the termination limit, but will not affect the slope in either case. Substituting eq. **(5.3)** into eq. **(5.2)** gives eq. **(5.5)**. Using the power law parameters found in *Tab. 5.1* and *Tab. 5.2*, it can be shown that at low e, a small amount of combination will lead to the apparent power law pre-factor in the termination limit (which is evaluated from eq. **(5.5)**: the expression is $A^2 (\frac{1+\lambda}{2})^{2(a-1)}$) exceeding that of the transfer limit, although the degree of combination necessary decreases as e increases, due to the tendency of the pre-factors for the two limits to diverge.

$$<k_t> (r_{tr} = 0) = k_t^{1,1} A^2 (\frac{1+\lambda}{2}\overline{DP}_n)^{2(a-1)} \qquad \textbf{(5.5)}$$

We now turn to the case of mixed termination / transfer. A series of calculations were made with the gm termination model and $e = 0.2$. Firstly, r_t was varied while r_{tr} was held constant at 1×10^{-4}. Setting $r_t = 0$ of course leads to $S_r = 10^4$, as the transfer limit applies. Increasing r_t

in a series from 1×10^{-7} to 1×10^{-2} steadily decreased the value of S_r. As a means of comparison with data calculated in the termination and transfer limits, S_r and S_t values were fitted with eq. **(5.1)**, yielding $A = 1.038$ and $a = 0.903$. Next, the opposite situation was examined: r_{tr} was varied while r_t was held constant at 2.37×10^{-4}. The latter value was chosen such that when $r_{tr} = 0$, as before, $S_r = 1.0\times10^{4}$. Increasing r_{tr} in a series from 1×10^{-6} to 5×10^{-3} steadily decreased the value of S_r. Fitting eq. **(5.1)** to the S_r and S_t values yielded $A = 1.076$ and $a = 0.899$. The results of the fits of eq. **(5.1)** to the above data can be rationalised as follows. The first data series begins in the transfer limit, and as r_t is increased, receeds from the transfer limit results and approaches the termination limit results. Thus we should expect the fit to give a lower intercept A and higher slope a, and comparison with the results of *Tab. 5.1* shows that this is so. The opposite situation applies in the second data series, so we expect a higher pre-factor and lower slope, and again this expectation is confirmed on comparison with the results of *Tab. 5.1*. With a low value of e as here, the proximity of the limits ensures that the deviation from the behaviour found in the limits is relatively small. Also, the slope a is affected to a lesser extent than is the pre-factor A, which may be fortunate as this is often of more interest – *c.f.* eq. **(5.2)**, measurement of a leads to determination of e, whereas measurement of A leads to determination of $k_t^{1,1}$.

Further analysis of the mixed kinetics situation follows on from a trend observed by Olaj *et al.*.[2] After calculations with similar conditions to those described above, they noted that[2] (using the notation of this thesis) A varies linearly with S_r. Note that Olaj *et al.*[2] assume that the LCA result, eq. **(4.39)**, holds in all cases, so that A is determined by the input value of e and calculated values of S_r and S_t. Since we have shown that the LCA result does not always hold, particularly that the exponent a differs from $1-e/2$ at high e, we seek a more general formulation of this result.

$$f_t = \frac{S_t - S_t'(r_{tr}=0)}{S_t'(r_t=0) - S_t'(r_{tr}=0)} \qquad \textbf{(5.6)}$$

In eq. **(5.6)**, the S_t' values are the values of S_t that would arise in the termination and transfer limits, as indicated, both at a constant value of S_r corresponding to the calculated value of S_t. In other words, f_t is the fractional 'character' of the value of S_t in terms of the two limits – in the termination limit, $f_t = 0$, and in the transfer limit, $f_t = 1$. This is analogous to the value of A in the work of Olaj *et al.*,[2] but does not depend on the LCA result. The values of S_t' in eq. **(5.6)** can be estimated from the calculated value of S_r and eq. **(5.1)** along with appropriate data from *Tab. 5.1* or *Tab. 5.2*.

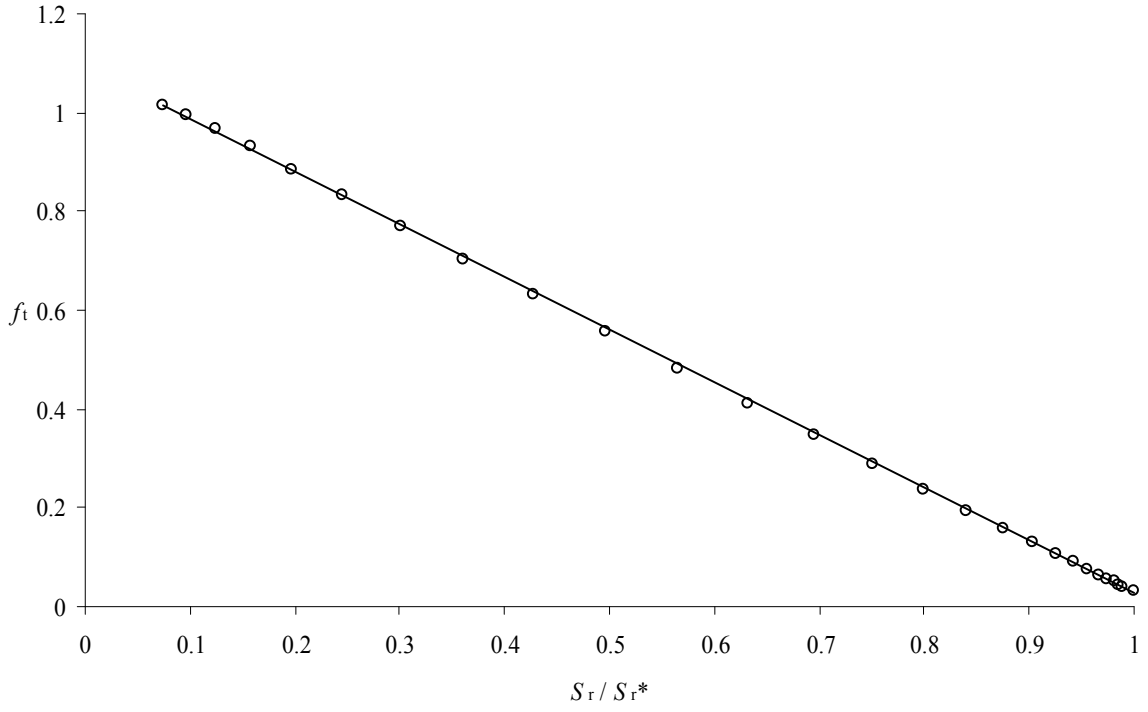

Fig. 5.6 Analysis of (S_r,S_t) values calculated at constant r_t, varying r_{tr} (see text for details) with S_t values used to calculate f_t according to eq. **(5.6)** (points). The parameters of the best fit line are $f_t = 1.067 - 1.093\ S_r / S_r^*$, where S_r^* is the value of S_r calculated with $r_{tr} = 0$ (here $S_r^* = 1.0\times10^4$).

The series of (S_r,S_t) data calculated with constant r_t and varying r_{tr} described above was analysed with eq. **(5.6)**. The results are shown in *Fig. 5.6*. The figure shows a linear relationship is followed, although it should be mentioned that this relationship breaks down as S_r decreases, probably due to the increasing inaccuracy of the power law fits used to calculate the S_t' values at low chain lengths. We should expect that when $S_r / S_r^* = 1$, $f_t = 0$ (the input value of r_{tr} was zero, thus the results are in the transfer limit). The aforementioned inaccuracy of the power law parameters is also responsible for the slightly positive value of f_t seen here. Nevertheless it could be imagined that if at each S_r value, the values of S_t in the two limits could be calculated exactly (rather than estimated from the power law as was done here), then an analysis as in *Fig. 5.6* would lead to linear best fit parameters such that $f_t = 1 - S_r / S_r^*$. Indeed, Olaj *et al.*[2] showed that assuming a relationship of this form leads to a fair approximation of (S_r, S_t) values with mixed kinetics using only LCA results calculated in the two limits.

The second dataset described above may be similarly analysed. In this case, the best linear relationship was found when the following equation was used:

$$f_r = \frac{S_r - S_r'(r_t=0)}{S_r'(r_{tr}=0) - S_t'(r_t=0)} \qquad \textbf{(5.7)}$$

The parameter f_r is analogous to f_t defined above (eq. **(5.7)**), the difference being that the S_r' values are calculated from the value of S_t that the steady state calculations yielded along with S_r.

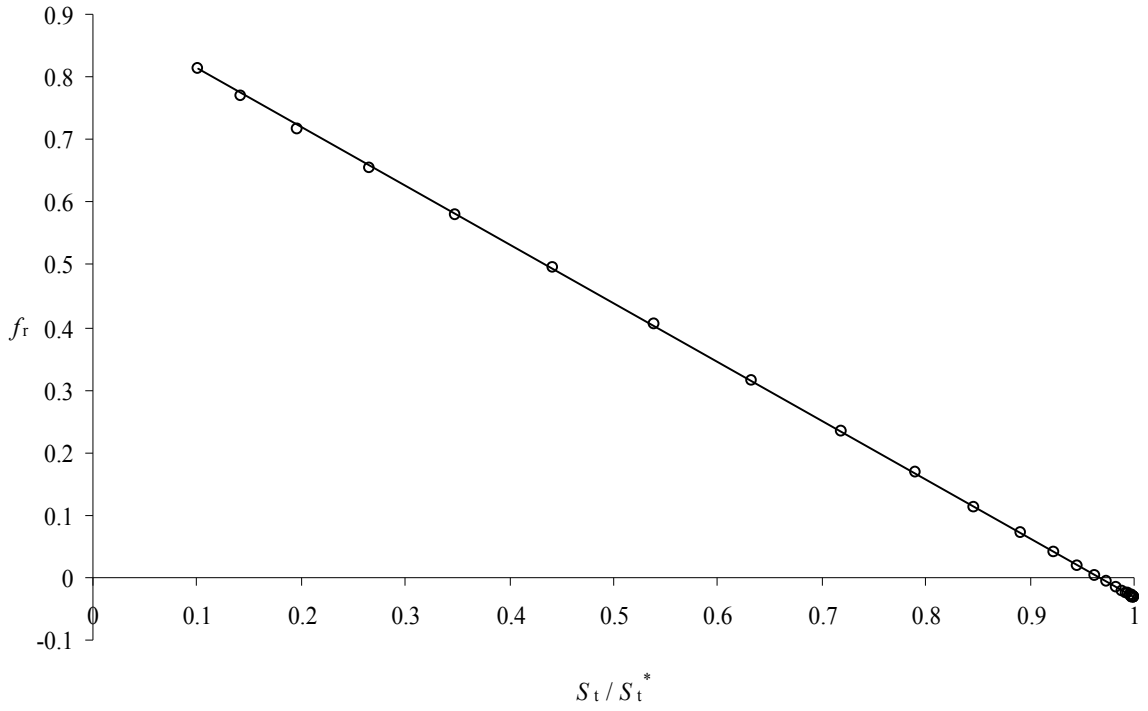

Fig. 5.7 Analysis of (S_r,S_t) values calculated at constant r_{tr}, varying r_t (see text for details) with S_r values used to calculate f_r according to eq. **(5.7)** (points). The parameters of the best fit line are $f_r = 0.905 - 0.937\ S_t / S_t^*$, where S_t^* is the value of S_t calculated with r_t=0 (here $S_t^* = 4.3\times10^3$).

From the figure it is evident that a linear relationship exists between f_r and S_t. Also, as was alluded to earlier, plotting the data in this way leads to a (slightly) better fit than by plotting *vs.* S_r. Similar limitations are evident here as with *Fig. 5.6* – the linearity breaks down at lower values of S_t, and although we would expect $f_r = 0$ when $S_t = S_t^*$, f_r is instead slightly negative. The relationship is nonetheless distinct enough to allow prediction of trends.

Effects of CLDT on the average rate coefficient for termination

It is useful to consider the effects of chain-length-dependent termination on the kinetics of FRP in terms of the chain-length averaged rate coefficient for termination, $\langle k_t \rangle$ (eq. **(4.28a)**). This allows comparison with the familiar 'classical' kinetics results, since when termination

is chain-length-independent, we have simply that $\langle k_t \rangle = k_t^{1,1}$. The intermediate form of eq. **(4.28a)** shows how $\langle k_t \rangle$ is a weighted average of the microscopic rate coefficients, $k_t^{i,j}$, with respect to the (normalised) radical chain-length distribution, $[R_i]/[R]$. Combining eq. **(4.28a)** with eqs. **(5.1)** and **(4.20)**, in the limits of dead chain formation by transfer and termination respectively, lead to eqs. **(5.8)** and **(5.9)**:

$$\langle k_t \rangle (r_t=0) = k_t^{1,1} A^2 r_{tr}^{2(1-a)} \qquad \textbf{(5.8)}$$

$$\langle k_t \rangle (r_{tr}=0) = k_t^{1,1} A^{2/a} r_t^{2(1-a)/a} \qquad \textbf{(5.9)}$$

These equations relate $\langle k_t \rangle$ with the two aggregate rate parameters, r_t and r_{tr}. They represent transformations of the power law eq. **(5.1)**, in that these are also power laws, and the same parameters a and A that described eq. **(5.1)** can also be used here. It has been established that these power law parameters depend on the value of e and the cross-termination model (gm, dm or hm in this work). With the analysis presented in *Tab. 5.1* and *Tab. 5.2*, bounds have been established on their values: in general $A \geq 1$ and $0 < a \leq 1$, and with CLI termination, both parameters are equal to one. The exponents of r_{tr} in eq. **(5.8)** and r_t in eq. **(5.9)** are therefore always positive. Increasing the transfer ratio r_{tr} (eq. **(4.22)**) leads to increased $\langle k_t \rangle$, since transfer produces shorter chains, which terminate more rapidly. Interpretation of eq. **(5.9)** in this manner is somewhat more complicated, since kinetic parameters contained in r_t (eq. **(4.21)**) are more numerous and more readily varied independently of each other. Increasing the rate of initiation, R_{init}, or decreasing the frequency of propagation, $k_p[M]$ (all else being equal) leads to shorter chains and higher $\langle k_t \rangle$. Increasing $k_t^{1,1}$, apart from the explicit dependence given in eq. **(5.9)** (all chains terminate more rapidly), also leads to shorter chains and therefore, higher $\langle k_t \rangle$.

Eqs. **(5.8)** and **(5.9)** have the obvious disadvantage that they may only be evaluated for the values of e for which power law fits have been determined from calculated (S_r,S_t) data, as in

Tab. 5.1 and *Tab. 5.2*, although it would be possible to fit and interpolate plots such as *Fig. 5.4* and *Fig. 5.5* to give values of A and a for any value of e. The results obtained with the LCA and gm termination model do not suffer this particular limitation, although their other deficiencies have been discussed previously. With these results, eqs. **(5.10)** and **(5.11)** are obtained.

$$\langle k_t \rangle \text{ (gm, LCA, } r_t=0) \;=\; k_t^{1,1} \left[\Gamma(1 - e/2)\right]^2 (r_{tr})^e \qquad \textbf{(5.10)}$$

$$\langle k_t \rangle \text{ (gm, LCA, } r_{tr}=0) \;=\; k_t^{1,1} \left[\Gamma\left(\frac{2}{2-e}\right)\right]^{-2} \left(\frac{2}{2-e} r_t\right)^{2e/(2-e)} \qquad \textbf{(5.11)}$$

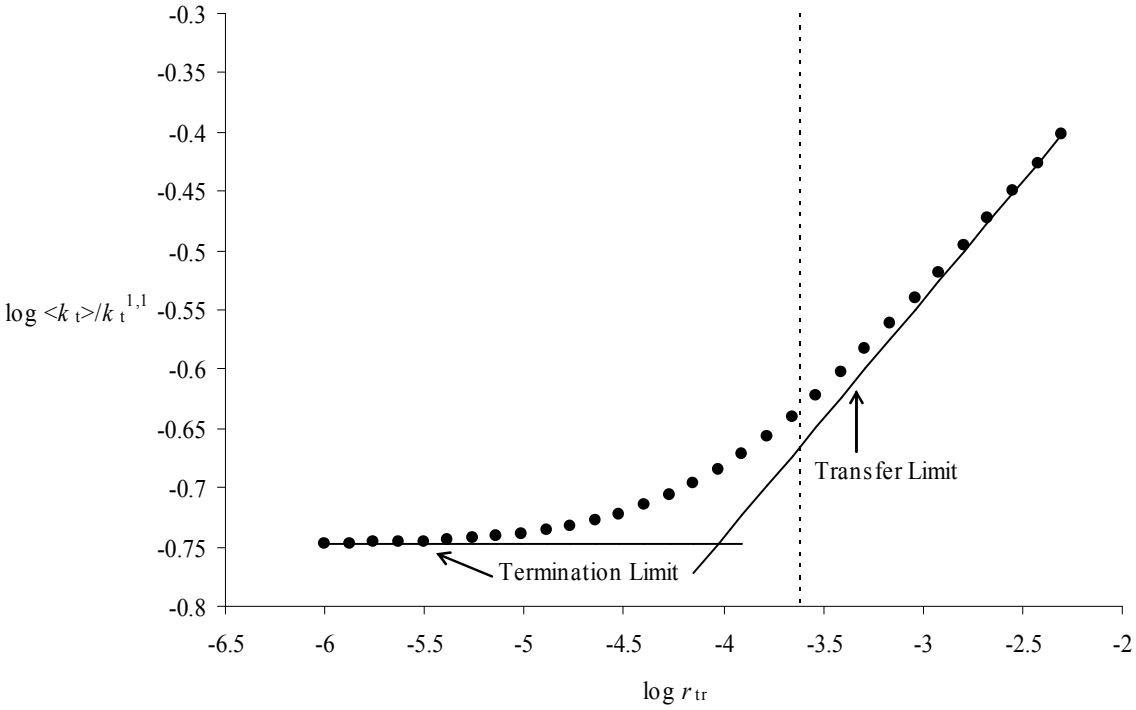

Fig. 5.8 Data of *Fig. 5.6* presented as log $\langle k_t \rangle / k_t^{1,1}$ (calculated from eq. **(4.28a)**) *vs.* log r_{tr} (points). The vertical dotted line indicates the constant value of r_t = 2.37×10^{-4}, plotted on the same axis as r_{tr}. Solid lines correspond to LCA results with the gm termination model in the transfer limit (r_t=0) and termination limit (r_{tr}=0), as indicated.

These expressions are good approximations for low e values. They also give upper bounds for the exponents with respect to r_{tr} (e) and r_t ($2e/(2-e)$) in the two limits.

To illustrate the effect of CLDT on $\langle k_t \rangle$ in situations of mixed termination and transfer, the data presented above in *Fig. 5.6* and *Fig. 5.7* is re-examined in *Fig. 5.8* and *Fig. 5.9*.

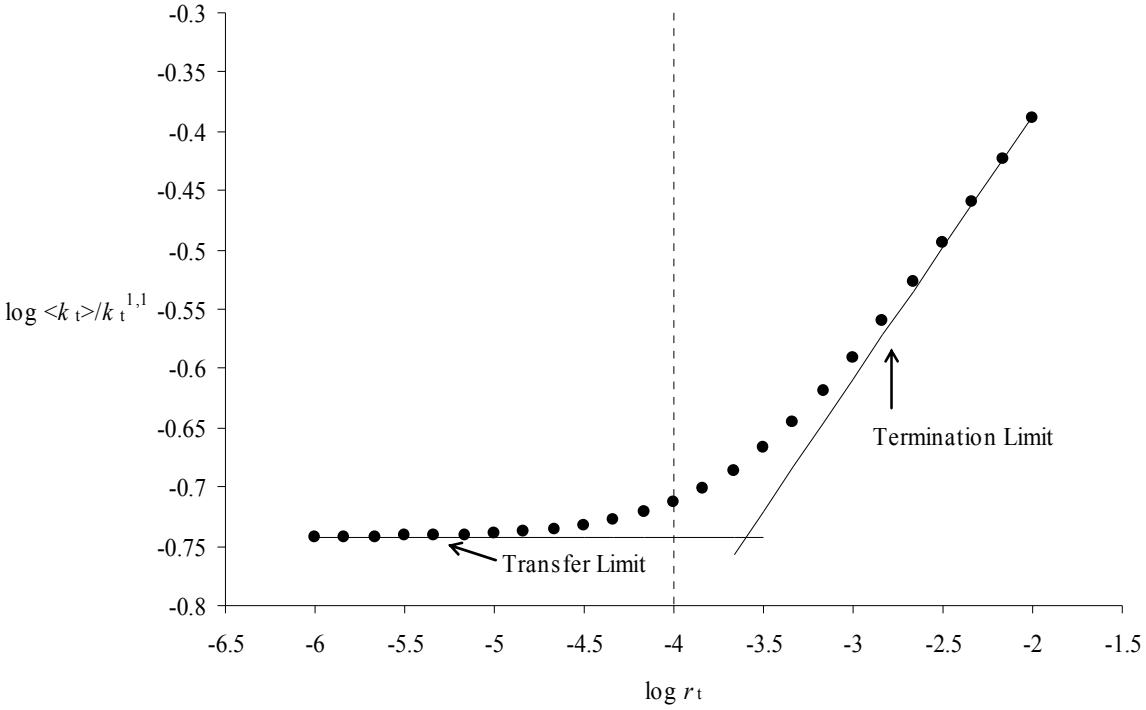

Fig. 5.9 Data of *Fig. 5.7* presented as log $\langle k_t \rangle / k_t^{1,1}$ (calculated from eq. **(4.28a)**) *vs.* log r_t (points). The vertical dotted line indicates the constant value of $r_{tr} = 1 \times 10^{-4}$, plotted on the same axis as r_t. Solid lines correspond to LCA results with the gm termination model in the transfer limit (r_t=0) and termination limit (r_{tr}=0), as indicated.

As the figures make clear, increasing either input parameter (r_t or r_{tr}) while leaving the other constant shifts the system nearer to the corresponding limit, and the apparent exponent with respect to that parameter also approaches that characteristic of the limit. Conversely,

decreasing one of the parameters while the other is nonzero leads to the other limit being approached, and at the same time the apparent exponent with respect to the varied parameter tends towards zero. It may be helpful when considering the above variations to recall that they are governed by eqs. **(5.1)** (in both the termination and transfer limits) and **(4.20)**, and depicted in *Fig. 5.3* and *Fig. 4.1*. This alternative perspective is considered since it corresponds more closely with experimental quantities.

Another point emphasised by the figures is that the parameters r_t and r_{tr} are not quite 'symmetrical' in that when they are equal (indicated by the vertical dotted lines in the figures), the system is actually closer to the transfer limit. This is a consequence of the fact that $S_t < S_r$ due to CLD termination. Naturally, the extent of this effect increases with increasing e.

5.3 Examples of Analysis of Experimental Data

The advantages of using classical kinetics to analyse FRP data are obvious – relatively simple algebraic relationships between data and model parameters (rate coefficients) exist, allowing use of generalised tools such as spreadsheet programs, rather than specialised simulation packages. However as we have seen, classical kinetics cannot be an adequate description of FRP kinetics: CLDT must be incorporated. Fortunately, this need not involve detailed modeling, since LCA results with the geometric mean termination model provide a good approximation under limiting conditions and low e, and are simple enough to calculate in a spreadsheet program. In this section we will follow this approach, analysing existing literature data for systems in conditions where LCA results are valid. This is partly to show that this approach can be used to uncover the CLDT parameters e and (an estimate of) $k_t^{1,1}$, and partly to illustrate how a detailed modeling approach (*i.e.* using the equations described in section 4.3) would lead to similar results.

Termination limit data

The data examined in this section are for bulk low-conversion polymerisation of methyl methacrylate (MMA) initiated by azobis(isobutyric acid methyl ester) (AIBME) at a range of temperatures.[5] The rate of thermal initiation is described by eq. **(5.12)**:

$$R_{\text{init}} = 2 f k_{\text{d}} [\text{I}] \qquad \textbf{(5.12)}$$

The temperature dependence of the initiator efficiency f and the initiator decomposition rate coefficient k_{d} for this system were determined by Stickler.[5] The initiator (AIBME) concentration is denoted by [I]. The steady-state rate of polymerisation under these conditions is described by the integrated rate law, eq. **(5.13)**:

$$-\ln(1-x) = k_{\text{p}} \sqrt{\frac{f k_{\text{d}} [\text{I}]}{\langle k_{\text{t}} \rangle}}\, t = k_{\text{app}} \sqrt{[\text{I}]}\, t \qquad \textbf{(5.13)}$$

Here, x is the fractional conversion of monomer into polymer, and t is time. In contrast to the equation used in Chapter 3, eq. **(3.12)**, propagation is assumed to be adequately described by the chain-length independent rate coefficient,[6] k_{p}.

Tab. 5.3 Temperature dependence of kinetic parameters for the bulk low-conversion polymerisation of MMA initiated by AIBME.

T (°C)	$f k_{\text{d}}$ $(\text{s}^{-1})^5$	k_{p} $(\text{L mol}^{-1}\ \text{s}^{-1})^6$	[M] $(\text{mol L}^{-1})^7$	r_{tr} [a)]
40	4.40×10^{-7}	498	9.20	7.95×10^{-6}
60	8.01×10^{-6}	834	8.95	1.38×10^{-5}
80	1.05×10^{-4}	1320	8.72	2.24×10^{-5}

a) Calculated using $k_{\text{tr,M}}$ values,[8] and assuming that all transfer in this system is due to transfer to monomer.

Also included in *Tab. 5.3* are values for the monomer concentration,[7] [M], and transfer ratio,[8] r_{tr}, both of which are used in data analysis, as will be discussed in due course.

Tab. 5.4 Experimental data gathered by Stickler[5] for polymerisation of MMA in near termination limit conditions.

T (°C)	[I] (mol L^{-1})	k_{app} ($L^{0.5}$ $mol^{-0.5}$ s^{-1})	$\overline{DP}_n$	$\langle k_t \rangle$ [b] (L mol^{-1} s^{-1})
40	4.00×10^{-1}	4.76×10^{-5}	1690	4.82×10^{7}
	1.71×10^{-1}	5.03×10^{-5}	2150	4.32×10^{7}
	7.25×10^{-2}	5.35×10^{-5}	3500	3.81×10^{7}
	3.99×10^{-2}	5.61×10^{-5}	4480	3.47×10^{7}
	1.50×10^{-2}	5.23×10^{-5}	6710	3.99×10^{7}
	3.88×10^{-3}	6.44×10^{-5}	14200	2.63×10^{7}
60	9.81×10^{-2}	2.86×10^{-4}	[a]	6.81×10^{7}
	4.90×10^{-2}	2.98×10^{-4}	[a]	6.27×10^{7}
	1.97×10^{-2}	3.65×10^{-4}	[a]	4.18×10^{7}
	9.76×10^{-3}	3.06×10^{-4}	2570	5.95×10^{7}
	3.76×10^{-3}	3.36×10^{-4}	4770	4.93×10^{7}
	9.76×10^{-4}	3.94×10^{-4}	8760	3.59×10^{7}
80	2.49×10^{-2}	1.71×10^{-3}	507	6.22×10^{7}
	1.22×10^{-2}	1.59×10^{-3}	1360	7.19×10^{7}
	2.50×10^{-3}	2.42×10^{-3}	1550	3.11×10^{7}
	1.03×10^{-3}	2.04×10^{-3}	3440	4.37×10^{7}
	2.56×10^{-4}	3.63×10^{-3}	11200	1.38×10^{7}

a) Data were not reported.[5]

b) Calculated from k_{app} and [I] values with eq. **(5.13)**, using data from *Tab. 5.3*.

The apparent rate coefficient for polymerisation, k_{app}, and the number average degree of polymerisation, $\overline{DP}_n$, were determined[5] as a function of initiator concentration. As indicated in eq. **(5.13)**, knowing k_{app} allows determination of $\langle k_t \rangle$, in conjunction with values of fk_d and k_p from *Tab. 5.3*.

We will consider two methods of extracting the CLDT parameters $k_t^{1,1}$ and e from the data in this section. The first method involves comparing $\langle k_t \rangle$ and $\overline{DP}_n$ data. We have seen previously that this allows immediate determination of e since $\langle k_t \rangle \sim (\overline{DP}_n)^{-e}$. Combining eqs. **(4.28b)**, **(4.40)** and **(5.3)** leads to eq. **(5.14)**:

$$\langle k_t \rangle = k_t^{1,1} \left[\Gamma\left(\frac{2}{2-e}\right) \right]^{e-2} \left[\frac{2}{(2-e)} \frac{2}{(1+\lambda)} \right]^{e} (\overline{DP}_n)^{-e} \qquad \textbf{(5.14)}$$

As previously discussed, this method has an intuitive appeal, given the analogous relationship between eq. **(5.14)** and eq. **(4.1)**. From a plot of log $\langle k_t \rangle$ *vs.* log $\overline{DP}_n$, the slope gives $-e$, which allows calculation of the terms involving the gamma function. The value of $k_t^{1,1}$ can then be determined from the intercept of the plot. In analysing this data it is assumed that $\lambda = 1$, in other words all termination is by disproportionation, which is reasonable for MMA

Tab. 5.5 CLDT parameters $k_t^{1,1}$ and e determined from the data of *Tab. 5.4* using the two methods discussed in the text.

Method	$\langle k_t \rangle$ *vs.* $\overline{DP}_n$		$\langle k_t \rangle$ *vs.* [I]	
T (°C)	$k_t^{1,1}$	e	$k_t^{1,1}$	e
40	2.5×10^8	0.24	1.6×10^8	0.20
60	1.2×10^9	0.41	2.2×10^8	0.21
80	1.1×10^9	0.48	1.0×10^9	0.48

monomer. The results of this analysis are presented in *Tab. 5.5*.

The second method for determination of the CLDT parameters involves comparing $\langle k_t \rangle$ and [I] data. Combining eq. **(5.9)** with the gm LCA results for A and a, and substituting eq. **(4.21)** for r_t gives eq. **(5.15)**:

$$\langle k_t \rangle = (k_t^{1,1})^{2/(2-e)} \left[\Gamma\left(\frac{2}{2-e}\right) \right]^{-2} \left[\frac{(f k_d)^{0.5}}{k_p[\mathrm{M}]} \left(\frac{4}{2-e}\right) \right]^{2e/(2-e)} [\mathrm{I}]^{e/(2-e)} \qquad \textbf{(5.15)}$$

Although eq. **(5.15)** may appear somewhat formidable, its application is similar to the method outlined for eq. **(5.14)**: finding the slope of a plot of log $\langle k_t \rangle$ *vs.*. log [I] allows determination of the value of e, whereupon evaluation of the middle part of the expression (the terms independent of $k_t^{1,1}$ and [I]) is possible. Evaluation of the intercept of the plot then leads to

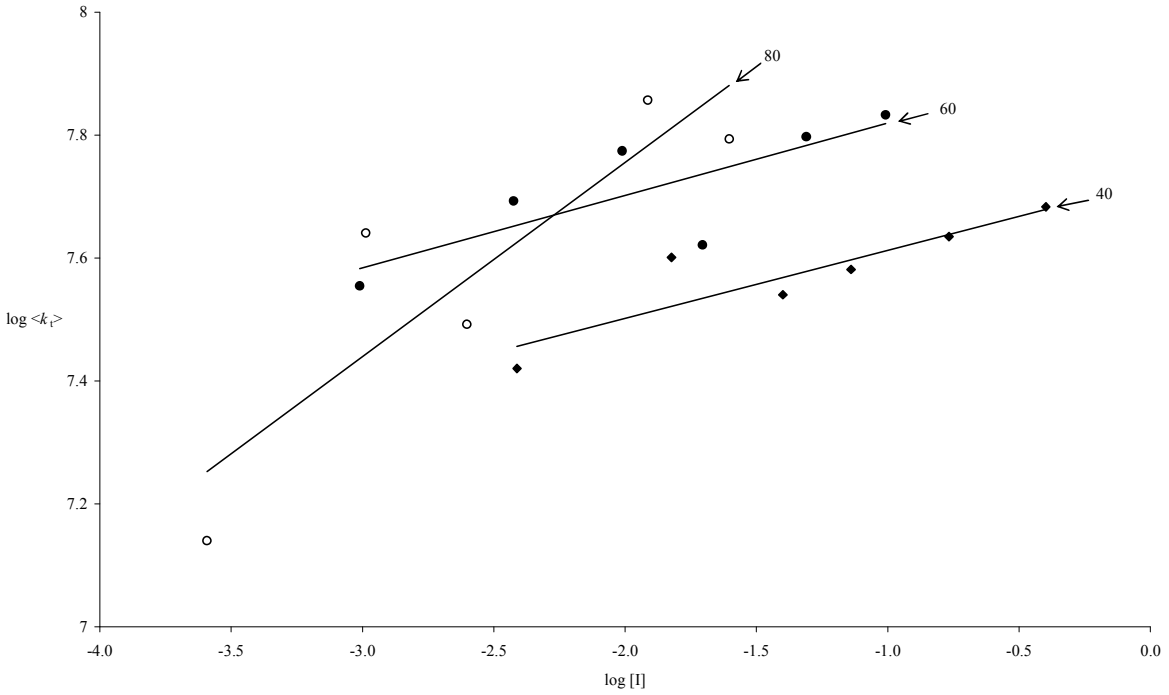

Fig. 5.10 Double logarithmic plot of $\langle k_t \rangle$ *vs.* [I] data taken from *Tab. 5.4*. Symbols indicate the temperature: diamonds, 40 °C; filled circles, 60 °C; open circles, 80 °C. Best fit lines are also shown for each set of data at constant temperature, as indicated.

$k_t^{1,1}$. Again, the results of the analysis are presented in *Tab. 5.5*.

Ideally of course, the results of both methods of analysis would be identical. Firstly, it should be noted that the observation of any effect at all from CLDT requires careful and extensive experiments – varying the initiator concentration over two orders of magnitude leads to variation in (the directly observed parameter) k_{app} of a factor of 2 or less. Given this, the consistency of the results determined by the two methods is encouraging. As *Fig. 5.10* shows, there is considerable scatter in the data, particularly for the 80 °C dataset. It is surprising then that this dataset shows the best agreement between the two methods. The lack of agreement in the 60 °C dataset is probably due to the limited range of $\overline{DP}_n$ data available at this temperature, leading to less accurately determined fit parameters. At 40 °C, the slightly higher $k_t^{1,1}$ value determined by using eq. **(5.14)** may be mitigated by the value of λ being less than one. While this is reasonable due to termination by combination having a lower activation energy than disproportionation,[9] the fact remains that the e values are also somewhat different between the two methods, and whatever the value of λ, it does not affect the determined value of e.

At this point it is worth examining the assumption made initially, that the system is in the termination limit. Using the values of $k_t^{1,1}$ found by the $\langle k_t \rangle$ *vs.* [I] method allows determination of r_t according to eq. **(4.21)**. Termination limit results will be applicable as long as r_t is greater than r_{tr} in all experimental data. At the lowest initiator concentration (and therefore lowest r_t value) used for each temperature, values of r_t were 2.3×10^{-4}, 3.5×10^{-4} and 9.1×10^{-4} at 40, 60 and 80 °C respectively. On comparison with r_{tr} values quoted in *Tab. 5.3*, it is clear that the value of r_t is always greater than 10 times the value of r_{tr}, so that the system must be very close to the termination limit, which validates the initial assumption that this was the case.

Some comments can be made on the relative merits of the two methods considered. The method involving comparison of $\langle k_t \rangle$ and [I] allows the more accurate determination of e to be made, since [I] can be determined far more accurately than can $\overline{DP}_n$, reducing the scatter in the data. There are also the added advantages that fewer measurements need to be made, and the fraction of disproportionation, λ, need not be known. There is still the problem of accurate measurement of initiation and propagation rate parameters, but these affect only the determination of $k_t^{1,1}$ and not e. Additionally, the type of mean operative in termination (whether gm, dm, hm or something else) is not known, so that $k_t^{1,1}$ cannot be absolutely determined in any case, so that it makes more sense to focus on accurately determining e. On the other hand, the method involving comparison of $\langle k_t \rangle$ and $\overline{DP}_n$ is not susceptible to the occurrence of transfer (at least, not to the same degree), and may lead to more accurate e values in systems where the extent of transfer is not known.

The determined values of $k_t^{1,1}$ and e are of secondary interest here, as was discussed earlier, the main point is to demonstrate and evaluate the methods that are used to determine them. The absolute values of $k_t^{1,1}$ are not physically realistic, due both to the unknown cross-termination model referred to earlier, and the neglect of the composite termination model discussed in chapters 2 and 3, which if included would lead to $k_t^{1,1}$ values more in line with small molecule measurements[10] (however, this would needlessly complicate the analysis). The trend of increased $k_t^{1,1}$ with temperature is of course expected, but the marked increase from the 60 °C to the 80 °C data is surprising, and unlikely to be real. The trend of e increasing with temperature is contrary to that found by Olaj.[11]

Transfer limit data

Unfortunately, studies of systems in the transfer limit that report rate as well as MWD data are relatively rare, in part because it is not well known that transfer limit data can yield useful

information on CLD termination. This point is counterintuitive, but quite significant. To briefly summarise the point (detailed in section 4.3), despite most dead chain formation occurring by transfer (the very definition of the transfer limit), and the radical chain-length distribution (RCLD) therefore being shaped by transfer, there must still be termination in a real FRP system, and since termination is chain-length dependent, the rate is affected by the nature of the CLD termination. In fact, as will soon be clear, analysis of this data is no more problematic - and in some ways simpler and less sensitive to experimental error - than analysis of termination limit data.

The first set of data considered in this section is that of Suddaby *et al.*,[12] who studied the free radical polymerisation of MMA and styrene at 60 °C in the presence of varying amounts of the catalytic chain transfer agent bis(boron difluorodimethylglyoximate) cobaltate(II) (COBF). This is a highly efficient transfer agent, and has the advantage of requiring such low concentrations to have its effect that the physical properties of the system are essentially unchanged, even at the highest concentrations used ([COBF]/[M] $\approx 2\times10^{-5}$). Contrast this with DDM, the transfer agent used in the work of Chapter 3, where much higher concentrations were required. The initiator was 2,2'-azobis(isobutyronitrile) (AIBN).

$$r_{tr} = \frac{k_{tr}^{X}[X]}{k_p[M]} = C_{trX}[X]/[M] \qquad \textbf{(5.16)}$$

In eq. **(5.16)**, which gives the aggregate rate parameter for transfer, r_{tr}, X denotes COBF. With such a highly active chain transfer agent, we can consider r_{tr} to be given by eq. **(5.16)** instead of the more strictly correct eq. **(4.22)**. In other words, transfer to monomer and other chain transfer reactions will be neglected in this section.

Tab. 5.6 Experimental parameters[12] and literature data for MMA and Styrene at 60 °C.

Series	Monomer	[I] (mol L^{-1})	$f k_d$ (s^{-1})[13]	k_p (L mol^{-1} s^{-1})[6,14]	[M] (mol L^{-1})[7,15]	C_{trX}[12]
A	MMA [a)]	1.17×10^{-2}	6.13×10^{-6}	834	2.98	2.07×10^{4}
B	MMA	3.52×10^{-2}	6.13×10^{-6}	834	8.95	3.69×10^{4}
C	Styrene	3.52×10^{-2}	6.13×10^{-6}	341	8.35	1.39×10^{3}

a) Solvent (Toluene) : monomer volume ratio was 2:1.

Experimental parameters for this system are tabulated in *Tab. 5.6*. Additional kinetic parameters that are used for subsequent analysis of the data are also tabulated. The value of $f k_d$ is taken from a study of AIBN-initiated styrene polymerisation,[13] and while this quantity is certainly likely to vary with monomer identity and solvent concentration, in the absence of more detailed information this value is used throughout. The value of k_p for MMA is similarly expected to depend on solvent concentration,[16] however again this effect must be neglected due to lack of information. The values of C_{trX} were determined by Suddaby *et al.*[12] using the Mayo method.

As with the termination limit data, we will contrast two methods of analysis based on the LCA results given in section 4.4. The geometric mean termination model will be used - despite existence of analytic results for the arguably more correct diffusion mean model - in order that derived values of $k_t^{1,1}$ are directly comparable with values found in the termination limit, where only the geometric mean termination model leads to simple expressions. The first method involves comparing $\langle k_t \rangle$ and $\overline{DP}_n$ data. Combining eqs. **(4.28b)**, **(4.41)** and **(5.4)** leads to eq. **(5.17)**:

$$\langle k_t \rangle = k_t^{1,1} \Gamma(1 - e/2)^2 (\overline{DP}_n)^{-e} \qquad \textbf{(5.17)}$$

Eq. **(5.17)** may be used to determine $k_t^{1,1}$ and e in the following way. From a plot of log $\langle k_t \rangle$ *vs.* log $\overline{DP}_n$, the slope gives -e, which allows calculation of the terms involving the gamma function. The value of $k_t^{1,1}$ can then be determined from the intercept of the plot. The second method involves comparison of $\langle k_t \rangle$ data with the experimental variable, [X]/[M]. Eqs. **(5.10)** and **(5.16)** combine to give eq. **(5.18)**:

$$\langle k_t \rangle = k_t^{1,1} \Gamma(1 - e/2)^2 (C_{trX})^e ([X]/[M])^e \qquad \textbf{(5.18)}$$

Tab. 5.7 Rate and molecular weight data from ref. [12].

Series	[X]/[M]	$\overline{DP}_n$	% conversion [a]	$\langle k_t \rangle$ [b] (L mol^{-1} s^{-1})
	0	969	7.43	6.78×10^{6}
	2.61×10^{-7}	118	6.37	9.33×10^{6}
A	5.22×10^{-7}	70	5.86	1.11×10^{7}
	1.04×10^{-6}	42	5.48	1.27×10^{7}
	2.09×10^{-6}	22	5.24	1.40×10^{7}
	0	1654	6.80	2.45×10^{7}
	2.37×10^{-8}	719	7.59	1.95×10^{7}
B	4.75×10^{-8}	437	6.48	2.70×10^{7}
	9.49×10^{-8}	230	6.21	2.95×10^{7}
	1.90×10^{-7}	133	5.73	3.48×10^{7}
	0	671	1.60	7.79×10^{7}
	5.11×10^{-6}	97	1.36	1.08×10^{8}
C	1.02×10^{-5}	63	1.34	1.11×10^{8}
	1.53×10^{-5}	42	1.2	1.39×10^{8}
	2.04×10^{-5}	33	1.17	1.46×10^{8}

a) Reaction time was 15 minutes in all experiments.

b) Calculated from conversion data using eq. **(5.13)** and corresponding values of k_p, $f k_d$ and [I] given in *Tab. 5.6*.

Note that as well as experimental data, eq. **(5.18)** also requires knowledge of the transfer ratio, C_{trX}, in much the same way as eq. **(5.15)** required knowledge of initiation and propagation parameters. According to eq. **(5.18)** a plot of log $\langle k_t \rangle$ *vs.* log [X]/[M] will have a slope of *e*, and the intercept may be used to determine $k_t^{1,1}$.

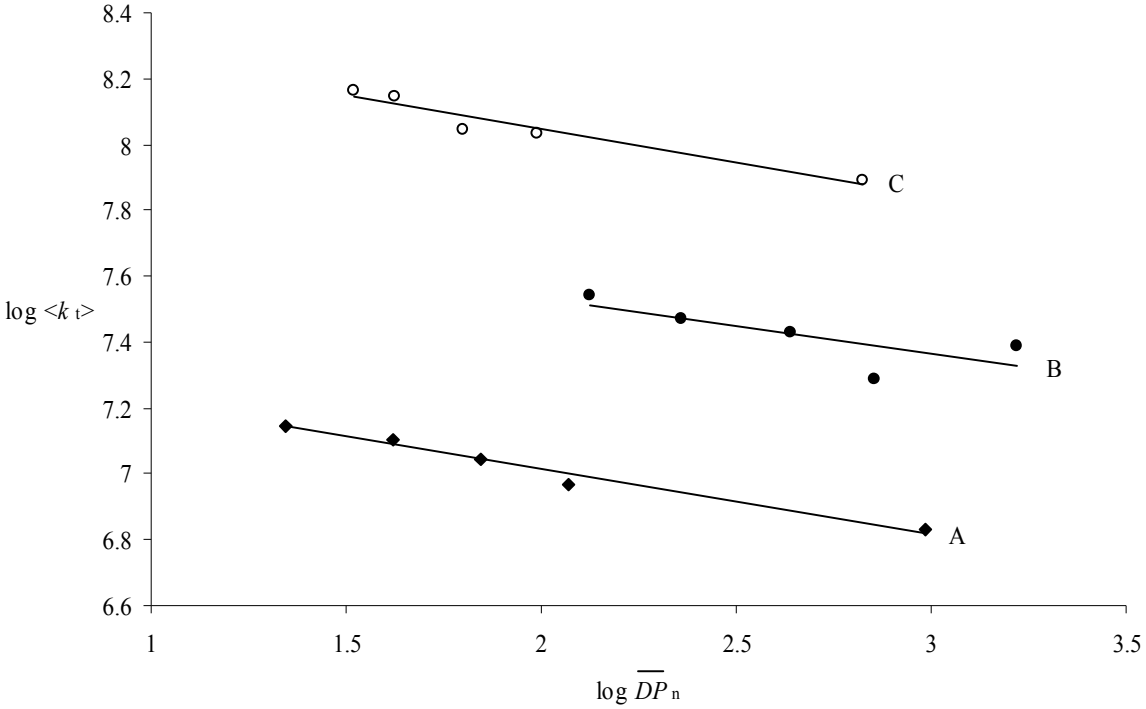

Fig. 5.11 Double logarithmic plot of $\langle k_t \rangle$ *vs.* $\overline{DP}_n$ data from *Tab. 5.7*. Symbols indicate datasets A, B and C from the table. Best fit lines for each dataset are also shown.

In *Fig. 5.11* and *Fig. 5.12*, the data of *Tab. 5.7* were plotted according to the methods described above, and linear best fits calculated. Eqs. **(5.17)** and **(5.18)** were used to determine $k_t^{1,1}$ and *e* from the parameters of the best fit lines. The results of this analysis are presented in *Tab. 5.8*. Agreement between the $k_t^{1,1}$ and *e* values derived for the two methods is almost perfect for series A and C, and fairly good for series B. It should be noted that the data for

[X]/[M] = 0 cannot be in the transfer limit, and in particular cannot be analysed with eq. **(5.18)** since $\langle k_t \rangle = 0$ is predicted in this case. However, it is felt that the extra information given by these data justifies their inclusion in the $\langle k_t \rangle$ *vs.* $\overline{DP}_n$ datasets fitted with eq. **(5.17)**, and depicted in *Fig. 5.11*. The data of *Tab. 5.1* indicate that the error associated with using the transfer limit expression to fit termination limit data should be much smaller than the error associated with the experimental data, especially considering the low *e* values (0.1 – 0.3) that have been determined for this data. Some deviation should be expected in the parameters $k_t^{1,1}$ and *e* derived with the two methods, simply because different datasets are used. Bearing in mind the relatively poor agreement found between the two methods for series B, it is interesting to note that when the [X]/[M] = 0 data is excluded from the $\langle k_t \rangle$ *vs.*

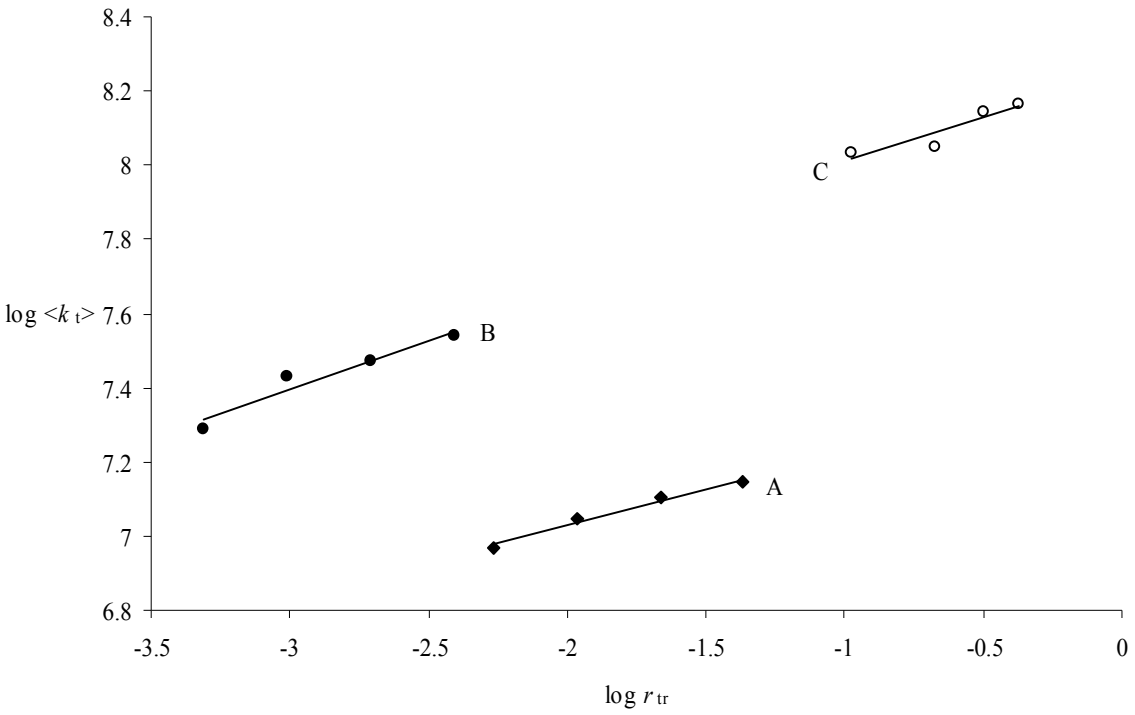

Fig. 5.12 Double logarithmic plot of $\langle k_t \rangle$ *vs.* r_{tr} (calculated from eq. **(5.16)**) data from *Tab. 5.7*. Symbols indicate datasets A, B and C from the table. Best fit lines for each dataset are also shown.

$\overline{DP}_n$ fit for this series a value of e of 0.32 is found, which is in good agreement with the value of e of 0.27 found with the $<k_t>$ *vs.* [X]/[M] data.

The question of whether or not the data is in the transfer limit can now be addressed. Recall that this issue depends on the relative magnitudes of the aggregate parameters r_t and r_{tr}, *i.e.* the extent to which $r_{tr} > r_t$. Using values of $k_t^{1,1}$ derived with the $<k_t>$ *vs.* $\overline{DP}_n$ method will give a conservative estimate of r_t using eq. **(4.21)** (since these $k_t^{1,1}$ values are lower than those found with the $<k_t>$ *vs.* [X]/[M] method). These values are compared with values of r_{tr} calculated according to eq. **(5.16)**, using C_{trX} values given in *Tab. 5.6* and the minimum non-zero values of [X]/[M] for each data series. These values of r_t and r_{tr} are displayed in *Tab. 5.8*. For series A, the value of r_t is about a factor of 5 lower than the minimum value of r_{tr}, so that all of the data points with [X]/[M] > 0 must be very close to the transfer limit. For series

Tab. 5.8 CLDT parameters $k_t^{1,1}$ and e determined from the data of *Tab. 5.7* using the two methods discussed in the text.

Method	$<k_t>$ *vs.* $\overline{DP}_n$		$<k_t>$ *vs.* [X]/[M]			
Series	$k_t^{1,1}$	e	$k_t^{1,1}$	e	r_{tr} [a)]	r_t [b)]
A	2.2×10^{7}	0.20	2.3×10^{7}	0.19	5.40×10^{-3}	1.02×10^{-3}
B	6.7×10^{7}	0.17	1.1×10^{8}	0.27	8.77×10^{-4}	1.02×10^{-3}
C	2.5×10^{8}	0.20	2.8×10^{8}	0.23	7.10×10^{-3}	5.13×10^{-3}

a) Calculated with eq. **(5.16)** using C_{trX} values determined in ref. [12] and the minimum non-zero value of [X]/[M] for each series.

b) Calculated with eq. **(4.21)** using $k_t^{1,1}$ derived with the $<k_t>$ *vs.* $\overline{DP}_n$ method and other parameters from *Tab. 5.6*

B, the value of r_t is also 1.02×10^{-3} (coincidentally). As this value is somewhat greater than the minimum value of r_{tr} for this series, it would be reasonable to expect to see some curvature in a plot of $\langle k_t \rangle$ *vs.* [X]/[M] due to mixed kinetics, as in *Fig. 5.8*. However *Fig. 5.12* shows no evidence of this curvature - this is probably due to experimental error. Series C however is safely within the transfer regime as the value of r_t is somewhat less than the minimum value of r_{tr} for the series. Overall, the assumption that this data is in the transfer limit has been shown to be self-consistent with this method of analysis. The lower value of $k_t^{1,1}$ in MMA with added toluene (series A) is expected, since toluene is more viscous than MMA. In general, the values of $k_t^{1,1}$ and e found are roughly consistent with the values found by other workers (see Chapter 2).

A similar study was carried out by Kukulj *et al.*[17] These workers studied the same systems studied by Suddaby *et al.*[12] analysed above. In addition to repeating measurements in the conditions of the earlier work, the temperature was also varied. This allows the determination of the temperature dependence of the CLD termination parameters $k_t^{1,1}$ and e as a check against the values determined from termination limit data (see above). As previously

Tab. 5.9 Temperature dependencies of kinetic parameters used in analysis of the data of Kukulj *et al.*[17]

Parameter	Monomer	Temperature dependence	Reference
k_p (L mol^{-1} s^{-1})	Styrene	$10^{7.63}\times\exp(-32.51\times10^3/RT)$	14
	MMA	$10^{6.427}\times\exp(-22.36\times10^3/RT)$	6
[M] (mol L^{-1})	Styrene	$10^3\times(0.92427 - 9.20\times10^{-4}\times(T/°C))/104.1$	15
	MMA	$10^3/(100.1\times(1.025934 + 0.001494\times(T/°C)))$	7
$f k_d$ (s^{-1})	Both	$\exp(32.585 - 123.5\times10^3/RT)$	13
C_{trX}	Styrene	$1.21\times10^{-4}\times\exp(41.8\times10^3/RT)$	17
	MMA	$6.21\times10^3\times\exp(4.63\times10^3/RT)$	17

established, initiation, propagation and transfer rate parameters are required to make a full analysis of the data for chain-length-dependent termination parameters. The temperature dependence of these parameters, which are available in the literature, are presented in *Tab. 5.9*.

For each temperature the experimental variable [X]/[M] was varied. These values were not tabulated in ref. [17], instead they were inferred from the experimental section of that paper, which also indicates that the initiator concentration in all experiments was 0.0273 mol L^{-1}.

Number average chain length ($\overline{DP}_n$) and conversion data were measured for each sample. However reaction times were not tabulated, so that it was not possible to calculate absolute $<k_t>$ from the data with eq. **(5.13)**. Instead, the relative $<k_t>$ with respect to the experiments at [X]/[M] = 0 was determined with eq. **(5.19)**, which is derived from eq. **(5.13)** with the assumption that all parameters except conversion (*viz.* reaction time, initiator concentration, initiation and propagation rate coefficients) remain constant between two experiments at the same temperature. It was explicitly stated[17] that reaction time was constant, and the other parameters ought to be constant when only transfer agent concentration is varied, therefore these assumptions are valid for this data.

$$<k_t>/<k_t>_0 = [\ln(1-x_0)/\ln(1-x)]^2 \qquad \textbf{(5.19)}$$

In eq. **(5.19)**, the subscript 0 indicates that the quantity pertains for [X]/[M] = 0. Calculating relative $<k_t>$ is somewhat unsatisfactory since e can be determined but $k_t^{1,1}$ cannot be determined (at least not directly). This also implies that it is not possible to quantify the balance of termination and transfer by calculating r_t and r_{tr} (since r_t depends on $k_t^{1,1}$), although a qualitative determination can be made. Note that relative $<k_t>$ increases with increasing [X]/[M], consistent with eq. **(5.18)** and a positive value of e. *Tab. 5.10* contains the data for MMA and *Tab. 5.11* contains the data for styrene.

Tab. 5.10 Conversion and molecular weight data for MMA from ref. [17].

Temperature (°C)	[X]/[M] [a)]	$\overline{DP}_n$	% conversion	$\langle k_t \rangle / \langle k_t \rangle_0$
40	0.00	4.99×10^{3}	5.80	1.00
	1.91×10^{-7}	4.06×10^{2}	4.68	1.55
	3.81×10^{-7}	1.73×10^{2}	4.40	1.76
	5.72×10^{-7}	8.66×10^{1}	3.92	2.23
50	0.00	4.05×10^{3}	6.16	1.00
	1.91×10^{-7}	2.50×10^{2}	4.92	1.59
	3.81×10^{-7}	1.13×10^{2}	4.95	1.57
	5.72×10^{-7}	6.85×10^{1}	4.66	1.78
	7.62×10^{-7}	5.98×10^{1}	4.32	2.07
60	0.00	2.36×10^{3}	5.23	1.00
	1.91×10^{-7}	2.08×10^{2}	4.52	1.35
	3.81×10^{-7}	1.04×10^{2}	4.36	1.45
	5.72×10^{-7}	5.34×10^{1}	4.16	1.60
	7.62×10^{-7}	5.10×10^{1}	4.12	1.63
70	0.00	1.26×10^{3}	6.21	1.00
	1.91×10^{-7}	1.77×10^{2}	5.52	1.27
	3.81×10^{-7}	9.29×10^{1}	5.26	1.41
	5.72×10^{-7}	6.40×10^{1}	5.13	1.48
	7.62×10^{-7}	4.62×10^{1}	5.00	1.56

a) Calculated from values given in experimental procedure[17].

From *Tab. 5.10* it can be seen that in the MMA data, the range of $\overline{DP}_n$ values at each temperature moves to lower values as the temperature is increased. This is unexpected since in the transfer limit $\overline{DP}_n = r_{tr}^{-1}$, with r_{tr} given by eq. **(5.16)**. The range of [X]/[M] values used is constant, however *Tab. 5.9* indicates that C_{trX} has a negative activation energy and thus decreases with temperature. Careful inspection of the paper[17] indicates that the data of *Tab.*

5.10 was not used to determine the temperature dependence of C_{trX} – a different dataset, which was not tabulated, was used for this purpose. Indeed, when the Mayo method used in the paper is applied to the data of *Tab. 5.10*, the C_{trX} values obtained increase with temperature, exactly as would have been expected based on the above argument. It is difficult to say which of the two datasets is more reliable, since no details of the data used to determine C_{trX} were presented[17].

Whatever the situation with C_{trX}, it is clear that values of $\overline{DP}_n$ are quite low (less than 50) at

Tab. 5.11 Conversion and molecular weight data for styrene from ref. [17].

Temperature (°C)	[X]/[M] [a)]	$\overline{DP}_n$	% conversion	$<k_t>/<k_t>_0$
40	0.00	1.37×10^{3}	3.56	1.00
	6.82×10^{-7}	8.34×10^{2}	3.31	1.16
	1.36×10^{-6}	5.44×10^{2}	3.26	1.20
	2.04×10^{-6}	3.70×10^{2}	3.19	1.25
	2.73×10^{-6}	3.04×10^{2}	3.09	1.33
50	0.00	7.78×10^{2}	4.2	1.00
	6.82×10^{-7}	6.33×10^{2}	4.07	1.07
	1.36×10^{-6}	4.05×10^{2}	3.85	1.19
	2.04×10^{-6}	3.48×10^{2}	3.88	1.18
60	0.00	6.96×10^{2}	4.47	1.00
	6.82×10^{-7}	4.68×10^{2}	4.35	1.06
	1.36×10^{-6}	3.55×10^{2}	4.36	1.05
	2.04×10^{-6}	2.85×10^{2}	4.2	1.14
70	0.00	4.05×10^{2}	4.7	1.00
	0.00	4.05×10^{2}	4.69	1.00
	6.82×10^{-7}	3.65×10^{2}	4.63	1.03
	1.36×10^{-6}	3.47×10^{2}	4.6	1.05
	2.04×10^{-6}	2.89×10^{2}	4.55	1.07

a) Calculated from values given in experimental procedure[17].

higher temperatures and transfer agent concentrations. Given the findings of Chapter 3, we may expect CLD propagation to be important in this system. It is not intended to attempt to model this, but merely to point out that this presents a limitation to the methods of analysis that will be used to determine the CLD termination parameters.

Two features of the data of *Tab. 5.11* are worth mentioning at this stage. Firstly, as with the MMA data, the values of [X]/[M] and $\overline{DP}_n$ given here are not consistent with the value of C_{trX} due to a different dataset being used to determine it.[17] Secondly, at higher temperatures it is apparent that addition of transfer agent has only a small effect on $\langle k_t \rangle$. This is an indication that the system is not in the transfer limit, and this is borne out by subsequent data analysis.

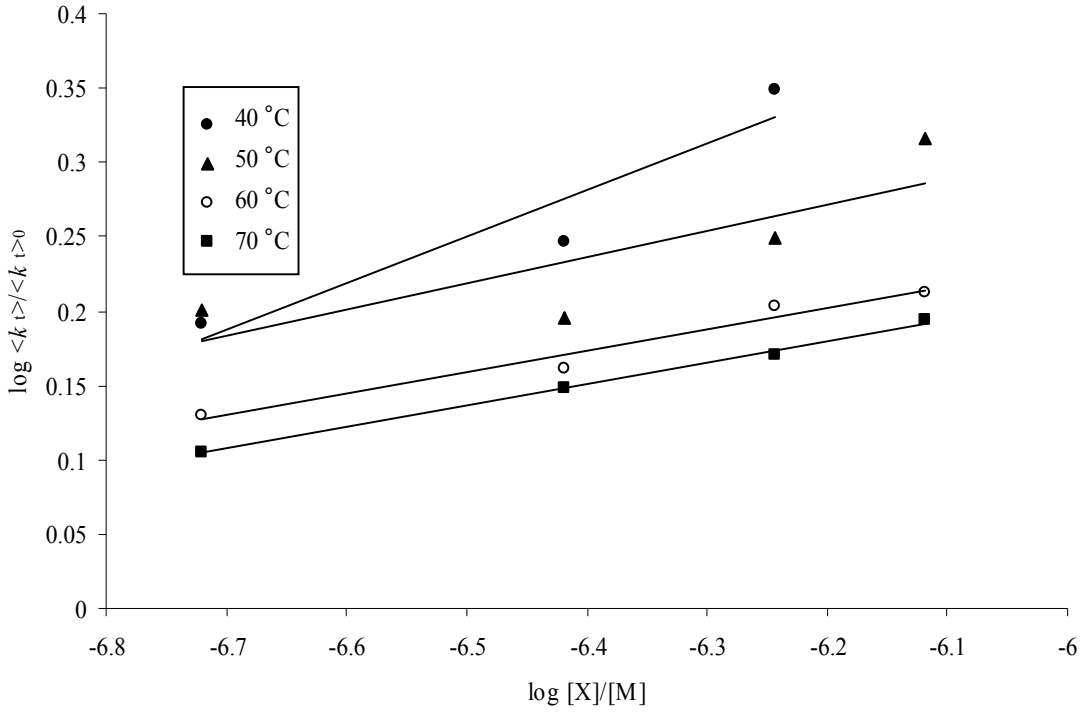

Fig. 5.13 Double logarithmic plot of relative $\langle k_t \rangle$ *vs.* [X]/[M] for MMA. Symbols denote temperature, as indicated. Best fit lines for datasets at each temperature are also shown.

Chain-length dependent termination parameters are determined as follows. The data of *Tab. 5.10* is plotted in *Fig. 5.13* and *Fig. 5.14*, and the data of *Tab. 5.11* is plotted in *Fig. 5.15* and *Fig. 5.16*. Best fit linear parameters are then used to determine e and $k_t^{1,1}/\langle k_t \rangle_0$ with eq. **(5.18)** (*Fig. 5.13* and *Fig. 5.15*) and with eq. **(5.17)** (*Fig. 5.14* and *Fig. 5.16*). These values are summarised in *Tab. 5.12*.

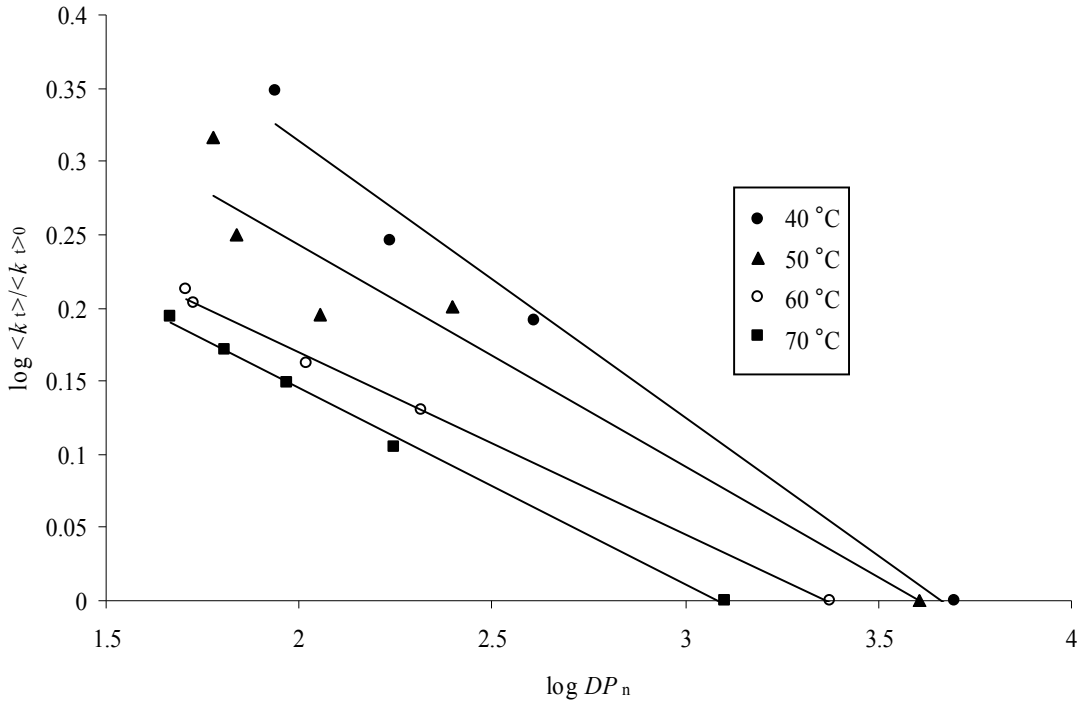

Fig. 5.14 Double logarithmic plot of relative $\langle k_t \rangle$ *vs.* $\overline{DP}_n$ for MMA. Symbols denote temperature, as indicated. Best fit lines for datasets at each temperature are also shown.

We now consider the data and determined CLD termination parameters for MMA. *Fig. 5.13* and *Fig. 5.14* show that there is often considerable scatter in the experimental data, in particular for the data at 40 °C and 50 °C. For this data *Fig. 5.13* is suggestive of a curve with increasing slope (as in *Fig. 5.8*) indicating that the data is not in the transfer limit, although it

is difficult to say this with certainty from 3 or 4 data points. However, comparison of the CLD termination parameters derived with the two methods shown in *Tab. 5.12* reveals that the values are in reasonable agreement, for the most part. Also, it is clear from *Fig. 5.8* that use of data not in the transfer limit would lead to determined values of e and $k_t^{1,1}$ being lower than their true values. In fact the opposite is observed: if we assume that values determined with eq. **(5.17)** are more accurate, since they are almost independent of the degree of termination *vs.* transfer, we would expect CLD termination values determined with eq. **(5.18)** to be lower. It is therefore more likely that the data is fairly close to the transfer limit and the different values determined by the two methods are attributable to experimental error (although it is curious that values determined with eq. **(5.18)** are higher for *all* four temperatures). Note that the slight differences between the CLD termination values

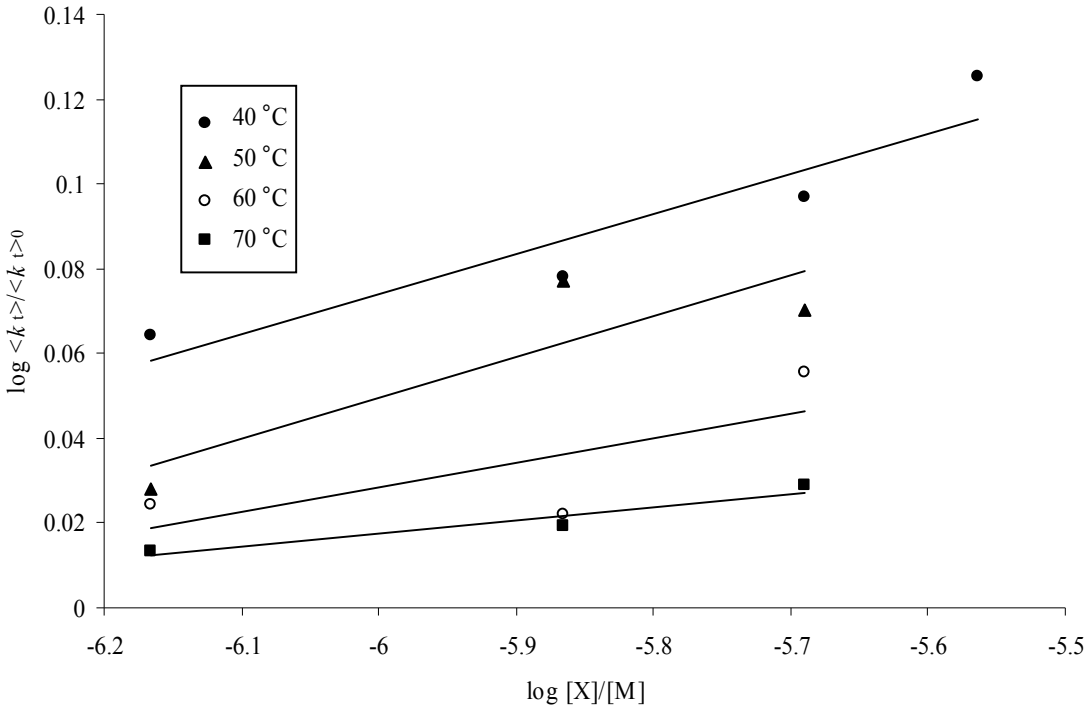

Fig. 5.15 Double logarithmic plot of relative $<k_t>$ *vs.* [X]/[M] for styrene. Symbols denote temperature, as indicated. Best fit lines for datasets at each temperature are also shown.

determined by Kukulj *et al.*[17] and those of *Tab. 5.12* are due to the use of eq. **(5.19)**, which correctly accounts for consumption of monomer during polymerisation, to determine relative $\langle k_t \rangle$.

We now consider the data and determined CLD termination parameters for styrene. *Fig. 5.15* and *Fig. 5.16* show some scatter, and as with the MMA data there is some suggestion that instead of a linear trend, a curve with an increasing slope would provide a better fit. In this case, comparison of the CLD termination parameters derived with the two methods shown in *Tab. 5.12* shows that the values determined with eq. **(5.17)** are greater than those determined with eq. **(5.18)** at each temperature. Comparison of these two figures with the figures for MMA show quite clearly what was noted previously - that the addition of chain transfer agent to the styrene system has a much less pronounced effect than it did for MMA. Overall it seems likely that the system is not in the transfer limit at any of the four temperatures, which somewhat decreases confidence in the accuracy of the determined CLD termination parameters. Despite this, the values determined with eq. **(5.17)** are probably more affected by scatter in the experimental data than by the system not being in the transfer limit – as previously discussed, $\langle k_t \rangle$ at a particular value of $\overline{DP}_n$ at low values of e is relatively unaffected by being in the termination or transfer limit. However, the occurrence of combination will change this situation somewhat, causing e to be underestimated (see eq. **(5.5)** and the section 'modeling transfer limit data'). It is evident from *Tab. 5.12* however that the underestimation of e incurred by the $\langle k_t \rangle$ *vs.* $\overline{DP}_n$ method is less than the underestimation of e incurred by the $\langle k_t \rangle$ *vs.* r_{tr} method when the system is not in the transfer limit.

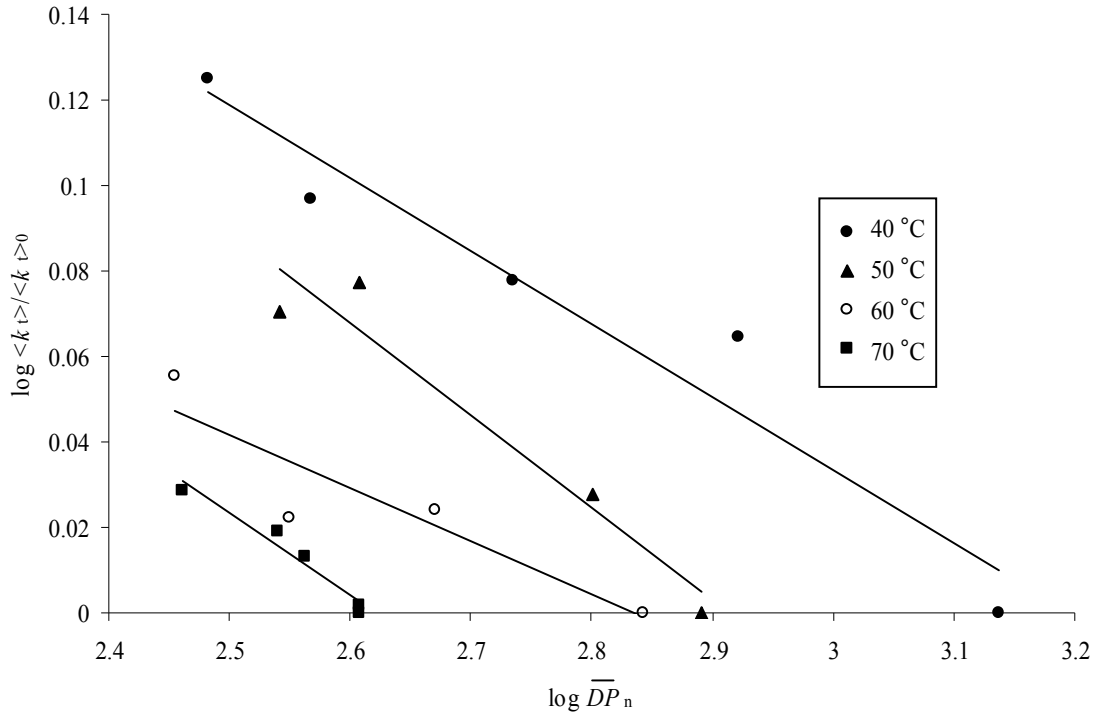

Fig. 5.16 Double logarithmic plot of relative $\langle k_t \rangle$ *vs.* $\overline{DP}_n$ for styrene. Symbols denote temperature, as indicated. Best fit lines for datasets at each temperature are also shown.

With the knowledge of values of e from *Tab. 5.12*, the data of *Tab. 5.10* and *Tab. 5.11* present an opportunity for the direct determination of $k_t^{1,1}$. Values of $\overline{DP}_n$ at [X]/[M] = 0 are in the termination limit, so that eq. **(5.3)** and eq. **(4.35)** for S_r should be applicable, and since e is known with reasonable certainty from analysis with eq. **(5.17)**, r_t can be determined. In eq. **(5.3)**, the fraction of termination by disproportionation λ is assumed to be 0 for styrene and 1 for MMA. Then, $k_t^{1,1}$ can be estimated since the other parameters comprising r_t (see eq. **(4.21)**) are known from *Tab. 5.9*. The results of the analysis just outlined are also presented in *Tab. 5.12*. Evidently there is considerable scatter in the $k_t^{1,1}$ values obtained. In order to reduce this somewhat, an average value of e was determined for each monomer, and $k_t^{1,1}$

values recalculated using this value of *e*. Taking styrene as an example, analysis of the latter set of data yields an activation energy for $k_t^{1,1}$ of 1.2 kJ/mol. The activation energy is expected to be of the order of 10 kJ/mol.[9] However it is plausible that a higher activation energy is consistent with the data due to the large amount of scatter, as well as uncertainty in the parameters of *Tab. 5.9*. Also it was assumed that the initiator concentration was constant in all experiments as this was implied in the experimental procedure[17], however if this was not the case it could also account for the unexpected trend in $k_t^{1,1}$ values.

Tab. 5.12 Monomer and temperature dependence of chain-length dependent termination parameters determined from the data of Kukulj *et al.*[17].

Monomer	Temp. (°C)	e [a)]	$\frac{k_t^{1,1}}{\langle k_t \rangle_0}$ [a)]	e [b)]	$\frac{k_t^{1,1}}{\langle k_t \rangle_0}$ [b)]	$k_t^{1,1}$ (L mol^{-1} s^{-1}) [c)]	$k_t^{1,1}$ (L mol^{-1} s^{-1}) [d)]
MMA	40	0.19	4.3	0.31	5.7	9.7×10^7	7.1×10^7
	50	0.15	3.2	0.18	3.3	4.1×10^7	4.0×10^7
	60	0.12	2.4	0.14	2.5	3.7×10^7	4.4×10^7
	70	0.13	2.4	0.14	2.4	5.4×10^7	6.0×10^7
Styrene	40	0.17	3.1	0.09	2.1	2.9×10^8	3.0×10^8
	50	0.22	3.7	0.10	2.1	5.0×10^8	4.1×10^8
	60	0.12	2.1	0.06	1.6	1.9×10^8	2.5×10^8
	70	0.19	2.8	0.03	1.3	3.9×10^8	3.6×10^8

a) Data in *Tab. 5.10* and *Tab. 5.11* analysed using eq. **(5.17)**.

b) Data in *Tab. 5.10* and *Tab. 5.11* analysed using eq. **(5.18)**.

c) Calculated from $\overline{DP}_n$ values with r_{tr}=0 using *e* values found using eq. **(5.17)** (see text for details).

d) Calculated from $\overline{DP}_n$ values as in [c)] with average values of *e* (0.15 for MMA and 0.18 for styrene).

The issue of the accuracy of the determination of the activation energy of $k_t^{1,1}$ is analysed in more detail here. *Fig. 5.17* shows the temperature dependence of the styrene $k_t^{1,1}$ values of *Tab. 5.12*. As mentioned earlier, using an average value of e to calculate $k_t^{1,1}$ reduces scatter. Using these values of $k_t^{1,1}$ and allowing both the frequency factor A and activation energy E_a to vary gives the fit indicated by the thick line in the figure. The parameters are E_a = 1.2 kJ/mol and $A = 5.0\times10^8$ L mol^{-1} s^{-1}. This is a very low activation energy even for a diffusion controlled reaction – in fact the estimated standard deviation of this parameter is 4.4 kJ/mol, higher than the actual value. Of course this is not statistically rigorous since the data is processed, therefore a comparison with measured data is sought (*viz.* $\overline{DP}_n$ measurements). A more realistic fit is obtained by fixing the activation energy at 10 kJ/mol – this is the thin line in the figure. The frequency factor A for this fit is 1.2×10^{10} L mol^{-1} s^{-1}. This frequency factor is more physically reasonable and lends support to the use of the use of these parameters despite the fact that they give a slightly inferior fit to the experimental data.

Values of $k_t^{1,1}$ given by these fits are then used to calculate $\overline{DP}_n$. These values are displayed in *Fig. 5.18* along with the original experimental data, where it is evident that these values of $k_t^{1,1}$ lead to a reasonable agreement with the experimental data, despite the large amount of scatter seen in the previous figure. This is because the temperature dependence of $\overline{DP}_n$ is only affected to a small extent by the temperature dependence of $k_t^{1,1}$. Consideration of eq. **(4.35)** demonstrates that the temperature dependence of $\overline{DP}_n$ is proportional to the 'activation energy' of r_t, which is given by eq. **(5.20)**. In deriving this equation it is assumed that e, [I] and [M] are independent of temperature:

$$E_a\,(\overline{DP}_n) \sim \frac{1}{2}\,(E_a(k_t^{1,1}) + E_a(f\,k_d)) - E_a(k_p) \qquad \textbf{(5.20)}$$

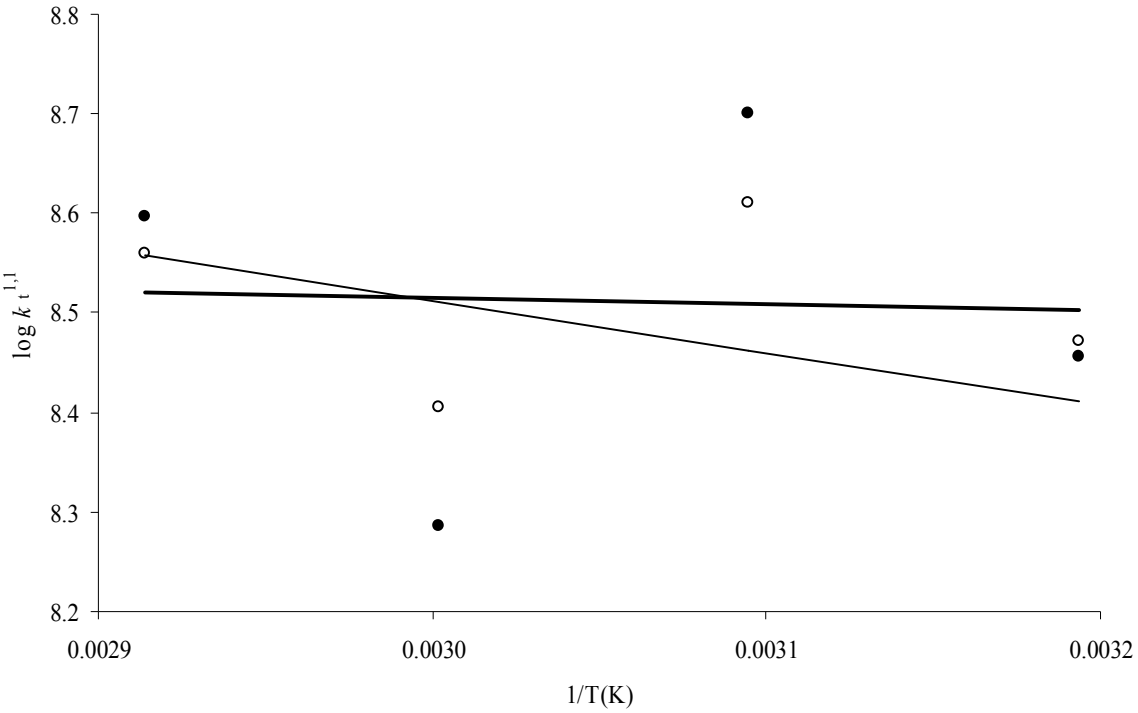

Fig. 5.17 Arrhenius plot for $k_t^{1,1}$. Solid circles correspond to the $k_t^{1,1}$ values in the left-hand column of *Tab. 5.12*, and hollow circles correspond to the right-hand column. The thin line is the best fit with an activation energy of 10 kJ/mol and the thick line is the best fit with the activation energy allowed to vary.

With the activation energies for $f\,k_d$ and k_p given in *Tab. 5.9*, E_a ($\overline{DP}_n$) is proportional to 29 + $E_a(k_t^{1,1})/2$ kJ/mol. With such large contributions from terms due to initiation and propagation, and the scatter in the data, the difference between activation energies for $k_t^{1,1}$ of 1.2 and 10 kJ/mol are almost indistinguishable.

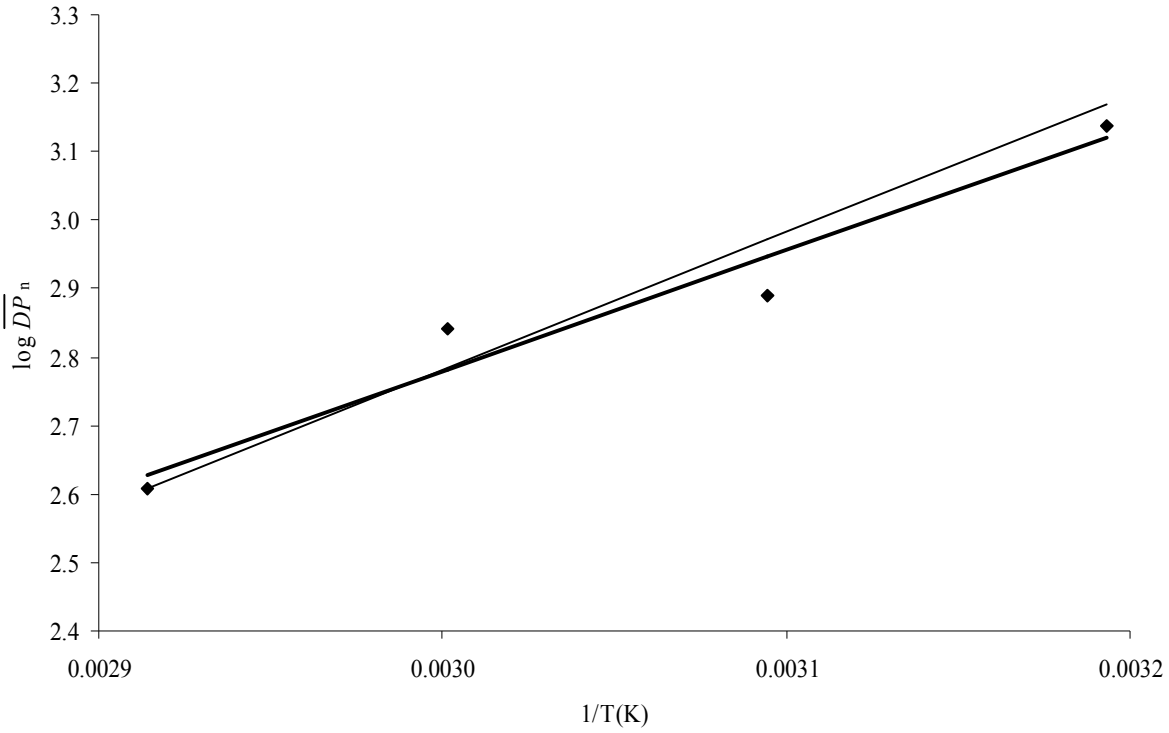

Fig. 5.18 Temperature dependence of the number-average molecular weight $\overline{DP}_n$. Diamonds are experimental values from *Tab. 5.11*. Lines are calculated with eq. **(4.35)** using $k_t^{1,1}$ values derived from fits of *Fig. 5.17* (The thin line is the best fit with an activation energy of 10 kJ/mol and the thick line is the best fit with the activation energy allowed to vary).

Modeling transfer limit data

Having determined the parameters of *Tab. 5.12* and also noted that the styrene data appears not to be in the transfer limit, it is worth investigating the degree to which full modeling (with mixed termination / transfer kinetics) is capable of reproducing the data. The r_t values determined above were used to predict the relative RCLD using eq. **(4.31)**, from which $\langle k_t \rangle$ and $\overline{DP}_n$ values were calculated (eqs. **(4.28a)** and **(4.29b)**). As *Fig. 5.19* shows, the $\overline{DP}_n$

values at $\langle k_t \rangle = \langle k_t \rangle_0$ (*i.e.* $r_{tr}=0$) are well reproduced by the model (as would be expected since these were the values used to determine the model parameters). The rest of the data is not so well reproduced, and it is clear that the slopes of the predicted curves are all too low. However it must be said that the correct qualitative trends are evident. This result is a little surprising since *Fig. 5.16* seems to support a linear relationship between $\langle k_t \rangle$ and $\overline{DP}_n$ with slope -*e*. Note however that the lines in *Fig. 5.19* are almost straight, so that the expectation of linearity is not challenged. This result can be explained by returning to an observation made in section 5.2 on the effect of the occurrence of combination – that combination raises the value of the pre-factor in the power law for $\langle k_t \rangle$ *vs.* $\overline{DP}_n$. Taking the data at 40 °C as an

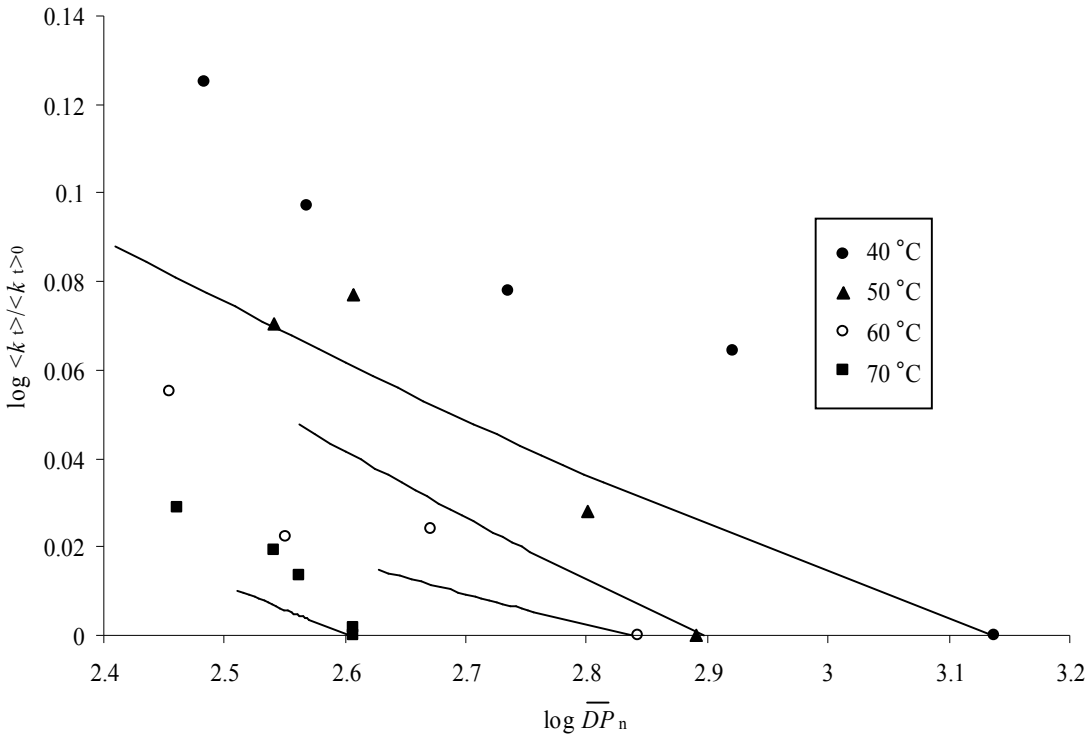

Fig. 5.19 Double logarithmic plot of relative $\langle k_t \rangle$ *vs.* $\overline{DP}_n$ for styrene. Symbols denote temperature, as indicated. Lines are for datasets at each temperature and are predicted with eq. **(4.31)** (see text for details).

example, in the termination limit with $\lambda = 0$ this pre-factor is 1.244, calculated with eq. **(5.5)** with eq. **(4.40)** for the value of A. However in the transfer limit the pre-factor is 1.117 (using eq. **(4.41)** for the value of A). This is consistent with the curves of *Fig. 5.19* - at the highest $\overline{DP}_n$ values they are in the termination limit and as $\overline{DP}_n$ decreases they move toward the transfer limit, although this transition is not complete even at the lowest $\overline{DP}_n$ values. This occurrence is enough to significantly reduce the slope from the expected value of e to that seen in the figure. One can be confident that calculations with still higher transfer agent concentrations would see the slopes of the curves in *Fig. 5.19* become more negative, eventually converging on the value of e as the transfer limit is approached.

The same predicted dataset is used to present *Fig. 5.20*. Much like the previous figure, the

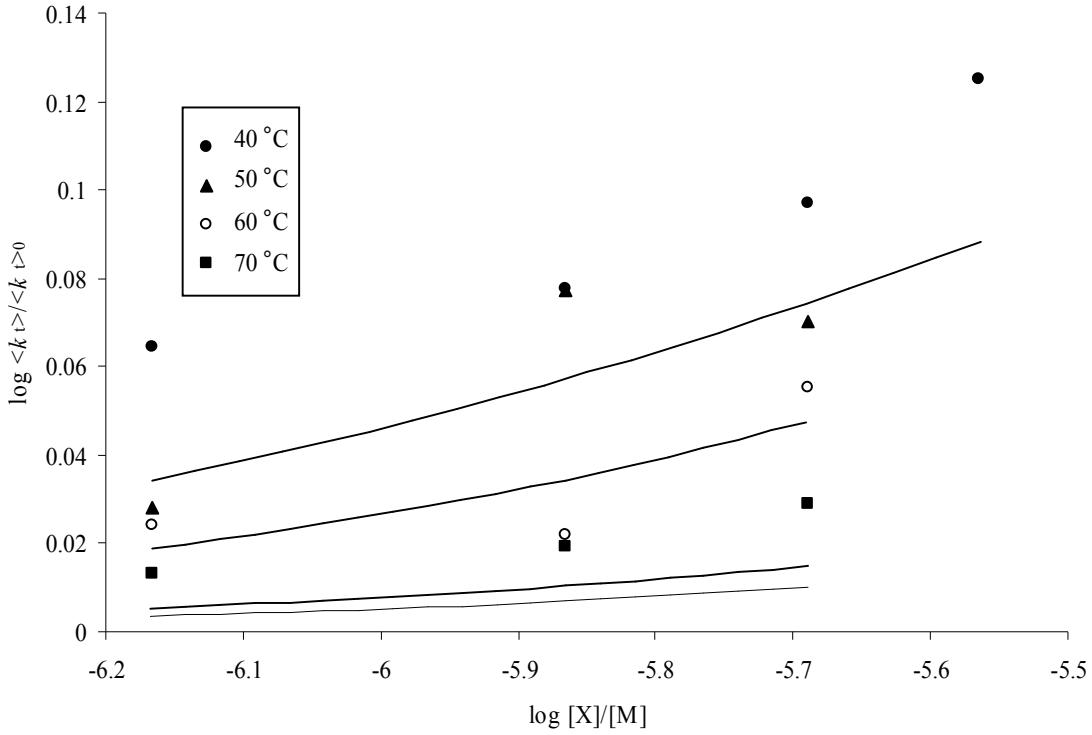

Fig. 5.20 Double logarithmic plot of relative $\langle k_t \rangle$ *vs.* [X]/[M] for styrene. Symbols denote temperature, as indicated. Lines are for datasets at each temperature and are predicted with eq. **(4.31)**.

qualitative trend of the data is reproduced but the fit is not very good. As expected from *Fig. 5.8* the predicted curves are distinctly nonlinear.

Given the difficulties presented by knowing only relative $<k_t>$, the possibility was investigated that the reaction time was constant in all experiments. This was quickly discarded because reproducing $<k_t>_0$ values at each temperature by varying $k_t^{1,1}$ lead to an activation energy for $k_t^{1,1}$ of 150 kJ/mol, which is much higher than expected for a diffusion controlled reaction. Since it follows from eq. **(5.13)** that $<k_t>$ is proportional to reaction time squared, experimental reaction time must have been decreased substantially with temperature.

Somewhat unexpectedly, the finding that the data of *Tab. 5.11* for styrene is not in the transfer limit suggests the possibility of indirect determination of $k_t^{1,1}$ by modeling, attempting to fit the shape of the curve of $<k_t>$ *vs.* [X]/[M] found with mixed transfer and termination (see *Fig. 5.8*). Eq. **(4.31)** was used and $k_t^{1,1}$ allowed to vary. The value of e used was 0.17 (the average of the values found at different temperatures), and other necessary parameters were taken from *Tab. 5.9*. The values of $k_t^{1,1}$ that gave these fits were non-physical as they decreased with increasing temperature. However this situation is not as problematic as it may seem, since particularly for the higher two temperatures, the data is relatively insensitive to the value of $k_t^{1,1}$, as $<k_t>$ is almost constant over the experimental range of [X]/[M] values. Thus a series of $k_t^{1,1}$ values that increased with temperature could fit the data almost as well.

5.4 Conclusion

Section 5.2 showed that the analytic expressions developed in Chapter 4 are surprisingly general, and where these analytic expressions are not exact, the model results always fit eq. **(5.1)**. This is a two-edged sword in that it makes discrimination between various termination

models difficult but also unnecessary if the aim is to extract basic parameters such as $k_t^{1,1}$ and e from experimental data.

In section 5.3 was exemplified how to use the theory of Chapter 4 and Section 5.2 to analyse experimental data in order to extract information about CLDT. The parameter values thus obtained are self-consistent in that rate data gives parameters agreeing with $\overline{DP}_n$ data. Further, these values are in agreement with best estimates from other experimental techniques. These other experimental techniques mostly require sophisticated, non-steady-state experiments, *e.g.* PLP. What this chapter has shown is that good parameter values can be obtained from simple steady-state data if only such data is analysed properly. While the equations involved are admittedly not simple, it should be evident from this chapter that nor are they prohibitively complicated. In particular, it is a very simple exercise to determine the slope of a plot, and there is always, as has been shown, a simple relationship between the slope and e.

While these methods do not *always* lead to a consistent set of parameters describing the data, careful use of them does at least indicate when more complete modeling is necessary, and also give a starting approximation to the model parameters. It must be noted that simply using the Mayo method to determine C_{trX} and eq. **(5.17)** to determine $k_t^{1,1}$ and e in isolation gives no warning of inconsistency. Perhaps a better fit may be achieved by allowing C_{trX} to vary, proceeding in a similar manner to Chapter 3, however for the purposes of this work it is sufficient to note that linear methods such as these do not always provide the full picture. Given the scatter in this experimental data, more complete modeling may not lead to significant improvement in the fit of the model to experiment, but in general the procedure developed in Chapter 3 is appropriate to these types of systems. In particular the data considered here does not justify addition to the model of composite termination or CLDP.

For MMA in the transfer limit, contrary to termination limit data we see *e* decrease with temperature. However, neither trend is particularly strongly supported by the data. It is noted that Olaj *et al.* predict that *e* will decrease with temperature.[11] For styrene, values of *e* are consistently lower when analysed using eq. **(5.18)**. This is almost certainly because the data are not in transfer limit.

5.5 Postscript

Some of the results of this chapter have been published in Smith, G. B.; Russell, G. T. *Macromol. Symp.* **2007**, *248*, 1-11.

References

(1) de Gennes, P. G.; Léger, L. *Ann. Rev. Phys. Chem.* **1982**, *33*, 49-61.

(2) Olaj, O. F.; Zifferer, G. *Macromolecules* **1987**, *20*, 850-861.

(3) Russell, G. T. *Aust. J. Chem.* **2002**, *55*, 399-414.

(4) Rudin, A. *The Elements of Polymer Science and Engineering*; 1st ed.; Academic Press: Orlando and London, 1982.

(5) Stickler, M. *Makromol. Chem.* **1986**, *187*, 1765-1775.

(6) Beuermann, S.; Buback, M.; Davis, T. P.; Gilbert, R. G.; Hutchinson, R. A.; Olaj, O. F.; Russell, G. T.; Schweer, J.; van Herk, A. M. *Macromol. Chem. Phys.* **1997**, *198*, 1545-1560.

(7) Eastmond, G. C. *Makromol. Chem., Macromol. Symp.* **1987**, *10/11*, 71-87.

(8) Stickler, M.; Meyerhoff, G. *Makromol. Chem.* **1978**, *179*, 2729-2745.

(9) Moad, G.; Solomon, D. H. *The Chemistry of Free Radical Polymerization*; 1st ed.; Pergamon: Oxford, 1995.

(10) Fischer, H.; Paul, H. *Acc. Chem. Res.* **1987**, *20*, 200-206.

(11) Olaj, O. F.; Vana, P. *J. Polym. Sci., Polym. Chem. Ed.* **2000**, *38*, 697-705.

(12) Suddaby, K. G.; Maloney, D. R.; Haddleton, D. M. *Macromolecules* **1997**, *30*, 702-713.

(13) Berger, K. C. *Makromol. Chem.* **1975**, *176*, 3575-3592.

(14) Buback, M.; Gilbert, R. G.; Hutchinson, R. A.; Klumperman, B.; Kuchta, F.-D.; Manders, B. G.; O'Driscoll, K. F.; Russell, G. T.; Schweer, J. *Macromol. Chem. Phys.* **1995**, *196*, 3267-3280.

(15) Matheson, M. S.; Auer, E. E.; Bevilacqua, E. B.; Hart, E. J. *J. Am. Chem. Soc.* **1951**, *73*, 1700-1706.

(16) Olaj, O. F.; Schnöll-Bitai, I. *Monatsh. Chem.* **1999**, *130*, 731-740.

(17) Kukulj, D.; Davis, T. P. *Macromol. Chem. Phys.* **1998**, *199*, 1697-1708.

6 Theoretical Validation of Single-Pulse Pulsed-Laser Polymerisation as a Method for Investigating Chain-Length-Dependent Termination

Abstract

Ideally, single-pulse pulsed-laser polymerisation (SP PLP) experiments are marked by a simple relation between time and radical chain length. Thus time-resolved data from such experiments have the potential to directly reflect the chain-length dependence of the termination reaction. However this capability is hostage to various assumptions. These are investigated by performing a series of theory *vs.* theory comparisons. On the one hand, assumption-free simulations of the kinetics of SP PLP experiments are carried out. The results thus generated are compared with the predictions of equations derived by making assumptions. In this way it is possible to gauge the rectitude of data-analysis methods based on the equations. In turn, the following assumptions are investigated: (1) That of radicals being of length 0 at time 0; (2) That of all radicals terminating at the same rate at any instant; (3) That of transfer being negligible; (4) That of termination being described by a simple power-law; and (5) That of propagation being chain-length independent in rate. All these assumptions are probed in relation to analysis of SP PLP kinetic data, while assumptions (1) and (4) are looked at in relation to the analysis of molecular weight distributions. While some surprising findings do emerge, for the most part it is found that data-analysis methods are reasonably robust. Further, it is possible to make these methods even more accurate by adopting some refinements that are recommended. In general the outstanding potential of SP PLP experiments for investigating the chain-length dependence of the termination reaction is validated.

6.1 Introduction

Pulsed lasers have revolutionised the study of free-radical polymerisation (FRP) kinetics.[1] Although musings on this topic were made as early as the late 1970s,[2] it was not until the mid-1980s that concrete proposals first appeared for using pulsed-laser polymerisation (PLP) to determine propagation rate coefficients,[3] k_p, and the coupled parameter k_t/k_p,[4-6] thus providing access to termination rate coefficients, k_t. Since then the method for k_p determination has become an almost routine tool of FRP workers.[1,7-11] While it is the most celebrated use of PLP, a little appreciated irony is that one is not obliged to use pulsed lasers in order to measure k_p in this way: in fact any means of periodic initiation will do the job,[12] as has been confirmed, for example, by the accurate measurement of k_p using rotating sector[13,14] and intermittent addition of rapidly decomposing initiator[15]. This situation may be contrasted with that for k_t: even though Buback recognised very early on[16,17] that, for the study of termination kinetics, PLP offers a unique advantage over other means of carrying out FRP, this opportunity remains largely unexploited by the FRP community. Making this situation even stranger is that it cannot be said that there exist any superior methods for the study of termination kinetics.[18]

To be more precise it is Buback's so-called single-pulse PLP (SP PLP) method[5] that is uniquely positioned for studying termination. This method involves time-resolved monitoring of the polymerisation that is consequent upon irradiation by a single laser pulse of a photoinitiator-containing system. The pulse creates a sufficiently large concentration of radicals, c_R, that the rate of termination far exceeds the rate of any background initiation processes. Thus the way in which c_R evolves with time, which is the information delivered by a SP PLP experiment, directly reflects how the rate of termination evolves with time. While traditional post-effect experiments deliver the same information,[18] the distinct feature of the

SP PLP approach is that the radical chain-length distribution (RCLD) is approximately monodisperse at any instant. This is the case because c_R is negligible immediately prior to irradiation, at time $t = 0$, and because the pulse itself, with a typical duration of 20 ns, creates radicals instantaneously on the timescale of propagation. Thus at $t = 0$ all the radicals are the same small length. Assuming negligible subsequent creation of small radicals by either transfer or extraneous initiation processes, it follows that at any instant all radicals are of essentially the same (evolving) size, because all the radicals were born at $t = 0$. So the termination rate at any instant reflects the rate coefficient for termination between radicals of the size pertaining at that instant. In the so-called 'classical' approach to FRP kinetics this is not of any significance, because k_t is regarded as being invariant with radical size. However it is now well accepted that termination, because it is diffusion controlled, is chain-length dependent in rate.[19,20] It is therefore evident not just that SP PLP has the ability to probe this important dependency, but that it is unique in its capacity to do so.

As developed and extensively exploited, Buback's SP PLP approach has employed NIR spectroscopy[21] to monitor the evolution of monomer concentration, c_M, with time. Unfortunately this gives rise to what has been termed 'the second-derivative problem':[22] that model-free extraction of $k_t(t)$ is difficult, because in effect it is the second derivative of measurements made on a fast timescale.[23,24] So even though $c_M(t)$ traces have yielded good-quality information on the chain-length dependence of termination for ethylene[17,25] and for acrylates and methacrylates,[22] it has always been evident that it would be better if c_R could be measured directly. This may be achieved using EPR spectroscopy, and first results for its use in conjunction with SP PLP have just been reported:[26] measurements of c_R on a millisecond (or faster) timescale have enabled $k_t(t)$ for dodecyl methacrylate to be determined. Because this approach, so called SP PLP EPR, is held by an IUPAC task group to be of great potential

for investigating termination kinetics,[18] it is timely to carry out kinetic simulations that probe the validity of this method. This is what will be done in this chapter. While there has been previous work in this vein,[23] it targeted the experimental approach in which $c_M(t)$ is measured, whereas the present work will consider the SP PLP EPR method, in which $c_R(t)$ is measured. Further, this chapter will focus on important mechanistic issues that have only recently come to light and therefore were not addressed by the earlier work.

6.2 Simulation Details

The following population balance equations are those corresponding to a FRP reaction scheme comprising of initiation, chain-length-dependent propagation (CLDP), chain-length-dependent termination (CLDT) and transfer to a small-molecule species (whether monomer, solvent or chain transfer agent):[20,27]

$$\frac{dc_{R1}}{dt} = R_{init} + k_{trX}\, c_X\, c_R - k_p^1\, c_M\, c_{R1} - k_{trX}\, c_X\, c_{R1} - 2\, c_{R1} \sum_{j=1}^{\infty} k_t^{1,j}\, c_{Rj} \qquad \textbf{(6.1)}$$

$$\frac{dc_{Ri}}{dt} = k_p^{i\text{-}1}\, c_M\, c_{Ri\text{-}1} - k_p^i\, c_M\, c_{Ri} - k_{trX}\, c_X\, c_{Ri} - 2\, c_{Ri} \sum_{j=1}^{\infty} k_t^{i,j}\, c_{Rj},\ i = 2, \infty \qquad \textbf{(6.2)}$$

$$\frac{dc_{Di}}{dt} = 2\,\lambda\, c_{Ri} \sum_{j=1}^{\infty} k_t^{i,j}\, c_{Rj} + k_{trX}\, c_X\, c_{Ri} + (1-\lambda) \sum_{j=1}^{i-1} k_t^{j,i-j}\, c_{Rj}\, c_{Ri-j},\ i = 1, \infty \qquad \textbf{(6.3)}$$

In these equations c denotes a concentration and k a rate coefficient, while the attendant subscript signifies the respective species or reaction involved. For example, c_M denotes monomer concentration and k_{trX} the rate coefficient for transfer to small-molecule species X. The other abbreviations used in these respects are 'p' for propagation, 't' for termination, R for radical and D for dead chain. Superscripts refer to degree of polymerisation, for example

D^i denotes a dead polymer molecule of chain length i and $k_p{}^i$ the propagation rate coefficient for a R^i species. Lastly, λ denotes the fraction of termination by disproportionation and R_{init} the rate of initiation. With regard to the latter quantity, it is important to note that eq. **(6.1)** quite reasonably assumes that propagation of photoinitiator-derived radicals is relatively fast.

As there is no general solution to eqs. **(6.1)-(6.3)**, we used in-house software to solve these equations numerically. This was done using the simple Euler method with a time-step of the order of $0.1(k_p c_M)^{-1}$. Perhaps surprisingly, this rudimentary numerical recipe has been found to give both impeccable accuracy and expeditious computational speed for the above system of equations,[28] with a SP PLP simulation of this work requiring of order minutes of CPU time on a desktop PC. We ascertained that the commercially available Predici® package[29] has comparable run-times when used for the same purpose.

In a SP PLP experiment there is only one burst of photoinitation, which is therefore simulated simply by setting $c_{R1} = \rho$ at $t = 0$, where ρ is the concentration of polymerising radicals produced by a laser pulse. This work assumed an ideal photoinitiator, *i.e.*, one with a negligible rate of dark-time initiation: $R_{init} = 0$ was used for $t > 0$. Because a SP PLP experiment involves only a small amount of polymerisation, it was thoroughly justified to use constant values of c_M and c_X in simulations, although it is stressed that this was done purely for convenience – it would be extremely easy also to include and solve the differential equation for each of these quantities. Unless otherwise stated, homotermination rate coefficients were stipulated in the following standard fashion:

$$k_t{}^{i,i} = k_t{}^{1,1}\, i^{-e} \qquad \textbf{(6.4)}$$

Here the parameter $k_t{}^{1,1}$ is the rate coefficient for termination between two radicals of chain length $i = 1$, while the exponent e quantifies the strength of the chain-length dependence of

termination. For cross-termination rate coefficients, $k_t^{i,j}$ where $i \neq j$, the diffusion-mean model was used: $k_t^{i,j} = 0.5(k_t^{i,i} + k_t^{j,j})$.[20] At any instant one may use

$$\langle k_t \rangle = \sum_{i=1}^{\infty} \sum_{j=1}^{\infty} k_t^{i,j} \frac{c_{Ri}}{c_R} \frac{c_{Rj}}{c_R} \qquad \textbf{(6.5)}$$

to evaluate the overall (chain-length-averaged) rate coefficient for termination, $\langle k_t \rangle$.

Because this work is inspired by SP PLP experiments involving bulk dodecyl methacrylate (DMA) at 0˚C,[26] parameter values for simulations were chosen with this particular system in mind: k_p = 240 L mol^{-1} s^{-1},[9] c_M = 3.5 mol L^{-1},[30] $\rho = 1 \times 10^{-5}$ mol L^{-1} (inferred from other quoted results as being a measured value of Ref. [26]), $k_t^{1,1} = 8 \times 10^6$ L mol^{-1} s^{-1}, e = 0.5 and k_{trX} = 0. These values of $k_t^{1,1}$ and e have been selected because they reproduce the reported SP PLP kinetics over the first 0.1 s of radical concentration decay (compare Figure 3 of Ref. [26] with *Fig. 6.1* below). Although this is a very low value for $k_t^{1,1}$, it is perhaps realistic on account of the low temperature, high viscosity and large monomeric size. Further, it is actually only the coupled value $k_t^{1,1}\rho$ that must be physically reasonable, because, as will be established in the following section, SP PLP kinetics are determined by $k_p c_M$ and $k_t^{1,1}\rho$, not these four values individually. Unless otherwise stated, simulations will use the just-given parameter values, including $k_p^i = k_p$ for all i (*i.e.*, chain-length-independent propagation). However the trends observed obviously hold for SP PLP experiments in general.

6.3 Background Considerations

For SP PLP such that $k_p^i = k_p$, $k_t^{i,j} = k_t$, $k_{trX} = 0$ and $R_{init} = 0$, the solution to eqs. **(6.1)** and **(6.2)** is[31,32]

$$c_{Ri} = c_R(t)\exp(-k_p c_M t)\frac{(k_p c_M t)^{i-1}}{(i-1)!} \quad \textbf{(6.6)}$$

where the evolution of the overall radical concentration with time is given by[6,25]

$$c_R(t) = \frac{\rho}{2k_t\rho t + 1} \quad \textbf{(6.7)}$$

Eq. **(6.6)** is a Poisson distribution of number-average degree of polymerisation

$$i = k_p c_M t + 1 \quad \textbf{(6.8)}$$

and variance $k_p c_M t$. Once beyond very small chain lengths, this represents a very narrow RCLD. Therefore it would seem reasonable to make the approximation that all radicals have chain length given by eq. **(6.8)**. Substituting into eq. **(6.4)**, one thus obtains $\langle k_t \rangle = k_t^{1,1}(k_p c_M t+1)^{-e}$ for the variation of $\langle k_t \rangle$ with time during a SP PLP. This may now be substituted into $-dc_R/dt = 2\langle k_t \rangle c_R^2$ and integration carried out, giving the result (assuming only $e \neq 1$)

$$\frac{\rho}{c_R} - 1 = \frac{2\rho k_t^{1,1}}{k_p c_M(1-e)}[(k_p c_M t+1)^{1-e} - 1] \quad \textbf{(6.9)}$$

For the case of $e = 0$, this correctly reduces to eq. **(6.7)**.

In the event of $e < 1$, the long-time limit of eq. **(6.9)** is

$$\frac{\rho}{c_R} - 1 = \frac{2\rho k_t^{1,1}(k_p c_M)^{-e}}{(1-e)} t^{1-e} \quad \textbf{(6.10)}$$

This equation has been presented by Buback et al, both recently[22,26] and some time ago,[17,25] and by other workers.[33,34] In all instances it was derived as eq. **(6.9)** above but by assuming $i = k_p c_M t$ (*c.f.* eq. **(6.8)**), which necessitates having $e < 1$ in order that the $t = 0$ limit of

integration is defined. Analytic integration of the ensuing expression for $-dc_M/dt = k_p c_M c_R$ has been investigated,[35] and it would be fair to say that the matter is exceedingly complicated. Hence it is understandable that Buback *et al.* have adopted alternative approaches with $c_M(t)$ data from SP PLP experiments: in early work[17,25] they fitted experimental $dc_M(t)/dt$ data to the expression for $-k_p c_M c_R(t)$ that follows from eq. **(6.10)**, while recently[22] they fitted experimental $c_M(t)$ data by numerically integrating this theoretical expression for $-k_p c_M c_R(t)$. However, with the availability now of directly measured $c_R(t)$ data from SP PLP EPR experiments, Buback *et al.* have devised and used the following elegant approach:[26] if data is plotted as $\log(\rho/c_R - 1)$ *vs.* $\log t$, then eq. **(6.10)** implies that the slope of such a plot will give e and thence the intercept $\rho k_t^{1,1}$, from which $k_t^{1,1}$ is accessible because ρ, the value of c_R at $t = 0$, is of course measured as part of an experiment. It is this approach for analysing data that will be the primary focus of this chapter.

To start off with it is illuminating to compare the predictions of eqs. **(6.9)** and **(6.10)**. This is done in *Fig. 6.1* for the standard parameter set of this work and using the reported range of experimental times.[26] At long times the two sets of calculations do indeed merge, however at early experimental times there are appreciable differences. Although the eq. **(6.9)** results are of course not perfectly linear, they are nevertheless very well fit by a straight line, as is shown in *Fig. 6.1*, and as experimental data they would be described as linear. If this line of best fit in *Fig. 6.1* is analysed according to eq. **(6.10)**, which is the procedure used in Ref. [26], then from the slope one would obtain $e = 0.44$ (*c.f.* the input value of 0.5). Using this value of e, one would then obtain from the intercept that $k_t^{1,1} = 6.0 \times 10^6$ L mol^{-1} s^{-1} (*c.f.* 8.0×10^6 L mol^{-1} s^{-1}). It is apparent that because the value of e is underestimated, giving artificially high values of $k_t^{i,i}$, this must be compensated for by $k_t^{1,1}$ also being underestimated, so as to

lower values of $k_t^{i,i}$ (see eq. **(6.4)**) and thus give a better approximation to the observed $\langle k_t \rangle(t)$.

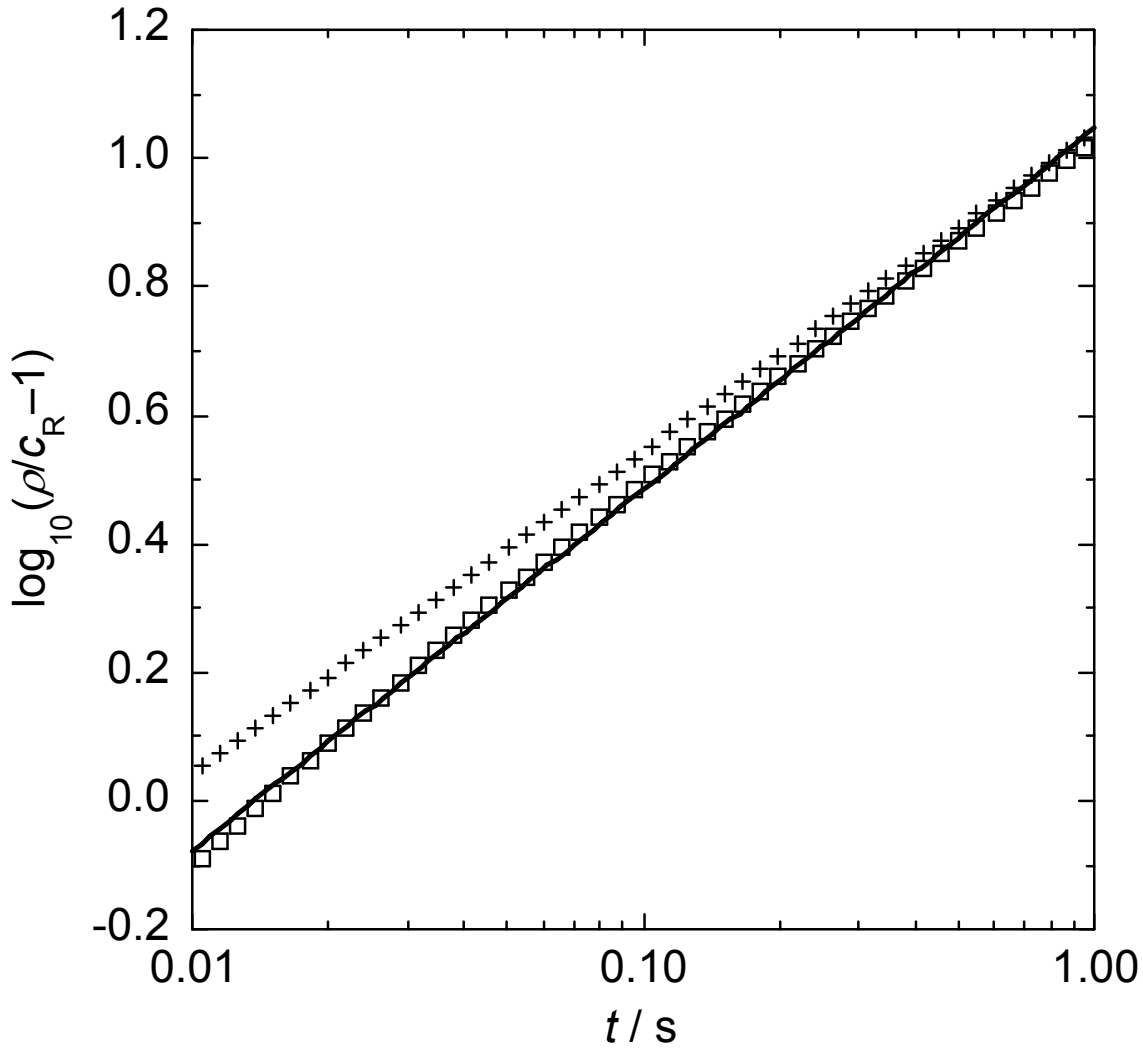

Fig. 6.1 Values of $\rho/c_R - 1$ *vs.* time calculated according to eq. **(6.9)** (□) and eq. **(6.10)** (+) using $k_p c_M = 840\ s^{-1}$, $\rho k_t^{1,1} = 8 \times 10^1\ s^{-1}$ and $e = 0.5$. The best-fit line to the eq. **(6.9)** points is also shown.

The analysis that has just been carried out assumes that eq. **(6.9)** is a more correct description of reality than eq. **(6.10)**. This might be questioned on the basis that primary radicals do not necessarily propagate quickly, and therefore $i = k_p c_M t$, leading to eq. **(6.10)**, might be a better description of average radical chain length than $i = k_p c_M t+1$, leading to eq. **(6.9)**. However such a debate is misguided in that the real issue here is how $<k_t>$ varies with time. If one assumes $i = k_p c_M t$, then eq. **(6.4)** gives that $<k_t>$ is infinite at $t = 0$, which clearly is unrealistic. In fact this is the reason that eq. **(6.10)** can only be derived assuming $e < 1$: because if $e > 1$, then $<k_t>$ is so high at t very close to 0 that all radicals terminate instantaneously. But even for $e < 1$, the initial rate of termination is unjustifiably overestimated by this approach. On the other hand, whatever the actual situation with regard to the speed of primary radical termination, it is evident that setting up the equations such that $i = 1$ at $t = 0$, which gives $<k_t> = k_t^{1,1}$ at $t = 0$, produces a much more realistic value of the termination rate coefficient at these crucial early times. Thus eq. **(6.9)** must give the more realistic variation of $c_R(t)$, whereas eq. **(6.10)** must underestimate the real c_R, as is evident in *Fig. 6.1*, with the extent of the error reducing with time. Because of the latter, the slope of the eq. **(6.9)** points must be greater than $1–e$, as indeed is found. Of course the extent to which this is the case will depend on the time-range of the fit and on the parameter values at hand. For example, if the *Fig. 6.1* data is fitted only over $0.01 \leq t/s \leq 0.1$, then $1–e = 0.60$ (hence $e = 0.40$) is inferred, while calculations with $e = 0.2$ result in $1–e = 0.82$ being inferred, which is much closer to the ideally expected value of 0.8. This reflects that as e becomes smaller, eq. **(6.10)** must become more accurate.

In Ref. [26], SP PLP EPR data was analysed using eq. **(6.10)**, and for low-conversion (15% or less) DMA polymerisations it was found that $e \approx 0.50$-0.55 at early times ($0.01 \leq t/s \leq 0.1$). However, on the basis of what has been learned above, it would seem reasonable to suggest

that $e \approx 0.6$ must be more in accord with this DMA data (see Section 6.6 for more on this). Although linear fitting using eq. **(6.10)** is an attractive way of analysing SP PLP EPR data, a more refined approach is to carry out non-linear least squares fitting using eq. **(6.9)** (probably best in the form $c_R(t)$), for this will yield more accurate estimates of e and $k_t^{1,1}$. Therefore this new approach is recommended.

6.4 The Monodispersity Assumption

The so-called 'monodispersity assumption'[23] is that all radicals are the same chain length. Because of the stochastic nature of propagation, this can never be the case (for $t > 0$). However, for $e = 0$ both eqs. **(6.9)** and **(6.10)** reduce to eq. **(6.7)**, which gives $c_R(t)$ exactly, even though the RCLD is not monodisperse. This emphasises that what is actually being assumed in deriving eqs. **(6.9)** and **(6.10)** is that all termination interactions are described by the one termination rate coefficient (which changes in value from instant to instant). Therefore one might better refer to the 'mono-termination assumption'. In reality chain-length-dependent termination will mean that those radicals that lag in chain length will experience elevated rates of termination, while those that race ahead in their growth will experience reduced rates of termination. Thus the RCLD will erode faster at low chain lengths and slower at high chain lengths, meaning that this distribution is not perfectly Poissonian and that eq. **(6.8)** does not *exactly* give the number-average chain length of the radicals. The former has been illustrated by Olaj *et al.*,[36] who investigated this phenomenon in the context of periodic PLP. Here the context is SP PLP, necessitating a different type of examination in order to gauge the accuracy of the monodispersity assumption: simulation output is to be compared with the predictions of eq. **(6.9)** (this rather than eq. **(6.10)** is to be used because the simulations assume that photoinitiation creates c_{R1} species at $t = 0$). Such

comparisons are presented in *Fig. 6.2* for the standard parameter set with both e = 0.5 and 0.2.

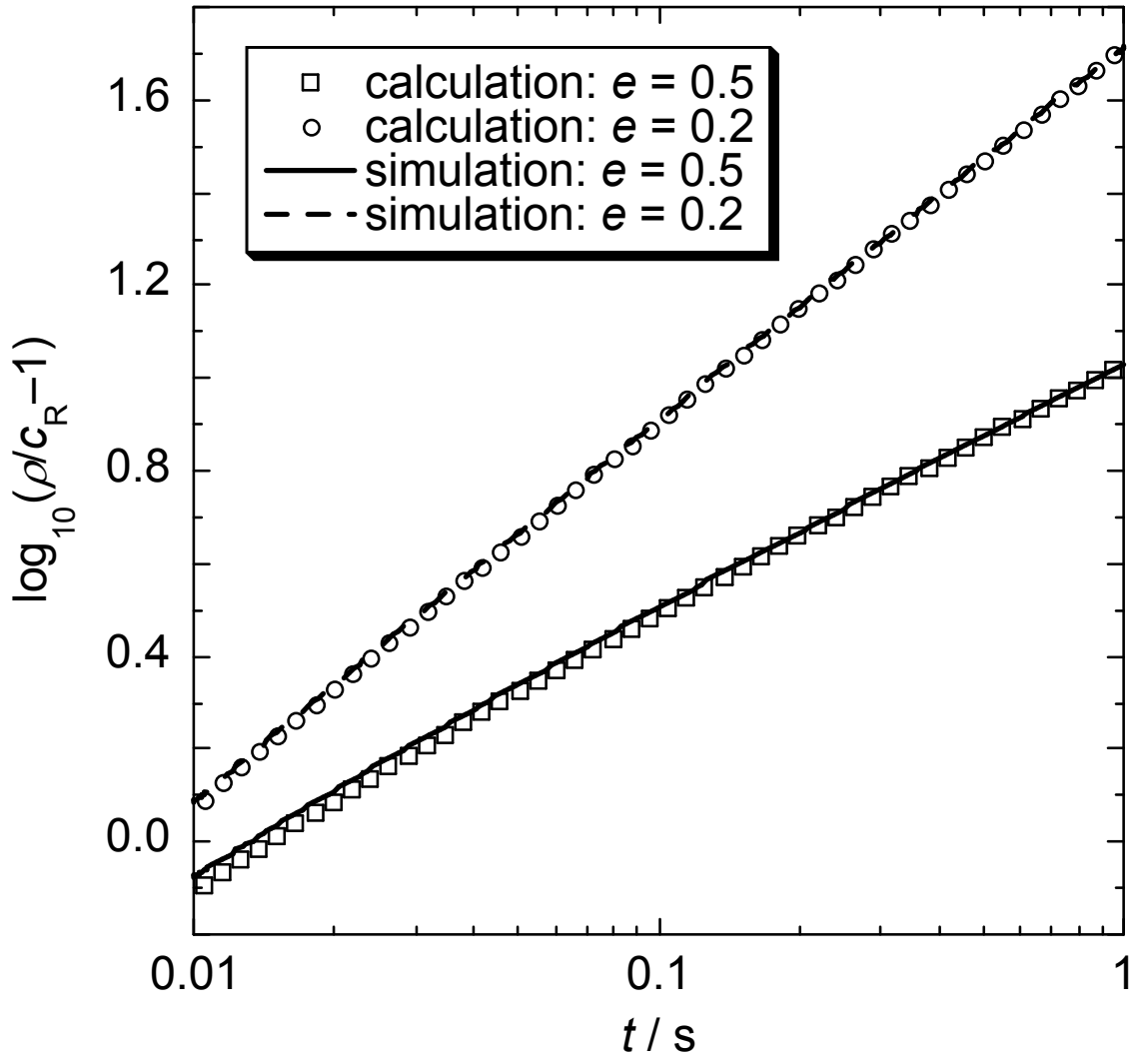

Fig. 6.2 Calculated (points, using eq. **(6.9)**) and simulated (lines) values of $\rho/c_R - 1$ *vs.* time using $k_p c_M$ = 840 s^{-1}, $\rho k_t^{1,1}$ = 8 × 10^1 s^{-1} and e = 0.5 and 0.2 as indicated.

Fig. 6.2 establishes the near faultless accuracy of the monodispersity assumption: the exact values of c_R, as obtained *via* simulation, agree essentially perfectly with the approximate values calculated using eq. **(6.9)**, thereby vindicating the implicit assumption of the previous section that eq. **(6.9)** can be regarded as exact. As expected the accuracy of eq. **(6.9)** diminishes as *e* increases, due to the greater difference between $k_t^{i,i}$ values for the shorter and longer radicals present at any instant: this is evident in that eq. **(6.9)** is slightly less accurate for $e = 0.5$, which results make it clear that eq. **(6.9)** slightly overestimates c_R (*i.e.*, it underestimates the true rate of termination). However, even for $e = 0.5$ the discrepancy between the exact results and those of eq. **(6.9)** is far less than will be the level of noise in experimental measurements of c_R. In fact consideration of *Fig. 6.1* and *Fig. 6.2* reveals that the use of eq. **(6.10)** to analyse data will be a far greater source of error than the monodispersity assumption. This emphasises the point that eq. **(6.9)** should be used for analysing data.

In summary, the results of *Fig. 6.2* are a spectacular vindication of the fundamental principle behind the use of SP PLP to probe the chain-length dependence of termination, this principle being that all radicals present at any instant can be regarded as experiencing the frequency of termination of a radical of (close to) average length for that instant.

6.5 Chain Transfer

The monodispersity assumption can also be invalidated by the occurrence of chain transfer to small-molecule species, a process that will continuously create small radicals. Obviously this undermines the capacity to learn about $k_t^{i,i}$ from SP PLP, and so it is logical to try to eliminate such processes. Therefore the inclusion of a chain transfer agent should be avoided, while only solvents that are resistant to chain transfer should be employed. Even if these steps are taken, nothing can be done to eliminate chain transfer to monomer. With this in mind it is

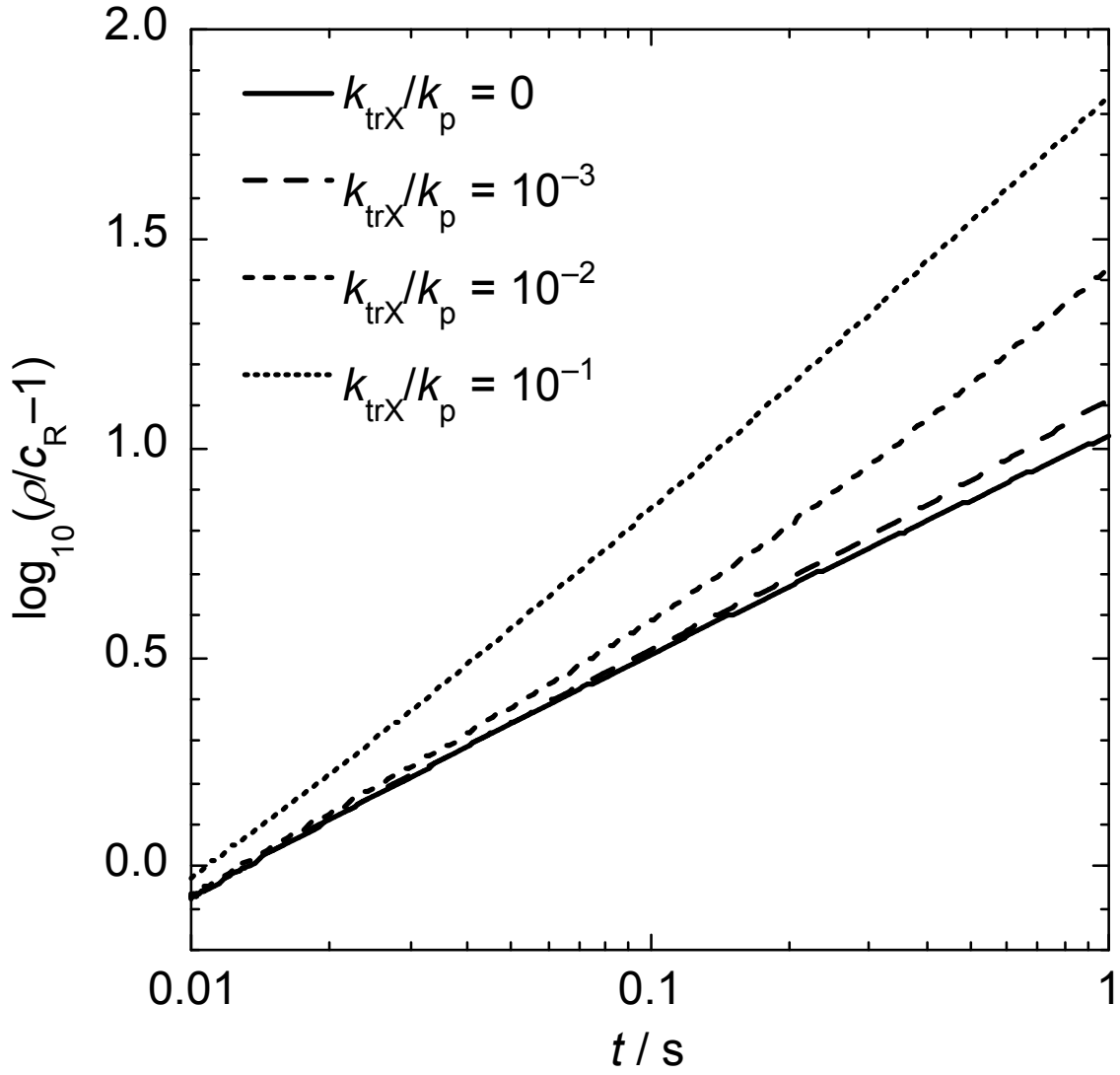

Fig. 6.3 Values of $\rho/c_R - 1$ *vs.* time from simulations using $k_p c_M = 840$ s^{-1}, $\rho k_t^{1,1} = 8 \times 10^1$ s^{-1}, $e = 0.5$ and k_{trX}/k_p as indicated.

of interest to see how fast this process must be for it to have an influence on SP PLP kinetics, and so simulations were carried out with $c_X = c_M$ – see eqs. **(6.1)-(6.3)** – and varying k_{trX}. Results are presented in *Fig. 6.3*.

The first thing that is evident from *Fig. 6.3* is that transfer hastens the decay of the radical concentration (*i.e.*, it gives rise to lower values of c_R, and thus to higher values of $\rho/c_R - 1$), and the higher the value of k_{trX}, the stronger this effect. This is all as expected: the creation of small radicals increases the overall rate coefficient for termination (see eq. **(6.5)**). However for $k_{trX}/k_p = 10^{-4}$ there is no tangible effect (hence these results are not shown), while even for $k_{trX}/k_p = 10^{-3}$ the effect is barely noticeable. This may be rationalised as follows. The frequency of transfer is given by $k_{trX}c_M = (k_{trX}/k_p)(k_p c_M)$, which equals 0.84 s^{-1} for the values at hand. This means that a radical undergoes transfer every 1.2 s on average. So in a SP PLP experiment lasting 1 s, as simulated in *Fig. 6.3*, approximately half the radicals will undergo transfer. Evidently this is sufficient transfer to start influencing the termination kinetics, as makes intuitive sense. What this argument reveals is that the impact of transfer is determined by the relative timescales of transfer and of the SP PLP experiment, of duration t_d: the rule-of-thumb will be that if $(k_{trX}c_X)^{-1} > t_d$, then transfer is not significant and eq. **(6.9)** will describe the SP PLP kinetics accurately. On the other hand, for $k_{trX}c_X > 1/t_d$, as is the case for the $k_{trX}/k_p = 10^{-2}$ and 10^{-1} simulations of *Fig. 6.3*, one cannot learn about $k_t^{i,i}$ from fitting eq. **(6.9)** to experimental data. Rather, one would have to fit data *via* simulations in which transfer is included, or else only analyse data over a reduced timescale such that $k_{trX}c_X < 1/t$. The validity of the latter approach is confirmed by *Fig. 6.3*, *e.g.* consider the $k_{trX}/k_p = 10^{-2}$ data up to 0.1 s.

Turning now to real data, the value $k_{trM}/k_p = 2.1 \times 10^{-6}$ has been measured at 0°C for chain transfer to monomer in polymerisation of methyl methacrylate (MMA),[37] which has very similar $k_p c_M$ to DMA.[9,30] So even if k_{trM}/k_p is somewhat higher for DMA on account of its pendant dodecyl groups, it is safe to say that transfer can have been playing no role in the experiments of Ref. [26], in which $t_d \approx 1$ s is indicated. This validates the work of Ref. [26].

However, one must become more wary of transfer as temperature increases. For example, at 140˚C the value of k_{trM}/k_p for MMA is 42 times greater than at 0˚C[37] while k_p is 28 times greater.[8] Thus k_{trM} is greater by about 10^3, meaning that transfer would impact upon an SP PLP experiment of duration 1 s. Of course 140˚C is an uncommonly high temperature, and thus this discussion establishes that at normal polymerisation temperatures, chain transfer to monomer can probably be neglected for SP PLP experiments involving methacrylates (unless t_d is unusually long). However, for acrylates the situation is unlikely to be so favourable. In this respect it is important to be clear that it is k_{trM} that decides the issue, not k_{trM}/k_p: while this ratio may be similar for acrylates and methacrylates, the much higher k_p of acrylates[1] mean that k_{trM} are also much higher, thereby complicating the interpretation of SP PLP experiments.

Especially in view of the transfer situation for acrylates, it is enlightening to consider the simulations of *Fig. 6.3* in greater detail so that a more profound understanding of SP PLP termination kinetics is reached. In this respect it is first of all noteworthy that the plots of *Fig. 6.3* become steeper as k_{trX}/k_p is increased. For example, the line of best-fit to the $k_{trX}/k_p = 10^{-1}$ data has slope 0.94, meaning $e \approx 0.06$ will be obtained *via* fitting of either eq. **(6.9)** or eq. **(6.10)**. In other words, even though it has been generated using $e = 0.5$, this data looks as though it evidences termination that is essentially chain-length independent. The reason for this is that $\langle k_t \rangle$ is effectively constant for most of the simulation, as is shown in *Fig. 6.4*, which presents the variation of $\langle k_t \rangle$ with time from each of the simulations of *Fig. 6.3*.

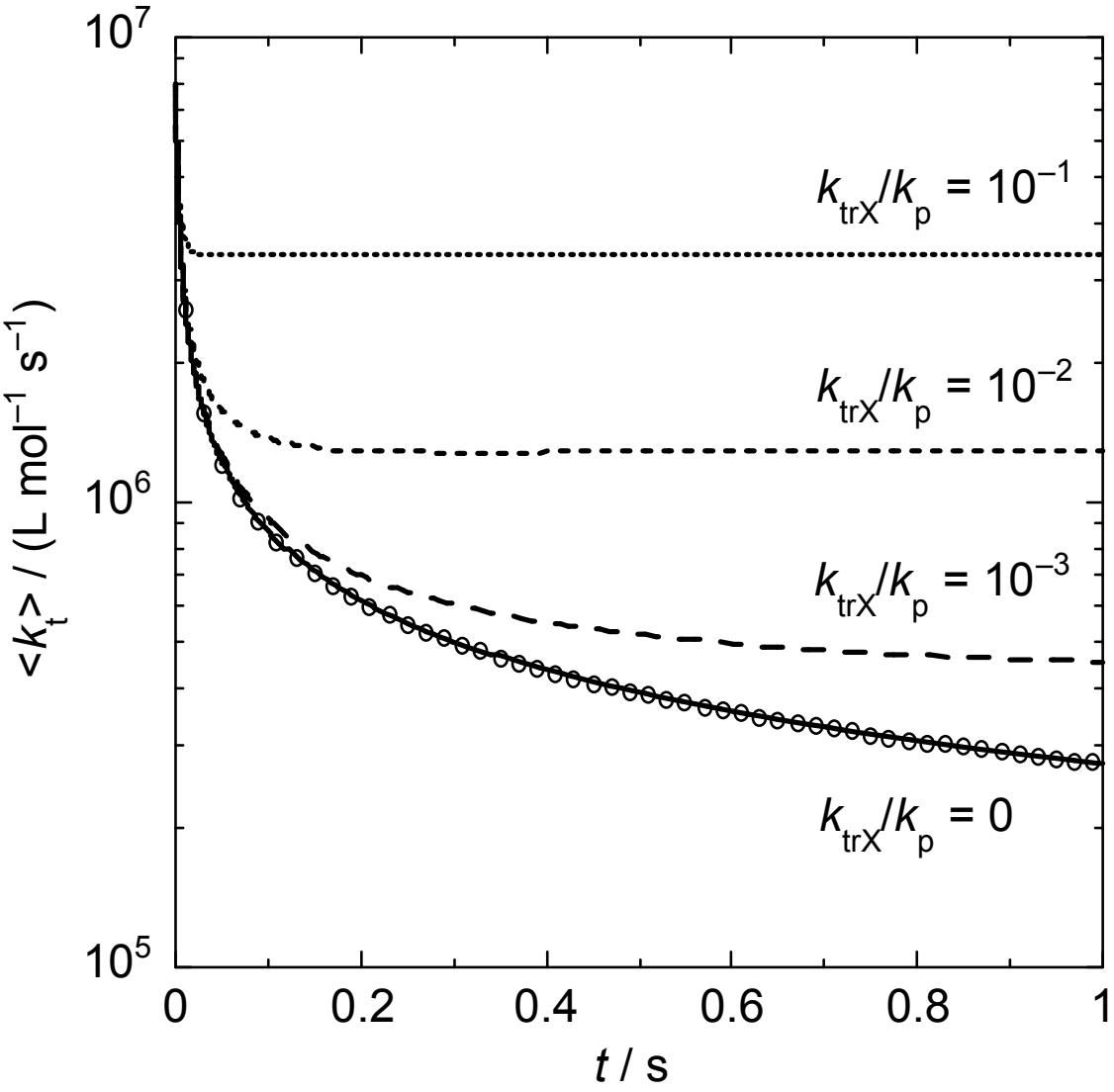

Fig. 6.4 Values of chain-length-averaged termination rate coefficient, $<k_t>$, *vs.* time from simulations (lines) using $k_p c_M = 840$ s^{-1}, $\rho = 1 \times 10^{-5}$ mol L^{-1}, $k_t^{1,1} = 8 \times 10^6$ L mol^{-1} s^{-1}, $e = 0.5$ and k_{trX}/k_p as indicated. Also shown (circles) are values of $k_t^{1,1}(k_p c_M t+1)^{-e}$.

The first comment to make about *Fig. 6.4* in fact concerns the results for the case of no transfer: $<k_t>(t)$ agrees essentially exactly with $k_t^{1,1}(k_p c_M t+1)^{-e}$ (the points in *Fig. 6.4*). This confirms the capacity of SP PLP experiments to recover $k_t^{i,i}$, where $i(t)$ is given by eq. **(6.8)**.

Of course this is already implicit in the results of *Fig. 6.2*, but it is instructive to see the rectitude of the monodispersity assumption re-confirmed in this (perhaps more intuitive) way.

Secondly, *Fig. 6.4* illustrates that the effect of transfer is to make $\langle k_t \rangle$ decline from the value $k_t^{1,1}$ at $t = 0$ (all simulations) to a time-invariant value, as opposed to the ongoing decline that occurs in the absence of transfer, which is due to the remaining radicals becoming longer and

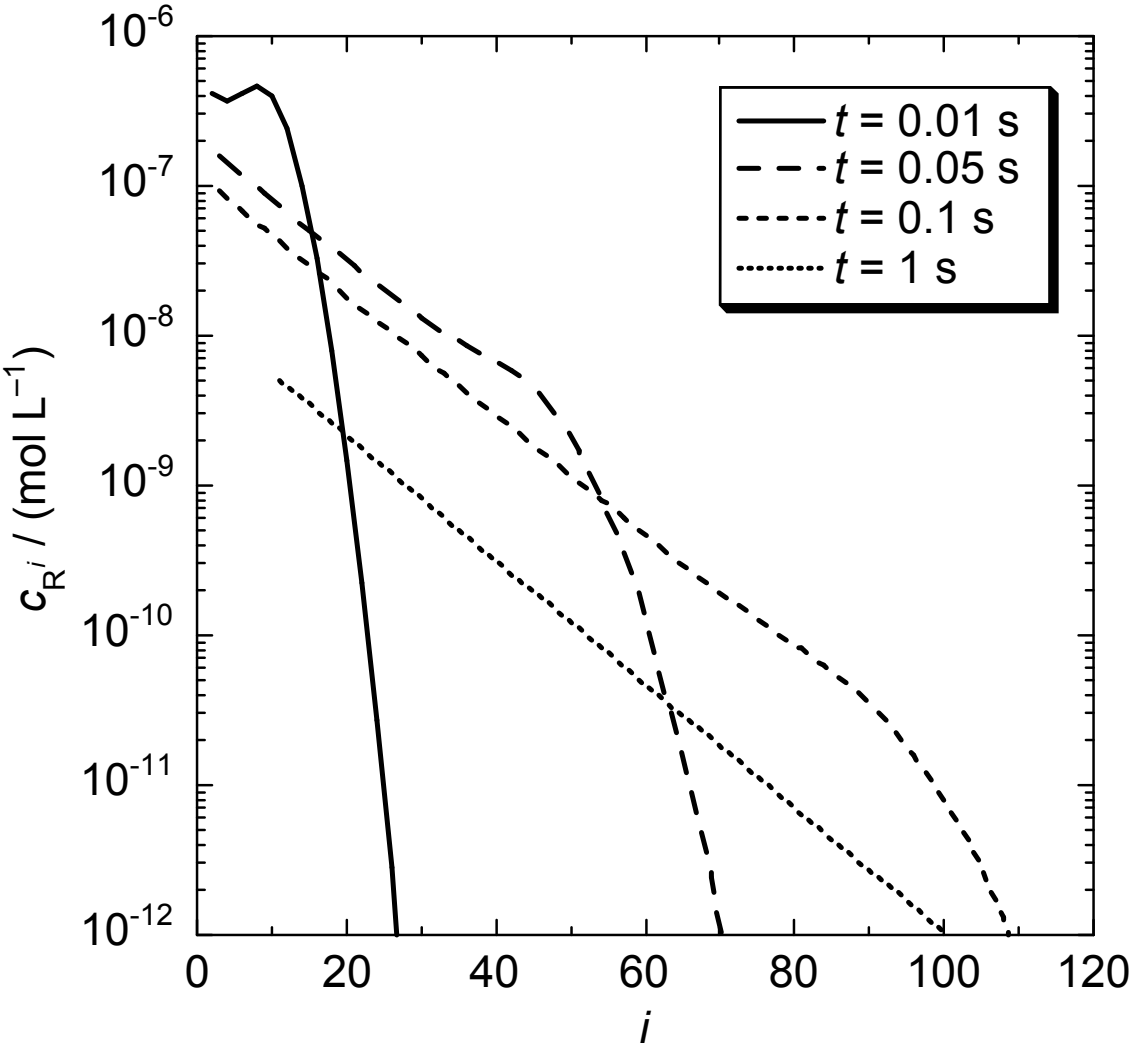

Fig. 6.5 Concentration of radicals of chain length i, c_{Ri}, at four different times, as indicated, from simulation using $k_p c_M = 840$ s^{-1}, $\rho k_t^{1,1} = 8 \times 10^1$ s^{-1}, $e = 0.5$ and $k_{trX}/k_p = 10^{-1}$.

longer. The reason for the plateau in $<k_t>$ is that as time passes, the radical chain-length distribution (RCLD) is converted by transfer from a Poisson-like distribution into a classical (Schulz-Flory) distribution, which of course is exponential-like. This is illustrated in *Fig. 6.5*, which shows c_{Ri} values from different times of the simulation with $k_{trX}/k_p = 0.1$. Although it is clear from *Fig. 6.5* that values of c_{Ri} continue to decline with time even once they have become transfer-determined, a noteworthy feature of such a RCLD is that c_{Ri}/c_R is independent of c_R. Thus once sufficient time has elapsed for the RCLD to become transfer-determined, $<k_t>$ becomes constant – see eq. **(6.5)** – even though c_R is decreasing (due to the continued occurrence of termination) and even though termination is chain-length dependent. The latter is a very important concept to grasp: a time-invariant $<k_t>$ can be fully consistent with CLDT and does not necessarily evidence chain-length-independent termination.

It is now easy to understand two more features of *Fig. 6.4*: (1) The higher the value of k_{trX}, the faster the plateau value of $<k_t>$ is attained. This is just because as k_{trX} increases, the RCLD becomes transfer-determined more quickly. Thus the faster is transfer, the greater the time period over which $<k_t>$ is relatively constant. This is also manifest from the way in which the plots of *Fig. 6.3* approach a slope of 1 as k_{trX}/k_p increases. As has been made clear, it is vital that such SP PLP data not be interpreted as evidence of chain-length-independent termination – it could equally be evidence of CLDT with transfer-control of the RCLD.[38] (2) As k_{trX}/k_p increases, the plateau value of $<k_t>$ increases.[38] This is because higher k_{trX}/k_p results in the RCLD becoming more and more weighted toward small chain lengths, and consequently in $<k_t>$ being higher (see eq. **(6.5)**).

Fig. 6.5 may also be used to explain a barely evident but highly intriguing result of *Fig. 6.4*: that in the simulations with $k_{trX}/k_p = 10^{-1}$ and 10^{-2}, the value of $<k_t>$ actually increases

slightly at long times. This phenomenon has also been remarked upon previously,[23] but there it went unexplained, and its authenticity could not be guaranteed because of the use of coarse-graining in carrying out simulations: this introduces inaccuracy, and because it artificially accelerates the rate of propagation it is regarded as suspect for use in PLP simulations,[39] for which it may therefore give artefactual results. However the present simulations are not coarse-grained, and so the increasing $\langle k_t \rangle(t)$ at long times can be taken as being a genuine result. It is counter-intuitive in that as time goes on one would expect the ever-lengthening radicals from the laser pulse to give rise to a smaller $\langle k_t \rangle$. *Fig. 6.5* solves this conundrum, for it makes clear that as time goes on there is conversion of radicals from the Poisson-like part at the high-*i* end of RCLD to the Schulz-Flory part. Once a time has been reached where the Poisson-like part has a greater average size than the transfer-determined RCLD, it is clear how this process results in a higher $\langle k_t \rangle$. Of course the magnitude of this effect is too small to be experimentally observed, amounting only to a 1% increase even in the $k_{trX}/k_p = 0.1$ simulation, where it was strongest. However this apparent paradox is felt to be of conceptual interest, and hence it has been elucidated here.

In fact one may question the relevance of all the above discussion surrounding *Fig. 6.4* and *Fig. 6.5* given that the parameter values used in the simulations are for DMA with non-physically high values of k_{trX}. Therefore it is stressed that the principles that have emerged are general and so will apply to any SP PLP system with dominant transfer. It is not unreasonable to suggest that many acrylate systems are quite likely of this nature, which may explain why data consistent with a constant $\langle k_t \rangle$ has generally been obtained in investigations of acrylates.[1]

Of course the other possible explanation for data that is consistent with a constant $\langle k_t \rangle$ is that the value of *e* is low (see the $e = 0.2$ results of *Fig. 6.2*). In this context it is appropriate to

mention that as e becomes lower, the effect of transfer is diminished. This is because the smaller the value of e, the smaller the differential between $k_t^{1,1}$ and $k_t^{i,i}$ (see eq. **(6.4)**), and thus the lower the capacity of transfer to increase the rate of termination, with transfer having no influence on termination in the limit of $e = 0$. For the purposes of illustrating the effects of transfer, only $e = 0.5$ results have been presented here.

Finally, it should be mentioned that the monodispersity assumption will also be violated if there is significant dark-time initiation. This could easily be investigated by using $R_{init} > 0$ in simulations, as has been done elsewhere but in a different context.[23] However the choice of an appropriate photoinitiator avoids this potential difficulty in a well-designed SP PLP experiment, and therefore there is felt to be no need to explore this issue here.

6.6 Composite Termination Model

As a result of careful consideration of what is known with relative surety about termination under dilute solution conditions, Smith *et al.*[27] (see Chapter 2) have concluded that eq. **(6.4)** is unlikely to hold across all chain lengths and that in fact the chain-length dependence of termination must be stronger at small chain lengths than the well-established weak dependence at long chain lengths. It was therefore proposed that[27]

$$k_t^{i,i} = k_t^{1,1}\, i^{-e_S}, \quad i \le i_c$$

$$= k_t^{1,1}\, (i_c)^{-e_S+e_L}\, i^{-e_L}, \quad i > i_c \qquad \textbf{(6.11)}$$

This was termed a 'composite' model for termination. The values $e_S \approx 0.5$, $e_L \approx 0.2$ and $i_c \approx 100$ were proposed[27] not with any religious fervor, but rather as a pragmatic opening gambit, it being clear that they were consistent with all credible termination data. It is rather amazing then that just a short time later the novel SP PLP EPR experiments of Buback *et al.* appeared

to confirm not just that eq. **(6.11)** holds for DMA at low conversion, but that it does so with *exactly* the suggested parameter values.[26] The basis for this conclusion was that when plotted as $\log(\rho/c_R-1)$ *vs.* $\log t$, the experimental data is well described by two straight lines, one at early times of slope 0.5 (suggesting $e_S \approx 1–0.5$), one at long times of slope 0.8 (suggesting $e_L \approx 0.2$), and the two lines intersecting at a time of about $100/(k_p c_M)$ (suggesting $i_c \approx 100$). What this analysis assumed without proof is that just as eq. **(6.4)**, the one-*e* model for $k_t^{i,i}$, gives rise to a quasi-linear variation of $\log(\rho/c_R-1)$ with $\log t$ (see Section 6.3), so the two-*e* model of eq. **(6.11)** will yield a plot with a second linear regime of slope $1–e_L$. It is therefore required to examine the correctness of this approach by rigorously investigating the effect that the composite termination model has on SP PLP kinetics.

First of all it is appropriate to use eq. **(6.11)** in conjunction with the monodispersity assumption. Taking $i = k_p c_M t+1$ and proceeding as in Section 6.3, it is derived (after some algebra) that

$$\frac{\rho}{c_R} - 1 = \frac{2\rho k_t^{1,1}[(k_p c_M t+1)^{1-e_S}-1]}{k_p c_M(1-e_S)}, \quad t \le t_c$$

$$= \frac{2\rho k_t^{1,1}[(i_c)^{1-e_S}-1]}{k_p c_M(1-e_S)} - \frac{2\rho k_t^{1,1}(i_c)^{1-e_S}}{k_p c_M(1-e_L)} + \frac{2\rho k_t^{0}(k_p c_M t+1)^{1-e_L}}{k_p c_M(1-e_L)}, \quad t > t_c \qquad \textbf{(6.12)}$$

where $t_c = (i_c-1)/(k_p c_M)$ is the time at which the cross-over from short-chain to long-chain termination behavior occurs, and $k_t^0 = k_t^{1,1}\,(i_c)^{-e_S+e_L}$ is the apparent value of $k_t^{1,1}$ if only long-chain termination is considered (see eq. **(6.11)**). It can be shown that the function given in eq. **(6.12)** is continuous at $t = t_c$ and that the second part reduces to first part in the event of $e_S = e_L$. Of course this first part of eq. **(6.12)** is the same as eq. **(6.9)**, but the expression for $t > t_c$ is perhaps more complicated than anticipated. Matters are barely relieved in this respect

by instead using the simpler but slightly erroneous $i = k_p c_M t$, for then the following analogue of eq. **(6.10)** is obtained:

$$\frac{\rho}{c_R} - 1 = \frac{2\rho k_t^{1,1}(k_p c_M)^{-e_S} t^{1-e_S}}{1-e_S}, \quad t \le t_c$$

$$= \frac{2\rho k_t^{1,1}(i_c)^{1-e_S}}{k_p c_M(1-e_S)} - \frac{2\rho k_t^{1,1}(i_c)^{1-e_S}}{k_p c_M(1-e_L)} + \frac{2\rho k_t^{0}(k_p c_M)^{-e_L} t^{1-e_L}}{1-e_L}, \quad t > t_c \qquad \textbf{(6.13)}$$

Note that for this expression the slightly different value of $t_c = i_c/(k_p c_M)$ pertains (for obvious reasons). What is interesting here, and thoroughly vindicates presenting these equations, is that even when $i = k_p c_M t$ is used, it is evident that a non-linear variation of $\log(\rho/c_R - 1)$ with $\log t$ is obtained for $t > t_c$, which is contrary to what was assumed in analysing data in Ref. [26]. However, in the limit of long time, and when $e_L < 1$, both the above equations reduce to

$$\frac{\rho}{c_R} - 1 = \frac{2\rho k_t^{0}(k_p c_M)^{-e_L} t^{1-e_L}}{1-e_L} \qquad \textbf{(6.14)}$$

This is the desired power-law form, in fact this equation is identical to eq. **(6.10)** except in that $k_t^{1,1}$ has been replaced by k_t^0. So providing an SP PLP experiment is carried out long enough that it reaches the above long-time regime, the data may be analysed in the standard fashion to obtain e_L from the slope and k_t^0 from the intercept. In the expected event of $e_S > e_L$, the value of k_t^0 will be less than $k_t^{1,1}$, and naturally one should be careful not to interpret k_t^0 as being an estimate of $k_t^{1,1}$. In principle one could obtain $k_t^{1,1}$ from k_t^0 if e_S, e_L and i_c were all known, however a more feasible avenue to $k_t^{1,1}$ is likely to be from early-time data (see Section 6.3).

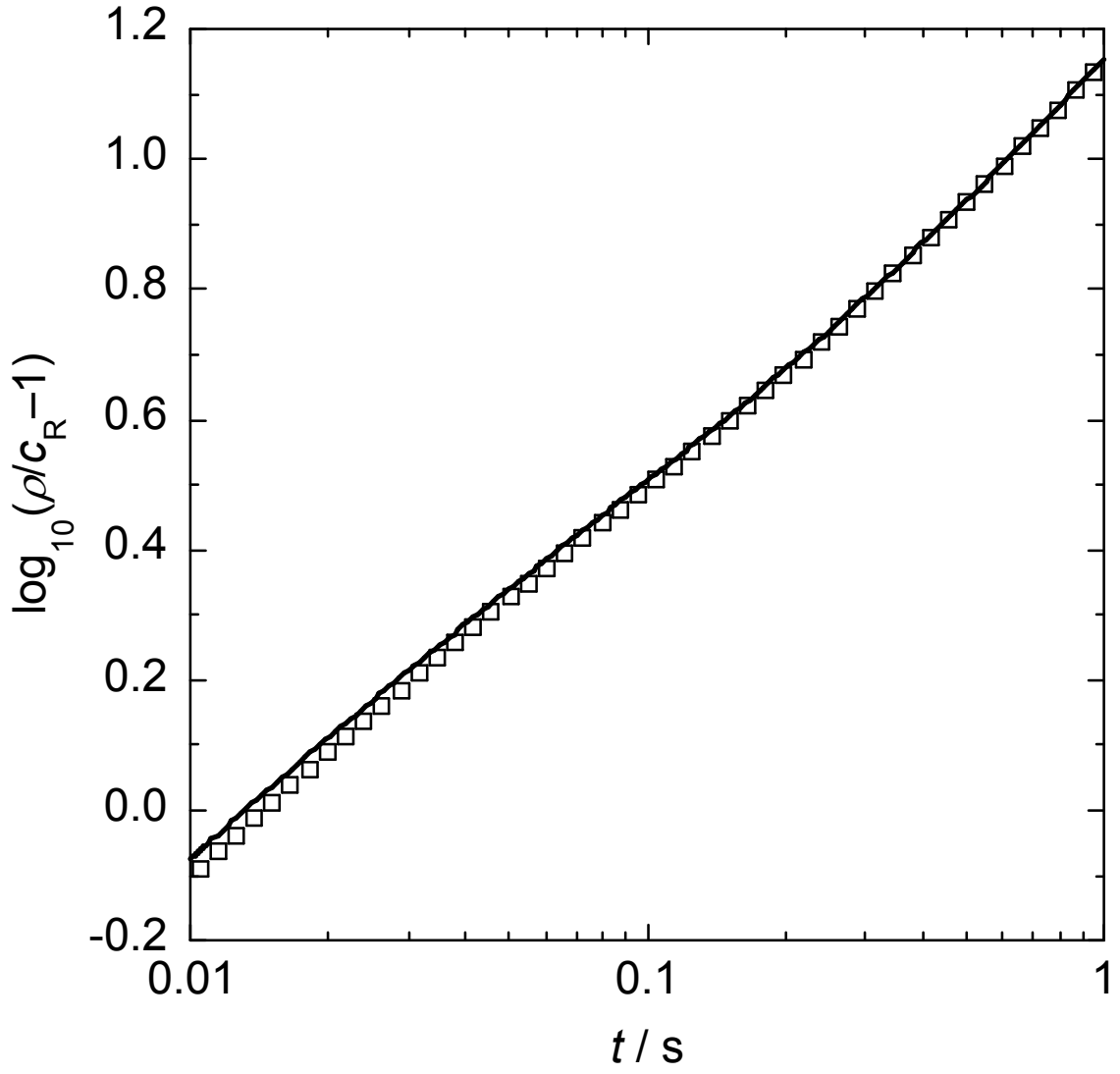

Fig. 6.6 Calculated (points, using eq. **(6.12)**) and simulated (line) values of ρ/c_R-1 *vs.* time using $k_p c_M = 840\ s^{-1}$, $\rho k_t^{1,1} = 8 \times 10^1\ s^{-1}$, $e_S = 0.5$, $e_L = 0.2$ and $i_c = 100$.

Before exploring eqs. **(6.12)**, **(6.13)** and **(6.14)**, it is a good idea to establish the accuracy of eq. **(6.12)**. This is done in *Fig. 6.6*, where results are presented from using the standard parameter set of this work together with $e_S = 0.5$, $e_L = 0.2$ and $i_c = 100$ (as seemingly found in Ref. [26]). It is evident that as in *Fig. 6.2*, the *exact* results from the simulation agree almost perfectly with the *approximate* results from eq. **(6.12)**. This verifies that the monodispersity

assumption also works excellently when termination is according to a composite (two-*e*) model, and so to all intents and purposes eq. **(6.12)** may be regarded as exact.

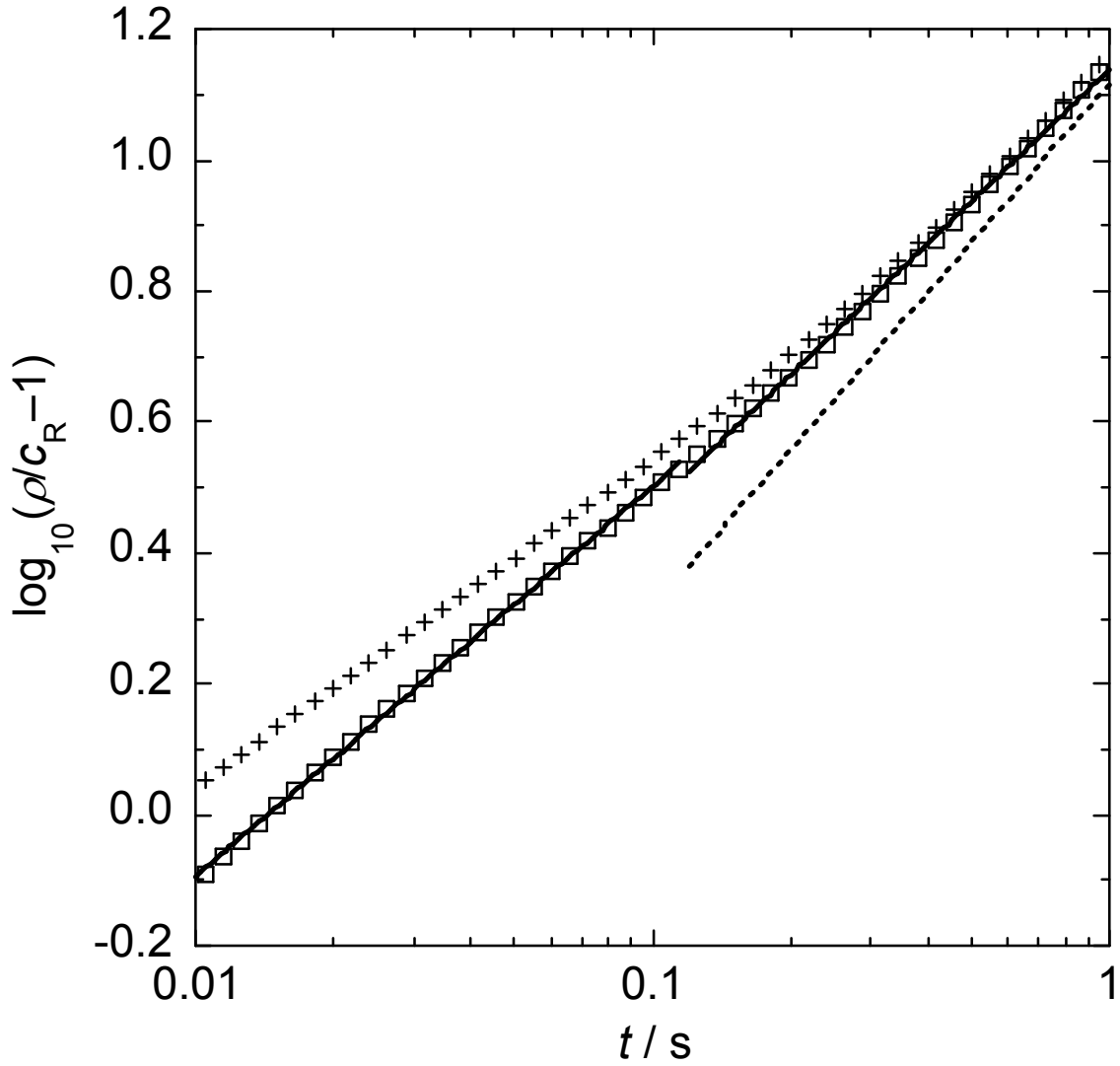

Fig. 6.7 Values of $\rho/c_R - 1$ *vs.* time calculated according to eq. **(6.12)** (□), eq. **(6.13)** (+) and eq. **(6.14)** (-----) using $k_p c_M = 840\ s^{-1}$, $\rho k_t^{1,1} = 8 \times 10^1\ s^{-1}$, $e_S = 0.5$, $e_L = 0.2$ and $i_c = 100$. Also shown are the best-fit lines (——) to the eq. **(6.12)** points for the two time intervals $t < t_c$ and $t > t_c$.

With the above in mind one may address the issue of how to extract composite-termination-model parameters from SP PLP data. This is done in *Fig. 6.7*, which presents evaluations of eqs. **(6.12)**, **(6.13)** and **(6.14)** for the same parameters as above. The first comment to make on *Fig. 6.7* is that it shows that eq. **(6.13)** becomes accurate at long times. This is as expected, because as t increases the difference between $k_p c_M t$ (the expression for $i(t)$ behind eq. **(6.13)**) and $k_p c_M t+1$ (behind eq. **(6.12)**) becomes negligible, and so the $\langle k_t \rangle(t)$ assumed in deriving each equation become the same. Thus the shape of eq. **(6.12)** data for $t > t_c$ is not dependent on the choice of $i(t)$, something that is important to remember in what now follows.

Next, and of far greater gravity, one sees from *Fig. 6.7* that eq. **(6.14)** is a poor description of the exact long-time values. In this context it is essential to reiterate that the time range of *Fig. 6.7* is precisely that of the data of Ref. [26]. Of particular concern is that the eq. **(6.12)** results are noticeably flatter than those of eq. **(6.14)**, which of course have a slope of $1-e_L = 0.80$. This may be compared with the slope of the shown linear fit to eq. **(6.12)** for $t > t_c = 0.118$ s, which is 0.67. This suggests the value $e_L = 0.33$, which is highly erroneous given that $e_L = 0.20$ was used to generate these results. The close coincidence of the intercepts (*i.e.*, $\log(t/\text{s}) = 0$ values) of the *Fig. 6.7* lines is no consolation, because procuring an accurate k_t^0 from the intercept relies on e_L being accurately known (see eq. **(6.14)**), which, as just pointed out, it will not be. Further, with different parameter values there is no guarantee that eq. **(6.14)** will remain accurate at $t = 1$ s. Thus it must be concluded that the determination of e_L and $k_t^{1,1}$ from *linear* fitting of long-time SP PLP data is problematic.

In fact the whole approach of fitting two straight lines to data is troublesome. This has been done for the eq. **(6.12)** (pseudo-exact) data in *Fig. 6.7*. While it is evident that this data is excellently described by two straight lines intersecting at close to $t = t_c$, this exercise was only possible because the value of t_c was known. Without such prior knowledge it would not

be possible to decide the location of the boundary between termination regimes, because it is evident that the data is actually curved. Further, the two best-fit lines of *Fig. 6.7* have slopes of 0.60 ($t < t_c$) and 0.67 ($t > t_c$), suggesting $e_S \approx 0.40$ and $e_L \approx 0.33$ respectively, both of which are inaccurate. To recover the experimental slope of 0.5 for $t < t_c$ in fact one must use $e_S = 0.64$ in eq. **(6.12)**, while the curvature in eq. **(6.12)** is such that even $e_S = 0.5$ and $e_L = 0$ only gives a slope of 0.77 for $t_c < t \leq 1$ s, which is still not quite as high as the reported value of 0.8.[26] On the other hand, we found that if the values $e_S = 0.5$, $e_L = 0.1$ and $i_c = 50$ are used, then eq. **(6.12)** looks very much like the long-time experimental data for DMA,[26] with a slope of 0.80 being found for $0.118 < t/\text{s} \leq 1$. From all this one can conclude that the double-linear analysis of Ref. [26] is likely to have underestimated e_S (*i.e.*, the value is probably more like 0.65 than 0.5), overestimated e_L (more like 0.1 than 0.2) and overestimated i_c (closer to 50 than 100). Thus the experimental data is still strong evidence for the composite termination model, but with parameter values somewhat different to those inferred.

From the present experiences two recommendations may be made: (1) Linear fitting to obtain e_L should be of SP PLP EPR data from times well beyond t_c. This is because at times immediately following t_c, data retains a memory of the different termination kinetics that pertained before t_c. In *Fig. 6.7* it is evident that this memory does not fully recede until about a decade of time beyond t_c has elapsed, for eq. **(6.14)** only becomes accurate for $t > 1$ s. Thus it is clear that one must expect to wait a long time for $\log(\rho/c_R - 1)$ *vs.* $\log t$ to become truly linear, and so experiments need to be carried out to very long times for accurate determination of e_L from linear fitting. Unfortunately this will bring transfer much more into play as an undermining influence (see Section 6.5). Therefore better practice is to: (2) Carry out non-linear least squares fitting of eq. **(6.12)** to data (in which context it is pointed out that the mathematical form of eq. **(6.12)** is simpler than it appears, *e.g.* the first two terms are just

a constant). Such fitting will explicitly allow for $\log(\rho/c_R-1)$ *vs.* log*t* to be curved, as indeed the data of Ref. [26] seems to be when viewed anew.

It has been seen in this section that even eq. **(6.11)**, a simple two-state model for the variation of *e* with *i*, results in a complex variation of $\log(\rho/c_R-1)$ with log*t*. More complicated termination models must therefore result in even more complex variations, ones that would be difficult to discern unambiguously in experimental data. So while eq. **(6.11)** is no doubt an over-simplification of reality, it is probably rare that SP PLP EPR data could with confidence reveal anything more complicated about the chain-length dependence of termination.

6.7 Chain-length-dependent Propagation

Following the stimulus provided by relatively recent theoretical[40] and experimental[41] work, the influence on FRP kinetics of chain-length-dependent propagation (CLDP) has become a topic of some interest. This is of relevance to the SP PLP data of Ref. [26], because these experiments probed the chain-length dependence of termination at relatively low chain lengths, and it is precisely at such chain lengths that CLDP will be operative. The reason this will impact upon SP PLP kinetics is that CLDP results in accelerated growth of radicals. Thus eq. **(6.8)**, the simple correlation between time and chain length that underlies all SP PLP analysis methods for obtaining $k_t^{i,i}$, is invalidated. For example, eq. **(6.8)** may predict that average radical length is 5 at a certain time, but because of CLDP it may actually be 10. Hence use of eq. **(6.8)** will overestimate the actual rate coefficient termination, meaning that false conclusions are drawn from SP PLP data.

With this in mind it is timely to investigate the influence of CLDP on SP PLP kinetics. This requires the variation of k_p^i with *i* for employment in simulations. For this purpose the expression[42]

$$k_p^i = k_p^\infty \left[1 + 15.8 \exp\left(\frac{-\ln 2}{1.12}(i-1)\right)\right] \qquad \textbf{(6.15)}$$

was used, where k_p^∞, the long-chain value of k_p, was as has been used for all k_p^i up until this point. eq. **(6.15)** has been shown[42] to describe MMA steady-state[42] and PLP[43] data, and as well it is consistent with theory[40] and a measured value of k_p^1 for MMA[44]. So whether or not

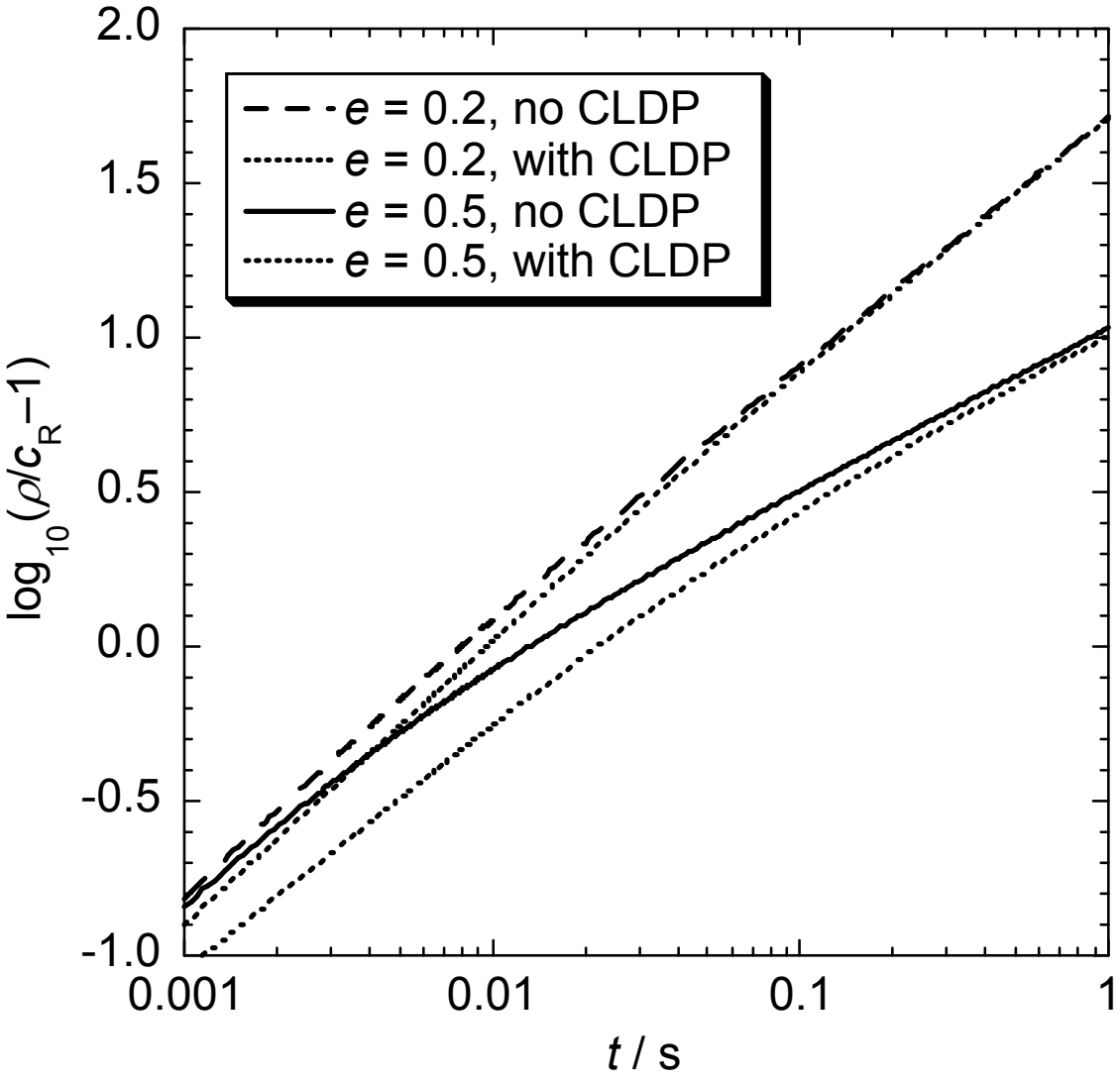

Fig. 6.8 Values of $\rho/c_R - 1$ *vs.* time from simulations using $k_p^\infty c_M = 840$ s^{-1}, $\rho k_t^{1,1} = 8 \times 10^1$ s^{-1}, and $e = 0.2$ and 0.5 as indicated. The simulations were carried out with and without chain-length-dependent propagation (CLDP, eq. **(6.15)**) as indicated.

eq. **(6.15)** is precisely correct, it is representative enough of the nature and magnitude of CLDP to enable the effect of this phenomenon on SP PLP kinetics to be gauged, which is the task at hand. Results are presented in *Fig. 6.8*, which gives the output from simulations using $e = 0.2$ and 0.5 (*i.e.*, the one-*e* model for termination), both with and without CLDP. Thus the results without CLDP are the same as those of *Fig. 6.2*, although an extra decade of time is presented in order to display what happens at very early times, when $i < 10$ and hence the effect of CLDP is strongest: eq. **(6.15)** is an exponential decay from $k_p^1 = 16.8k_p^\infty$ to $k_p^{10} = 1.06k_p^\infty$.

What is immediately clear from *Fig. 6.8* is that CLDP lowers values of $\rho/c_R - 1$. This is because faster propagation produces radicals of higher chain lengths than would otherwise be the case, which terminate more slowly, and hence c_R is higher. It is also clear from *Fig. 6.8* that the effect of CLDP on $c_R(t)$ diminishes with time. Again, this is easily understood: as time goes on and the effect of CLDP on i recedes, $\langle k_t \rangle(t)$ in the absence of CLDP catches up with that when CLDP holds. However it is important to note that the effect of CLDP on the observed kinetics persists well beyond the time at which k_p^i becomes equal to its long-chain value. This is most clearly seen from the $e = 0.5$ results, which are still slightly different at $t = 1$ s. It is worth pointing out that the logarithmic scale obscures this difference; the value of $c_R(t = 1\text{ s})$ is 8.5×10^{-7} mol L^{-1} with no CLDP, and 8.9×10^{-7} mol L^{-1} with CLDP. The time $t = 1$ s corresponds to $i = 841$ in the simulations of *Fig. 6.8*, whereas $k_p^i \approx k_p^\infty$ for $i > 10$. Thus one may not argue that the effects of CLDP will be absent from SP PLP kinetics once chain lengths are such that $k_p^i \approx k_p^\infty$. Rather, what is more important in this regard is the value of *e*: *Fig. 6.8* shows that for $e = 0.2$ there is only a very minor effect of CLDP on SP PLP kinetics at early times, while at long times the influence is vanishingly small. Although in this case

there is still the same accelerated growth of radicals as with $e = 0.5$, it is not of the same consequence because differences in $k_t^{i,i}$ are much smaller.

In terms of data analysis, the effect to note from *Fig. 6.8* is that CLDP increases the slope of a plot of $\log(\rho/c_R - 1)$ *vs.* $\log t$. This means that one will underestimate the value of e from the slope. For example, the linear fit of the $e = 0.5$ data with CLDP over $0.01 \leq t/\text{s} \leq 1$, the experimental time range of Ref. [26], has slope of 0.63, from which one would infer $e = 0.37$, which is markedly smaller than the actual value of 0.50 (although remember that this analysis also includes the effect of eq. **(6.10)** not being exact, as detailed in Section 6.3). Thus CLDP is another effect which makes the Ref. [26] value of $e_S = 0.5$ most likely an underestimate.

Given what has been found above, the question arises as to whether the effect of CLDP on SP PLP kinetics can be treated analytically. The way to do this is to integrate $\mathrm{d}i = k_p^i c_M \mathrm{d}t$ so as to obtain $i(t)$ for the particular CLDP at hand (*c.f.* the simple eq. **(6.8)**). One then proceeds as in Section 6.3. This exercise has been carried out for the case of $k_p^i = k_p^1 i^{-a}$.[35] Relevantly, it was found that $(\rho/c_R - 1) \sim t^{1-e/(1+a)}$,[35] *i.e.*, the slope of $\log(\rho/c_R - 1)$ *vs.* $\log t$ is increased by CLDP (because $a > 0$). This is in qualitative accord with what has been found above. However, a power-law model for CLDP is non-physical in that it is too weak at small i and too strong at high i (at which k_p^i is constant rather than continuing to decrease). Developing analytic equations that utilise the mathematically more challenging but physically more correct model of eq. **(6.15)** remains to be attempted.

Lastly, mention is made of a recently proposed method for obtaining $k_t^{i,i}$ through careful analysis of rate data from living free-radical polymerisation (LFRP).[45] As has been pointed out,[18] the concept underpinning this method is exactly that behind the SP PLP EPR method, even if the equations involved are different (because the LFRP method involves steady-state

polymerisation). One may thus anticipate that the LFRP method will be affected by chain transfer, composite termination and CLDP in the same qualitative ways as have been found in this chapter for the SP PLP EPR method.

6.8 Molecular Weight Distributions

Whether it is carried out by measurement of $c_M(t)$[17,22,25] or of $c_R(t)$,[26] Buback's SP PLP method involves following the disappearance of reactant. However kinetics may also be investigated by monitoring the appearance of product, which in the case of the termination reaction is dead polymer. While it is not feasible to do this on a sub-millisecond timescale for the creation of dead polymer, the realisation was made by Olaj, Vana *et al.* that the molecular weight distribution (MWD) at the end of a SP PLP experiment is effectively a meticulous record of the rate of appearance of dead polymer as a function of time.[33] This is because D^i species are formed by termination (by disproportionation or combination) of R^i species, which, according to the monodispersity assumption, exist at one instant only, and at that instant all termination interactions have rate coefficient $k_t^{i,i}$. Thus for the special case of SP PLP, the amount of dead polymer of chain length i must provide a direct window onto the value of $k_t^{i,i}$. That this is just a variation on the theme of Buback's fundamental SP PLP idea[17,25] is clear. Because this chapter is an investigation of this idea, it is apposite that this method of Olaj, Vana *et al.*[33] for determining $k_t^{i,i}$ also be put under the spotlight.

The mechanics of putting the idea of Olaj, Vana *et al.* into action, including admitting both combination and disproportionation, are as follows[33] (as adapted for present purposes). For SP PLP in the absence of transfer, eq. **(6.3)** becomes

$$\frac{dc_{Di}}{dt} = 2\lambda c_{Ri} k_t^{i,i} c_{Ri} + (1-\lambda) k_t^{i/2,i/2} c_{Ri/2} c_{Ri/2} \qquad \textbf{(6.16)}$$

Here a genuine monodispersity assumption has been made: it has been taken that *all* radicals have *exactly* the same chain length at any instant (this is stronger than the previously required mono-termination assumption, which is just that all radicals terminate with the same rate coefficient at any instant). If this chain length is taken as being $i = k_p c_M t$, then eq. **(6.10)** for $c_R(t)$ may be used in eq. **(6.16)**, with $t = i/(k_p c_M)$ giving the value of c_{Ri} for the disproportionation contribution and $t = i/(2k_p c_M)$ giving the value of $c_{Ri/2}$ for the combination part. Next one needs to grasp that $di = k_p c_M dt$ holds for chains formed by disproportionation while $di = 2k_p c_M dt$ holds for chains formed by combination (where i now refers to the length of dead polymer, not living radicals). This enables conversion from dt to di in eq. **(6.16)**, giving the final result

$$\frac{dc_{Di}}{di} = \lambda \rho C i^{-e}\left(1 + \frac{C}{1-e} i^{1-e}\right)^{-2} + (1-\lambda)\frac{\rho C}{4}(i/2)^{-e}\left(1 + \frac{C}{1-e}(i/2)^{1-e}\right)^{-2} \quad \textbf{(6.17)}$$

where $C = 2k_t^{1,1}\rho/(k_p c_M)$. This equation may look impossibly obscure, but the derivation has tried to emphasise just how simply it can be arrived at. Of particular note is that the correct balance between the disproportionation and combination contributions is automatically achieved by using eq. **(6.3)** as a starting point in the derivation. It is also stressed that eq. **(6.17)** gives concentrations from *one pulse only* of SP PLP.

Eq. **(6.17)** of course gives the *continuous* number-chain length distribution (CLD) expected from SP PLP. To convert to the *discrete* form of the number-CLD, as is yielded, for example, by simulations, one simply notes that it involves steps of 1 in chain length, *i.e.*, $di = 1$. Thus eq. **(6.17)** also gives c_{Di}, the discrete number-CLD. Olaj, Vana *et al.*[33] divided eq. **(6.17)** by $\rho(1+\lambda)/2$, the total concentration of dead chains that must eventually arise from an initial concentration ρ of radicals, and worked with the thus resulting *normalised* CLD. However

eq. **(6.17)** is of fascination in that it predicts *absolute* values of dead-chain concentrations, as are also furnished by simulations. Therefore eq. **(6.17)** will here be used as it stands.

To test the accuracy of eq. **(6.17)**, simulations were carried out with the standard parameter set of this work and both e = 0.2 and e = 0.5. To simplify matters the value λ = 1 was employed (as would be appropriate for a monomer like DMA). In *Fig. 6.9* are presented values of c_{Di} at the end of each simulation as well as the corresponding predictions of eq. **(6.17)**. The truncated nature of the c_{Di} from simulations is because these were ceased at t = 1 s, corresponding to an average i of about 841 for radicals (see eq. **(6.8)**). This is sufficient time to give complete formation of dead chains with i up to about 800, and accordingly it is evident that eq. **(6.17)** seems to provide a very good description of this portion of the simulation data. However a less flattering picture is revealed by *Fig. 6.10*, where the same data is presented as i^2c_{Di}, the so-called size exclusion chromatography (SEC) or hypermass form of the CLD. This emphasises that eq. **(6.17)** underestimates the true value of c_{Di}, and that the extent of the discrepancy becomes greater as e increases. This may be understood as arising from the fact that eq. **(6.10)** underestimates $c_R(t)$ (as shown in *Fig. 6.1*) because $i = k_pc_Mt$ overestimates the very initial rate of termination (see Section 6.3). A lower value of c_R results in a lower rate of termination and hence in a deficiency of dead chains, as revealed by *Fig. 6.10*. Further, the greater the value of e, the greater the extent to which c_R is underestimated (see Section 6.3), and hence the greater the inaccuracy of eq. **(6.17)**, as confirmed by the results of *Fig. 6.10*. One could alleviate this situation by using eq. **(6.9)**, based on $i = k_pc_Mt+1$, rather than eq. **(6.10)** in proceeding from eq. **(6.16)** in order to generate a more correct version of eq. **(6.17)**. This will be done in the following section.

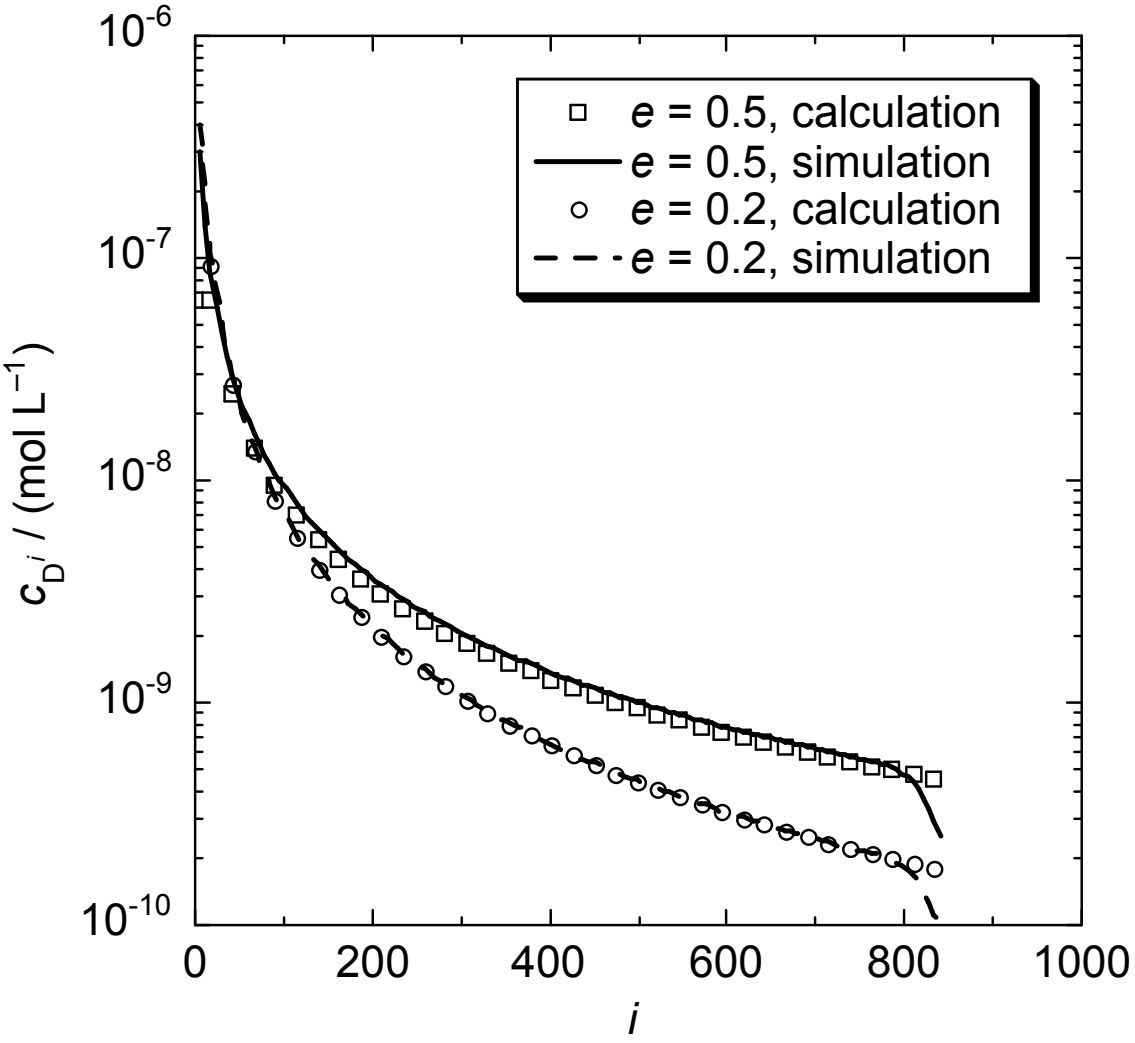

Fig. 6.9 Calculated (points, using eq. **(6.17)**) and simulated (lines) values of c_{Di}, the concentration of dead chains of length i, as obtained using $k_p c_M = 840$ s^{-1}, $\rho k_t^{1,1} = 8 \times 10^1$ s^{-1}, $\lambda = 1$ and $e = 0.5$ and 0.2 as indicated.

A motivation for presenting results as $i^2 c_{Di}$ is that Olaj, Vana *et al.* fitted their equivalent of eq. **(6.17)** to this form of experimental data in order to obtain e and C.[33] Although this was done for styrene and MMA systems, which will have different parameter values to those used here (most notably, $k_t^{1,1}$ will be much higher), one may still use the present simulations to

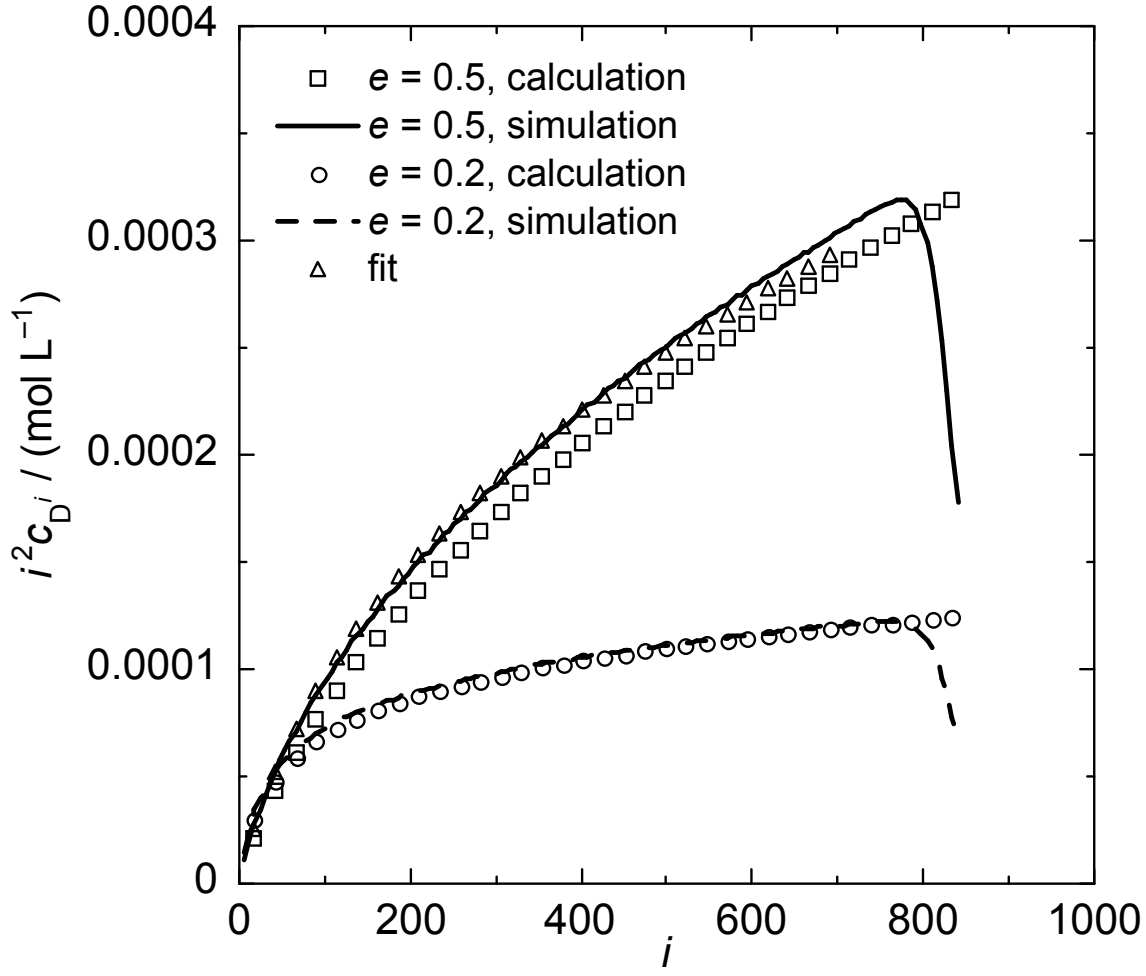

Fig. 6.10 Data of *Fig. 6.9* presented as i^2c_{Di} *vs.* chain length *i*. Additionally presented is a best-fit (triangles) of eq. **(6.17)** to the $e = 0.5$ simulation data (see text for details).

gauge the correctness of these endeavours of Ref. [33]. With this in mind, non-linear least squares fitting of the SEC-CLD form of eq. **(6.17)** to the $e = 0.5$ simulation data ($i \leq 700$ only) was carried out. This of course mimics the fitting of experimental data performed in Ref. [33]. The resulting best-fit parameter values are $e = 0.42$ and $k_t^{1,1} = 6.3 \times 10^6$ L mol^{-1} s^{-1}, as compared with the simulation input values of 0.50 and 8.0×10^6 L mol^{-1} s^{-1} respectively. While this agreement is reasonable, the fact that it is still somewhat astray is not at all

betrayed by the quality of the fit, which is excellent, as shown in *Fig. 6.10* (see the triangles). In other words, one has little indication that somewhat inaccurate parameter values have been obtained. The fact that both e and $k_t^{i,i}$ are underestimated is fully consistent with fitting of eq. **(6.10)** to $c_R(t)$ data also resulting in underestimation of both these values, as discussed and explained in Section 6.3. One must therefore conclude that the value $e = 0.2$ inferred from experimental data in Ref. [33] is probably a slight underestimate of the true value. Nevertheless the fundamental finding of this paragraph is that reasonable estimates of e are obtained by the method of Ref. [33].

This chapter has investigated several issues that complicate SP PLP kinetics. Of most immediate interest in terms of the method of Ref. [33] is how it is affected by the composite termination model. This is because Ref. [33] carried out fitting from $i = 1$ up to a maximum chain length, and it was found that as this maximum chain length was reduced from over 1000 down to as low as 100, the obtained value of e increased from about 0.2 to as high as 0.8. On the face of it this looks like evidence for e being higher at small chain lengths, in accord with the composite termination model. To investigate whether this is really so, a simulation was carried out with $e_S = 0.5$, $e_L = 0.2$ and $i_c = 100$. The results are presented in *Fig. 6.11*.

The first and most astonishing finding of *Fig. 6.11* is that rather than the composite-model results lying between those for $e = 0.2$ and $e = 0.5$, as one would expect, in fact they lie above them. How is this so? Well up until radicals reach $i = 100$, the composite-model kinetics are the same as those for $e = 0.5$. Thus at the point at which radicals reach $i = 100$, both models have identical c_R. However, at this point values of $k_t^{i,i}$ will diverge. Specifically, $k_t^{i,i}$ will be higher for the composite model, which has $e = 0.2$ for $i > 100$. Because c_R is the same but $k_t^{i,i}$ is higher, the rate of termination will be higher for the composite termination model, and thus

more dead chains will form. So this explains the thoroughly unexpected result of i^2c_{Di} being higher for the composite termination model than for $e = 0.5$.

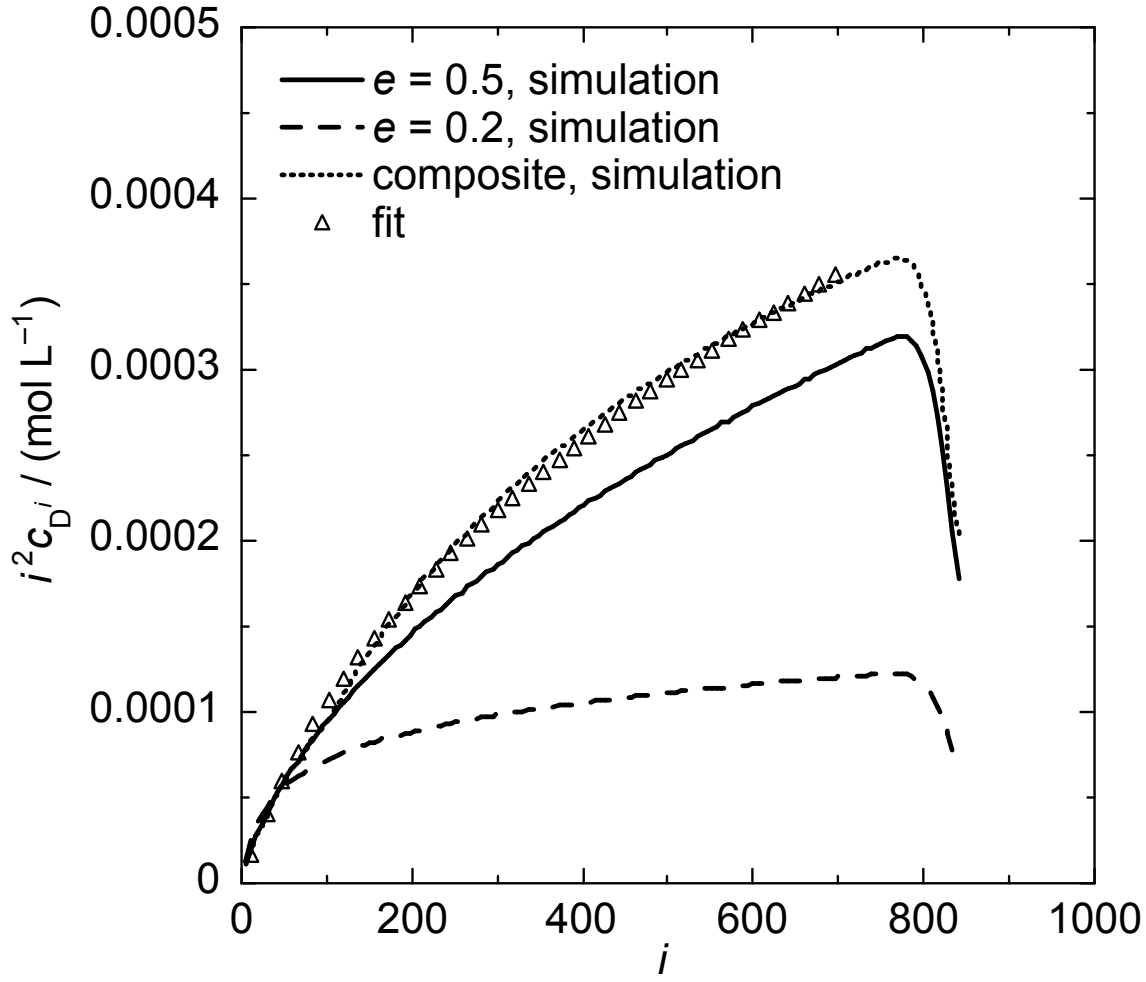

Fig. 6.11 Values of i^2c_{Di} *vs.* chain length i from simulations using $k_pc_M = 840$ s^{-1}, $\rho k_t^{1,1} = 8 \times 10^1$ s^{-1}, $\lambda = 1$ and $e = 0.5$, 0.2 and composite termination ($e_S = 0.5$, $e_L = 0.2$ and $i_c = 100$) as indicated. Also presented is a best-fit (triangles) of eq. **(6.17)** to the composite-termination data (see text for details).

Next, we fitted eq. **(6.17)** to the composite-model results. The best fit for $i \leq 700$ is shown in *Fig. 6.11* (the triangles). It is clear that a very satisfying fit is obtained. So even though a two-*e* termination model was used to generate the data, it is almost perfectly described by an

equation assuming a constant value of e. Because the fitting is mostly of data with $i > i_c$ (= 100), one would therefore anticipate that the value of e obtained from fitting is close in value to e_L. However in fact the fit of Fig. 6.11 was generated with $e = 0.44$ and $k_t^{1,1} = 5.3 \times 10^6$ L mol^{-1} s^{-1}. So the obtained value of e is actually a good estimate of e_S, and does not at all reflect e_L. Further, the following results were obtained for fitting over different ranges of chain length, mimicking the work of Ref. [33]: for i up to 500, $e = 0.44$; i up to 300, $e = 0.42$; and i up to 200, $e = 0.39$. So there is no evidence of any increase in e, contrary to what was found in Ref. [33]. Thus one can say that if the low-i SEC data of Ref. [33] is of good quality, then it is probably evidencing that e is much greater than 0.5 at small chain lengths.

Understanding of many of the surprising results that have been obtained above is enhanced by noting that in the limit of high i, eq. **(6.17)** becomes

$$i^2 c_{Di} = i^e \frac{\rho}{C} (1-e)^2 (\lambda + [1-\lambda]2^{-e}) \qquad \textbf{(6.18)}$$

This result also requires having $e < 1$, but that has already been assumed in using eq. **(6.10)**. eq. **(6.18)**, which has in fact been presented before,[34] reveals how remarkably simple are the SEC-CLDs of *Fig. 6.10*: to good approximation they are just power laws, something that is obvious in hindsight (the $e = 0.5$ results look like $i^{0.5}$, the $e = 0.2$ like $i^{0.2}$). It is now clear that the parameter e predominantly determines the *shape* of the SEC-CLD, while $\rho/C = k_p c_M/(2k_t^{1,1})$ predominantly determines the *magnitude*.

The accuracy of eq. **(6.18)** is investigated in *Fig. 6.12*, which re-presents the $e = 0.5$ simulation data of *Fig. 6.10* and also presents evaluations of eq. **(6.18)** and eq. **(6.17)**. It is apparent that values of eq. **(6.18)** overestimate the simulation data, to a greater extent than eq. **(6.17)** underestimated it. Despite this, the shape of the curve is well reproduced by eq. **(6.18)**.

Since values of $i^2 c_{Di}$ continue to increase with i, the apparently constant difference between the values of eqs. **(6.17)** and **(6.18)** becomes insignificant in relative terms at sufficiently high chain length. However, the value of i at which the two equations merge was found to be unphysically high (results not presented), which shows the danger of assuming that eq. **(6.18)** holds *a priori*.

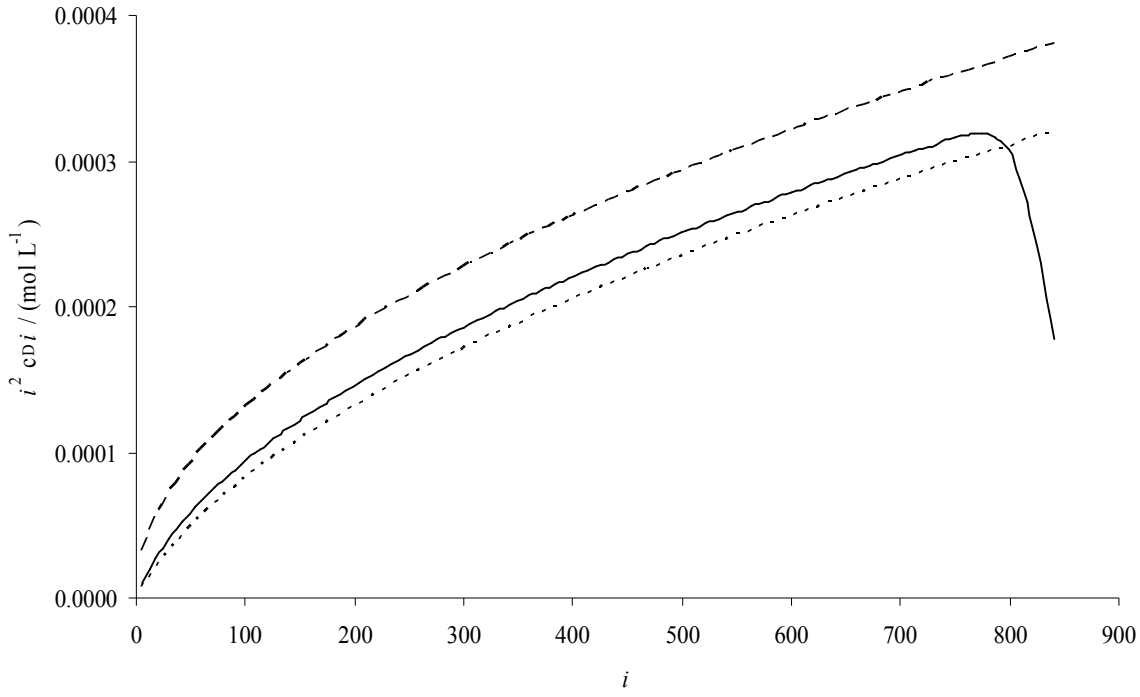

Fig. 6.12 Values of $i^2 c_{Di}$ *vs.* chain length i using $k_p c_M = 840\ s^{-1}$, $\rho k_t^{1,1} = 8 \times 10^1\ s^{-1}$, $\lambda = 1$ and $e = 0.5$ from simulations (solid line), eq. **(6.17)** (short-dashed line) and eq. **(6.18)** (long-dashed line).

In view of eq. **(6.18)** it can be recommended that MWD data from SP PLP experiments should be plotted as the logarithm of the SEC-CLD *vs.* log$i$. At high i such a plot should be linear, with the slope being equal to e. If the data is from high enough chain length, then from the intercept one can obtain $k_t^{1,1}$ if $k_p c_M$ and λ are known (e being available from the slope),

however this also requires that absolute values of c_{Di} can be inferred from experimental data, which is as good as impossible to achieve accurately in practice.[33] So at this stage the fitting of MWD data from SP PLP experiments should really only be regarded as a method for determining e, as its influence is not affected by the inclusion of scaling constants in eqs. **(6.17)** and **(6.18)**.[33]

From eq. **(6.18)** it is now clear why fitting of eq. **(6.17)** to the composite-model data yielded e = 0.44 (*Fig. 6.11*), higher than the value obtained (0.42) from fitting e = 0.5 data (*Fig. 6.10*): it is because $i^2 c_{Di}$ values are higher for the composite model, which means e must be higher. On the other hand, eq. **(6.18)** makes clear that the SEC-CLD from the composite model must eventually show $i^{0.2}$ behaviour (since e_L = 0.2), and therefore must drop below the SEC-CLD from using e = 0.5 (which will show $i^{0.5}$ behaviour at high i). These expectations were confirmed by carrying out a simulation to t = 10 s. Results are presented in *Fig. 6.13*, which shows the CLD from the composite model crossing over with that from e = 0.5 at a chain length of approximately 1700. Also presented in *Fig. 6.13* are (one-parameter) fits of $i^{0.5}$ and $i^{0.2}$ over the range of chain length 5000-8000, confirming that this simple behaviour is displayed at high chain length. That said, it is equally evident that even at these extremely high chain lengths, limiting long-time behaviour is still not perfectly displayed. Further, the constant of proportionality from fitting is different to that predicted by eq. **(6.18)**. For example, with e = 0.5 eq. **(6.18)** predicts a constant of proportionality of 1.31×10^{-5} mol L^{-1}, while the best fit value is 1.25×10^{-5} mol L^{-1}. This is consistent with the observation made above that eq. **(6.18)** overestimates values of $i^2 c_{Di}$.

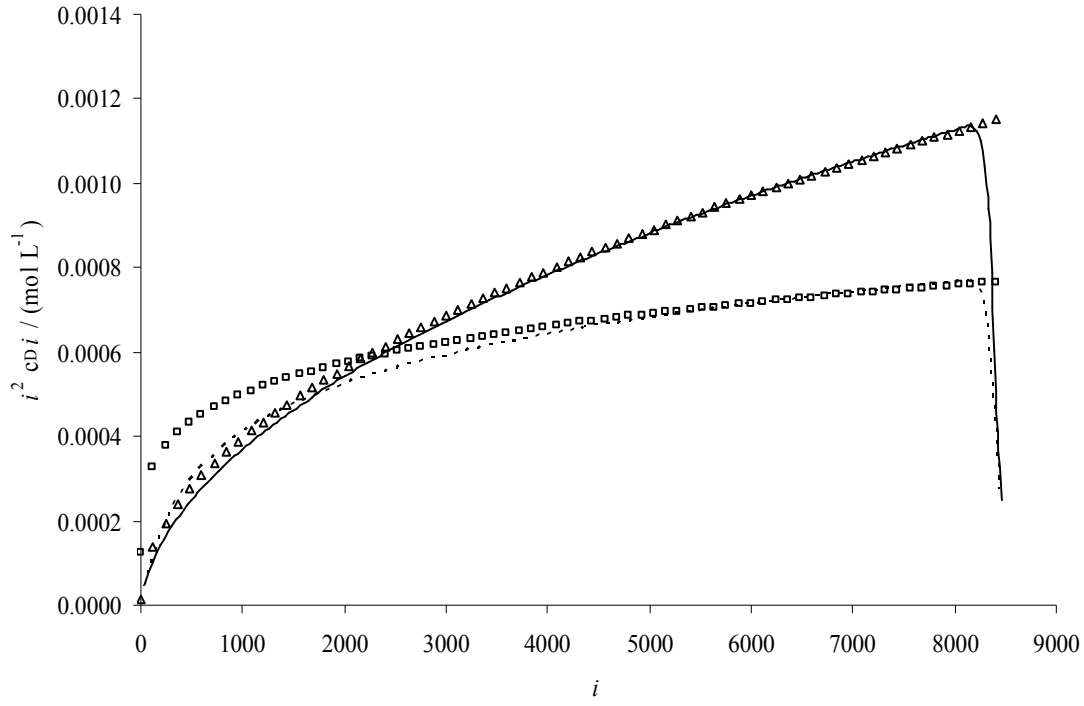

Fig. 6.13 Values of $i^2 c_{Di}$ *vs.* chain length i using $k_p c_M = 840$ s^{-1}, $\rho k_t^{1,1} = 8 \times 10^1$ s^{-1} and $\lambda = 1$. Simulations are indicated by lines (solid: $e = 0.5$, dashed: composite termination ($e_S = 0.5$, $e_L = 0.2$ and $i_c = 100$)), and fits (see text) to simulated data are indicated by symbols (squares: $i^{0.2}$ fit to composite termination data, triangles: $i^{0.5}$ fit to $e = 0.5$ data).

As is implicit in the discussion above, eq. **(6.18)** makes the remarkable prediction that the SEC-CLD from a SP PLP will continue to rise without bound as i increases, as indeed was observed in simulations (and all experimental data presented in Ref. [33] is monotonic increasing). About this result it is necessary to say two things: (1) It does not mean that c_{Di} increases as i increases, for it is very evident from *Fig. 6.9* that the opposite is the case. Rather, all it means is that i^2 increases faster than c_{Di} decreases. (2) Unbounded increase of $i^2 c_{Di}$ with i can never occur in real systems because chain transfer will eventually occur. The capacity of chain transfer to undermine the method of this section is something that has not

yet been probed here, as all simulations up to this point have used $k_{trX} = 0$. However, intuition is that if a radical has a high probability of terminating before it reaches chain length $k_p c_M/(k_{trX} c_X)$, then the CLD will be little affected by transfer. As this statement makes clear, it would seem that the timescales of several processes are involved in determining if transfer will perturb a SP PLP MWD experiment.

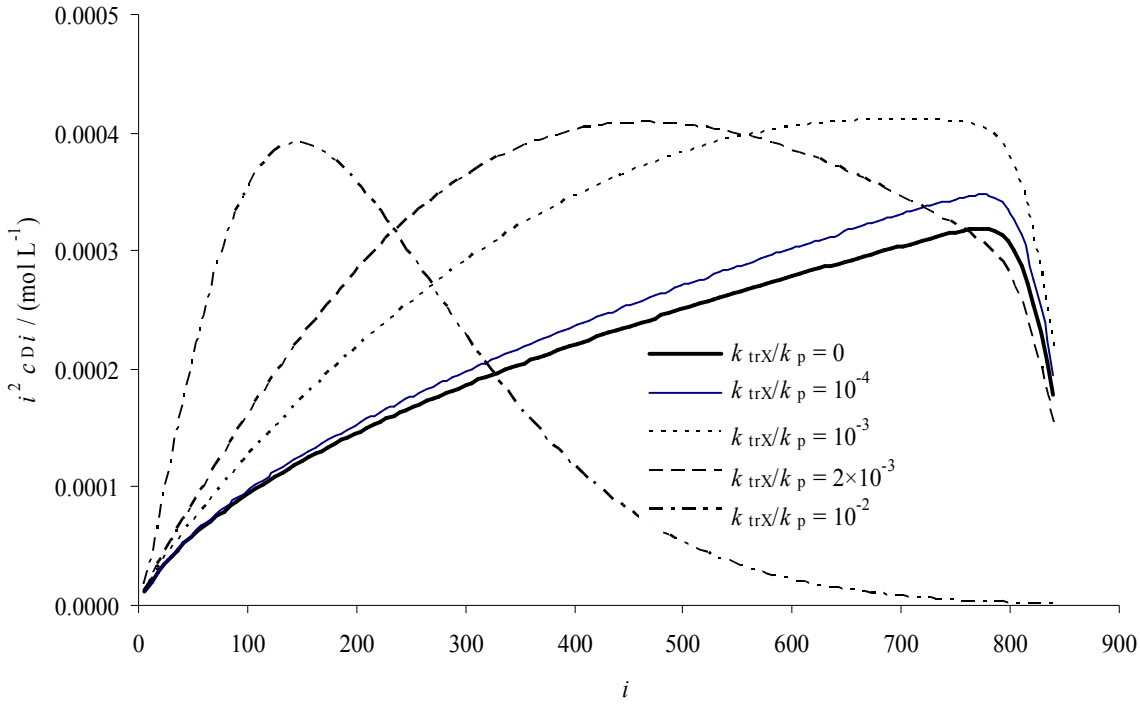

Fig. 6.14 Values of $i^2 c_{Di}$ *vs.* chain length i using $k_p c_M = 840$ s^{-1}, $\rho k_t^{1,1} = 8 \times 10^1$ s^{-1}, $\lambda = 1$, $e = 0.5$, and k_{trX}/k_p as indicated.

Now we will investigate transfer. *Fig. 6.14* depicts the effect of transfer on the simulated SEC CLD with $e = 0.5$. As expected, transfer produces SEC CLDs of the familiar 'peak' shape, with the peak (very approximately) at $k_p c_M/(k_{trX} c_X)$. The figure shows how the MWD is sensitive to transfer, more so than was $c_R(t)$: in *Fig. 6.3* a plot with $k_{trX}/k_p = 10^{-4}$ is indistinguishable from the plot with $k_{trX}/k_p = 0$, whereas in *Fig. 6.14* the MWD is noticeably

affected by the same degree transfer. The explanation for this is that transfer directly affects the MWD by producing dead chains, whereas $c_R(t)$ is only affected indirectly by producing short chains (which subsequently terminate more rapidly, as detailed in section 6.5).

From this section it seems reasonable to conclude that interpretation of SP PLP MWD results in order to learn about $k_t^{i,i}$ is more problematic than that of SP PLP EPR experiments. This is especially so when it is remembered that SEC data is unavoidably distorted by column broadening, something that has not been considered here (that said, it is evident that the MWDs generated by SP PLP: are very broad, meaning that they are probably little affected by column broadening). Even so, there is no disputing that MWD data from SP PLP experiments must be a useful adjunct to EPR data for learning about termination kinetics: the elegance of the idea underpinning SP PLP MWD experiments ensures this. And of course the SP PLP MWD experiment has the virtue of being extremely simple to conduct, for it *only* involves the determination of the MWD at the end of an SP PLP experiment, as opposed to requiring fast time-scale measurements of c_R (or c_M). Another aspect in which the EPR and MWD methods are complementary is the dependence of the sensitivity of the data on time / chain length. The EPR method is most sensitive to early-time / low-chain-length data as this is when the signal due to c_R is still relatively high, while the MWD method is weak at low chain lengths due to reliance on the SEC method, which necessarily gives small signals at low chain lengths. Conversely, EPR signals will be weak at long times (when c_R is low) while SEC signals are amplified at high chain lengths due to the i^2 weighting.

6.9 Molecular Weight Distributions – Analytic Equations Revisited

It was seen in the preceding section that eq. **(6.17)** can be inaccurate because it uses $i = k_p c_M t$, which gives a highly erroneous rate of termination at very early times (see Section 6.3). This may be remedied as follows. eq. **(6.9)** may be written as follows:

$$c_R^{-1} = \rho^{-1} + \frac{C}{1-e}(i^{1-e} - 1) \qquad \textbf{(6.19)}$$

where $C = 2k_t^{1,1}\rho/(k_p c_M)$ as used previously. This is now substituted into eq. **(6.16)**, and it is easily obtained that

$$\frac{dc_{Di}}{di} = \lambda \rho C i^{-e}\left(1 + \frac{C}{1-e}\left[i^{1-e} - 1\right]\right)^{-2}$$

$$+ (1-\lambda)\frac{\rho C}{4}(i/2)^{-e}\left(1 + \frac{C}{1-e}\left[(i/2)^{1-e} - 1\right]\right)^{-2} \qquad \textbf{(6.20)}$$

Fig. 6.15 re-presents the data of *Fig. 6.10* but with predictions of eq. **(6.20)** now also included. It is evident that eq. **(6.20)** represents a significant improvement over eq. **(6.17)**,

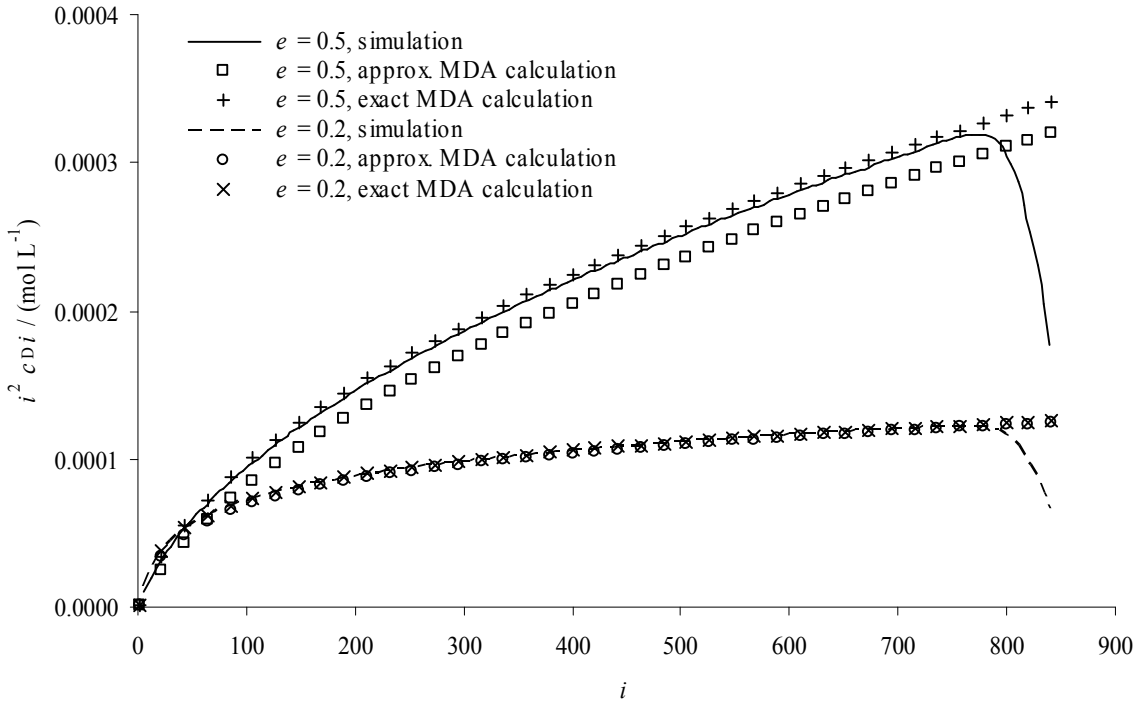

Fig. 6.15 Calculated (points, using the 'approx. MDA' eq. **(6.17)** or 'exact MDA' eq. **(6.20)**) and simulated (lines) values of $i^2 c_{Di}$, as obtained using $k_p c_M$ = 840 s^{-1}, $\rho k_t^{1,1} = 8 \times 10^1$ s^{-1}, $\lambda = 1$ and $e = 0.5$ and 0.2 as indicated.

and is spectacularly accurate, which confirms how well the MDA works also for MWDs from SP PLP. It is also relevant to note that in the long-time limit, eq. **(6.20)** also gives eq. **(6.18)**.

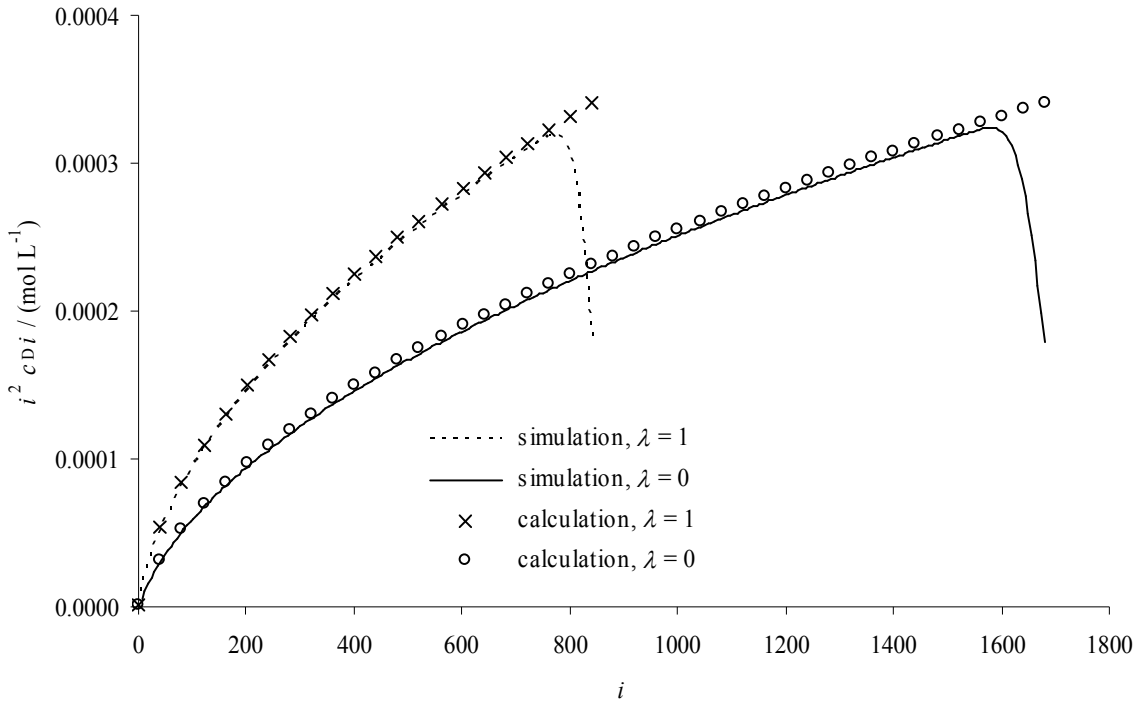

Fig. 6.16 Calculated (points, using eq. **(6.20)**) and simulated (lines) values of $i^2 c_{Di}$, as obtained using $k_p c_M = 840$ s^{-1}, $\rho k_t^{1,1} = 8 \times 10^1$ s^{-1}, $e = 0.5$ and $\lambda = 0$ and 1 as indicated.

It is of interest to examine the effect of combination. Therefore a simulation has been carried out with the standard parameter set, and $e = 0.5$, but with $\lambda = 0$ rather than 1. The result is shown in *Fig. 6.16*. Because of the time taken to evaluate the combination sum of eq. **(6.3)**, there is a significant computational cost associated with including combination: the simulation with $\lambda = 0$ took about 8 times longer than that with $\lambda = 1$ (both SP PLP simulations were carried out to $t = 1$ s). This is despite the fact that it is possible to use a much higher timestep in solving eq. **(6.3)**[28] than was required to accurately solve eqs. **(6.1)**

and **(6.2)**. Also presented in *Fig. 6.16* are simulation results carried out with $\lambda = 1$, together with the predictions of eq. **(6.20)**. It is once again evident that the MDA is spectacularly accurate, and this accuracy is uncompromised by the occurrence of combination. The physical effect that is of interest is that combination causes a noticeably lesser amount of polymer at low chain lengths. In the high-i limit, eq. **(6.18)** can be used to make the prediction that values of $i^2 c_{\mathrm{D}i}$ due to disproportionation and combination would have the same shape, but different magnitude (the scaling factor being given by 2^{-e}). This behaviour is evident in *Fig. 6.16*. A curious consequence of this prediction is that when $e = 0$, both disproportionation and combination should give the same, constant high-i-limit value of $i^2 c_{\mathrm{D}i}$, despite the total concentrations of dead polymer necessarily being quite different. What must be kept in mind when considering this is that a constant value of $i^2 c_{\mathrm{D}i}$ implies that increasing i^2 is exactly counterbalanced by decreasing $c_{\mathrm{D}i}$, so that the high-i part of the CLD does not necessarily represent a significant fraction of the *number* CLD.

6.10 Effect of Chain-length-dependent Propagation on Molecular Weight Distributions

A curious aspect of the experimental results of Ref. [33] is the paucity of chains at low chain lengths, with data actually being concave up at very low i, which of course is impossible for a strict power-law dependence such that $e < 1$. The thought occurs that chain-length-dependent propagation must also have this effect: because small chains will propagate more rapidly, there is a reduced chance of them undergoing termination, and therefore fewer small chains will be formed. *Fig. 6.17* shows that this effect is found in simulations, with this particular CLDP producing fewer dead chains up to chain length 5. Subsequently however, as i increases and k_{p}^{i} approaches the long-chain value of k_{p}^{∞}, CLDP produces *more* dead chains, a somewhat unexpected result.

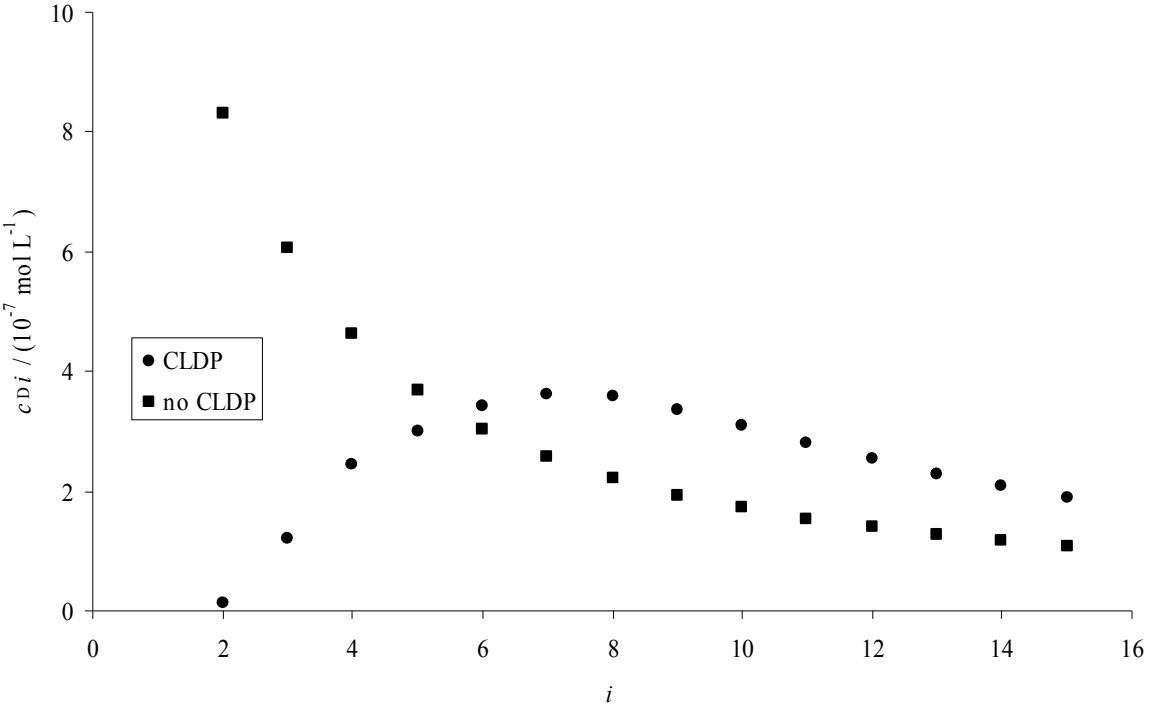

Fig. 6.17 Values of c_{Di} at low chain lengths i using $k_p^{\infty}c_M$ = 840 s^{-1}, $\rho k_t^{1,1} = 8 \times 10^1$ s^{-1}, and e = 0.5. The simulations were carried out with and without chain-length-dependent propagation (CLDP, eq. **(6.15)**) as indicated.

Fig. 6.18 shows that the surprising effect noted above not only persists through the entire DCLD, but is also of significant magnitude. Several effects conspire to ensure this. At a particular time, c_R is higher with CLDP than without it (see *Fig. 6.8*). Since the rate of formation of dead chains is proportional to c_R^2, a greater quantity of dead chains must be formed with CLDP. Also, the squared dependence accentuates differences in c_R. There is also believed to be another subtle effect due to CLDP: with faster propagation of short chains, radicals will reach a particular chain length at an earlier time, and with less time for termination to occur the concentration of radicals will be higher than with chain-length-independent propagation, increasing the rate of formation of dead chains of that chain length.

With all of that said, it is also clear that this effect depends on an interplay between CLDP and CLDT, and from *Fig. 6.18* it is evident that lower *e* decreases the magnitude of the effect.

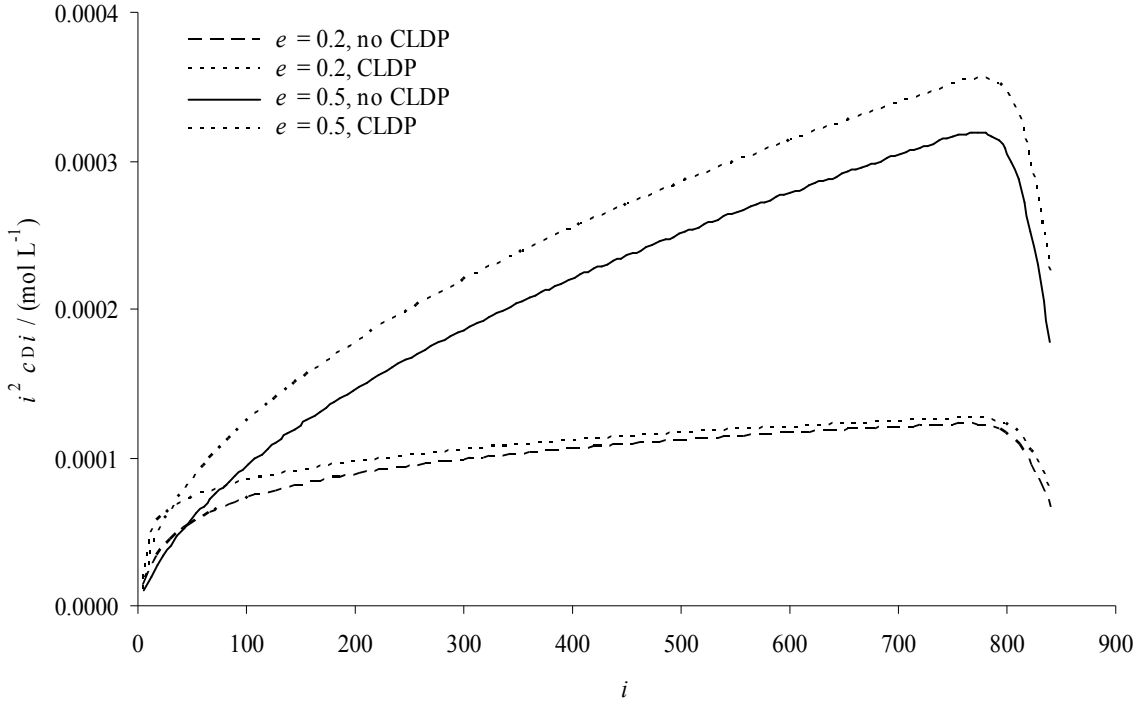

Fig. 6.18 Values of $i^2 c_{Di}$ *vs.* chain length *i* obtained using $k_p^{\infty} c_M = 840\ s^{-1}$, $\rho k_t^{1,1} = 8 \times 10^1\ s^{-1}$, and $e = 0.2$ and 0.5 as indicated. The simulations were carried out with and without chain-length-dependent propagation (CLDP, eq. **(6.15)**) as indicated.

6.11 Conclusion

In deriving equations associated with the SP PLP method, the major assumption of which one is conscious is the monodispersity assumption. This work has shown that this assumption is spectacularly accurate (see *Fig. 6.2* and *Fig. 6.6*). However the same cannot be said for the many less visible assumptions of which one usually is not aware. It would be wonderful if the world were such that $\langle k_t \rangle = k_t^{1,1}(k_p c_M t)^{-e}$ was accurate at very early times (Section 6.3), that

transfer to monomer was always negligible (Section 6.5), that $k_t^{i,i}$ was always given by a simple power law (Section 6.6) and that propagation was chain-length independent (Section 6.7). But the world is not this simply behaved, and it has been shown that the breakdown of each of these approximations can exert a perturbation of significant magnitude on SP PLP data. Because of this it has to be concluded that completely rigorous interpretation of SP PLP data necessarily requires modeling *via* simulations using eqs. **(6.1)-(6.3)** without simplification. Further, experimental data would ideally consist of both $c_R(t)$ and the final MWD from the one SP PLP experiment, so that both approaches for extracting $k_t^{i,i}$ from SP PLP data could be used in harmony rather than in isolation (as has been the case to date).

All the above said, it is still warranted to conclude this chapter on a positive note. SP PLP data may be *perturbed* by real phenomena such as chain transfer to monomer, the variation of *e* with chain length, and chain-length-dependent propagation. However, under usual circumstances the SP PLP method for determining $k_t^{i,i}$ remains reasonably robust in the face of these effects; further, this robustness may be increased by employing refinements to current data-analysis methods that have been suggested here. Hence it may be said that the exquisite idea behind the use of SP PLP for direct probing of the chain-length dependence of termination is also a viable idea. And in terms of FRP experiments for this purpose, this idea is probably as good as it gets.

6.12 Postscript

The work of the above chapter was largely published as Smith, G. B.; Russell, G. T. *Z. Phys. Chem.* **2005**, *219*, 295-323. Not included in this publication were *Fig. 6.12* - *Fig. 6.18*, in other words part of Section 6.8, and all of Sections 6.9 and 6.10. A significant development since the publication of Smith, G. B.; Russell, G. T. *Z. Phys. Chem.* **2005**, *219*, 295-323 is

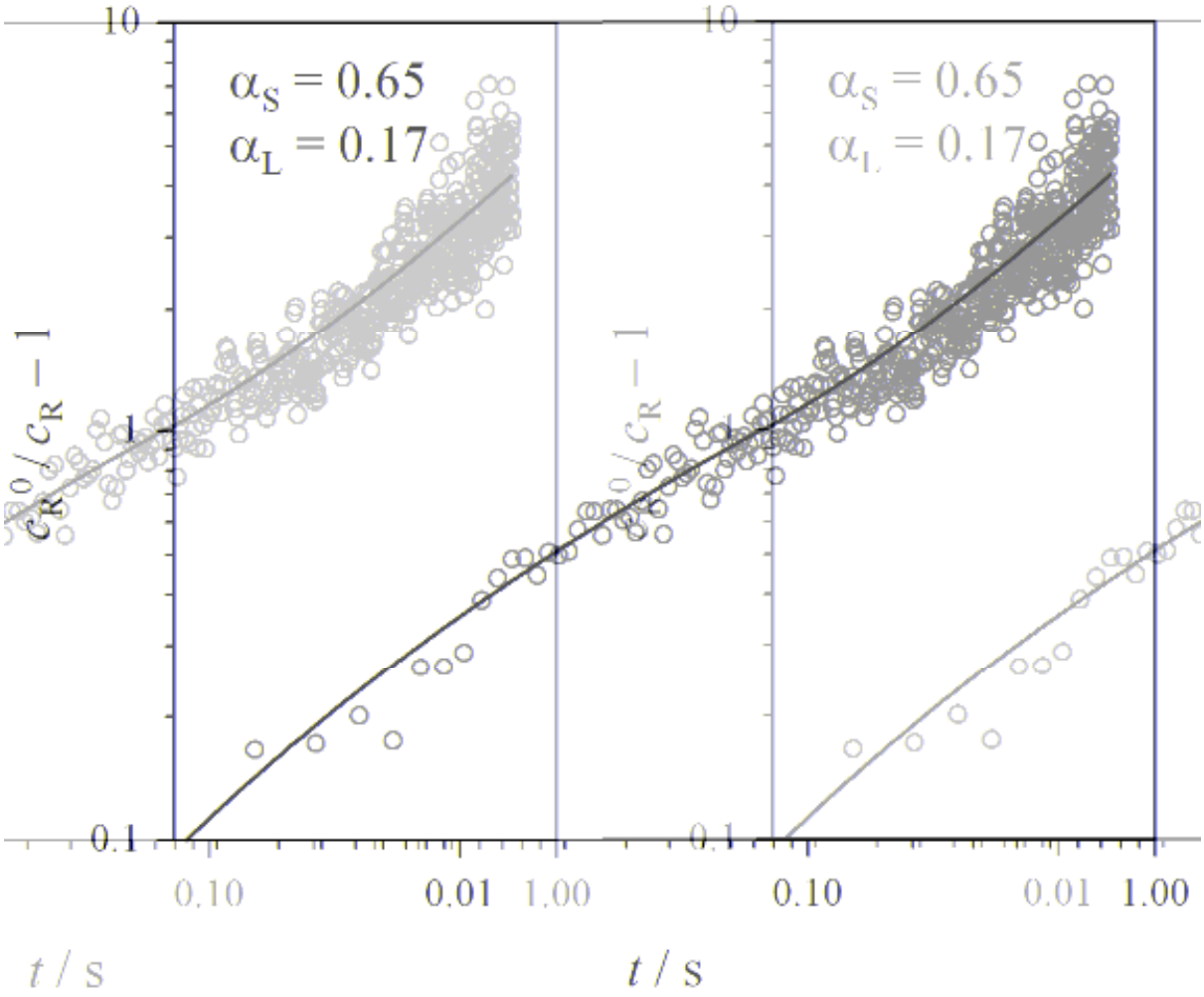

Fig. 6.19 Log-log plot of (ρ/c_R – 1) versus time for SP–PLP–EPR data of dodecyl methacrylate at 0 °C and 12.9 % conversion. Points: experiment; line: eq. **(6.12)** with $k_t^{1,1}$ = 1.5 × 10^7 L mol^{-1} s^{-1}, e_S = 0.65, e_L = 0.17 and i_c = 50. Reproduced from ref. [46] (where, as is evident, slightly different notation was used).

that the theory of this work has been applied in analysis of SP-PLP-EPR data. Specifically, eq. **(6.12)** has been fitted to data for dodecyl methacrylate, benzyl methacrylate and cyclohexyl methacrylate.[46] In all instances, eq. **(6.12)** was found to give a superb fit to data, and to return more accurate parameter estimates than the simple double-linear approach originally used.[26] An example is presented in *Fig. 6.19*.[46] Especially noteworthy is the capacity of eq. **(6.12)** to fit data at very early times, data that was previously either ignored[26] or falsely interpreted as chain-length independent termination ($e \approx 0$) at oligomeric chain lengths for dibutyl itaconate.[47] In fact, this early time region of high slope (≈ 1) is still perfectly described by $e_S \approx 0.5$ once the "+1 effect" – in other words, the fact that chain length starts at 1 rather than 0, and thus the rate of termination is not infinite at $t = 0$ – is taken into account, as is the case with eq. **(6.12)**.

References

(1) Beuermann, S.; Buback, M. *Prog. Polym. Sci.* **2002**, *27*, 191-254.

(2) Aleksandrov, A. P.; Genkin, V. N.; Kitai, M. S.; Smirnova, I. M.; Sokolov, V. V. *Sov. J. Quantum Electron.* **1977**, *7*, 547-550.

(3) Olaj, O. F.; Bitai, I.; Hinkelmann, F. *Makromol. Chem.* **1987**, *188*, 1689-1702.

(4) Olaj, O. F.; Bitai, I.; Gleixner, G. *Makromol. Chem.* **1985**, *186*, 2569-2580.

(5) Buback, M.; Hippler, H.; Schweer, J.; Vögele, H.-P. *Makromol. Chem., Rapid Commun.* **1986**, *7*, 261-265.

(6) Brackemann, H.; Buback, M.; Vögele, H.-P. *Makromol. Chem.* **1986**, *187*, 1977-1992.

(7) Buback, M.; Gilbert, R. G.; Hutchinson, R. A.; Klumperman, B.; Kuchta, F.-D.; Manders, B. G.; O'Driscoll, K. F.; Russell, G. T.; Schweer, J. *Macromol. Chem. Phys.* **1995**, *196*, 3267-3280.

(8) Beuermann, S.; Buback, M.; Davis, T. P.; Gilbert, R. G.; Hutchinson, R. A.; Olaj, O. F.; Russell, G. T.; Schweer, J.; van Herk, A. M. *Macromol. Chem. Phys.* **1997**, *198*, 1545-1560.

(9) Beuermann, S.; Buback, M.; Davis, T. P.; Gilbert, R. G.; Hutchinson, R. A.; Kajiwara, A.; Klumperman, B.; Russell, G. T. *Macromol. Chem. Phys.* **2000**, *201*, 1355-1364.

(10) Beuermann, S.; Buback, M.; Davis, T. P.; García, N.; Gilbert, R. G.; Hutchinson, R. A.; Kajiwara, A.; Kamachi, M.; Lacík, I.; Russell, G. T. *Macromol. Chem. Phys.* **2003**, *204*, 1338-1350.

(11) van Herk, A. M. J. Macromol. Sci., Rev. Macromol. Chem. Phys. **1997**, C37, 633-648.

(12) Olaj, O. F.; Zifferer, G. *Makromol. Chem., Theory Simul.* **1992**, *1*, 71-90.

(13) Olaj, O. F.; Kremminger, P.; Schnöll-Bitai, I. *Makromol. Chem., Rapid Commun.* **1988**, *9*, 771-779.

(14) Olaj, O. F.; Schnöll-Bitai, I.; Kremminger, P. *Eur. Polym. J.* **1989**, *25*, 535-541.

(15) Olaj, O. F.; Schnöll-Bitai, I. *Makromol. Chem., Rapid Commun.* **1991**, *12*, 373-380.

(16) Buback, M.; Schweer, J. Die Makromolekulare Chemie, Rapid Communications **1988**, 9, 145-149.

(17) Buback, M.; Schweer, J. Die Makromolekulare Chemie, Rapid Communications **1988**, 9, 699-704.

(18) Barner-Kowollik, C.; Buback, M.; Egorov, M.; Fukuda, T.; Goto, A.; Olaj, O. F.; Russell, G. T.; Vana, P.; Yamada, B.; Zetterlund, P. B. *Progress in Polymer Science* **2004**, submitted.

(19) Buback, M.; Egorov, M.; Gilbert, R. G.; Kaminsky, V.; Olaj, O. F.; Russell, G. T.; Vana, P.; Zifferer, G. *Macromol. Chem. Phys.* **2002**, *203*, 2570-2582.

(20) Russell, G. T. *Aust. J. Chem.* **2002**, *55*, 399-414.

(21) Buback, M. *Angew. Chem., Int. Ed. Engl.* **1991**, *30*, 641-653.

(22) Buback, M.; Egorov, M.; Feldermann, A. *Macromolecules* **2004**, *37*, 1768-1776.

(23) de Kock, J. B. L.; Klumperman, B.; van Herk, A. M.; German, A. L. *Macromolecules* **1997**, *30*, 6743-6753.

(24) de Kock, J. B. L., Ph.D. Thesis, Technical University of Eindhoven, 1999

(25) Buback, M.; Schweer, J. *Z. Phys. Chem. (Munich)* **1989**, *161*, 153-165.

(26) Buback, M.; Egorov, M.; Junkers, T.; Panchenko, E. *Macromol. Rapid Commun.* **2004**, in press.

(27) Smith, G. B.; Russell, G. T.; Heuts, J. P. A. *Macromol. Theory Simul.* **2003**, *12*, 299-314.

(28) Rees, M. T. L., Ph.D. Thesis, The University of Canterbury, 1999

(29) Wulkow, M. *Macromol. Theory Simul.* **1996**, *5*, 393-416.

(30) Hutchinson, R. A.; Beuermann, S.; Paquet, D. A., Jr.; McMinn, J. H. *Macromolecules* **1997**, *30*, 3490-3493.

(31) Hutchinson, R. A.; Richards, J. R.; Aronson, M. T. *Macromolecules* **1994**, *27*, 4530-4537.

(32) Kornherr, A.; Zifferer, G.; Olaj, O. F. *Macromol. Theory Simul.* **1999**, *8*, 260-271.

(33) Olaj, O. F.; Vana, P.; Kornherr, A.; Zifferer, G. *Macromol. Chem. Phys.* **1999**, *200*, 2031-2039.

(34) Nikitin, A. N.; Evseev, A. V. *Macromol. Theory Simul.* **1997**, *6*, 1191-1210.

(35) Schnöll-Bitai, I.; Zifferer, G.; Olaj, O. F. *Die Makromolekulare Chemie, Rapid Communications* **1988**, *9*, 659-670.

(36) Olaj, O. F.; Kornherr, A.; Zifferer, G. *Macromol. Theory Simul.* **1997**, *6*, 655-666.

(37) Stickler, M.; Meyerhoff, G. *Makromol. Chem.* **1978**, *179*, 2729-2745.

(38) Smith, G. B.; van Berkel, K. Y.; Russell, G. T., manuscript in preparation.

(39) Russell, G. T. *Macromol. Theory Simul.* **1994**, *3*, 439-468.

(40) Heuts, J. P. A.; Gilbert, R. G.; Radom, L. *Macromolecules* **1995**, *28*, 8771-8781.

(41) Olaj, O. F.; Vana, P.; Zoder, M.; Kornherr, A.; Zifferer, G. *Macromol. Rapid Commun.* **2000**, *21*, 913-920.

(42) Smith, G. B.; Russell, G. T.; Yin, M.; Heuts, J. P. A. *European Polymer Journal* **2005**, *41*, 225-230.

(43) Willemse, R. X. E.; Staal, B. B. P.; van Herk, A. M.; Pierik, S. C. J.; Klumperman, B. *Macromolecules* **2003**, *36*, 9797-9803.

(44) Gridnev, A. A.; Ittel, S. D. *Macromolecules* **1996**, *29*, 5864-5874.

(45) Vana, P.; Davis, T. P.; Barner-Kowollik, C. *Macromol. Rapid Commun.* **2002**, *23*, 952-956.

(46) Buback, M.; Müller, E.; Russell, G. T. *J. Phys. Chem. A* **2006**, *110*, 3222-3230.

(47) Buback, M.; Egorov, M.; Junkers, T.; Panchenko, E. *Macromol. Chem. Phys.* **2005**, *206*, 333-341.

7 Conclusion and Outlook

This thesis has shown that one must acknowledge chain-length dependent termination (CLDT) and propagation (CLDP): even if they are not ostensibly apparent in a certain radical polymerisation system, then rather than concluding that they are not in operation, one should ask why their effect has been masked.

It could be said that the addition of a number of adjustable parameters to the model for RP kinetics (*viz.* e_S, e_L and i_c for CLDT and C and $i_{½}$ for CLDP) might enable the fitting of any conceivable dataset. There is truth to this, however this view would neglect that this is actually the minimum number of parameters necessary to describe physical reality, and also that the parameters have clear physical interpretations which, if these interpretations are kept in mind in fitting data, could not explain every anomalous situation. For instance, one should have $e_S > e_L > 0$, and C, $i_{½} > 0$.

An important point to appreciate about masking the effects of CLDT concerns the so-called 'transfer limit': It obscures expected effects of CLDT (see Chapter 5) such as the dependence of rate on initiator concentration deviating from the prediction of classical kinetics. Then in other situations one has that the effects of CLDP and CLDT on rate largely cancel each other out, once again perhaps giving the false impression of classical kinetics (see Chapter 3).

Effects due to CLDP, which may have been dismissed as artefactual in the past, should be studied, since theory indicates that they are real phenomena: the 'dip' at low chain lengths in the number molecular weight distribution (MWD) (see Chapter 6) and the low polydispersity index of MWDs formed at low chain lengths (see Chapter 3) are both implied by theory to be due to the effect of CLDP. It is now evident that both of these have been observed in reality without any such appreciation of the data being possible at the time.[1,2]

In Chapter 4 it was seen that all polymerisation reactions with the potential for chain-length-dependent reactivities have been acknowledged to be so, with one exception: chain transfer (CLDTr). There is currently no information on this, but it is reasonable to expect that if propagation is chain-length-dependent, chain transfer may also be so due to the similar reaction coordinates followed by these two reactions.[3] Indeed, this possibility has very recently been explored *via* kinetic simulations,[4] but the next step is obviously for some concrete data on this phenomenon to be obtained.

Indeed, it is clear from this thesis that theory is now in advance of experiment, and a vital direction for future work is for improved experimental data on CLDT, CLDP and CLDTr to be obtained, so that the theory of this work can be better exploited in understanding RP.

Finally, the systems studied in this thesis have all been at low conversion. The theory however, is not restricted in terms of conversion. Thus it would be timely to use this theory to build on what has been learnt at low conversion in order to investigate intermediate conversion phenomena such as the Trommsdorff effect. In fact this was the original aim of this Ph.D., but other interesting things intervened!

References

(1) Heuts, J. P. A.; Davis, T. P.; Russell, G. T. *Macromolecules* **1999**, *32*, 6019-6030.

(2) Zammit, M. D.; Davis, T. P.; Haddleton, D. M.; Suddaby, K. G. *Macromolecules* **1997**, *30*, 1915-1920.

(3) Heuts, J. P. A. In *Handbook of Radical Polymerization*; Matyjaszewski, K., Davis, T. P., Eds.; Wiley and Sons Inc.: New York, NY, 2002; pp 1-76.

(4) Heuts, J. P. A.; Russell, G. T.; Smith, G. B. *Aust. J. Chem.* **2007**, submitted.

8 Appendix: Numerical Solution of Differential Equations - Simulation Program Details

In order to perform modeling work such as described in Chapter 2,[1] Chapter 6[2] and elsewhere,[3] a simulation program was developed to solve the equations that describe Pulsed-Laser-initiated radical Polymerisation (PLP). The program was implemented on a desktop PC using the C programming language, with all non-integer variables declared double precision (except time, which was declared long double precision). Some technical details of the operation of this program are given in this appendix. Other workers[4-6] have undertaken similar efforts in order to model polymerisation systems.

Considered here is a model system with the following parameters: the concentration of radicals added per laser pulse, $\rho = 5\times10^{-8}$ mol L^{-1}; the (chain-length independent) rate coefficient for termination, $k_t = 1\times10^{9}$ L mol^{-1} s^{-1} (note that with chain-length independent termination, as we have here, results depend only on the product $\rho\, k_t$, e.g., identical results would be obtained with $\rho = 5\times10^{-7}$ mol L^{-1} and $k_t = 1\times10^{8}$ L mol^{-1} s^{-1}); the propagation frequency, $k_p[M] = 2000$ s^{-1}; the frequency of transfer, $f_{tr} = 0$; the fraction of dead chains formed by disproportionation, $\lambda = 1$; and the time between laser pulses, $t_d = 0.2$ s. See Chapters 1, 2 or 6 for more details on the physical meaning of these parameters.

The output of the program is compared with that of the PLP simulation package PREDICI © in *Fig. 8.1*. It can be seen from the figure that by decreasing PREDICI's 'time integration accuracy', the accurate results obtained by the program developed for this thesis are approached. It is noteworthy that these results were obtained on the same computer, and while the program developed here took 2 minutes, PREDICI's results (in order of decreasing 'time integration accuracy' parameter) took 23 minutes and 4 hours. It is clear that the

program developed here performs exceptionally well on this model system. Below are noted the numerical strategies employed by this program that contribute to its superior performance.

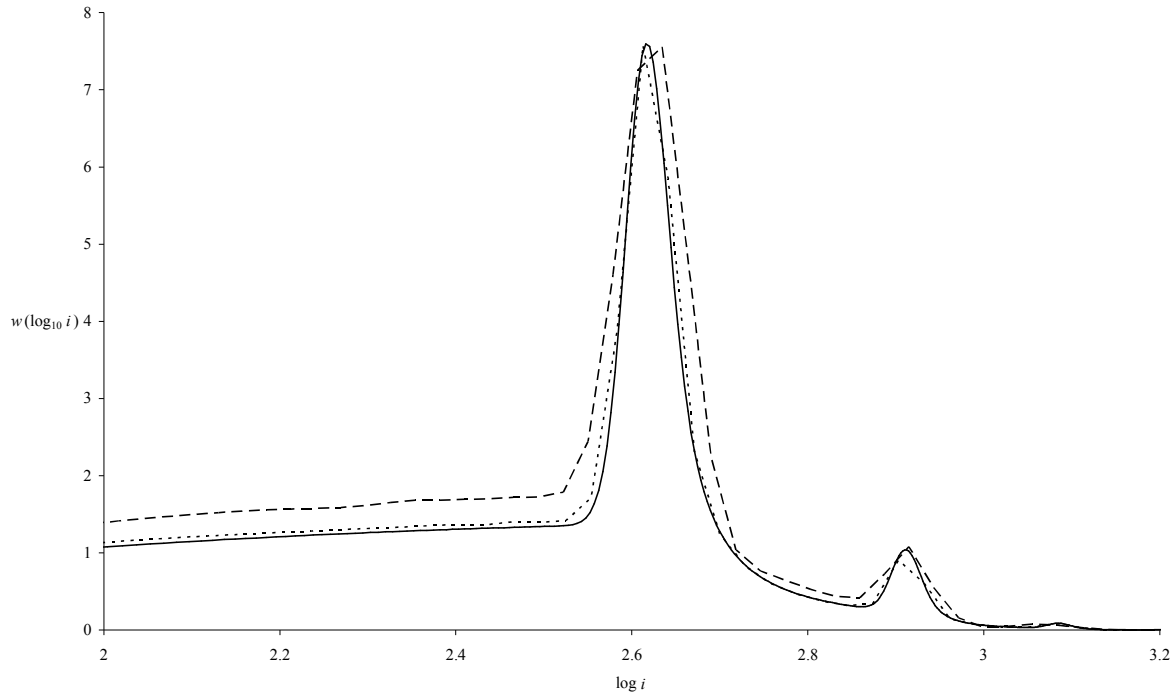

Fig. 8.1 Simulated PLP-SEC distributions (as $w(\log_{10} i)$) with the model parameters of this appendix (see text above). The data represented by the solid line was obtained with the program developed for this thesis with a timestep $h = 1\times10^{-5}$ s (see text below), and the data represented by the other two lines were obtained from PREDICI © with 'time integration accuracy' of 0.01 (dotted line) and 0.05 (dashed line).

Numerical solution of Differential Equations

The program uses the simple Euler method to solve differential equations for several reasons. Firstly, it is exceedingly simple to implement (see Chapter 1). Secondly, if programs are developed in a modular fashion, such that DE solving is logically separated from calculations

pertaining to the kinetic modeling, the Euler method can easily be 'upgraded' to higher order methods such as Modified Euler or Runge-Kutta[7] should additional accuracy/efficiency be required. Finally, however, it was found that the latter is not necessary, so the Euler method was always used with a constant timestep, $h \leq 1/(k_p[M])$.[7] In fact, a timestep of $h = 1/(10k_p[M])$ was typically used for the work of this thesis and can be recommended.

Truncation chain length

The chain length up to which it is necessary to calculate the radical and dead chain distributions in order to obtain suitably accurate results is called the truncation chain length. This cannot be known in advance, since the calculation of the MWD is rather the point of performing simulations! It is therefore tempting to set a very high value of the truncation chain length as a parameter for the program, in order to avoid the situation where a calculation is carried out, but the results are invalidated by the discovery, at the end of the calculation, that the truncation chain length was not quite high enough and a significant portion of the distribution was omitted. On the other hand, doing this actually guarantees that the calculation will be lengthy, since the truncation chain length determines the number of equations to be solved.

In practice what has been done in this program is to allocate memory sufficient to perform calculations to a very high chain length, but treat the truncation chain length as a program variable, z, which can initially be set to a very low value since the initial conditions are that all radical and dead polymer chain concentrations are zero. Subsequently, at each timestep the program checks the condition

$$\frac{d[R_z]}{dt} > 0 \qquad \textbf{(8.1)}$$

If eq. **(8.1)** is satisfied, z is increased by one. It might be suspected that this procedure could introduce errors of its own, but this was found not to be the case: for reasonable values of the timestep h, when the value on the LHS of eq. **(8.1)** exceeded zero it was hardly greater than the minimum possible value for a double precision formatted number.

Estimation of a maximum truncation chain-length at early simulation times

The procedure of the preceding section allows z to be adjusted dynamically without incurring error in the calculation, however it should not be allowed to increase without bound, for obvious reasons. Ideally it would be possible to use some characteristic of the MWD calculated at early times, before z has become prohibitively large, to estimate the eventual maximum value of z that will give acceptable accuracy in the final results.

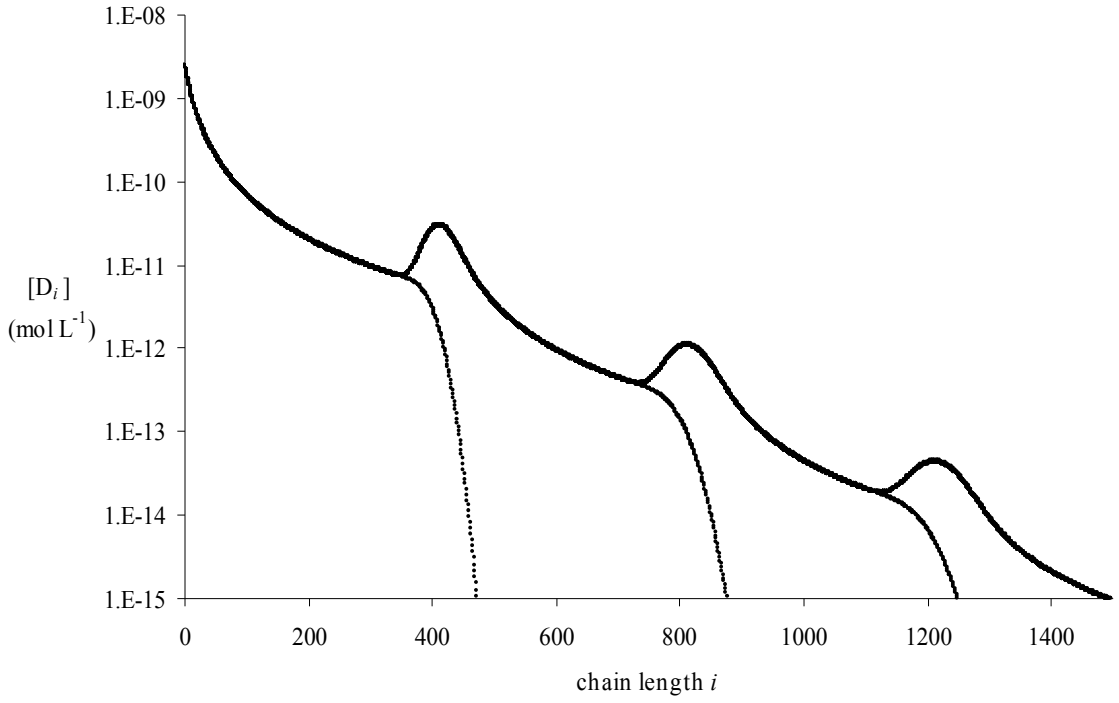

Fig. 8.2 Dead chain-length distributions [D_i] vs. i (note the log-linear scale) added during successive pulse intervals (*i.e.* created during 0-0.2, 0.2-0.4, 0.4-0.6 and 0.6-0.8 s) for the system under consideration (see text above).

As is evident from *Fig. 8.2*, after a small number of pulse intervals t_d have elapsed, the number distribution of dead chains added by successive pulses is (very approximately) exponential, *i.e.* a plot of log [D_i] *vs. i* is approximately linear. This is the characteristic used to estimate the maximum value of *z* that should be used. The fraction f_L of dead chains that are longer than the truncation chain length is defined as

$$f_L = \sum_{j=z}^{\infty} [D_j] \; / \; \sum_{j=1}^{\infty} [D_j] \qquad \textbf{(8.2)}$$

Let *m* be the slope of a plot of log [D_i] *vs. i* (calculated in the simulation just before a new pulse is applied). Assuming that an exactly exponential distribution will eventually be produced by PLP, it can be shown that a desired value of f_L will be attained when *z* is given by eq. **(8.3)**:

$$z = \log(f_L) / m \qquad \textbf{(8.3)}$$

Typically $f_L = 10^{-6}$ was used. Later in this appendix it will be specifically explained how this equation is used to set *z*.

This method is weak when the pulse repetition rate is low, and fails entirely when only a single pulse is simulated with no transfer, as in Chapter 6. This is because by the time a good estimate of the maximum truncation chain length can be calculated, the actual truncation chain length being used by the simulation far exceeds the estimate. However, the method excels for moderate and high pulse repetition rates, as we have in the model parameters of this appendix. To further appreciate this point, see also *Fig. 8.3*. Actual PLP experiments usually have $t_d < 1$s, and in such circumstances the method described above works well.

Differential equations for chains longer than the truncation chain length

Once the truncation chain length is judged to have been reached by the simulation, it is still desirable to retain some information about longer chains than this. This can be done by adding the following additional reaction to the kinetic scheme:

$$R_{z\text{-}1} + M \xrightarrow{k_p^{\infty}} R_L \qquad \textbf{(8.4)}$$

A differential equation can then be derived for $[R_L]$, the total concentration of all radical chains with a chain length of z or greater. Similarly for dead chains; $[D_L]$ is increased by termination by disproportionation or transfer of long radicals, or termination by combination of two radicals whose combined chain length is greater than z. Most programmers implicitly assume $[R_L] = 0$, which is an impediment to accuracy. The procedure above allows an economical z to be set without sacrificing accuracy. To put the matter simply, $[R_L]$ species do affect kinetics but do not need to be treated by individual chain length.

Check for pseudo-steady state conditions

After a sufficiently large number of pulses, the concentration of radicals that is removed by termination in the interval between successive laser pulses becomes equal to the concentration of radicals that is added by the laser pulse, and the variation of the total radical concentration with time is entirely periodic. Once this condition is satisfied, the individual radical concentrations (for all but the longest chain lengths, which by this time are probably subsumed in 'long' chains, $[R_L]$) will also be entirely periodic, and the dead chain-length distribution added during any given pulse interval will be identical to that added during the previous pulse period (see *Fig. 8.2*). Thus, there is no need for further calculation at this point, as the results are entirely predictable from results already calculated. In this program, the MWD added by successive pulses is compared (by calculating the square root of the

average sum of squared relative differences), and when the change is judged sufficiently small (typically less than 10^{-6}), pseudo-steady state conditions are assumed to hold, and the calculation is halted. A less stringent criterion based on the value of the total radical concentration either just before or just after the laser pulse is added could alternatively be used, however this is not recommended for reasons soon to be discussed. The output simulation results are then just those for the final simulated pulse interval (because in reality this is the situation that will hold for hundreds of pulses in a PLP experiment). Obviously simulation time is thus minimised by the program detecting exactly how long it needs to operate and not operating any longer than required.

Timestep for dead chain-length distribution

The DEs for the radical chain-length distribution (RCLD) are coupled to each other, and so the same timestep absolutely must be used to simulate the whole radical distribution. The situation with the dead chain-length distribution (DCLD) however is not so stringent: the DCLD is coupled to the RCLD only, and so a different timestep may freely be used to evaluate the DCLD. This is especially important in systems where combination occurs, as the calculation of the terms due to combination in the DEs is very expensive (one must sum the contribution of all pairs of radical chain lengths that can produce a dead chain of a particular chain length). It has been found that using a timestep for the DCLD that is 5-10 times higher than that used for the RCLD does not incur significant error. This strategy makes the calculation of the DCLD essentially free if only disproportionation and transfer occur (as most of the calculation time is spent on evaluating the RCLD), and significantly reduces the time taken by the calculation if combination occurs.

Implicit in the above discussion is the concept that if combination does not occur in the system of interest, care should be taken not to evaluate the terms due to it in the program. The

program used for this thesis does this (*i.e.* the combination sum is skipped for $\lambda = 1$). It is possible that the slow operation times of PREDICI in the comparative simulations of *Fig. 8.1* are largely due to this factor.

Use of symmetry in calculating terms due to combination

The combination term in the DEs for the DCLD is usually written

$$\frac{d[D_i]}{dt}(\text{combination}) = (1-\lambda)\sum_{j=1}^{i-1} k_t^{j,i-j}[R_j][R_{i-j}] \qquad \textbf{(8.5)}$$

It is easy to see that consideration of symmetry can reduce the computational effort required to calculate this term, since $k_t^{i,j} = k_t^{j,i}$ for all conceivable physically realistic termination models. For example consider combination to produce chains of length 4: these may be formed by pairs of radicals of length 1 and 3, 2 and 2, or 3 and 1. The terms in eq. **(8.5)** due to the first and last aforementioned pairs are equal. Indeed, consideration of this symmetry roughly halves the time taken to calculate combination terms. Where combination occurs, evaluation of the sum of eq. **(8.5)** is a large fraction of total calculation time, hence every effort to reduce the cost of this calculation (see also the preceding section) results in a significant gain in terms of overall computational efficiency.

Behaviour of the simulation for the model system

Fig. 8.3 shows the way in which the strategies outlined above interact in the numerical solution of the model system outlined at the start of this appendix. Initially, z is low since the only radicals present are the monomeric radicals generated by the first laser pulse. With the addition of the second laser pulse, the total radical concentration is slightly higher than it was after the first pulse, since not all radicals terminated in the interval between pulses. The first estimate of the maximum truncation chain length becomes available, but it is not used since

experience shows that this first estimate is likely to be inaccurate. After three pulse intervals (*i.e.* $t = 0.6$ s) the estimate of z according to eq. **(8.3)** is less than 10% different from that after two pulse intervals (*i.e.* $t = 0.4$ s). From experience this is deemed sufficiently accurate, and therefore the value of z is set at the eq. **(8.3)** (as shown in the figure), and is not allowed to increase further after this time. If the current value of z is greater than the estimated maximum truncation chain length that has been judged to be accurate, the concentrations of radicals and dead chains greater than the new truncation chain length are all immediately added to the 'long' concentration for their respective distribution ($[R_i]$ and $[D_i]$). It can be seen that at this point, the concentration of long radicals begins to increase, and soon reaches a pseudo-steady state. After 8 pulse intervals (1.6 seconds), comparison of the MWD added during successive pulse intervals (see *Fig. 8.2*) shows that pseudo-steady state conditions apply, and therefore the simulation is halted.

Two further points should be made about the results of *Fig. 8.3*: (1) There was a great increase in computational speed at $t = 0.6$ s, the point at which the truncation chain length was reduced to the unchanging value of about 1700 (in this case). This illustrates the advantage of clever choice of z. (2) The overall radical concentration approaches pseudo-steady state much faster than the entire distribution (compare the [R] and $[R_L]$ profiles in the figure). This emphasises that one should use the entire distribution to determine when pseudo-steady state has been reached, otherwise the MWD at long chain lengths will be inaccurate.

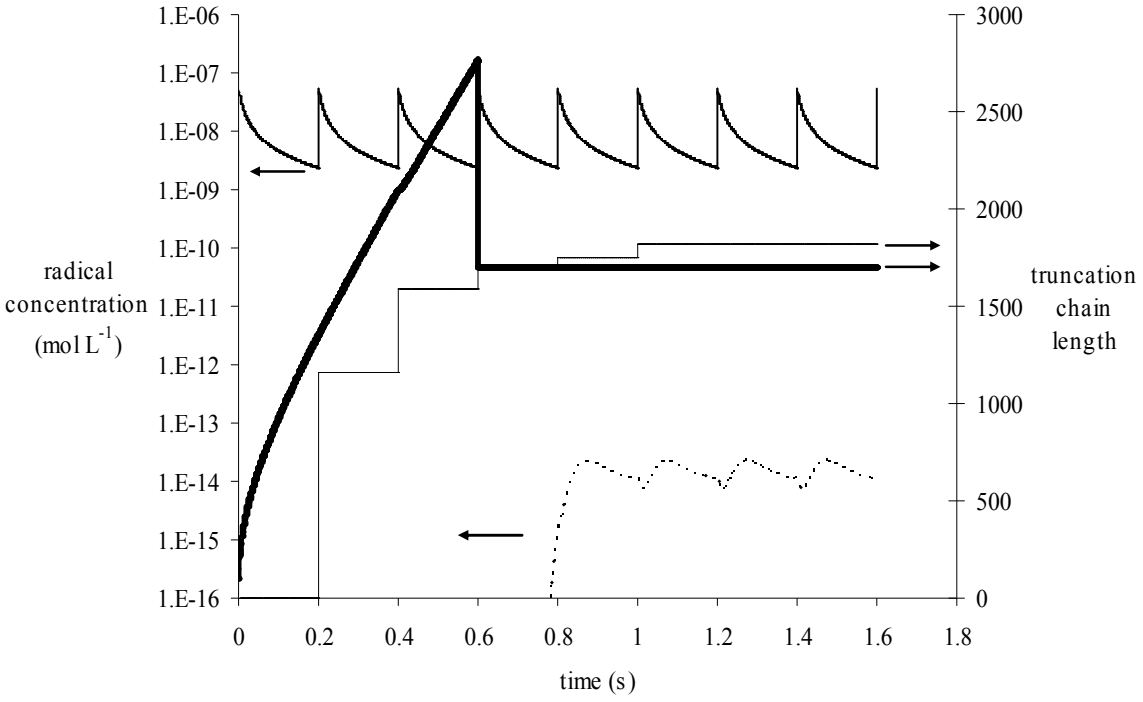

Fig. 8.3 Time evolution of radical concentration (left hand axis, as indicated by arrows) and truncation chain length (right hand axis, as indicated by arrows) for the parameters used in this appendix (see text above). For radical concentrations, the solid line depicts the total radical concentration, while the dotted line depicts the concentration of 'long' radicals (see text). For truncation chain lengths, the solid line depicts the (variable) truncation chain length z used at a particular time, while the dotted line depicts the maximum value of the truncation chain length estimated from eq. **(8.3)** with the arrival of each pulse.

Conclusion

To return to the fact noted at the beginning of this appendix, that the program developed for this thesis performs far better than PREDICI © for the system considered here, it could be said that the program's speed is due to a combination of *lack* of sophistication in areas where

sophistication is not required or helpful for this particular system (DE solvers of higher order, and variable timestep methods), and increased sophistication in areas where it is helpful (control of truncation chain length, and checking for pseudo-steady state conditions).

In order for higher order methods to be useful, they must counterbalance, with increased accuracy, the additional function evaluations of the DEs which the methods demand (*e.g.* 4 function evaluations per timestep for the 4th order Runge-Kutta method, *vs.* one function evaluation for the Euler method). Since all of these methods must use a maximum timestep of $1/(k_p[M])$,[7] the extra accuracy gained, although it can be considerable, often comes at the expense of too much additional computational time.

References

(1) Smith, G. B.; Russell, G. T.; Heuts, J. P. A. *Macromol. Theory Simul.* **2003**, *12*, 299-314.

(2) Smith, G. B.; Russell, G. T. *Z. Phys. Chem.* **2005**, *219*, 295-323.

(3) Tanaka, K.; Yamada, B.; Fellows, C. M.; Gilbert, R. G.; Davis, T. P.; Yee, L. H.; Smith, G. B.; Rees, M. T. L.; Russell, G. T. *J. Polym. Sci., Polym. Chem. Ed.* **2001**, *39*, 3902-3915.

(4) Buttè, A.; Storti, G.; Morbidelli, M. *Macromol. Symp.* **2002**, *182*, 181-194.

(5) Johnson, C. H. J.; Moad, G.; Solomon, D. H.; Spurling, T. H.; Vearing, D. J. *Aust. J. Chem.* **1990**, *43*, 1215-1230.

(6) Moad, G.; Anderson, A. G.; Ercole, F.; Johnson, C. H. J.; Krstina, J.; Moad, C. L.; Rizzardo, E.; Spurling, T. H.; Thang, S. H. *Am. Chem. Soc., Symp. Ser.* **1998**, *685*, 332-360.

(7) Rees, M. T. L., Ph.D. Thesis, The University of Canterbury, 1999

9 Appendix: Steady State Solutions - Simulation Program Details

This appendix concerns steady state free-radical polymerisation calculations. The model is developed and equations presented in Chapter 4. This appendix gives procedural details of the program, and dependence of performance on specified tolerances.

Procedure

The general procedure for calculations is described in this section. Some steps are optional if certain models are used, but the order of the steps is general.

A) Set values of input parameters. If the parameters that comprise r_t and r_{tr} are specified individually, calculate the aggregate parameters:

$$r_t = \frac{\sqrt{2\, k_t^{1,1}\, R_{init}}}{f_p^{\infty}} \tag{9.1}$$

$$r_{tr} = \frac{f_{tr}}{f_p^{\infty}} \tag{9.2}$$

Specify the model parameters for the chain-length dependence of propagation and termination:

$$k_p^{\,i} = k_p^{\infty}\, N(i) \tag{9.3}$$

$$k_t^{i,j} = k_t^{1,1}\, M(i,j) \tag{9.4}$$

Specify convergence tolerances ε_z and ε_{it} (see below). Where output data is to be produced which could potentially be very high volume (such as chain length distributions), specify the frequency of output.

B) Calculate the reduced radical chain-length distribution (rRCLD), starting at $i = 1$ with $P_0 = 1$, and in the first instance using the geometric mean model (eq. **(9.5)**); note that $M(i,i) = i^{-e}$ for the one-*e* model. As the chain length is increased, calculate P_L (eq. **(9.6)**) and S_r (eq. **(9.7)**) in parallel with the rRCLD, stopping when the truncation tolerance is reached (eq. **(9.8)**), a good value to use being $\varepsilon_z = 10^{-6}$:

$$\frac{P_i}{P_{i\text{-}1}} = \frac{N(i\text{-}1)}{N(i) + r_{tr} + r_t\sqrt{M(i,i)}} \qquad \textbf{(9.5)}$$

$$\frac{P_L}{P_{i\text{-}1}} = \frac{1}{r_{tr} + r_t\sqrt{M(i,i)}} \qquad \textbf{(9.6)}$$

$$S_r = \sum_{j=1}^{i\text{-}1} P_j + P_L \qquad \textbf{(9.7)}$$

$$P_L / S_r \leq \varepsilon_z \qquad \textbf{(9.8)}$$

It can be seen that these equations may also be used for the transfer limit ($r_t = 0$). Due to the similarity of **(9.5)** and **(9.6)**, it is recommended to first calculate $r_{tr} + r_t\sqrt{M(i,i)}$ before using this one number in both equations. This procedure is non-iterative, and the only limit to accuracy is the *z* up until which the rRLCD is calculated. This holds even for the termination limit ($r_{tr} = 0$), in which there are one-line, closed expressions for $\langle k_t \rangle$, $\overline{DP}_n$, $\overline{DP}_w$, *etc.*[1,2]: these expressions are all in the long chain limit, whereas the above approach does not make this assumption. The two types of methods are complementary, as at short chain lengths the closed expressions are inaccurate (see Chapter 5) but the non-iterative procedure outlined above can be quickly evaluated. In contrast, at long chain lengths the opposite situation applies: closed expressions are more accurate while the non-iterative procedure takes longer to calculate. Note that such one-line closed expressions exist only for the termination and

transfer limits; in the general case one has no option but to use the above approach (notwithstanding the approximate procedure developed by Olaj *et al.*[2]).

Regardless of which termination model is used, the solution with the geometric mean may be cheaply calculated and makes the best possible starting approximation for further calculations.

C) Iterate until iteration tolerance is reached. For the diffusion mean:

$$\frac{P_i}{P_{i\text{-}1}} = \frac{N(i\text{-}1)}{N(i) + \frac{S_r(\text{old})^{-1} + r_{tr}}{2} + M(i,i)\,\frac{r_t^2}{2\,(S_r(\text{old})^{-1} - r_{tr})}} \qquad \textbf{(9.9)}$$

$$\frac{P_L}{P_{i\text{-}1}} = \frac{1}{\frac{S_r(\text{old})^{-1} + r_{tr}}{2} + M(i,i)\,\frac{r_t^2}{2\,(S_r(\text{old})^{-1} - r_{tr})}} \qquad \textbf{(9.10)}$$

$$\frac{S_r(\text{old}) - S_r}{S_r(\text{old})} \leq \varepsilon_{it} \qquad \textbf{(9.11)}$$

It was found to be best to use the value of S_r from the previous iteration (S_r(old)) in eq. **(9.9)** and **(9.10)**, rather than updating it at every chain length i. However, eq. **(9.7)** and **(9.8)** are also used unmodified, so S_r should still be calculated in parallel with the rRCLD. Eq. **(9.11)** is used to judge convergence of iterations after the truncation criterion eq. **(9.8)** is satisfied; typically $\varepsilon_{it} = 10^{-7}$ was used.

For a general termination model (for instance the harmonic mean model) the following should be used:

$$\frac{P_i}{P_{i\text{-}1}} = \frac{N(i\text{-}1)}{N(i) + r_{tr} + \frac{r_t^2}{1 - r_{tr}S_r}\sum_{j=1}^{z} M(i,j)\,P_j} \qquad \textbf{(9.12)}$$

$$\frac{P_L}{P_{i\text{-}1}} = \frac{1}{r_{tr} + \frac{r_t^2}{1 - r_{tr}S_r} \sum_{j=1}^{z} M(z,j)\, P_j} \qquad \textbf{(9.13)}$$

The fact that the term $\sum_{j=1}^{z} M(i,j)\, P_j$ must be calculated for each i clearly makes the evaluation of the steady state solution of a general termination model much more computationally expensive than for the gm or dm models.

D) Calculate output values: S_t, $\langle k_t \rangle$, $\overline{DP}_n$, the RCLD and DLCD, *etc*:

$$S_t = (1 - r_{tr}\, S_r) / r_t \qquad \textbf{(9.14)}$$

$$(S_t)^2 = \sum_{i=1}^{z} \sum_{j=1}^{z} M(i,j)\, P_i\, P_j \qquad \textbf{(9.15)}$$

S_t may be simply calculated from eq. **(9.14)**, as is implicitly done in the equations for the rRCLD above, or it may be calculated from eq. **(9.15)** as a further check on the accuracy of the rRCLD (checking whether indeed $r_t\, S_t + r_{tr}\, S_r = 1$ as expected, see Chapter 4). Eq. **(9.15)** may be simplified for the gm and dm models (see Chapter 4).

$$[R_0] = \sqrt{\frac{R_{init}}{2\, k_t^{1,1}}} / S_t \qquad \textbf{(9.16)}$$

Eq. **(9.16)** may then be used to calculate $[R_0]$, and thus recover the original radical distribution $[R_i] = [R_0]\, P_i$, if so desired. The chain length averaged rate coefficient for termination, $\langle k_t \rangle$, may be calculated from eq. **(9.17)**, and the number average degree of polymerisation may be calculated from eq. **(9.18)**.

$$\langle k_t \rangle = k_t^{1,1} \left(\frac{S_t}{S_r} \right)^2 \qquad \textbf{(9.17)}$$

$$\overline{DP}_{\mathrm{n}} = \frac{1 + S_{\mathrm{r}}}{r_{\mathrm{tr}} S_{\mathrm{r}} + \frac{1+\lambda}{2}(1 - r_{\mathrm{tr}} S_{\mathrm{r}})} \qquad \textbf{(9.18)}$$

Note that eq. **(9.18)** applies with the occurrence of termination by combination, but it is not necessary to calculate combination terms to find $\overline{DP}_{\mathrm{n}}$. If the full DCLD is required, eq. **(9.19)** may be employed (which does require evaluation of combination terms):

$$[D_i] \sim r_{\mathrm{tr}} P_i + \lambda \left(N(i\text{-}1) P_{i\text{-}1} - N(i) P_i - r_{\mathrm{tr}} P_i\right) + \frac{1-\lambda}{2} \frac{r_{\mathrm{t}}}{S_{\mathrm{t}}} \sum_{j=1}^{i-1} M(i\text{-}j,j) P_{i-j} P_j \qquad \textbf{(9.19)}$$

Oscillating solutions

In some situations, it is found that the values delivered by eqs. **(9.12)** and **(9.13)** display oscillatory behaviour. This may be ameliorated by adjusting values to be a mean of the two most recent estimates for P_i, *e.g.* the geometric mean or arithmetic mean. It is stressed that such situations are relatively uncommon, however it was found, for example, that this adjustment procedure helped in some cases when the harmonic mean model for $k_{\mathrm{t}}^{i,j}$ was employed. Specifically, geometric mean averaging was used, and it approximately halved the number of iterations required to reach convergence.

Performance

All other input parameters being equal, performance of the calculation depends on the tolerances for truncation and iteration. Since truncation logically precedes iteration, iteration tolerance should be of the same order as truncation tolerance for best efficiency. Use of the rRCLD affords great increases in performance over the use of the RCLD itself, despite the slightly more complicated derivation: far fewer iterations are required, particularly near the transfer limit where the RCLD method requires thousands of iterations, but the rRCLD does

not require significantly more iterations in this situation than it does near the termination limit. As an example, a sample calculation with the dm near the transfer limit ($r_{tr} = 10^{-4}$, $r_t = 10^{-6}$, $e = 0.5$) required only 3 iterations for convergence, using the already given e values and the gm distribution as the starting guess. It is stressed that the combination of using the gm distribution as a starting guess, and using the rRCLD to perform calculations rather than the RCLD, leads to a major reduction in the number of iterations required to reach convergence.

References

(1) Olaj, O. F.; Zifferer, G.; Gleixner, G. *Makromol. Chem., Rapid Commun.* **1985**, *6*, 773-784.

(2) Olaj, O. F.; Zifferer, G.; Gleixner, G. *Macromolecules* **1987**, *20*, 839-850.